

**Dynamic Phasor Modeling of Modular Multilevel Converters for Hybrid
AC/DC Power Systems**

by

Abraham Rojas Tarango

A thesis submitted in partial fulfilment of the requirements for the degree of
Master of Science
in
Energy Systems

Department of Electrical and Computer Engineering
University of Alberta

© Abraham Rojas Tarango, 2020

Abstract

This thesis develops a time averaged model (TAM) and a dynamic phasor model (DPM) of a generalised modular multilevel converter (MMC) structure that can be used to represent four different MMC topologies. These four topologies include two different classes of next generation MMCs that are garnering attention for use in hybrid AC/DC power systems: (i) DC/DC/AC MMCs that combine DC/DC and AC/DC conversion stages into a single converter structure, and (ii) DC/DC MMCs. The former enables controlled power exchange between two DC systems and an AC grid while the latter is a key building block of future DC grids. A TAM is developed in the $\alpha\beta 0$ frame that includes all dynamics in a converter, barring switching harmonics. This model is useful when detailed studies of the converter dynamics are required, but the long simulation time of the switched model is an impediment. A DPM is then derived from the TAM that takes into account multiple harmonic components to ensure an accurate representation of the practical converter behaviour across a wide range of operating points. This model permits the elaboration of a steady-state solution procedure to solve for the full state solution at

an arbitrary operating point, enabling systematic study of the DC/DC/AC and DC/DC MMCs using industry standard numerical software tools. Extensive simulations and steady-state analyses are carried out to investigate the converters' behaviour, including how the current stresses and capacitor voltage ripples change due to varying parameters such as DC and AC systems power flows.

Dedication

*To my wife, without whom all of this would not have been possible. I admire your
bravery for agreeing to leave behind your life, and become my own.*

Acknowledgments

I would like to first express my deepest appreciation and gratitude to my supervisor, Professor Gregory J. Kish. For the last two and a half years he has given me the best guidance, advice, and encouragement any student could ever desire. His patience and technical expertise were fundamental for this work, and will always be cherished.

I also wish to give my sincere gratitude to the members of the thesis examination committee, Professor Yunwei Li and Professor Hao Liang, for the time they took to review this work and their valuable feedback.

I am incredibly grateful to the many people who have been with me throughout this process. My wife, Reyna, who has been by my side always and helped me through the most difficult times. My mother, Luz Elena, my father, Edgardo, and my brother, Edgar, who have been a pillar of support my whole life, I would not be where I am today without them. Nahum, who really has made me push my limits, and has always been available to provide me with assistance. Bekah and Dave, whose help and friendship has been invaluable.

The financial support of CONACyT-SENER's "*sustentabilidad energetica*" fellowship is gratefully acknowledged.

Contents

Nomenclature	xvi
1 Introduction	1
1.1 Background	1
1.2 MMC Topologies for Future DC and Hybrid AC/DC Power Systems . . .	4
1.2.1 DC/DC Converters	5
1.2.2 DC/DC/AC Converters	9
1.2.3 Availability of Analytical Models	10
1.3 Thesis Scope	15
2 Power Transfer Mechanisms of DC/DC and Multiport DC/DC/AC MMCs	17
2.1 Conventional AC/DC MMC	18
2.2 DC/DC MMC	24
2.3 DC/DC/AC MMC	27
2.4 Regulation of Capacitor Voltage and External Network Power Injections	30
2.5 Multiport MMC Structure for Simultaneous DC/ DC/ AC Conversion	31

3	Converter Dynamic Modelling	33
3.1	Time-Averaged Model	33
3.1.1	Single Phase Leg for DC/DC/AC Conversion	35
3.1.2	Three-Phase Converter for DC/DC/AC Conversion	40
3.1.3	$\alpha\beta 0$ - Frame Mapping	42
3.1.4	Three-Phase Converter for DC/DC Conversion	47
3.1.5	Model Validation	48
3.2	Dynamic Phasor Model	53
3.2.1	DPM Derivation for DC/DC/AC Conversion	53
3.2.2	DPM Derivation for DC/DC Conversion	57
3.2.3	DPM Validation	58
3.3	Chapter summary	66
4	DC/DC/AC and DC/DC Converters Case Studies	69
4.1	DC/DC/AC Conversion	69
4.1.1	Challenges in steady-state analysis using TAM	70
4.1.2	Steady-State Solution Procedure	70
4.1.3	MP-DCDCAC Steady-State Analysis	74
4.1.3.1	400/200kV ($G_v=0.5$) Converter Design	76
4.1.3.2	400/320kV ($G_v=0.8$) Converter Design	79
4.1.4	BP-DCDCAC Steady-State Analysis	82
4.1.4.1	320/320kV ($G_v=1$) Converter Design	84
4.1.5	Varying Parameters Studies	88
4.2	DC/DC Conversion	91
4.2.1	Steady-State Solution Procedure	91
4.2.2	MP-DCDC Steady-State Analysis	92

4.2.2.1	500/250kV ($G_v=0.5$) Converter Design	93
4.2.2.2	400/320kV ($G_v=0.8$) Converter Design	96
4.2.3	BP-DCDC Steady-State Analysis	99
4.2.3.1	320/320kV ($G_v=1$) Converter Design	101
4.2.4	Varying Parameters Studies	103
4.3	Chapter Summary	105
5	Conclusion	106
5.1	Contributions	106
5.2	Future Work	108
	References	109
A	DC/DC/AC TAM Matrices	119
B	DC/DC TAM Matrices	123
C	DC/DC/AC DPM Matrices	126
D	DC/DC DPM Matrices	156
E	Accuracy of DC/DC/AC DPM	180

List of Tables

2.1	Practical switching states of the half-bridge submodule	19
2.2	Currents' harmonic components and power transfer mechanisms for each of the conversion cases	29
2.3	Currents' harmonic components and powers for each of the conversion cases	31
3.1	Simulation parameters for the switched/averaged simulations	49
3.2	Dominant harmonic components for each $\alpha\beta 0$ frame component in system Equation (3.31)	54
3.3	Simulation parameters for the averaged/DPM simulations	60
3.4	MP-DCDCAC State Variables Steady-State Comparison	65
3.5	MP-DCDC State Variables Steady-State Comparison	65
3.6	BP-DCDCAC State Variables Steady-State Comparison	66
3.7	BP-DCDC State Variables Steady-State Comparison	67
3.8	Summary of developed time-averaged models	68
3.9	Summary of developed DPMs	68
4.1	Simulation parameters for MP-DCDCAC using $G_v=0.5$	77
4.2	Simulation parameters for MP-DCDCAC using $G_v=0.8$	80
4.3	Simulation parameters for BP-DCDCAC	84

4.4	Simulation parameters for MP-DCDC using $G_v=0.5$	94
4.5	Simulation parameters for MP-DCDC using $G_v=0.8$	97
4.6	Simulation parameters for BP-DCDC	100
E.1	MP-DCDCAC State Variables Steady-State Comparison Using $30 \frac{kJ}{MW}$. .	181
E.2	MP-DCDC State Variables Steady-State Comparison Using $30 \frac{kJ}{MW}$. . .	181
E.3	BP-DCDCAC State Variables Steady-State Comparison Using $30 \frac{kJ}{MW}$. .	182
E.4	BP-DCDC State Variables Steady-State Comparison Using $30 \frac{kJ}{MW}$. . .	182

List of Figures

1.1	Conventional AC/DC MMC (a) three-phase topology, (b) standard sub-module configurations	4
1.2	DAB (or F2F) MMC	6
1.3	HVDC autotransformer [31]	7
1.4	M2DC [33]–[35] with magnetics solution for the filter	9
1.5	Examples of three-phase DC/DC/AC MMCs; (a) based on F2F MMC, (b) based on HVDC-AT [32], (c) based on M2DC [36], (d) Bipolar MMC with delta/zig-zag transformer [39], (e) Generalised DC/DC/AC chain-link structure [40], (f) multiport buck-boost converter [41]	11
1.6	Different detail in models for converters [43]	13
1.7	Dynamic phasors visualisation using series RL circuit	15
2.1	(a) single-phase DC/AC MMC, (b) useful switching states of half-bridge submodule and waveform produced by each state	19
2.2	$\Sigma\Delta$ transformation of the single-phase MMC, where the quantities from Equations (2.1) to (2.4) are transformed through Equation (2.6). The dotted, green terms represent DC quantities and dashed, red terms represent fundamental frequency components	22

2.3	M2DC with $\Sigma\Delta$ currents and voltages, where dotted, green terms represent DC quantities and solid, blue terms represent a combination of DC and AC quantities	24
2.4	M2DC with AC port, showing $\Sigma\Delta$ currents and voltages, where dotted, green terms represent DC quantities; dashed, red terms represent fundamental frequency components; and solid, blue terms represent a combination of both	28
2.5	MMC topologies under study in this thesis: (a) MP-DCDCAC, (b) MP-DCDC, (c) BP-DCDCAC, (d) BP-DCDC	32
3.1	Target converter structures for modelling: (a) Unified general structure, (b) MP-DCDCAC topology, (c) BP-DCDC topology, (d) MP-DCDCAC topology, (e) BP-DCDC topology	34
3.2	Average models for upper arm: (a) individual j^{th} submodule, (b) composite arm with N series-cascaded submodules, (c) compact representation of upper arm	35
3.3	Time-averaged model of a single-phase leg for DC/DC/AC conversion . .	36
3.4	Three-phase structure for DC/DC/AC conversion	41
3.5	Three-phase structure for DC/DC/AC conversion	44
3.6	MP-DCDCAC simulation results comparing the 14 state variables in the $\alpha\beta 0$ frame for the PLECS' switched model vs the time averaged model in Equation (3.31)	50
3.7	BP-DCDC simulation results comparing the 12 state variables in the $\alpha\beta 0$ frame for the PLECS' switched model vs the time averaged model in Equation (3.34)	51

3.8	Upper and lower phase a arms' voltages for the: (a) MP-DCDCAC and (b) BP-DCDC simulations, comparing the PLECS' switched model vs time averaged model in Equation (3.31) and Equation (3.34)	52
3.9	MP-DCDCAC; DPM and averaged model simulation results	61
3.10	MP-DCDC; DPM and averaged model simulation results	62
3.11	BP-DCDCAC; DPM and averaged model simulation results	63
3.12	BP-DCDC; DPM and averaged model simulation results	64
4.1	Process to obtain modulating signals using TAMs	70
4.2	Solution procedure visualisation	74
4.3	MP-DCDCAC converter with current direction convention	75
4.4	Steady-state MP-DCDCAC DPM waveforms for $G_v=0.5$ (400/200 kV); $P_{dc,1}=1$ pu, $P_{dc,2}=-0.5$ pu, $P_{ac}=-0.5$ pu	77
4.5	Steady-state MP-DCDCAC DPM waveforms for $G_v=0.5$ (400/200 kV); $P_{dc,1}=0.8$ pu, $P_{dc,2}=-1$ pu, $P_{ac}=0.2$ pu	78
4.6	Steady-state MP-DCDCAC DPM waveforms for $G_v=0.5$ (400/200 kV); $P_{dc,1}=0$ pu, $P_{dc,2}=0$ pu, $P_{ac}=0$ pu	78
4.7	Steady-state MP-DCDCAC DPM waveforms for $G_v=0.8$ (400/320 kV); $P_{dc,1}=0.8$ pu, $P_{dc,2}=-0.4$ pu, $P_{ac}=-0.4$ pu	80
4.8	Steady-state MP-DCDCAC DPM waveforms for $G_v=0.8$ (400/320 kV); $P_{dc,1}=0.3$ pu, $P_{dc,2}=-0.5$ pu, $P_{ac}=0.2$ pu	81
4.9	Steady-state MP-DCDCAC DPM waveforms for $G_v=0.8$ (400/320 kV); $P_{dc,1}=0$ pu, $P_{dc,2}=0$ pu, $P_{ac}=0$ pu	81
4.10	BP-DCDCAC converter with current direction convention	82
4.11	Steady-stateBP-DCDCAC DPM waveforms; $P_{dc,1}=0.5$ pu, $P_{dc,2}=0.5$ pu, $P_{ac}=-1$ pu	86

4.12	Steady-stateBP-DCDCAC DPM waveforms; $P_{dc,1}=0.25$ pu, $P_{dc,2}=-0.5$ pu, $P_{ac}=0.25$ pu	86
4.13	Steady-stateBP-DCDCAC DPM waveforms; $P_{dc,1}=-0.6$ pu, $P_{dc,2}=0.5$ pu, $P_{ac}=0.1$ pu	87
4.14	Steady-stateBP-DCDCAC DPM waveforms; $P_{dc,1}=0$ pu, $P_{dc,2}=0$ pu, $P_{ac}=0$ pu	87
4.15	Loci of steady-state studies for $G_v=0.5$ for the phase a upper and lower arms: (a) arms' peak current stress with $P_{ac}=0.5$ pu; (b) percent capacitor voltage ripple with $P_{ac}=0.5$; (c) arms' peak current stress with $P_{dc1}=1$ pu; (d) percent capacitor voltage ripple with $P_{dc1}=1$ pu	89
4.16	Loci of steady-state studies for $G_v=0.8$ for the phase a upper and lower arms: (a) arms' peak current stress with $P_{ac}=0.5$ pu; (b) percent capacitor voltage ripple with $P_{ac}=0.5$; (c) arms' peak current stress with $P_{dc1}=1$ pu; (d) percent capacitor voltage ripple with $P_{dc1}=1$ pu	90
4.17	MP-DCDC converter with current direction convention	93
4.18	Steady-state MP-DCDC DPM waveforms for $G_v=0.5$ (500/250 kV); $P_{dc,1}=1$ pu	95
4.19	Steady-state MP-DCDC DPM waveforms for $G_v=0.5$ (500/250 kV); $P_{dc,1}=-1$ pu	95
4.20	Steady-state MP-DCDC DPM waveforms for $G_v=0.5$ (500/250 kV); $P_{dc,1}=0$ pu	96
4.21	Steady-state MP-DCDC DPM waveforms for $G_v=0.8$ (400/320 kV); $P_{dc,1}=1$ pu	98
4.22	Steady-state MP-DCDC DPM waveforms for $G_v=0.8$ (400/320 kV); $P_{dc,1}=-1$ pu	98

4.23	Steady-state MP-DCDC DPM waveforms for $G_v=0.8$ (400/320 kV); $P_{dc,1}=0$ pu	99
4.24	BP-DCDC converter with current direction convention	100
4.25	Steady-state BP-DCDC DPM waveforms for $G_v=1$ (320/320 kV); $P_{dc,1}=1$ pu	102
4.26	Steady-state BP-DCDC DPM waveforms for $G_v=1$ (320/320 kV); $P_{dc,1}=-1$ pu	102
4.27	Steady-state BP-DCDC DPM waveforms for $G_v=1$ (320/320 kV); $P_{dc,1}=0$ pu	103
4.28	Loci of steady-state studies for the phase a upper and lower arms: (a) arms' peak current stress for $G_v=0.5$; (b) percent capacitor voltage ripple for $G_v=0.5$; (c) arms' peak current stress for $G_v=0.8$; (d) percent capacitor voltage ripple for $G_v=0.8$	104
E.1	MP-DCDCAC; DPM and averaged model simulation results using $30 \frac{kJ}{MW}$	183
E.2	MP-DCDC; DPM and averaged model simulation results using $30 \frac{kJ}{MW}$	184
E.3	BP-DCDCAC; DPM and averaged model simulation results using $30 \frac{kJ}{MW}$	185
E.4	BP-DCDC; DPM and averaged model simulation results using $30 \frac{kJ}{MW}$	186

Nomenclature

Acronym	Long Form
AC	Alternating Current
AT	Auto-Transformer
BESS	Battery Energy Storage System
BP-DCDC	Bipolar DC/DC Converter
BP-DCDCAC	Bipolar DC/DC/AC Converter
DAB	Dual Active Bridge
DC	Direct Current
DPM	Dynamic Phasor Model
EMI	Electromagnetic Interference
F2F	Front-to-Front
FFT	Fast-Fourier Transform
FBSM	Full-Bridge Submodules
HVAC	High-Voltage Alternating Current
HVDC	High-Voltage Direct Current
IGBT	Insulated-Gate Bipolar Transistor
KVL	Kirchhoffs Voltage Law
LCC	Line Commutated Converters
MMC	Modular Multilevel Converter
MP-DCDC	Multiport DC/DC Converter
MP-DCDCAC	Multiport DC/DC/AC Converter
MVDC	Medium-Voltage Direct Current
PV	Photovoltaic
SPWM	Sinusoidal Pulse Width Modulation
TAM	Time Averaged Model
VSC	Voltage Sourced Converter

Chapter 1

Introduction

1.1 Background

In the last couple decades of energy research, DC transmission has gathered a great amount of interest from academics and industry all around the world. This can be seen by the increase of this topic in recent literature; the journal papers containing DC transmission as a subject have almost tripled the last twenty years compared to the whole of the last century, going by the search results in the *IEEEXplore digital library*. The reason is not because DC transmission can supplant AC transmission, the latter being well suited for many of its current applications, but because recent research seems to indicate that the future requires a combination of both of these technologies (AC and DC). High-Voltage Direct Current (HVDC) can be used for very long transmission distances, to interconnect unsynchronised AC networks, to transmit more power than AC in a comparable corridor size, and for power quality functions in existing and future grids [1]. Another very prominent application for HVDC revolves around the ever-increasing renewable energy systems; the underwater transmission of energy harvested from off-shore

wind farms [2]–[4], the transmission of PV energy without the need of AC conversion [5], [6], and connections to BESSs [7], [8]. More recently, the development of multiterminal DC systems and DC grids using HVDC is being pursued [9]–[11]

Despite its many benefits, challenges arise for the use of HVDC when several connections are to be made. Most of the previously mentioned applications require only a sending end and a receiving end, called point-to-point, and their operation and design are well understood [12]. However, as more sources and uses for energy are added to various locations, an evolution beyond basic point-to-point connections is inevitable. This becomes even more so the case when the existing AC grid is taken into consideration. Interconnecting multiple DC sources and loads, as well as including the existing AC grid, is a very active area in recent research. Such blending of DC and AC transmission technologies has been envisioned for the future of energy distribution in Europe, dubbed a *supergrid* [13]. This type of network is projected to be able to extend through a very wide area, incorporating HVDC transmission to support the existing HVAC grid, and be able to meet the ever increasing energy needs [14].

The interconnection of AC and DC links, to form what might well be the hybrid AC/DC power system of the future, comes with several challenges. One of the most prominent of these is the power conversion needed between AC and DC systems, and between different DC voltage levels. To achieve these conversions, power electronic converters are required. There is a myriad of converters capable of achieving AC/DC conversion, but for the purpose of HVDC only recent advancements in semiconductor technology allow some to be of consideration. Line commutating converters (LCCs) have been around for decades and are a mature technology, with high efficiency, and still recently being used in transmission projects around the world [15]; however, they suffer from the fact that rely on the AC system for commutation and absorb reactive power, as well as that power reversal requires the inverting of the voltage polarity. Voltage source converters

(VSCs) don't have any of the aforementioned disadvantages; moreover, they excel at controllability of power direction are therefore well suited for DC grid applications. Two and three level VSCs have the shortcoming of only being able to endure medium voltage rating before the large amount of series-connected semiconductors, usually IGBTs, start posing challenges such as high switching losses, reduced efficiency, and EMI problems [13].

Another type of VSC that has been gaining a lot of popularity since its inception is the modular multilevel converter (MMC) [16], a converter that distributes capacitors in the converter structure, instead of having them in parallel with the DC link, as illustrated by Figure 1.1a. For each phase in the converter there are two valves, or arms, each of them made up by N series cascaded submodules, each submodule a low-voltage DC/DC chopper cell with a capacitor. The output voltage of this converter has $N+1$ levels, giving it the ability of providing waveforms that are very close to a sinusoidal. Thus, the required filters at the output are considerably smaller than other VSCs. It also has low dv/dt , given the large number of steps in the AC waveforms, and can achieve high efficiency due to low switching losses.

Each of the N stacked submodules shown in Figure 1.1a, rated for a relatively low voltage, on the order of a couple of kilovolts, provides one either positive or negative step in the AC voltage, which results in a multi-level AC waveform that is very similar to a sinusoidal one. The submodules can be half-bridge or full-bridge, Figure 1.1b, the latter having the ability to operate in all four quadrants, in which both positive and negative voltages can be obtained in the submodule terminals, regardless of current direction [17].

It is widely considered that, for the upcoming need of interconnecting DC and AC grids, as well as the connection of different DC power systems, the MMCs is one of the most important converter technologies, and it's the reason they have been eagerly researched [13], [17]–[19]. The principle of this converter can also be applied to make

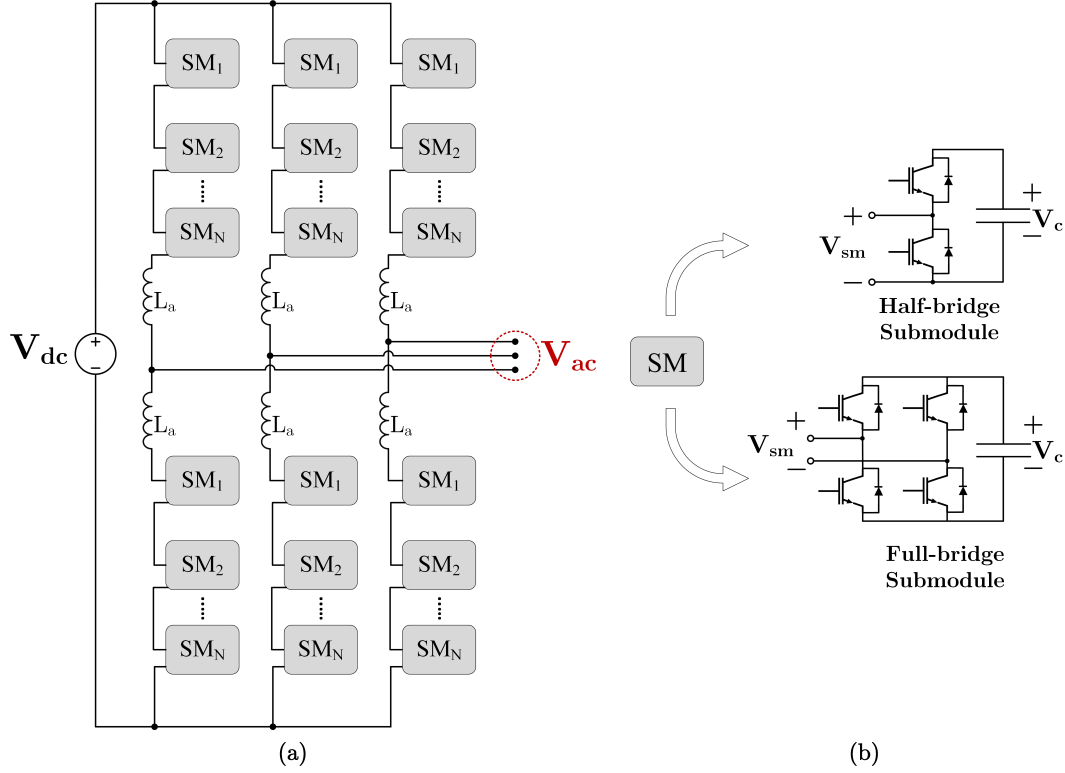


Figure 1.1: Conventional AC/DC MMC (a) three-phase topology, (b) standard submod-ule configurations

DC/DC converters, as will be discussed in the next section, but it is one more of the advantages making the MMC an attractive tool for the future of HVDC transmission.

1.2 MMC Topologies for Future DC and Hybrid AC/DC Power Systems

As previously stated, the MMC is the VSC of choice for HVDC grids. The AC/DC MMC has been well studied and its modelling and behaviour can be found in many papers, e.g., [20]–[24]. The application of the MMC concept to DC/DC conversion is,

on the other hand, much more recent and therefore not as well developed as the former. Several structures using MMCs have been investigated in published works with the objective of DC/DC conversion for use in HVDC. MMC type topologies that offer simultaneous DC/DC and AC/DC conversion have also recently emerged. These “multiport” converters are ideally suited for hybrid AC/DC power systems applications.

1.2.1 DC/DC Converters

One of the first MMC based DC/DC converter topologies proposed for an HVDC network is based on the well-known dual-active-bridge or front-to-front (DAB or F2F) topology [25], which was firstly investigated in the early 2010s [26]. The general topology of this converter is shown in Figure 1.2. As its name indicates, this converter is based on the principle of the dual-active-bridge, where two AC/DC MMCs are coupled through their AC sides by an AC transformer. The name front-to-front is used as a reference to the back-to-back converter configuration [27], in which two AC/DC converters are connected through their DC sides, to make an AC/AC converter. The DAB-MMC converter has been intensively studied, and many works on it can be found where its operation is described and analysed, e.g., [28]–[30]. The basic principle is that the DC power in one of the ports is converted in its totality to AC power, which then goes through voltage conversion in the transformer, then rectified back to DC by the other MMC. It can be seen that this conversion is a two-stage conversion, meaning that this converter will have twice the conduction and switching losses of a one-stage AC/DC conversion process. An advantage, however, is that it will have galvanic separation between the two DC ports. By selecting an appropriate turns ratio in the transformer, both buck and boost operation can be achieved, and since the AC section of the converter is completely internal it’s not bounded by any frequency requirements of the AC grids, nor by its waveform. It also

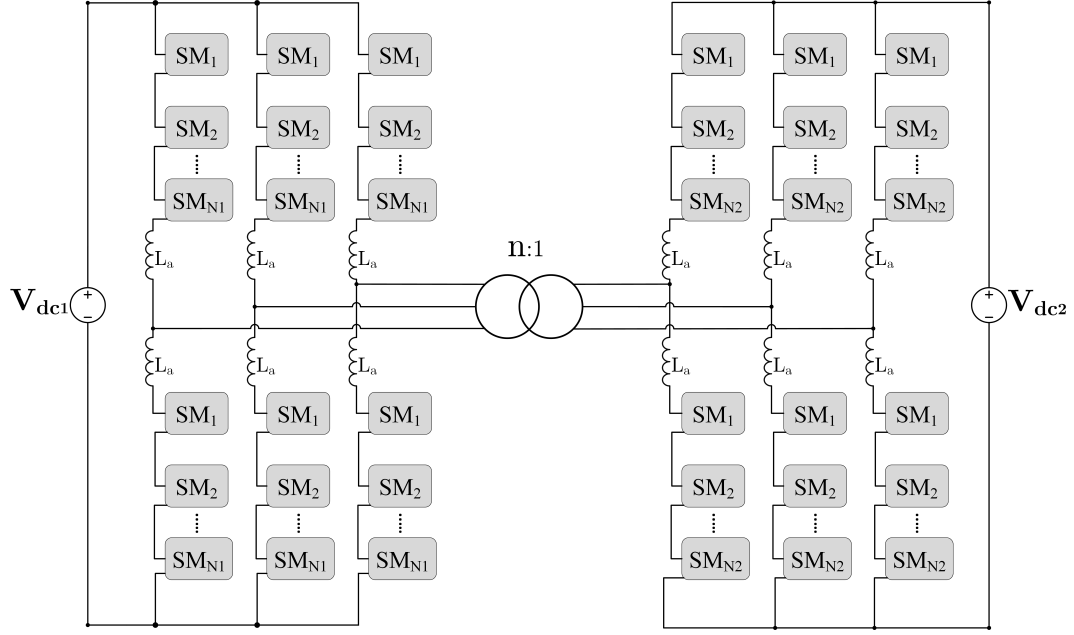


Figure 1.2: DAB (or F2F) MMC

offers bidirectional power flow.

Another topology for DC/DC conversion that uses the AC/DC MMC as a building block is the HVDC autotransformer (HVDC-AT), first introduced in [31] and whose general structure can be seen in Figure 1.3. As shown, the converter consists of two MMCs connected in series on their DC side, and their AC links are coupled together via a transformer. The first DC voltage, V_{dc1} or high-level DC voltage, is formed by the sum of both MMCs' DC voltages, while the second DC voltage, V_{dc2} or low-level DC voltage, is made by the lower MMC's DC voltage. The internal AC link is there to exchange average AC power between the two MMCs for capacitor voltage balancing; this power exchange, however, needs to be only a fraction of the dc power transfer, and therefore the power conversion is less than the full power conversion to be expected from the F2F converter.

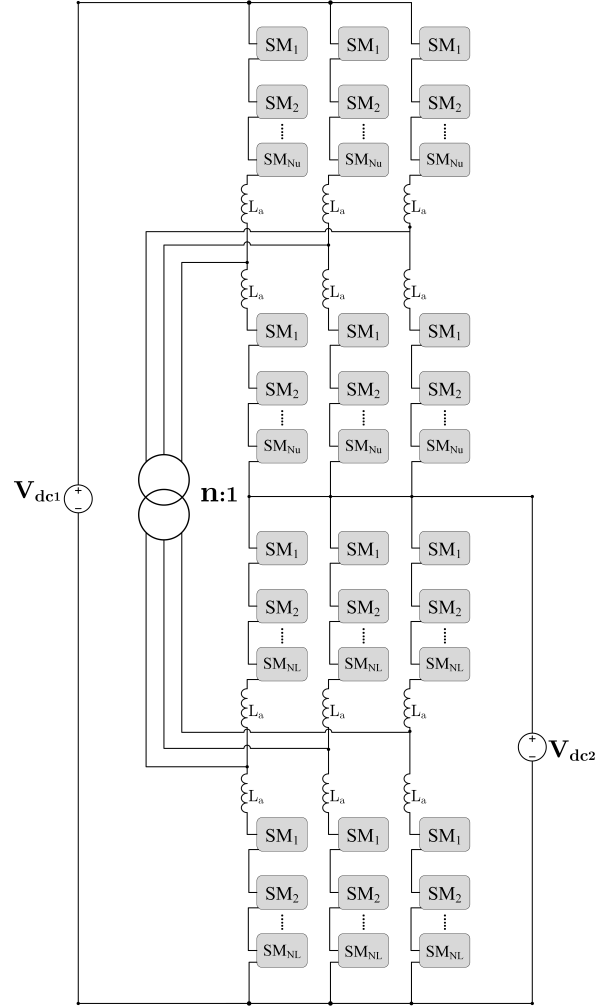


Figure 1.3: HVDC autotransformer [31]

The HVDC autotransformer is therefore a non-isolated partial power processing topology, where

$$P_{ac} = \left(1 - \frac{V_{dc2}}{V_{dc1}}\right) \cdot P_{dc} \quad (1.1)$$

is the power processed by the AC transformer. This converter is suitable for DC/DC applications in HVDC grids, while offering significant potential savings in capital cost

and losses relative to the F2F MMC; however, it does not provide galvanic separation, and DC fault blocking requires full-bridge submodules in the upper MMC [32].

In [33], a non-isolated DC/DC structure called tuned filter modular multilevel dc converter (TF-MMDCC) is proposed in which the power balance between the phase arms is maintained by a secondary power loop. The topology, shown in Figure 1.4, was also proposed by other research groups around the same time [34], [35] and is now commonly referred to as the Modular Multilevel DC Converter (M2DC). This converter bears structural similarity with the conventional MMC AC/DC converter, but requires an added filter in its output that has the purpose of blocking AC currents from going through to the second DC side. Internally circulating AC currents are needed to balance the capacitor voltages as in the case of the HVDC-AT, but without the use of an AC transformer. The filter can be implemented in different ways, including magnetics, passives, and active filtering. The magnetics solution is shown in Figure 1.4, where a zig-zag transformer is used. In [36] it is specified that the M2DC's intention is to work as a step-down, or a *buck*, converter. The M2DC can be used in a symmetrical monopole structure and employ the use of full-bridge submodules (FBSM) to achieve both step-up and step-down operation, known as buck-boost operation, and also to provide DC fault blocking [37]. Similar to the HVDC-AT, the M2DC is a non-isolated partial power processing topology where the amount of internal AC power processing is shown in Equation (1.1). A comparison between the mentioned converters (F2F, HVDC-AT, and M2DC) can be seen in [18], and a comprehensive overview of other non-isolated MMC-based DC/DC converters that share commonalities with the HVDC-AT and M2DC can be found in [19].

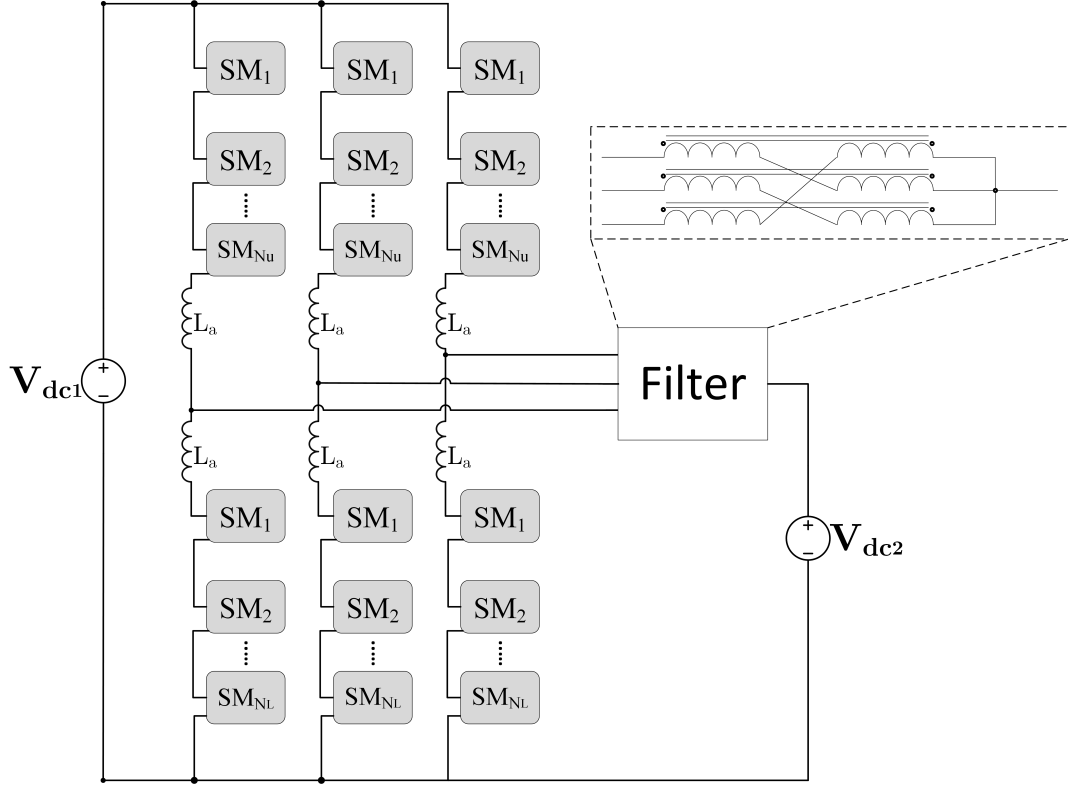


Figure 1.4: M2DC [33]–[35] with magnetics solution for the filter

1.2.2 DC/DC/AC Converters

All of the DC/DC converters described in Section 1.2.1 use internal AC currents to shuttle average AC power between arms for the purpose of capacitor power balancing. This suggests the potential to “tap” into this AC circuit for enabling power exchange with a local AC grid. i.e., to add an AC port to the existing DC/DC MMCs. The F2F and the HVDC-AT already have a transformer that, by adding windings, could be used to interconnect an AC grid [32], shown in Figure 1.5a and 1.5b, respectively. Of course, the price paid is increased transformer size and design complexity. The M2DC can also be endowed with an AC port, as shown in Figure 1.5c, where a transformer is added in

parallel with the filter block [36].

Patent [38] describes an M2DC where the AC port is instead taken at the converter midpoint. In [39], a delta/zig-zag transformer is used to combine the AC transformer and filter for the M2DC in Figure 1.5c. The resulting compact DC/DC/AC M2DC structure is shown in Figure 1.5d, where the total MVA rating of the delta/zig-zag transformer is less than the total MVA rating of all magnetics in Figure 1.5c. In [40], a generalised DC/DC/AC structure using a centre-tapped transformer is presented, that gives rise to two new topologies that could be used in future hybrid AC/DC power systems. The generalised topology is shown in Figure 1.5e, where three DC ports, d1-d3, can be used to connect to either a bipolar DC grid or two different DC grids. The control of these topologies allows for independent exchange of power between its DC and AC ports, and the state-space model is provided in [40]. In [41], four different multiport DC/DC/AC MMCs are presented; these include the three topologies in Figure 1.5a - 1.5c, and a fourth new topology, shown here in Figure 1.5f, which is equivalent to the buck-boost MMC in [42] with a transformer added for AC grid interconnection.

1.2.3 Availability of Analytical Models

For the study of new converter topologies, the mathematical modelling is a very useful tool; it allows for the creation of well-tuned controls to be made and permits the evaluation of the topology without having to resort to building a physical model. The conventional DC/AC MMC has been well studied, and has models and controls made for them that can be found in the literature, e.g. [20]–[24]. Since the HVDC DC/DC converters in Section 1.2.1 and the multiport DC/DC/AC MMCs in Section 1.2.2 are relatively new, little literature regarding their modelling and control is available.

When a converter is modelled, there is usually the question of how detailed the mod-

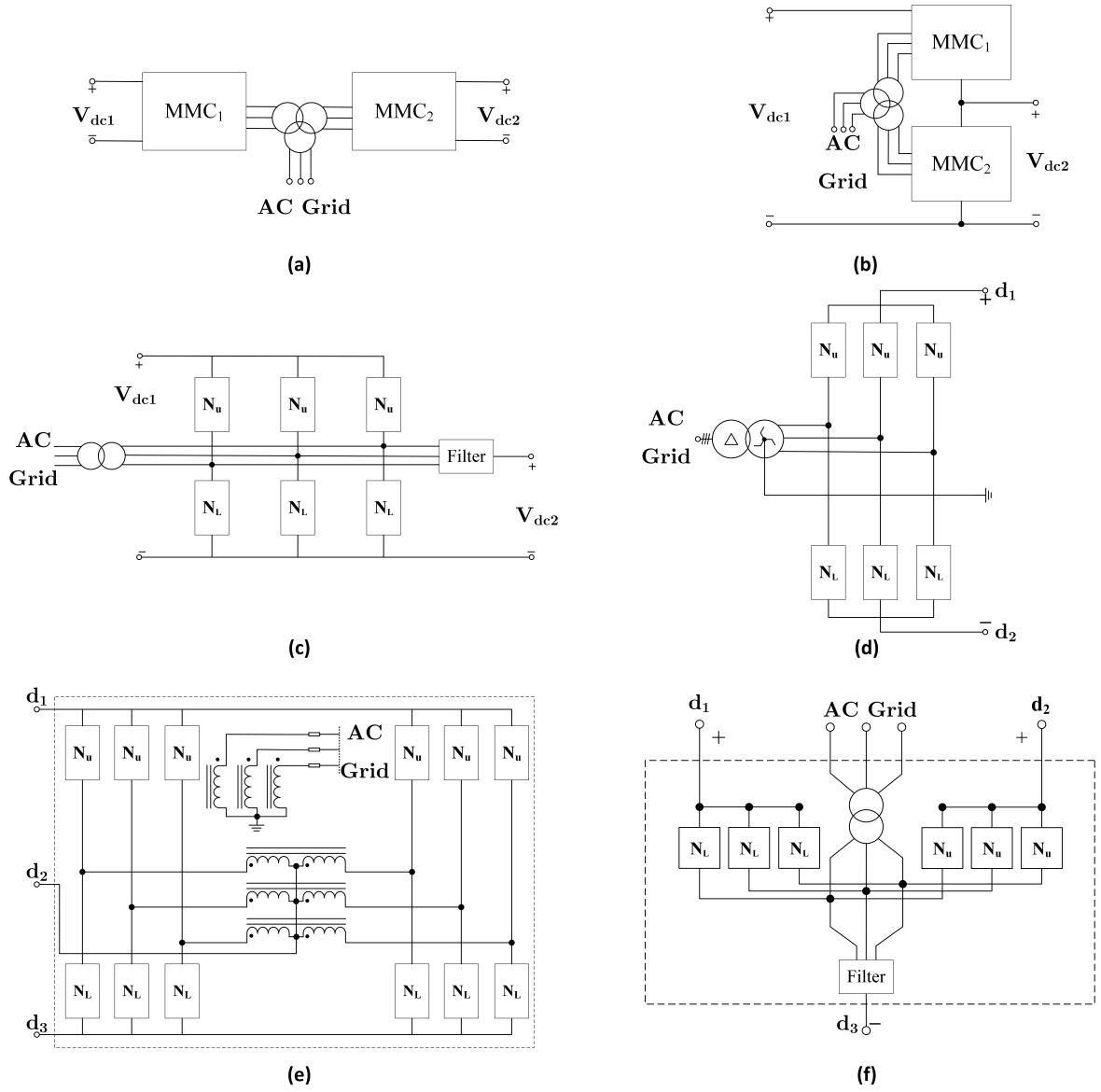


Figure 1.5: Examples of three-phase DC/DC/AC MMCs; (a) based on F2F MMC, (b) based on HVDC-AT [32], (c) based on M2DC [36], (d) Bipolar MMC with delta/zig-zag transformer [39], (e) Generalised DC/DC/AC chain-link structure [40], (f) multiport buck-boost converter [41]

elling will be, and this usually brings into question how much of the electronic components, namely switches, are to be included. Figure 1.6 [43] shows a depiction of different types of modelling accuracy that can be employed during the modelling of a converter, depending on the type of study. Making a fully detailed model, i.e. modelling every single semiconductor in the converter, would ideally be the best for all types of studies, since it would provide a completely faithful representation of the converter; nevertheless, this model would be very complex and computationally challenging even for a two or three level VSC. For an MMC, which has a much higher number of components, and therefore nodes in the admittance matrix, it would be very difficult if not impossible. Detailed equivalent models and switching function models still take into account the switching of the components, but do not model each submodule individually; these models are useful for electromagnetic transient studies and fault analyses [44]–[48]. An averaged model is made by replacing the semiconductors in a model with an equivalent controlled voltage or current source. The averaged model will naturally lose the information on individual switching cells, as well as the influence of diodes, and neglect the high order switching harmonics. However, it is a very good for accelerated simulations, controller design, and as a basis for creating a state space dynamic model [49]–[51]. In [52], a detailed explanation can be found regarding the modelling of DC/DC MMCs. This includes the large-signal dynamic model, and it is a good example of a full detailed model. Another example of modelling of DC/DC MMCs can be found in [53], where the averaged and the switched converter models of a single string of a DC-MMC are compared.

A very useful technique when modelling converters is the dynamic phasor model, first introduced for power electronic applications in [54] and more formally referred to as generalised averaging method. For linear control design and eigenvalue analysis, a linear time-invariant model is required; however, often, the averaged model of an MMC converter will have time-varying state variables at steady-state. This is because of the

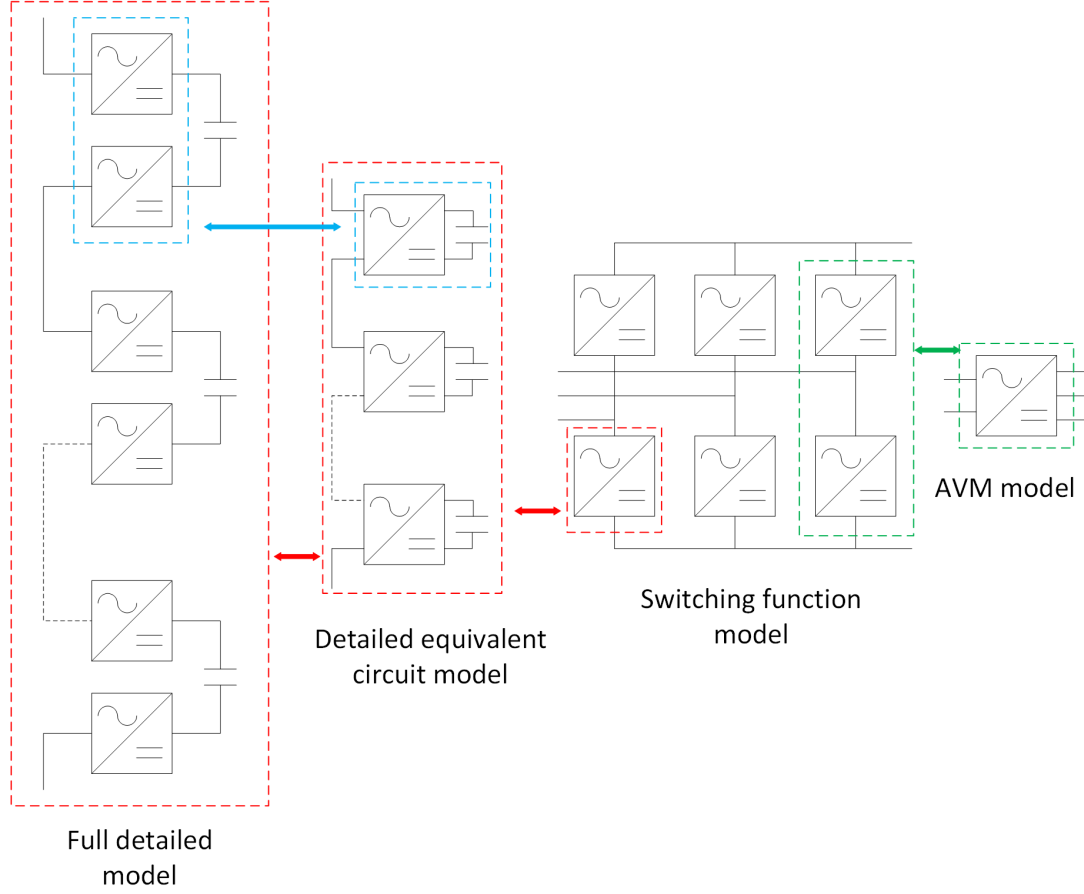


Figure 1.6: Different detail in models for converters [43]

existence of multiple frequency components in the converter. To tackle this, the concept of dynamic phasors can be used, in which the time-varying waveform is to be approximated with the coefficients from a Fourier series expansion. In other words, the sinusoidal quantities can be represented with phasors that are allowed to change over time. This becomes useful since in steady-state the equations that represent the converter dynamics will become time-invariant [55]. To illustrate, Figure 1.7a shows a simple RL circuit connected to an AC voltage source, with a switch that closes at $t=0.02$ seconds. Figure 1.7b shows two plots: the upper plot shows the time domain current $i(t)$; the lower plot shows

three current components that correspond to the dynamic phasor model of $i(t)$. The DC component, solid plot, can be seen overshooting after the switch closes, then converging to zero. The dashed and dotted plots show the AC fundamental components of $i(t)$ broken into cosine and sine components with amplitudes $X(t)$ and $Y(t)$, respectively, [56]. Observe the three states in the dynamic phasor model of $i(t)$ become DC valued (i.e., time-invariant) at steady-state. If the $X(t)$ and $Y(t)$ plots were to be multiplied by $\cos(\omega t)$ and $\sin(\omega t)$, respectively, and summed with the DC component, the resulting waveform would be $i(t)$. This method is widely used in converter analysis, for it provides very useful information of the converter operation and permits a more detailed control design than the conventional time averaged model. This modelling technique has been recently adopted in MMC studies [57]–[61].

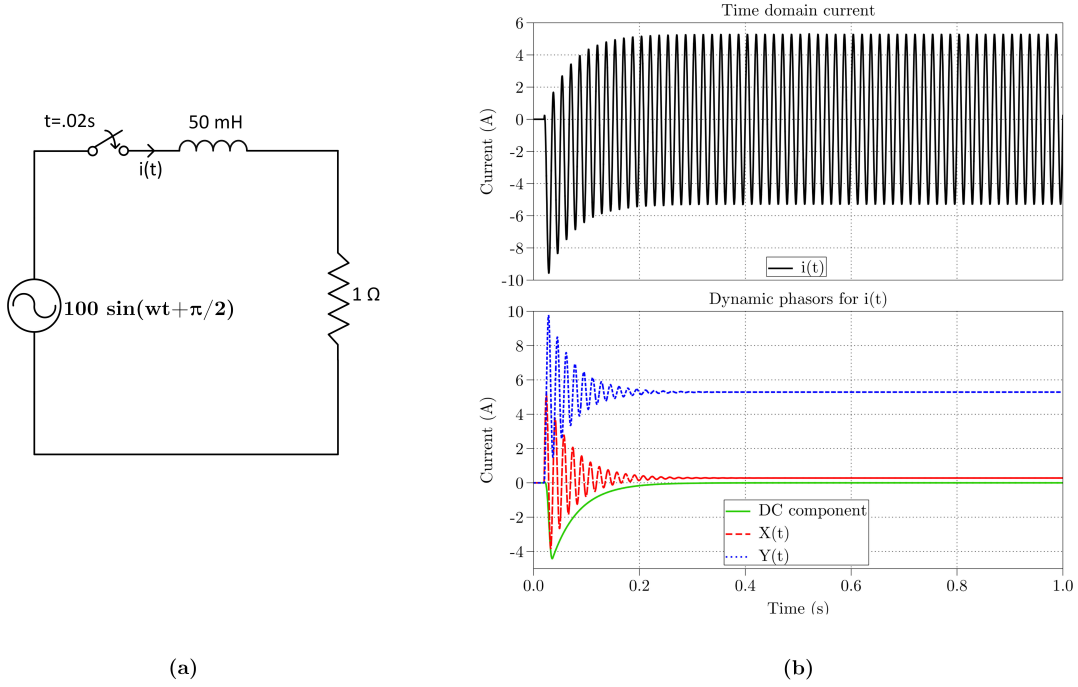


Figure 1.7: Dynamic phasors visualisation using series RL circuit

1.3 Thesis Scope

The most recent research in power systems suggests that interconnecting different DC and AC systems is to be a very important part of the future. However, at present, little work has been invested towards the development of analytical models for newest types of DC/DC/AC converters using MMC technology. This thesis aims to fill this gap.

This thesis first develops a time averaged dynamic model of a single-phase generalised DC/DC/AC MMC structure. A three-phase model is then synthesised from the single-phase model. A dynamic phasor model that includes multiple harmonic components is then developed from the state-space representation of the three-phase model, in which the state variables are time-invariant at steady-state. From this one model, four different

converter models are derived, two of which are DC/DC/AC, and two are DC/DC. Solution procedures, to solve for the input variables required for different operating points, are then developed for each converter. Using these solution procedures, steady-state analysis for each converter, in different operating points, are carried out.

Chapter 2

Power Transfer Mechanisms of DC/DC and Multiport DC/DC/AC MMCs

In this chapter a summary of the operation principles for the conventional DC/AC MMC, the DC/DC MMC, and the multiport DC/DC/AC MMC will be presented. The power transfer mechanisms for each of these topologies are also discussed.

For the purposes of this chapter only the steady-state operation of the converters is considered. Other assumptions employed in this chapter are: (I) The converter components are assumed to be ideal and lossless, by which the input power equals the output power, (II) The number of submodules employed in every converter is large enough to guarantee ideal sinusoidal waveforms, (III) The voltage sort and selection algorithm [22], [62] is used to balance the voltage in the capacitors within each arm, (IV) Only DC and fundamental frequency AC components are considered.

2.1 Conventional AC/DC MMC

As stated in Chapter 1, many studies on the conventional AC/DC MMC have been carried out and its operation is well understood [20]–[24], [43], [63], [64]. Here a brief overview of the principle of operation of the AC/DC MMC is presented.

Figure 2.1a shows the conventional single-phase AC/DC MMC structure, where the upper and lower arms can be seen comprising the leg of the converter. Correspondingly, each arm has a designated current, i_u and i_l , while the current that goes into the leg from the DC source is termed I_{dc} and the current that goes to the AC system is named i_s . To describe how the submodules are able to produce the different voltage levels that compose the AC voltage, the half-bridge submodule operation is described. The half-bridge submodule consists of two IGBTs, each of them with an antiparallel diode, and one capacitor. The two semiconductors are operated in a complementary manner, which is to say, when one has a gating signal on 1(ON), the other one has a 0(OFF). This entails that, for a half-bridge submodule, there are four useful switching states Figure 2.1b shows these four states of the submodule, while Table 2.1 provides an explanation of what happens in each of them. To form the AC voltage waveform, the capacitor on each submodule can either be inserted (S_1, S_3) or bypassed (S_2, S_4). The resulting waveform for each submodule can be seen as having two levels, and by stacking hundreds of them the many levels of the MMC can be achieved. It is also clear that the voltage provided by the submodule can only be positive, the direction of the current i_{SM} notwithstanding.

While the number of capacitors to be inserted in the upper and lower arms is specified by the modulation technique, such as space vector modulation, multicarrier sinusoidal pulse-width modulation, and nearest level modulation, determining which capacitors from each arm to be inserted is also something that needs to be addressed. Given

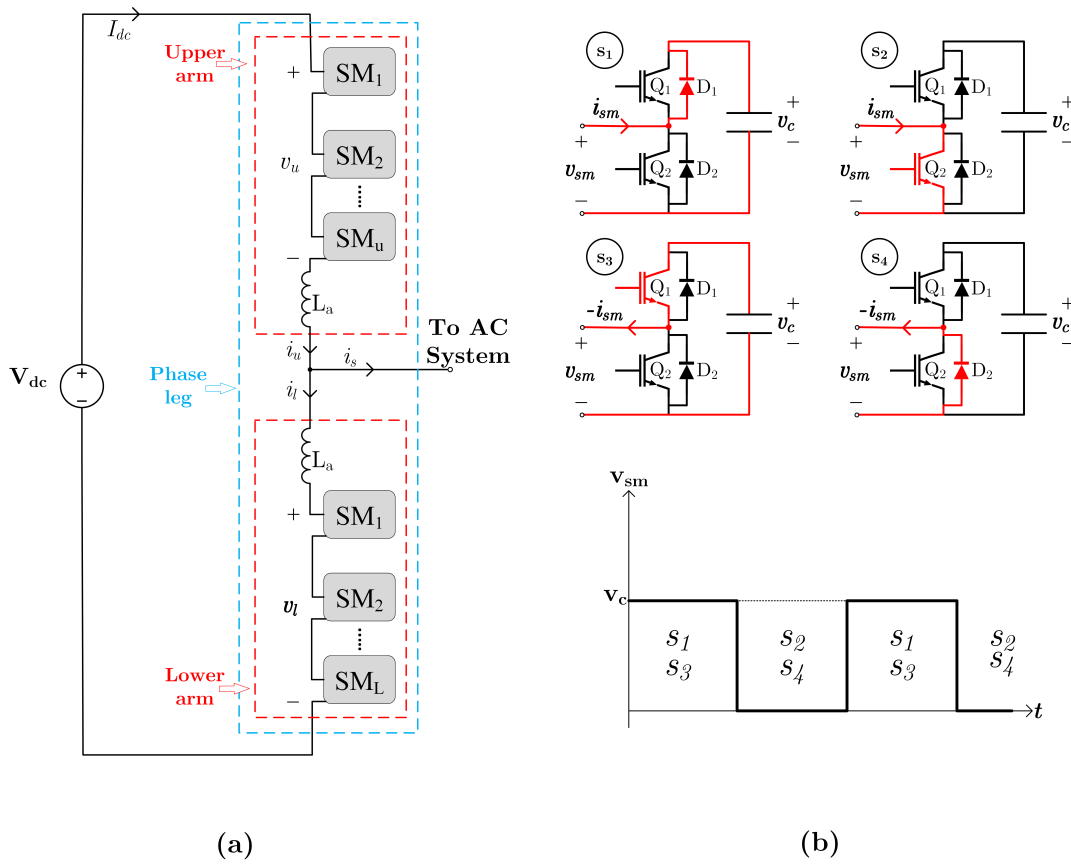


Figure 2.1: (a) single-phase DC/AC MMC, (b) useful switching states of half-bridge submodule and waveform produced by each state

Table 2.1: Practical switching states of the half-bridge submodule

States in Figure 2.1b	Capacitor State	D_1	D_2	i_{SM} flows through	v_{SM}
$S_1(+i_{SM})$	Inserted	1	0	D_1	$+v_c$
$S_2(+i_{SM})$	Bypassed	0	1	Q_2	0
$S_3(-i_{SM})$	Inserted	1	0	Q_1	$+v_c$
$S_4(-i_{SM})$	Bypassed	0	1	D_2	0

that there could potentially be hundreds of capacitors in each arm, these capacitors will change their voltage depending on which are inserted and the direction of current into

the capacitor. Since the goal is to maintain the capacitor's voltage as close to their rated value $\frac{V_{dc}}{N}$, there is the need for active balancing via control. Many techniques have been proposed for the balancing of the capacitor's voltage, although the most common is called "sort and selection algorithm" [22], [23], [65]. In this method the voltage of each capacitor is measured and then a sorting takes place which makes an order of the capacitors that will be inserted depending on the direction of the arm current.

The arm voltages in the MMC of Figure 2.1a can be described as:

$$v_u(t) = \frac{V_{dc}}{2} + \hat{V} \cos(\omega t), \quad (2.1)$$

$$v_l(t) = \frac{V_{dc}}{2} - \hat{V} \cos(\omega t), \quad (2.2)$$

where \hat{V} is the peak magnitude fundamental frequency voltage, which assuming the use of half-bridge submodules can take values between 0 and $\frac{V_{dc}}{2}$. Accordingly, the arms' currents are:

$$i_u(t) = I_{dc} + \frac{\hat{I}}{2} \cos(\omega t + \theta_i) \quad (2.3)$$

$$i_l(t) = I_{dc} - \frac{\hat{I}}{2} \cos(\omega t + \theta_i) \quad (2.4)$$

$$i_s(t) = I \cos(\omega t + \theta_i) \quad (2.5)$$

where \hat{I} is the peak magnitude fundamental frequency current.

In the analysis of MMCs, a common practice is to map the voltages and currents of the MMC into a coordinate system which decouples the terms that relate to the external AC system and the internal MMC quantities, and by doing so, separates the DC

and fundamental frequency components. This system is called sum-difference or “ $\Sigma\Delta$ ” coordinate system [62], [66]. After being transformed to this new domain, the voltages and currents can be referred to as the ones that are common to both arms (Σ) and the ones that are differential to each arm (Δ). The current and voltage transformation of the quantities Equations (2.1) to (2.4) for the single-phase MMC in Figure 2.1a are defined as:

$$\begin{bmatrix} i_{\Sigma} \\ i_{\Delta} \\ v_{\Sigma} \\ v_{\Delta} \end{bmatrix} = \begin{bmatrix} \frac{1}{2} & \frac{1}{2} & 0 & 0 \\ 1 & -1 & 0 & 0 \\ 0 & 0 & \frac{1}{2} & \frac{1}{2} \\ 0 & 0 & \frac{1}{2} & -\frac{1}{2} \end{bmatrix} \begin{bmatrix} i_u \\ i_l \\ v_u \\ v_l \end{bmatrix}. \quad (2.6)$$

The $\Sigma\Delta$ domain parameters in Equation (2.6) are illustrated in Figure 2.2. For the single-phase MMC, the abstract $\Sigma\Delta$ quantities ideally consist of DC and fundamental frequency components as follows:

$$i_{\Sigma} = I_{dc} \quad (2.7)$$

$$v_{\Sigma} = \frac{V_{dc}}{2} \quad (2.8)$$

$$i_{\Delta} = \hat{I}_{\Delta} \cos(\omega t + \theta_{i_{\Delta}}) \quad (2.9)$$

$$v_{\Delta} = \hat{V}_{\Delta} \cos(\omega t). \quad (2.10)$$

As noted by Equations (2.7) to (2.10) and Figure 2.2, the Σ terms are both common to both arms and DC quantities, whereas the Δ terms are differential to both arms and AC fundamental frequency quantities.

The $\Sigma\Delta$ reference frame is also useful for examining the DC/AC conversion process.

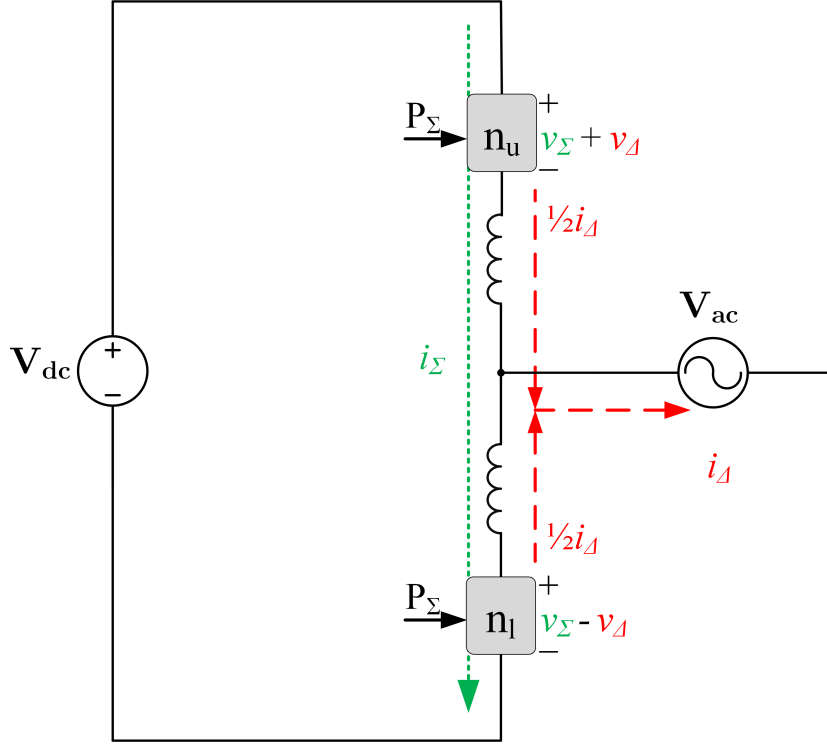


Figure 2.2: $\Sigma\Delta$ transformation of the single-phase MMC, where the quantities from Equations (2.1) to (2.4) are transformed through Equation (2.6). The dotted, green terms represent DC quantities and dashed, red terms represent fundamental frequency components

For the conventional AC/DC MMC, the average power absorbed by each arm can be calculated as follows:

$$P_u = \frac{1}{T} \int_0^T (v_\Sigma + v_\Delta) \left(i_\Sigma + \frac{\hat{I}_\Delta}{2} \right) dt = \frac{V_{dc} I_{dc}}{2} + \frac{\hat{V}_\Delta \hat{I}_\Delta}{4} \cos(\theta_{i_\Delta}) \quad (2.11)$$

$$P_l = \frac{1}{T} \int_0^T (v_\Sigma - v_\Delta) \left(i_\Sigma - \frac{\hat{I}_\Delta}{2} \right) dt = \frac{V_{dc} I_{dc}}{2} + \frac{\hat{V}_\Delta \hat{I}_\Delta}{4} \cos(\theta_{i_\Delta}). \quad (2.12)$$

Since the arms have only capacitive energy storage, at steady-state $P_u=P_l=0$, therefore:

$$P_u = P_l \Rightarrow \frac{V_{dc}I_{dc}}{2} = -\frac{\hat{V}_\Delta \hat{I}_\Delta}{4} \cos(\theta_{i_\Delta}). \quad (2.13)$$

Thus

$$P_{dc} = -P_{ac} \quad (2.14)$$

where

$$P_{dc} \triangleq V_{dc}I_{dc} \quad (2.15)$$

$$P_{ac} = P_{grid} \triangleq \frac{\hat{V}_\Delta \hat{I}_\Delta}{4} \cos(\theta_{i_\Delta}). \quad (2.16)$$

Equation (2.14) represents the arms power balance requirement for a single-phase AC/DC MMC. This implies that, assuming the grid is absorbing power, the arms inject average power of $\frac{P_{dc}}{2}$ per arm to the AC systems via the modulated AC quantities. It is also worth noting that both arms process the same amount of power, splitting the full input DC power between them. Thus, in the $\Sigma\Delta$ domain, the AC/DC power transfer mechanism is purely a common mode (Σ) component, as shown in Figure 2.2.

$$P_\Sigma = \frac{-P_{ac}}{2} \quad (2.17)$$

$$P_\Delta = 0. \quad (2.18)$$

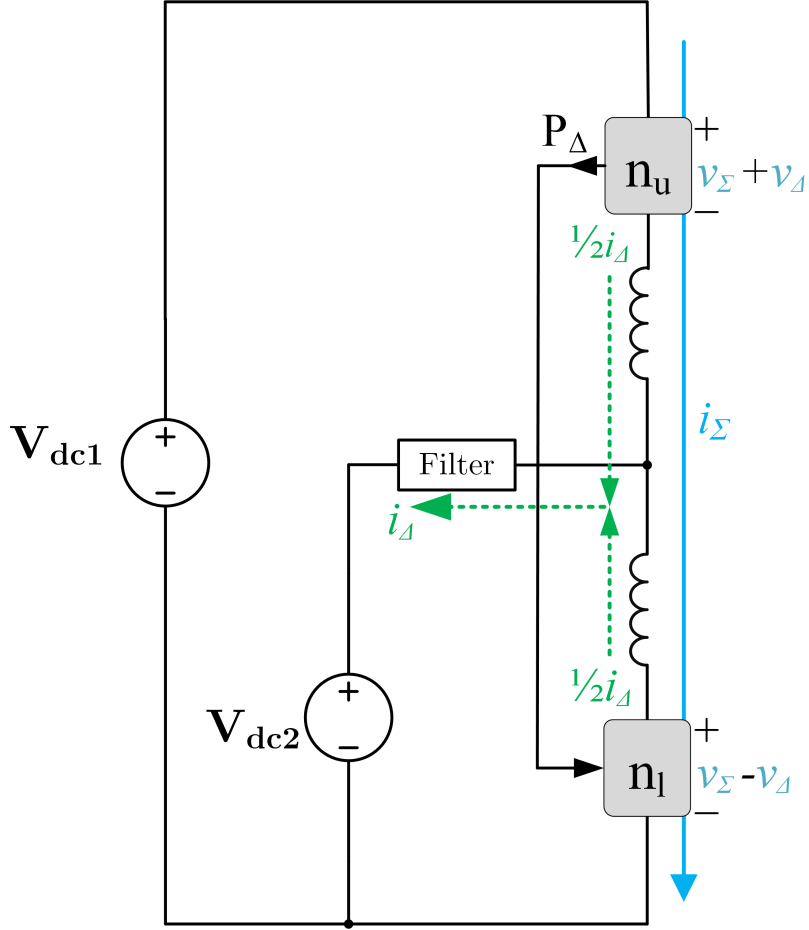


Figure 2.3: M2DC with $\Sigma\Delta$ currents and voltages, where dotted, green terms represent DC quantities and solid, blue terms represent a combination of DC and AC quantities

2.2 DC/DC MMC

The M2DC, described comprehensively in [33], [67]–[69], is a DC/DC MMC that can transfer power between two DC systems. Figure 2.3 illustrates the currents, voltages, and average power exchange between arms of the M2DC. The AC quantities synthesised in the arms do not exit through the midpoint of the converter, where a filter prevents anything but DC quantities from reaching the second voltage source, but are used to exchange

average AC power between the upper and lower arms to maintain power balance of the submodule capacitors. The DC step ratio G_v is used to indicate the voltage ratio between the two DC sources as

$$G_v = \frac{V_{dc2}}{V_{dc1}}, \quad (2.19)$$

and can take values from 0 to 1 for step-down operation. The $\Sigma\Delta$ quantities in Figure 2.3 ideally consist of DC and fundamental frequency components as follows:

$$i_\Sigma = \left(1 - \frac{1}{2G_v}\right) I_{dc} + \hat{I}_\Sigma \cos(\omega t + \theta_{i_\Sigma}) \quad (2.20)$$

$$v_\Sigma = \frac{V_{dc1}}{2} + \hat{V}_\Sigma \cos(\omega t + \theta_{v_\Sigma}) \quad (2.21)$$

$$i_\Delta = \frac{I_{dc}}{G_v} \quad (2.22)$$

$$V_\Delta = \left(\frac{1}{2} - G_v\right) V_{dc1} + \hat{V}_\Delta \cos(\omega t) \quad (2.23)$$

From Equation (2.20) it can be seen that, for the M2DC, i_Σ now has both AC and DC components, while in the conventional MMC (see Equation (2.7)) it was only DC. This is because the AC quantities no longer exit through the middle point. However, it can also be seen that i_Σ is purely AC at the step ratio of $G_v=0.5$. Equations (2.21) and (2.23) show that the arms' voltages have both Σ and Δ terms are comprised of DC and AC components. The ratio G_v , as in the case of the currents, sets how the DC voltage is split between the terms.

To maintain steady-state power balance for the submodules' capacitors, the M2DC's arms have to exchange average power between them.

Assuming $\hat{V}_\Delta \gg \hat{V}_\Sigma^1$, the average power absorbed by the upper and lower arms can be calculated as follows:

$$P_u = \frac{1}{T} \int_0^T (v_\Sigma + v_\Delta)(i_\Sigma + i_\Delta) dt = (1 - G_v) V_{dc1} I_{dc} + \frac{\hat{V}_\Delta \hat{I}_\Sigma}{2} \cos(\theta_{i\Sigma}) \quad (2.24)$$

$$P_l = \frac{1}{T} \int_0^T (v_\Sigma - v_\Delta)(i_\Sigma - i_\Delta) dt = -(1 - G_v) V_{dc1} I_{dc} - \frac{\hat{V}_\Delta \hat{I}_\Sigma}{2} \cos(\theta_{i\Sigma}). \quad (2.25)$$

From Equations (2.24) and (2.25), it can be observed that $P_u = -P_l$. This indicates that average AC power in one arm has to be shuttled to the other arm in order to maintain submodule capacitor power balance. Since the arms have only capacitive energy storage, at steady-state $P_u = P_l = 0$, therefore:

$$(1 - G_v) V_{dc1} I_{dc} = -\frac{\hat{V}_\Delta \hat{I}_\Sigma}{2} \cos(\theta_{i\Sigma}). \quad (2.26)$$

Thus, by defining:

$$P_{dc} \triangleq V_{dc1} I_{dc} \quad (2.27)$$

$$P_{ac} \triangleq -\frac{\hat{V}_\Delta \hat{I}_\Sigma}{2} \cos(\theta_{i\Sigma}), \quad (2.28)$$

we have:

$$(1 - G_v) P_{dc} = P_{ac}. \quad (2.29)$$

¹This assumption is valid for small arm choke impedances

Equation (2.29) represents the arms power balance requirement for the M2DC. Since this power is now differential mode to the arms in a single leg, P_{Δ} now exists in Figure 2.3, when it didn't in the conventional AC/DC MMC. No common mode power exists for this converter, therefore:

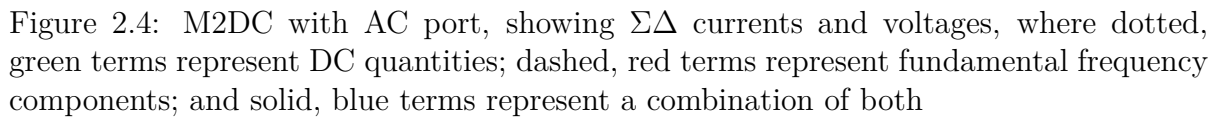
$$P_{\Sigma} = 0 \quad (2.30)$$

$$P_{\Delta} = (1 - G_v)P_{dc} \quad (2.31)$$

These equations are in contrast to Equations (2.17) and (2.18) for the AC/DC MMC.

2.3 DC/DC/AC MMC

As mentioned in Chapter 1, the M2DC can be adapted to include an AC port [36], [38], and several such topological variations can be found in the literature [39]–[41]. This converter fulfils the energy conversion objectives of the two converters presented in Sections 2.1 and 2.2 simultaneously. Because of this, its behaviour is also described as a simultaneous behaviour of those two. Figure 2.4 illustrates how these powers, currents, and voltages would look for a single-phase M2DC with an AC port. As it can be expected, the voltages and currents present in this converter are a combination of the quantities present in the AC/DC and DC/DC converters in Figures 2.2 and 2.3, and can be defined as:



$$V_{\Delta} = \left(\frac{1}{2} - G_v\right) V_{dc1} + \hat{V} \cos(\omega t). \quad (2.35)$$

28

them. For these reasons, the M2DC with an AC port requires simultaneous existence of P_Σ and P_Δ terms:

$$P_\Sigma = -\frac{P_{ac}}{2} \quad (2.36)$$

$$P_\Delta = (1 - G_v)P_{dc}. \quad (2.37)$$

Table 2.2: Currents' harmonic components and power transfer mechanisms for each of the conversion cases

Current	AC/DC	DC/DC	DC/DC/AC
i_Σ	DC	AC + DC*	AC + DC
i_Δ	AC	DC	DC + AC
Average Power	AC/DC	DC/DC	DC/DC/AC
P_Σ	$\hat{V}_\Delta, \hat{I}_\Delta$	-	$\hat{V}_\Delta, \hat{I}_\Delta$
P_Δ	-	$\hat{V}_\Delta, \hat{I}_\Sigma$	$\hat{V}_\Delta, \hat{I}_\Sigma$

*Exists when $G_v \neq 0.5$

Table 2.2 summarises the harmonic components of i_Σ and i_Δ present in AC/DC, DC/DC, and combined DC/DC/AC conversion. It also shows the arms' average powers, P_Σ and P_Δ , present in each conversion, and their constituent harmonic components. Each of the currents fulfils a role in each of the conversion cases. Since i_Δ represents the current that exits through the midpoint in all cases, this current regulates external power injection in all cases, whether it be real and reactive power injection to the grid when AC conversion is present, or DC power when DC/DC conversion is being performed.

2.4 Regulation of Capacitor Voltage and External Network Power Injections

Regulating the capacitor voltages of the upper and lower arms is an objective that must be accomplished by the converter, as briefly mentioned in Section 2.1. This can be accomplished by appropriate control of i_Σ . For this purpose, the targets of this regulation are defined as:

$$\Sigma V_{cap,\Sigma} = \frac{1}{2}\Sigma V_{cap,upper} + \frac{1}{2}\Sigma V_{cap,lower} \quad (2.38)$$

$$\Sigma V_{cap,\Delta} = \frac{1}{2}\Sigma V_{cap,upper} - \frac{1}{2}\Sigma V_{cap,lower}, \quad (2.39)$$

where $\Sigma V_{cap,upper}$ and $\Sigma V_{cap,lower}$ represent the sum of the submodule capacitor voltages for the upper and lower arms, respectively.

In the case of AC/DC conversion, the objective is to regulate $\Sigma V_{cap,\Sigma}$, by means of the DC component of i_Σ . When DC/DC conversion is present, $\Sigma V_{cap,\Delta}$ is to be regulated by the fundamental frequency component of i_Σ . It can be noted that the role of either the DC or the fundamental frequency component of the currents in the AC/DC conversion is fulfilled by the other component in the DC/DC conversion. E.g. the regulation of $\Sigma V_{cap,\Sigma}$ is fulfilled by the DC component of i_Σ in the AC/DC conversion, and the equivalent task in DC/DC conversion, the regulation of $\Sigma V_{cap,\Delta}$, is realised by the fundamental frequency component of i_Σ . The same symmetry occurs with the power injections to the external DC and AC grids. Table 2.3 summarises these points, where the superscript indicates with “dc” or a “1” if the component is the DC or the fundamental frequency component, respectively.

Table 2.3: Currents' harmonic components and powers for each of the conversion cases

Regulation Objective	AC/DC	DC/DC	DC/DC/AC
P_{grid}, Q_{grid}	i_{Δ}^1	-	i_{Δ}^1
P_{dc}	-	i_{Δ}^{dc}	i_{Δ}^{dc}
$\Sigma V_{cap,\Sigma}$	i_{Σ}^{dc}	-	i_{Σ}^{dc}
$\Sigma V_{cap,\Delta}$	-	i_{Σ}^1	i_{Σ}^1

2.5 Multiport MMC Structure for Simultaneous DC/ DC/ AC Conversion

This thesis is focused on simultaneous DC/DC and AC/DC conversion using MMCs, a topic of emerging interest for the future of power systems. For this purpose, the modelling of a converter that can interconnect two DC ports and an AC port, akin to the structure presented in Figure 2.4 is the first objective in this work. On the early stages of this enterprise it became clear that a single unified model could be applied to four different converter structures. Figure 2.5 illustrates these four topologies; two of them are for DC/DC/AC conversion, and two are for DC/DC conversion. Figure 2.5a and 2.5c are three-phase topologies with two DC ports and one AC port, suitable for DC/DC/AC conversion and termed multiport DC/DC/AC (MP-DCDCAC) and bipolar DC/DC/AC (BP-DCDCAC) converters, respectively. Figure 2.5b and 2.5d are two DC/DC converter topologies that result from removing the AC port from the aforementioned structures, and are called multiport DC/DC (MP-DCDC) and bipolar DC/DC (BP-DCDC) converters, respectively.

As it can be seen in Figure 2.5, the four topologies all use the exact same base converter structure, marked by a dotted square, which allows the use of the same unified

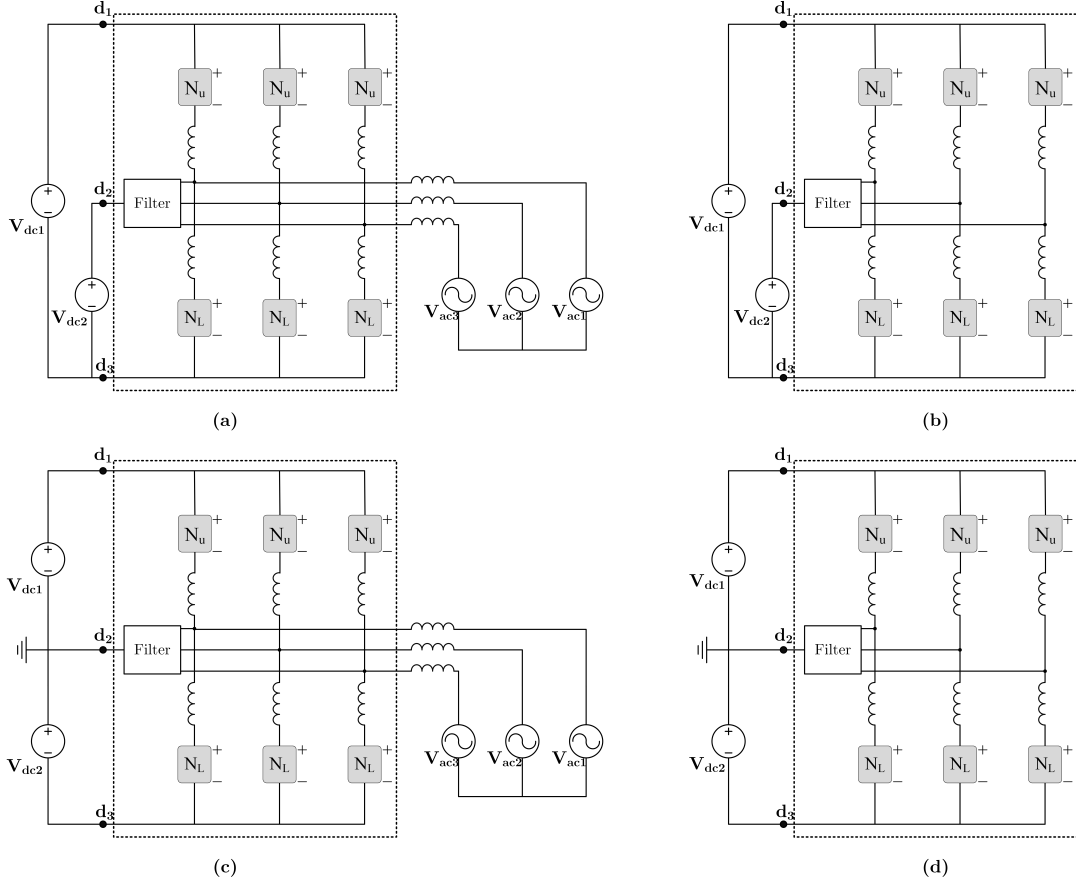


Figure 2.5: MMC topologies under study in this thesis: (a) MP-DCDCAC, (b) MP-DCDC, (c) BP-DCDCAC, (d) BP-DCDC

base model for all of them by only redefining the voltages in the DC ports (d_1 - d_3) and redefining the external AC grid connections. This can easily be done in the model with minimal changes. The base structure identified in Figure 2.5 is the primary point of interest of the next chapter, in which a unified mathematical model is obtained for it.

Chapter 3

Converter Dynamic Modelling

In this chapter, a generalised time-averaged three-phase dynamic model for the four converter structures firstly identified in Figure 2.5 and now shown here in Figure 3.1a, is developed. This process is carried out starting with a single-phase leg model and progresses to a complete three phase model for a representative converter structure. From this benchmark model, a multi-harmonic dynamic phasor model (DPM) is the derived. The model derivation is carried out using the MP-DCDCAC structure, Figure 3.1b, as the base topology to obtain the unified model that is later used to simulate all four converter structures shown in Figure 3.1. The validation of the developed models is carried out using a combination of PLECS, a time-domain software for power electronics circuits simulation, and SIMULINK, a MATLAB-based graphical programming environment.

3.1 Time-Averaged Model

This section presents the process of developing a three-phase unified model in the $\alpha\beta 0$ reference frame that represents the general structure of Figure 3.1a. This process is

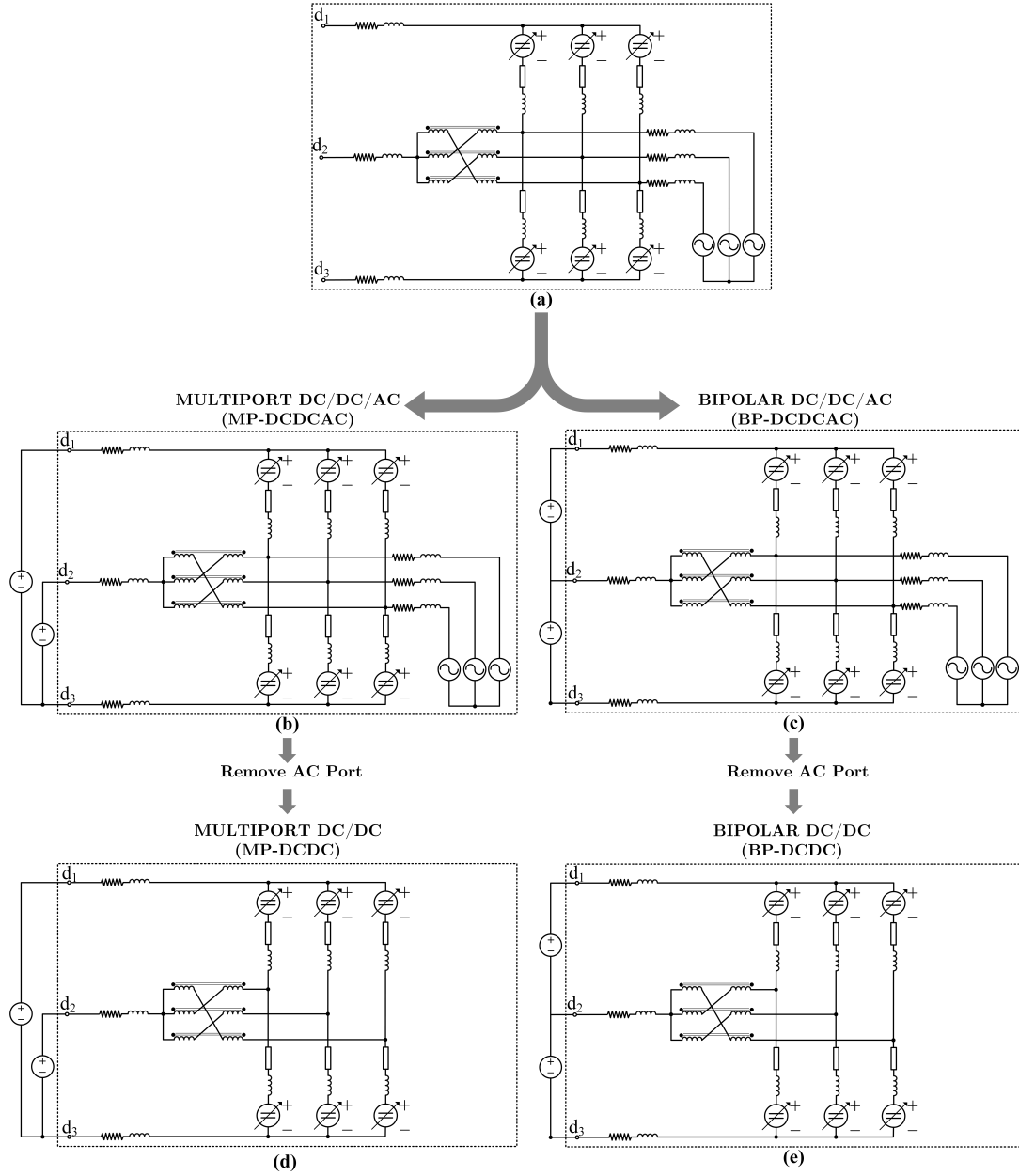


Figure 3.1: Target converter structures for modelling: (a) Unified general structure, (b) MP-DCDCAC topology, (c) BP-DCDC topology, (d) MP-DCDCAC topology, (e) BP-DCDC topology

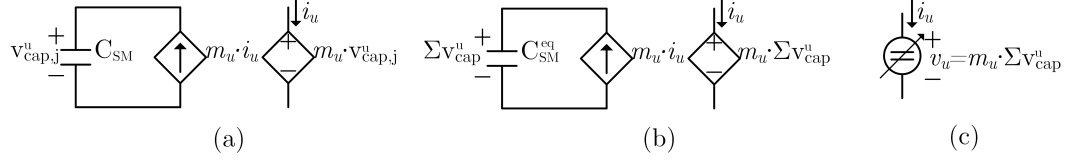


Figure 3.2: Average models for upper arm: (a) individual j^{th} submodule, (b) composite arm with N series-cascaded submodules, (c) compact representation of upper arm

done by using the MP-DCDCAC topology, shown in Figure 3.1b, and the model is later adapted to the other three topologies in Figure 3.1. The developed time averaged model (TAM) is validated with a switched model.

3.1.1 Single Phase Leg for DC/DC/AC Conversion

A time-averaged model for the submodules in the MMC arm is shown in Figure 3.2, taking for this example the upper arm [70]. A single submodule can be averaged over one switching period as shown in Figure 3.2a, where represents the voltage of the capacitor, C_{SM} , of the j th individual submodule in the upper arm, where j can take values from 0 to N; m represents the modulating signal for the arm, that can take values between 0 and 1, assuming the use of half-bridge submodules. Figure 3.2 illustrates how a single submodule can be represented as a voltage source controlled by the modulating signal that submodule would receive and the voltage a capacitor would have subjected to a current source controlled by the current in the arm and the modulating signal. Figure 3.2b illustrates the same methodology applied to the entire arm of N cascaded submodules, summing all the capacitance of one arm, C_{SM}^{eq} , and its voltage, ΣV_{cap}^u . Figure 3.2c shows a compact representation of the upper arm time averaged module.

The single-phase leg for DC/DC/AC conversion to be modelled is shown in Figure 3.3, where the currents and voltages are presented in the $\Sigma\Delta$ domain, as presented in Sec-

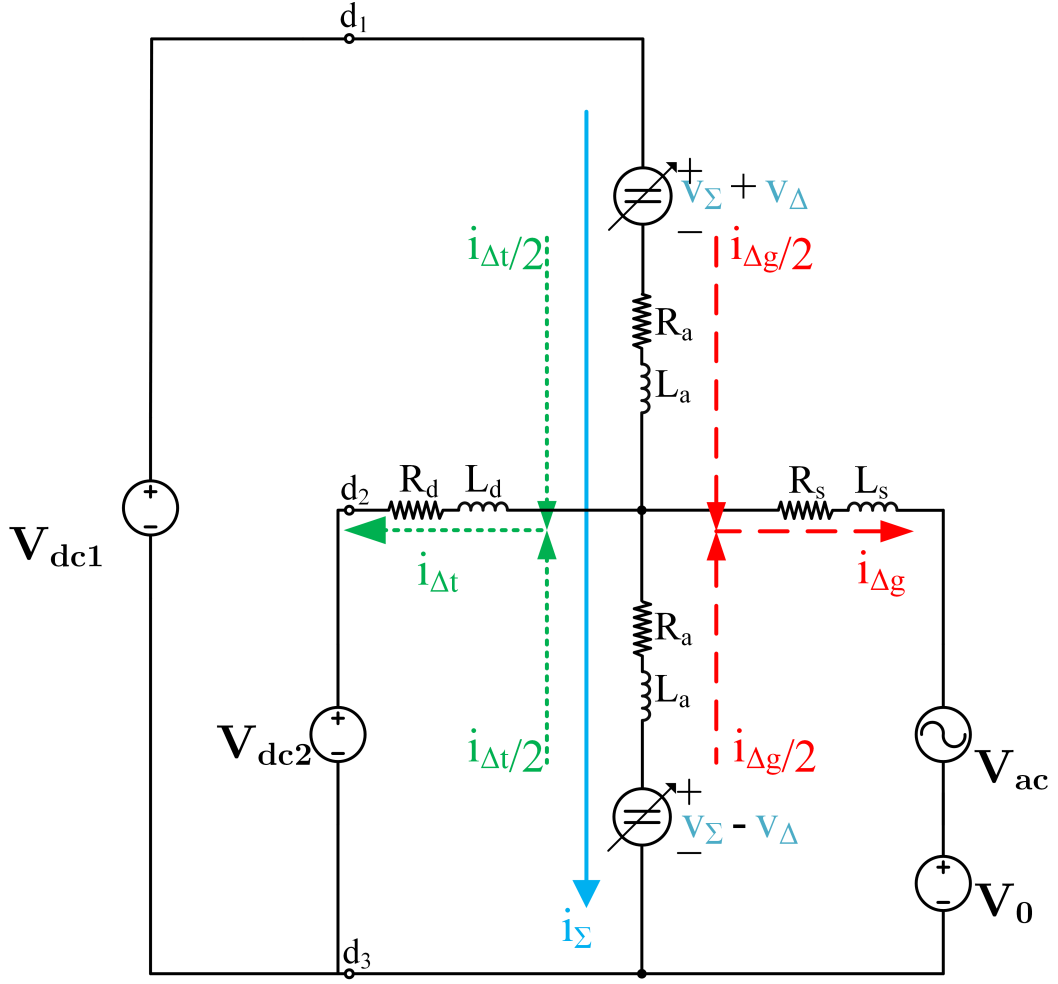


Figure 3.3: Time-averaged model of a single-phase leg for DC/DC/AC conversion

tion 2.1. Differential mode arm current i_Δ , first introduced in Figure 2.2 in the previous chapter, corresponds here to $i_\Delta = i_{\Delta t} + i_{\Delta c}$ which is the sum of the external AC and DC networks' currents; i_Σ , v_Σ , and v_Δ are the same as previously introduced in Equation (2.6). Three differential equations, from three different KVL loops, are written to represent the current dynamics and their relation with the arms' voltages as:

$$\begin{aligned}
L_a \frac{d}{dt} \left(i_\Sigma + \frac{i_{\Delta g}}{2} + \frac{i_{\Delta t}}{2} \right) + R_a \left(i_\Sigma + \frac{i_{\Delta g}}{2} + \frac{i_{\Delta t}}{2} \right) + L_d \frac{d}{dt} (i_{\Delta t}) \\
+ R_d(i_{\Delta t}) + V_{dc2} - V_{dc1} + V_\Sigma + V_\Delta = 0
\end{aligned} \tag{3.1}$$

$$\begin{aligned}
L_a \frac{d}{dt} \left(i_\Sigma - \frac{i_{\Delta g}}{2} - \frac{i_{\Delta t}}{2} \right) + R_a \left(i_\Sigma - \frac{i_{\Delta g}}{2} - \frac{i_{\Delta t}}{2} \right) - L_d \frac{d}{dt} (i_{\Delta t}) \\
- R_d(i_{\Delta t}) - V_{dc2} + V_\Sigma - V_\Delta = 0
\end{aligned} \tag{3.2}$$

$$L_s \frac{d}{dt} (i_{\Delta g}) + R_s(i_{\Delta g}) - L_d \frac{d}{dt} (i_{\Delta t}) - R_d(i_{\Delta t}) - V_{dc2} + V_{ac} + V_0 = 0. \tag{3.3}$$

In an effort to simplify the system in Equations (3.1) to (3.3) and decouple as many states as possible, three new equations are obtained by: adding Equation (3.1) and Equation (3.2); subtracting Equation (3.2) from Equation (3.1); solving for $\frac{d}{dt}(i_{\Delta t})$ in the previously obtained equation and replacing its value in Equation (3.3). The resulting equations are written in state-space form as:

$$l \frac{d}{dt}(\mathbf{x}_i) = a_{11} \cdot \mathbf{x}_i + b \cdot \mathbf{u} + n \cdot \mathbf{w}, \tag{3.4}$$

where the state, input, and disturbance vectors are respectively defined as:

$$\mathbf{x}_i = \begin{bmatrix} i_\Sigma & i_{\Delta g} & i_{\Delta t} \end{bmatrix}^T, \quad \mathbf{u} = \begin{bmatrix} v_\Sigma & v_\Delta \end{bmatrix}^T, \quad \mathbf{w} = \begin{bmatrix} V_{dc1} & V_{dc2} & V_{ac} & V_0 \end{bmatrix}^T. \tag{3.5}$$

The state-space matrices in Equation (3.4), l , a_{11} , b , n , are given by:

$$\begin{aligned}
l &= \begin{bmatrix} 2L_a & 0 & 0 \\ 0 & L_a & La + 2L_d \\ 0 & \frac{L_a L_d}{L_a + 2L_d} + L_s & 0 \end{bmatrix} \\
a_{11} &= \begin{bmatrix} -2R_a & 0 & 0 \\ 0 & -R_a & -R(R_a + 2R_d) \\ 0 & -\left(\frac{R_a L_d}{L_a + 2L_d} + R_s\right) & -\left(\frac{L_d(R_a + 2R_d)}{L - a + 2L_d} - R_d\right) \end{bmatrix} \\
b &= \begin{bmatrix} -2 & 0 \\ 0 & -2 \\ 0 & -\frac{2L_d}{L_a + 2L_d} \end{bmatrix} \\
n &= \begin{bmatrix} 1 & 0 & 0 & 0 \\ 1 & -2 & 0 & 0 \\ \frac{L_d}{L_a + 2L_d} & \left(1 - \frac{2L_d}{L_a + 2L_d}\right) & -1 & -1 \end{bmatrix}.
\end{aligned} \tag{3.6}$$

At this moment, the system in Equation (3.4) does not include the capacitor voltage dynamics, nor the modulating signals that are the inputs of interest. The equations that govern the capacitor voltages and currents, shown in Figure 3.2b for the upper arm, can be written for either arm as:

$$v_{u/l} = m_{u/l} \cdot \Sigma V_{cap}^{u/l} \tag{3.7}$$

$$m_{u/l} \cdot i_{u/l} = \frac{C_{u/l}}{N_{u/l}} \cdot \left(\Sigma V_{cap}^{u/l} \right), \tag{3.8}$$

where $C_{u/l}$ and $N_{u/l}$ represent the upper or lower arm submodule's capacitance and number of submodules, respectively. Each of the three terms in Equation (3.7) can also

be represented in the $\Sigma\Delta$ domain with the following transformation:

$$\begin{bmatrix} x_\Sigma \\ x_\Delta \end{bmatrix} = \begin{bmatrix} \frac{1}{2} & \frac{1}{2} \\ \frac{1}{2} & -\frac{1}{2} \end{bmatrix} \begin{bmatrix} x_u \\ x_L \end{bmatrix}, \quad (3.9)$$

where x can be v , m , or ΣV_{cap} . By doing so, $v_{u/l}$ in Equation (3.7) can be mapped into $\Sigma\Delta$ domain parameters v_Σ and v_Δ for both arms as:

$$\begin{bmatrix} V_\Sigma \\ V_\Delta \end{bmatrix} = \begin{bmatrix} m_\Sigma & m_\Delta \\ m_\Delta & m_\Sigma \end{bmatrix} \begin{bmatrix} \Sigma V_{cap,\Sigma} \\ \Sigma V_{cap,\Delta} \end{bmatrix}. \quad (3.10)$$

$[V_\Sigma, V_\Delta]^T$ in Equation (3.10) can replace \mathbf{u} in Equation (3.4) to introduce the modulating signals into the model. The multiplication of the modulating signals matrix in Equation (3.10) with b in Equation (3.6) results in:

$$a_{12} = \begin{bmatrix} -2m_\Sigma & -2m_\Delta \\ -2m_\Delta & -2m_\Sigma \\ \left(\frac{-2L_d}{L_a+2d}\right) m_\Delta & \left(\frac{-2L_d}{L_a+2d}\right) m_\Sigma \end{bmatrix}. \quad (3.11)$$

At this point, only the capacitor voltage dynamics are missing. By substituting the $\Sigma\Delta$ domain values into Equation (3.8) for each arm, the resulting equations become:

$$(m_\Sigma + m_\Delta) \left(i_\Sigma + \frac{i_{\Delta g}}{2} + \frac{i_{\Delta t}}{2} \right) = \left(\frac{C_u}{N_u} \right) \frac{d}{dt} (\Sigma V_{cap,\Sigma} + \Sigma V_{cap,\Delta}) \quad (3.12)$$

$$(m_\Sigma - m_\Delta) \left(i_\Sigma - \frac{i_{\Delta g}}{2} - \frac{i_{\Delta t}}{2} \right) = \left(\frac{C_u}{N_u} \right) \frac{d}{dt} (\Sigma V_{cap,\Sigma} - \Sigma V_{cap,\Delta}). \quad (3.13)$$

Equations (3.12) and (3.13) can be written in matrix form as:

$$c \frac{d}{dt} \mathbf{x}_v = a_{21} \cdot \mathbf{x}_i, \quad (3.14)$$

where $\mathbf{x}_v = [\Sigma V_{cap,\Sigma} \ \Sigma V_{cap,\Delta}]^T$, and:

$$\begin{aligned} c &= \begin{bmatrix} \frac{C_u}{N_u} & \frac{C_u}{N_u} \\ \frac{C_L}{N_L} & -\frac{C_L}{N_L} \end{bmatrix} \\ a_{21} &= \begin{bmatrix} m_\Sigma + m_\Delta & \frac{m_\Sigma + m_\Delta}{2} & \frac{m_\Sigma + m_\Delta}{2} \\ m_\Sigma - m_\Delta & \frac{m_\Sigma - m_\Delta}{2} & \frac{m_\Sigma - m_\Delta}{2} \end{bmatrix}. \end{aligned} \quad (3.15)$$

By including Equation (3.11) and Equation (3.14) into Equation (3.4), the set of differential equations that represent the time averaged arm current and capacitor voltage dynamics of the single-phase leg DC/DC/AC converter in Figure 3.3 can be written in state-space form as:

$$\frac{d}{dt} \begin{bmatrix} \mathbf{x}_i \\ \mathbf{x}_v \end{bmatrix} = \begin{bmatrix} l^{-1}a_{11} & l^{-1}a_{12} \\ c^{-1}a_{21} & 0_{2 \times 2} \end{bmatrix} \begin{bmatrix} \mathbf{x}_i \\ \mathbf{x}_v \end{bmatrix} + \begin{bmatrix} l^{-1}n \\ 0_{2 \times 4} \end{bmatrix} \begin{bmatrix} \mathbf{w} \end{bmatrix}, \quad (3.16)$$

where:

$$\mathbf{x}_i = \begin{bmatrix} i_\Sigma & i_{\Delta g} & i_{\Delta t} \end{bmatrix}^T, \quad (3.17)$$

$$\mathbf{x}_v = \begin{bmatrix} \Sigma V_{cap\Sigma} & \Sigma V_{cap\Delta} \end{bmatrix}^T, \quad (3.18)$$

$$\mathbf{w} = \begin{bmatrix} V_{dc1} & V_{dc2} & V_{ac} & V_0 \end{bmatrix}^T. \quad (3.19)$$

3.1.2 Three-Phase Converter for DC/DC/AC Conversion

The set of differential equations in Equation (3.16), that represents the single-phase converter in Figure 3.3, can be used to develop a three-phase model as shown in Figure 3.4. The state variables x_i and x_v in Equation (3.16) represent a single phase; by triplicating

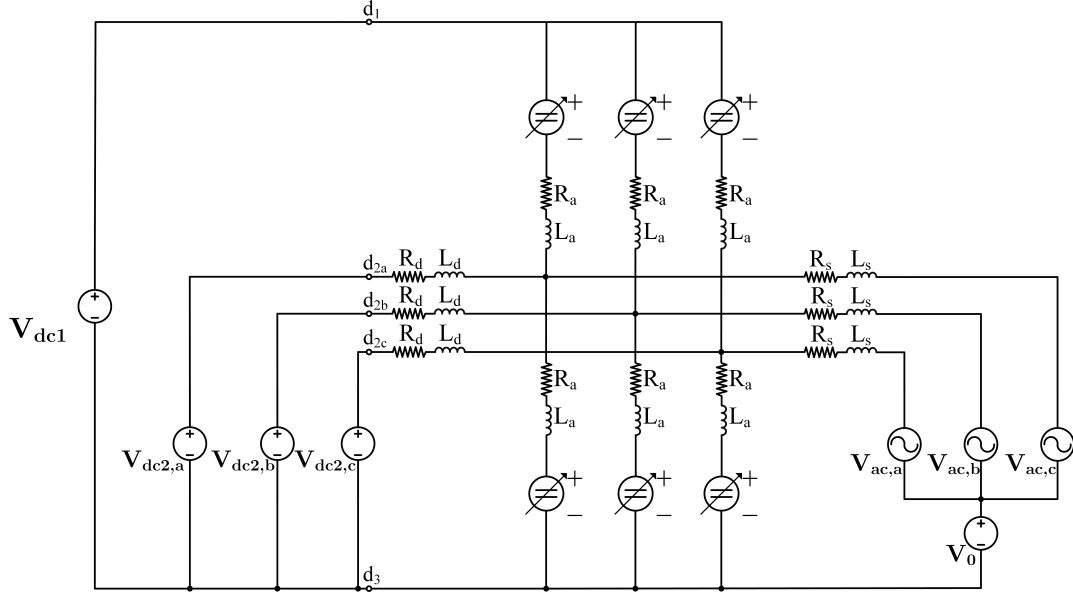


Figure 3.4: Three-phase structure for DC/DC/AC conversion

these state equations, the three-phase converter model can be expressed as:

$$\frac{d}{dt} \begin{bmatrix} \mathbf{X}_i \\ \mathbf{X}_v \end{bmatrix} = \begin{bmatrix} L^{-1}A_{11} & L^{-1}A_{12} \\ C^{-1}A_{21} & 0_{6 \times 6} \end{bmatrix} \begin{bmatrix} \mathbf{X}_i \\ \mathbf{X}_v \end{bmatrix} + \begin{bmatrix} L^{-1}N \\ 0_{6 \times 8} \end{bmatrix} [\mathbf{W}], \quad (3.20)$$

where the uppercase matrices in Equation (3.20) contain the information of their lowercase counterparts in Equation (3.16), augmented to represent the three-phase converter, in this manner:

$$U = \begin{bmatrix} u & 0 & 0 \\ 0 & u & 0 \\ 0 & 0 & u \end{bmatrix}. \quad (3.21)$$

The state and disturbance vectors in Equation (3.20) are now defined as:

$$\begin{aligned}
\mathbf{X}_i &= \begin{bmatrix} i_{\Sigma a} & i_{\Sigma b} & i_{\Sigma c} & i_{\Delta ga} & i_{\Delta gb} & i_{\Delta gc} & i_{\Delta ta} & i_{\Delta tb} & i_{\Delta tc} \end{bmatrix}^T \\
\mathbf{X}_v &= \begin{bmatrix} \Sigma V_{\Sigma a} & \Sigma V_{\Sigma b} & \Sigma V_{\Sigma c} & \Sigma V_{\Delta a} & \Sigma V_{\Delta b} & \Sigma V_{\Delta c} \end{bmatrix}^T \\
\mathbf{W} &= \begin{bmatrix} V_{dc1} & V_{dc2-a} & V_{dc2-b} & V_{dc2-c} & V_{ac-a} & V_{ac-b} & V_{ac-c} \end{bmatrix}^T.
\end{aligned} \tag{3.22}$$

The structure in Figure 3.4 has now three phases, which was the objective; however, the structure has at the moment three sources of DC voltage as the second DC port, which is unwanted. Now that the model has three phases, the magnetics filter (zig-zag transformer) presented in Section 2.1 is the ideal interface between the converter and the second DC port. The voltage source V_0 , which represent a voltage common to the a,b,c phases, is also undesirable in this model. Before making any such changes, the system can more easily be modified by transforming it into the well-known $\alpha\beta 0$ -frame [71].

3.1.3 $\alpha\beta 0$ - Frame Mapping

The Clarke transform is the method through which a system in abc -frame can be mapped into the $\alpha\beta 0$ -frame, and is defined as:

$$T_c = \begin{bmatrix} \frac{2}{3} & \frac{-1}{3} & \frac{-1}{3} \\ 0 & \frac{1}{\sqrt{3}} & \frac{2}{3} \\ \frac{1}{3} & \frac{1}{3} & \frac{1}{3} \end{bmatrix} \tag{3.23}$$

Each of the quantities in Equation (3.20) that are expressed in terms of the abc -frame, the fifteen state-variables, the six modulating signals, and the three-phase grid voltages, are mapped into the $\alpha\beta 0$ -frame as:

$$\mathbf{X}_{\alpha\beta 0} = T_c \cdot \mathbf{X}_{abc}, \quad (3.24)$$

where $\mathbf{X}_{\alpha\beta 0}$ and \mathbf{X}_{abc} represent vectors of three quantities in the $\alpha\beta 0$ -frame and abc -frame, respectively. Therefore, in Equation (3.20) every instance of abc quantities can be replaced with $\alpha\beta 0$ quantities by:

$$\mathbf{X}_{abc} = T_c^{-1} \cdot \mathbf{X}_{\alpha\beta 0}. \quad (3.25)$$

After the substitution, every set of three equations is pre-multiplied by T_C . This will yield a model whose state variables and modulating signals are all in the $\alpha\beta 0$ -frame, in the form of:

$$\frac{d}{dt} \begin{bmatrix} \mathbf{X}_{i\alpha\beta 0} \\ \mathbf{X}_{v\alpha\beta 0} \end{bmatrix} = \begin{bmatrix} L^{-1}A_{11} & L^{-1}T_3A_{12}T_3^{-1} \\ C^{-1}T_2A_{21}T_2^{-1} & 0_{6 \times 6} \end{bmatrix} \begin{bmatrix} \mathbf{X}_{i\alpha\beta 0} \\ \mathbf{X}_{v\alpha\beta 0} \end{bmatrix} + L^{-1} \begin{bmatrix} I_v & N_{\alpha\beta 0} \\ 0_{6 \times 1} & 0_{6 \times 7} \end{bmatrix} \begin{bmatrix} V_{dc1} \\ \mathbf{W}_{\alpha\beta 0} \end{bmatrix}, \quad (3.26)$$

where

$$\begin{aligned} \mathbf{X}_{i\alpha\beta 0} &= \begin{bmatrix} i_{\Sigma a} & i_{\Sigma b} & i_{\Sigma c} & i_{\Delta ga} & i_{\Delta gb} & i_{\Delta gc} & i_{\Delta ta} & i_{\Delta tb} & i_{\Delta tc} \end{bmatrix}^T \\ \mathbf{X}_{v\alpha\beta 0} &= \begin{bmatrix} \Sigma V_{\Sigma a} & \Sigma V_{\Sigma b} & \Sigma V_{\Sigma c} & \Sigma V_{\Delta a} & \Sigma V_{\Delta b} & \Sigma V_{\Delta c} \end{bmatrix}^T \\ \mathbf{W}_{\alpha\beta 0} &= \begin{bmatrix} V_{dc1} & V_{dc2-a} & V_{dc2-b} & V_{dc2-c} & V_{ac-a} & V_{ac-b} & V_{ac-c} \end{bmatrix}^T. \end{aligned} \quad (3.27)$$

T_3 and T_2 are 9x9 and 6x6 matrices, respectively, with diagonal T_C matrices. $N_{\alpha\beta 0}$ is the same as its abc counterpart in Equation (3.20), but removing the first column. I_v is a column vector defined as:

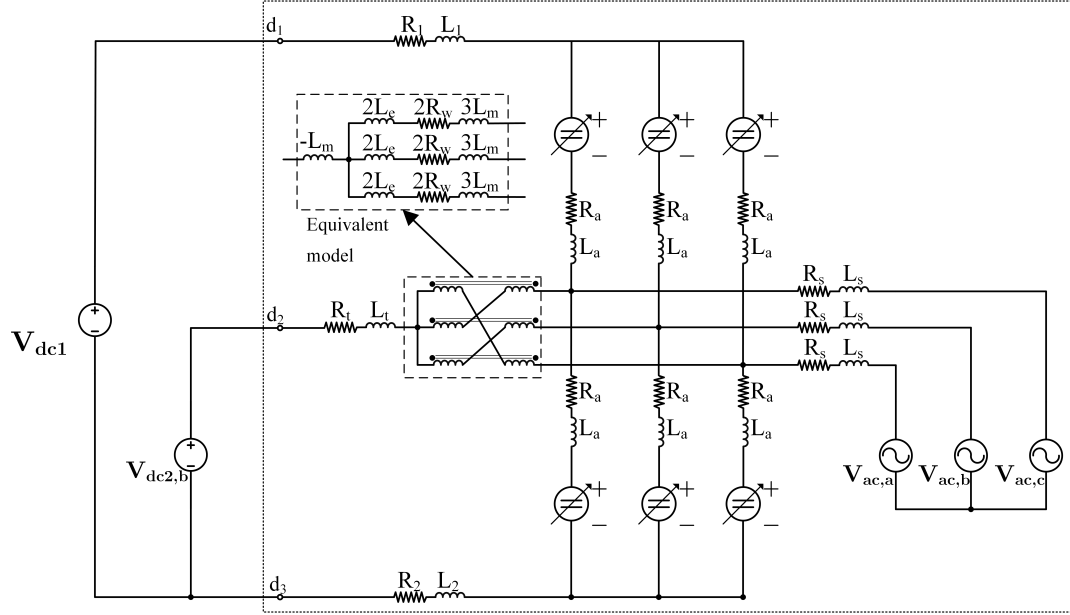


Figure 3.5: Three-phase structure for DC/DC/AC conversion

$$I_v = \begin{bmatrix} 0 & 0 & 1 & 0 & 0 & 1 & 0 & 0 & 1 \end{bmatrix}^T. \quad (3.28)$$

In the new system of Equation (3.26), the α and β components of the currents sum to zero when not in the phase legs, meaning that only θ sequence quantities enter the DC rails. Taking advantage of this phenomenon, three important modifications are made to the topology in Figure 3.4, since now only the equations that represent the zero components of the currents will be affected. The modifications are: (i) eliminate V_0 and leave the AC network neutral point floating, (ii) include a zig-zag transformer as the interface between the converter structure and only one d_2 port, and (iii) include line impedances for each of the three DC ports.

Modification (i) is applied by deleting from the model the sixth column from $N_{\alpha\beta 0}$, as well as the input V_0 from $\mathbf{W}_{\alpha\beta 0}$. In the structure, this amounts to removing the

zero-sequence path from the AC network to the bottom DC rail of the converter. By doing this, the state variable $i_{\Delta g0}$ ceases to exist, for there is no path for it to circulate. Therefore, the sixth column of the A_1 and A_2 are removed, as well as the sixth row of the whole model. The resulting system is reduced from fifteen to fourteen state variables.

Modification (ii) requires that the existing impedances that connect the three V_{dc2} sources and the converter be replaced with the equivalent model of a three-phase zig-zag transformer, shown in Figure 3.5. A zig-zag transformer is characterised by winding resistance, R_w , leakage inductance, L_e , and magnetising inductance, L_m . These three parameters can replace existing inductances L_d and R_d (in Figure 3.4) as:

$$L_d = 2L_e + 3L_m \quad (3.29)$$

$$R_d = 2R_w. \quad (3.30)$$

The $-L_m$ term in Figure 3.5 is required to properly model the zig-zag transformer, but this term is only seen by the current $i_{\Delta t0}$, as it is positioned after the three legs of the transformer have converged into one. The impedance to be added in port d_2 will similarly only be seen by the same current, and in the same manner, the impedances to be added in ports d_1 and d_3 , modification (iii), will only be seen by current $i_{\Sigma 0}$. This makes adding them to the model relatively simple. Since the only affected parts of the model will be the third and ninth columns and rows, it's simple to rewrite the equations of the KVL loops including these terms, much like in the first section of this chapter. The final structure is shown in Figure 3.5, while the final $\alpha\beta 0$ -frame model including all the aforementioned changes, is given by:

$$\frac{d}{dt} \begin{bmatrix} \mathbf{X}_i^* \\ \mathbf{X}_v^* \end{bmatrix} = \begin{bmatrix} \dot{A}_{11} & \dot{A}_{12} \\ \dot{A}_{21} & 0_{6 \times 6} \end{bmatrix} \begin{bmatrix} \mathbf{X}_i^* \\ \mathbf{X}_v^* \end{bmatrix} + \begin{bmatrix} \dot{N} \\ 0_{6 \times 5} \end{bmatrix} \begin{bmatrix} \mathbf{W}^* \end{bmatrix}, \quad (3.31)$$

where

$$\dot{A}_{11} = L^{-1}A_{11}^*; \quad \dot{A}_{12} = L^{-1}T_3A_{12}^*T_3^{-1}; \quad \dot{A}_{21} = C^{-1}T_2A_{21}^*T_2^{-1}; \quad \dot{N} = L^{-1}N^*. \quad (3.32)$$

In Equation (3.32), the matrices with an asterisk represent their counterparts in Equation (3.26), after going through the three aforementioned modifications.

The state and disturbance vectors in Equation (3.31) are defined by:

$$\begin{aligned} \mathbf{X}_i^* &= \begin{bmatrix} i_{\Sigma\alpha} & i_{\Sigma\beta} & i_{\Sigma 0} & i_{\Delta g\alpha} & i_{\Delta g\beta} & i_{\Delta t\alpha} & i_{\Delta t\beta} & i_{\Delta t0} \end{bmatrix}^{\mathbf{T}} \\ \mathbf{X}_v^* &= \begin{bmatrix} \Sigma V_{\Sigma\alpha} & \Sigma V_{\Sigma\beta} & \Sigma V_{\Sigma 0} & \Sigma V_{\Delta\alpha} & \Sigma V_{\Delta\beta} & \Sigma V_{\Delta 0} \end{bmatrix}^{\mathbf{T}} \\ \mathbf{W}^* &= \begin{bmatrix} V_{dc1} & V_{dc2} & V_{ac-\alpha} & V_{ac-\beta} & V_{ac-0} \end{bmatrix}^{\mathbf{T}}. \end{aligned} \quad (3.33)$$

The \dot{A} and \dot{N} matrices defined in Equation (3.32) are provided in full in Appendix A.

Note that Figure 3.5 now exactly matches the model of Figure 1.1(b). The transition to the $\alpha\beta\theta$ -frame has permitted several changes to be made to the converter in a simple manner, as well as it permits a more streamlined analysis than in the abc -frame; however, the $\alpha\beta\theta$ -frame is a stationary reference frame, which means that the states in the model are time-varying at steady-state. Solving for an equilibrium point, $\frac{d}{dt}\mathbf{X}_i^* = \frac{d}{dt}\mathbf{X}_v^* = 0$, would not yield any useful information, as the only solution it could provide would be a trivial one, with zero power transfers.

A further transformation could be applied to the model in Equation (3.31) that would

make the states DC-valued at steady-state, the well-known $dq0$ transformation. This transformation, however, would not solve the problem on its own, because although said transformation involves a rotating reference frame, it could only make one harmonic frequency DC-valued. If the $dq0$ -frame were to be used, multiple synchronous dq reference frames would be required. Instead, the $\alpha\beta0$ -frame offers a more elegant solution while also capturing unbalanced converter operation (can capture both positive and negative sequences). The concept of “dynamic phasor modelling”, as introduced in Section 1.2.3, is applied to achieve the conditions required for solving the system for equilibrium points instead. This process is presented in Section 3.2.

3.1.4 Three-Phase Converter for DC/DC Conversion

The model in Equation (3.31) can be used to accurately model either version of the DC/DC/AC converters with minor changes. To properly model, however, either version of the DC/DC converters, a bigger change has to be made to the model in Figure 3.5, and naturally in Equation (3.31) as well. The rows and columns that represent the AC network, i.e. all the terms related to $i_{\Delta g}$, have to be removed from the model. This results in a reduced model that is represented as:

$$\frac{d}{dt} \begin{bmatrix} \mathbf{X}_{ir}^* \\ \mathbf{X}_v^* \end{bmatrix} = \begin{bmatrix} \dot{A}_{11r} & \dot{A}_{12r} \\ \dot{A}_{21r} & 0_{6 \times 6} \end{bmatrix} \begin{bmatrix} \mathbf{X}_{ir}^* \\ \mathbf{X}_v^* \end{bmatrix} + \begin{bmatrix} \dot{N}_r \\ 0_{6 \times 5} \end{bmatrix} \begin{bmatrix} \mathbf{W}_r^* \end{bmatrix}, \quad (3.34)$$

where the subscript “ r ” means a reduced version of Equation (3.31), where the three-phase AC grid in Figure 3.5 has been eliminated. In Equation (3.34), matrices \dot{A}_{12r} and \dot{N}_r are obtained by removing the fourth and fifth row, matrix \dot{A}_{21r} by removing the fourth and fifth column, and matrix \dot{A}_{11r} by removing the fourth and fifth columns and rows, from their respective counterparts in Equation (3.31). The reduced state and input

vectors are defined as:

$$\begin{aligned} \mathbf{X}_{ir}^* &= \begin{bmatrix} i_{\Sigma\alpha} & i_{\Sigma\beta} & i_{\Sigma 0} & i_{\Delta t\alpha} & i_{\Delta t\beta} & i_{\Delta t0} \end{bmatrix}^T \\ \mathbf{W}_r^* &= \begin{bmatrix} V_{dc1} & V_{dc2} \end{bmatrix}^T. \end{aligned} \quad (3.35)$$

3.1.5 Model Validation

In this section, the validation of the developed models is carried out by comparing switched PLECS models of the MP-DCDCAC and BP-DCDC topologies in Figures 3.1(b) and 3.1(e), respectively, with their respective time averaged models in Equation (3.31) and Equation (3.34). All the simulations are run using open loop control. The open loop modulating signals are obtained by a solution procedure that will be explained in Chapter 4. Given this, the modulating signals are not specified here, and only the operating points for which the converters are set to validate them and their parameters are given. The simulations are carried out using the PLECS blockset in Simulink. The switched model used for the MMC arms was the one provided in the PLECS' demo "*HVDC Transmission System with MMCs*".

Table 3.1 shows the parameters used for the two simulations. The MP-DCDCAC converter is rated for 480 MW, and the operating point for this simulation is one in which half of its rated power is being transferred from the first DC port to the second DC port, and the other half is transferred to the AC port with a 0.9 power factor. The BP-DCDC converter is rated for 384 MW, and the operating point for this simulation is set to a transfer of 18% of rated power from the first DC port to the second DC port. In both cases, a disturbance at $t=2s$ in the form of a reduction of power transferred of 50% for the AC and 10% for the second DC port is triggered to demonstrate matching

of both models during steady-state and dynamic response.

Figure 3.6 and Figure 3.7 show how the waveforms for the time averaged and switched models of the MP-DCDCAC and BP-DCDC, respectively, have an excellent match in both simulations. To provide a more compact notation in the waveforms' results, the voltage state variables, i.e. Σv_Σ and Σv_Δ , are referred to only as v_Σ and v_Δ . It's worth noting that the current that goes through the d_2 port is equal to three times the state variable $i_{\Delta t0}$. Figure 3.8 shows the upper and lower arm voltage of phase a for both simulations, where the stepped voltage change from the switched model is contrasted by the smooth curve of the averaged model. Since a high degree of matching between the averaged and switched models is expected, as it has been shown in many works, i.e. [46], [51], [70], [72]–[74], the model is determined validated by confirming the excellent visual matching between the two models.

Table 3.1: Simulation parameters for the switched/averaged simulations

Parameter	MP-DCDCAC	BP-DCDC
$w, f_s w^*$	$2\pi 60$ rad/s, 10kHz	$2\pi 60$ rad/s, 10kHz
L_1, L_2, L_t, L_a, L_s	82 mH, 0, 40 mH, 50 mH, 20 mH	80 mH, 80 mH, 0, 50 mH, 0
L_e, L_m	9.8 mH, 28 H	9.8 mH, 28 H
R_1, R_2, R_t, R_a, R_s	2.1 Ω , 0 Ω , 1 Ω , 0.4 Ω , 0.6 Ω	2.1 Ω , 2.1 Ω , 0 Ω , 0.4 Ω , 0 Ω
R_w	0 Ω	0.1 Ω
C_u, C_L	20 mF	10 mF
N_u, N_L	38	38
V_{dc1}, V_{dc2}	400 kV, 200 kV	76 kV, 76 kV
<i>Peak L-N</i> V_{ac}	180 kV	-

* Carrier frequency for the SPWM for the switched model

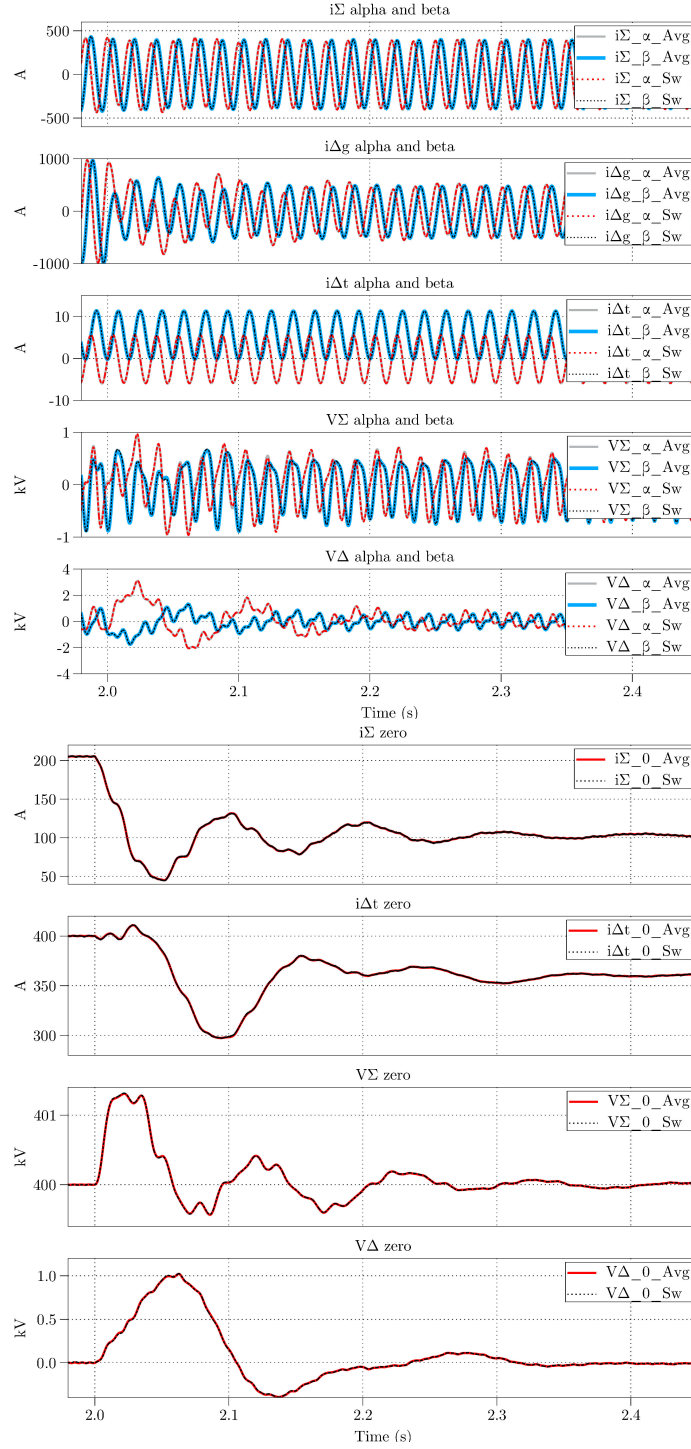


Figure 3.6: MP-DCDCAC simulation results comparing the 14 state variables in the $\alpha\beta 0$ frame for the PLECS' switched model vs the time averaged model in Equation (3.31)

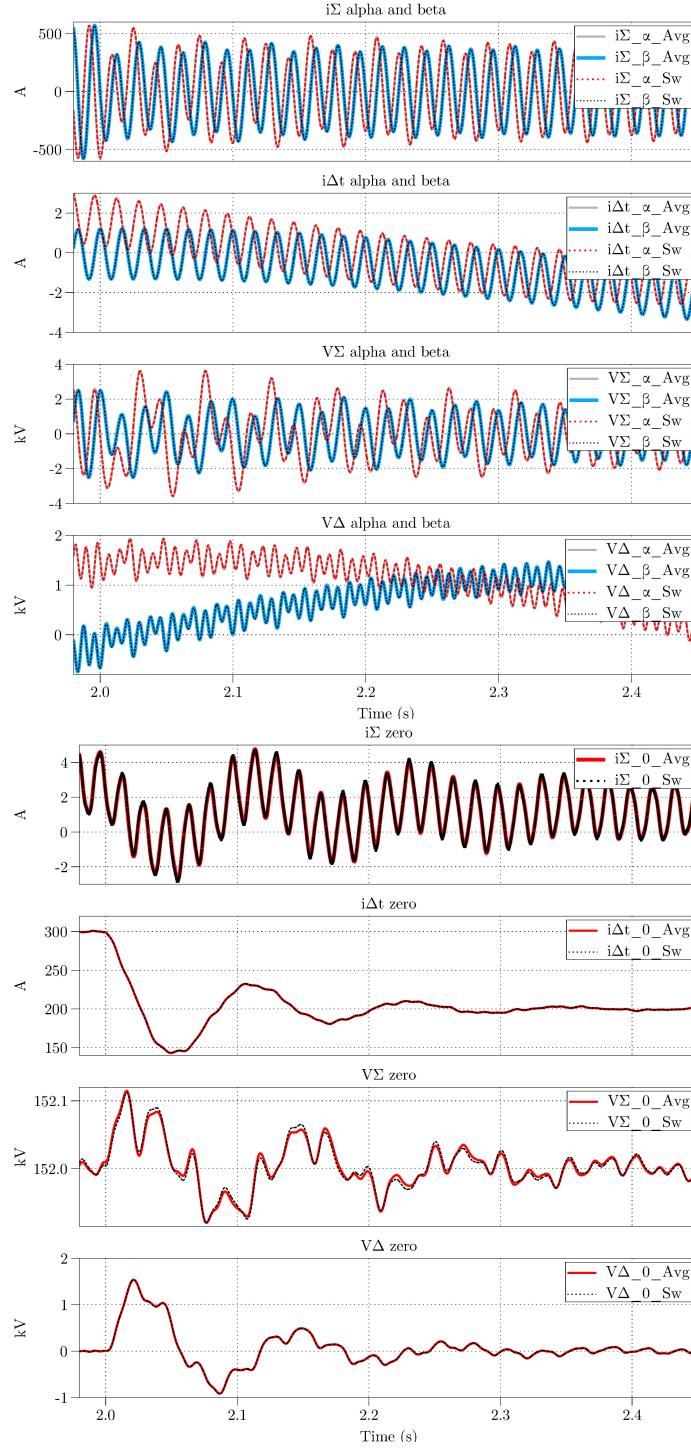


Figure 3.7: BP-DCDC simulation results comparing the 12 state variables in the $\alpha\beta$ 0 frame for the PLECS' switched model vs the time averaged model in Equation (3.34)

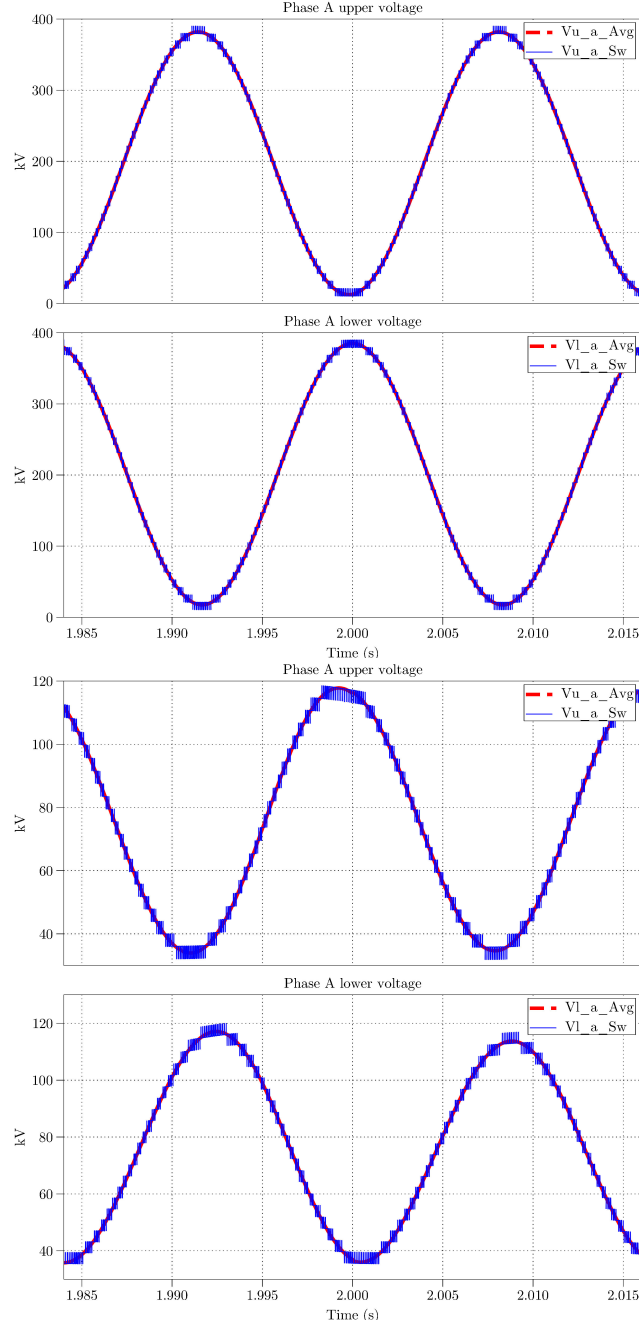


Figure 3.8: Upper and lower phase a arms' voltages for the: (a) MP-DCDCAC and (b) BP-DCDC simulations, comparing the PLECS' switched model vs time averaged model in Equation (3.31) and Equation (3.34)

3.2 Dynamic Phasor Model

In this section, the steps taken to develop a DPM of the MP-DCDCAC system given by Equation (3.31) are shown. This DPM can then be used, with minor modifications, to derive DPMs of the three remaining converter structures in Figure 3.1c - Figure 3.1e. All four DPMs are validated against their timeaveraged counterpart models developed in Section 3.1.

3.2.1 DPM Derivation for DC/DC/AC Conversion

The principle of dynamic phasors, introduced as generalised averaging method in [54] and applied to MMCs in [57]–[61], can be described as an averaging tool used to approximate time-varying waveforms with a Fourier series expansion that includes the time-varying nature of the waveforms in its complex coefficients. The approximation of a time-varying signal, $x(t)$, can be represented, for an arbitrary accuracy and on the interval $(t-T, t)$, as [54]:

$$x(t) \approx \sum_{k=-n}^{+n} \langle x \rangle_k(t) e^{jk\omega_s(t-T+s)}, \quad (3.36)$$

where k represents integers of the harmonics, n the range of harmonics to be considered for the Fourier expansion, $\omega_s = \frac{2\pi}{T}$, $s \in (t-T, t)$, and $\langle x \rangle_k(t)$ represents the complex Fourier coefficients, or the dynamic phasor of $x(t)$. Instead of using the complex exponential representation, the use of sines and cosines is adopted in this work, to allow the direct use of real quantities.

According to Equation (3.36), it is necessary to choose which harmonics are to be modelled. To pick which harmonics are to be selected for this converter, the system in Equation (3.31) is simulated in open-loop, with the control inputs chosen to approximate

a realistic operating point. The resulting waveforms indicate that the dominant harmonics for the states in Equation (3.31) can be categorised based on their $\alpha\beta 0$ components. Table 3.2 summarises the findings for these simulations.

Table 3.2: Dominant harmonic components for each $\alpha\beta 0$ frame component in system Equation (3.31)

$\alpha\beta 0$ component	DC	1^{st}	2^{nd}	3^{rd}
α		X	X	
β		X	X	
0	X			X

Therefore, the states in Equation (3.31) are to be approximated by a combination of DC and AC harmonic components as follows:

$$i_{\Sigma\alpha}(t) \approx I_{\Sigma\alpha}^{1\parallel} \cos(wt) + I_{\Sigma\alpha}^{1\perp} \sin(wt) + I_{\Sigma\alpha}^{2\parallel} \cos(2wt) + I_{\Sigma\alpha}^{2\perp} \sin(2wt) \quad (3.37)$$

$$i_{\Sigma\beta}(t) \approx I_{\Sigma\beta}^{1\parallel} \cos(wt) + I_{\Sigma\beta}^{1\perp} \sin(wt) + I_{\Sigma\beta}^{2\parallel} \cos(2wt) + I_{\Sigma\beta}^{2\perp} \sin(2wt) \quad (3.38)$$

$$i_{\Sigma 0}(t) \approx I_{\Sigma 0}^{dc} + I_{\Sigma 0}^{3\parallel} \cos(3wt) + I_{\Sigma 0}^{3\perp} \sin(2wt) \quad (3.39)$$

$$i_{\Delta g\alpha}(t) \approx I_{\Delta g\alpha}^{1\parallel} \cos(wt) + I_{\Delta g\alpha}^{1\perp} \sin(wt) + I_{\Delta g\alpha}^{2\parallel} \cos(2wt) + I_{\Delta g\alpha}^{2\perp} \sin(2wt) \quad (3.40)$$

$$i_{\Delta g\beta}(t) \approx I_{\Delta g\beta}^{1\parallel} \cos(wt) + I_{\Delta g\beta}^{1\perp} \sin(wt) + I_{\Delta g\beta}^{2\parallel} \cos(2wt) + I_{\Delta g\beta}^{2\perp} \sin(2wt) \quad (3.41)$$

$$i_{\Delta t\alpha}(t) \approx I_{\Delta t\alpha}^{1\parallel} \cos(wt) + I_{\Delta t\alpha}^{1\perp} \sin(wt) + I_{\Delta t\alpha}^{2\parallel} \cos(2wt) + I_{\Delta t\alpha}^{2\perp} \sin(2wt) \quad (3.42)$$

$$i_{\Delta t 0}(t) \approx I_{\Delta t 0}^{dc} + I_{\Delta t 0}^{3\parallel} \cos(3wt) + I_{\Delta t 0}^{3\perp} \sin(2wt) \quad (3.43)$$

$$i_{\Delta t\beta}(t) \approx I_{\Delta t\beta}^{1\parallel} \cos(wt) + I_{\Delta t\beta}^{1\perp} \sin(wt) + I_{\Delta t\beta}^{2\parallel} \cos(2wt) + I_{\Delta t\beta}^{2\perp} \sin(2wt) \quad (3.44)$$

$$\Sigma v_{\Sigma\alpha}(t) \approx \Sigma V_{\Sigma\alpha}^{1\parallel} \cos(wt) + \Sigma V_{\Sigma\alpha}^{1\perp} \sin(wt) + \Sigma V_{\Sigma\alpha}^{2\parallel} \cos(2wt) + \Sigma V_{\Sigma\alpha}^{2\perp} \sin(2wt) \quad (3.45)$$

$$\Sigma v_{\Sigma\beta}(t) \approx \Sigma V_{\Sigma\beta}^{1\parallel} \cos(wt) + \Sigma V_{\Sigma\beta}^{1\perp} \sin(wt) + \Sigma V_{\Sigma\beta}^{2\parallel} \cos(2wt) + \Sigma V_{\Sigma\beta}^{2\perp} \sin(2wt) \quad (3.46)$$

$$\Sigma v_{\Sigma 0}(t) \approx \Sigma V_{\Sigma 0}^{dc} + \Sigma V_{\Sigma 0}^{3\parallel} \cos(3wt) + \Sigma V_{\Sigma 0}^{3\perp} \sin(2wt) \quad (3.47)$$

$$\Sigma v_{\Delta\alpha}(t) \approx \Sigma V_{\Delta\alpha}^{1\parallel} \cos(wt) + \Sigma V_{\Delta\alpha}^{1\perp} \sin(wt) + \Sigma V_{\Delta\alpha}^{2\parallel} \cos(2wt) + \Sigma V_{\Delta\alpha}^{2\perp} \sin(2wt) \quad (3.48)$$

$$\Sigma v_{\Delta\beta}(t) \approx \Sigma V_{\Delta\beta}^{1\parallel} \cos(wt) + \Sigma V_{\Delta\beta}^{1\perp} \sin(wt) + \Sigma V_{\Delta\beta}^{2\parallel} \cos(2wt) + \Sigma V_{\Delta\beta}^{2\perp} \sin(2wt) \quad (3.49)$$

$$\Sigma v_{\Delta 0}(t) \approx \Sigma V_{\Delta 0}^{dc} + \Sigma V_{\Delta 0}^{3\parallel} \cos(3wt) + \Sigma V_{\Delta 0}^{3\perp} \sin(2wt). \quad (3.50)$$

The control inputs follow the same pattern, with their components assigned as follows:

$$m_{\Sigma\alpha}(t) = M_{\Sigma\alpha}^{1\parallel} \cos(wt) + M_{\Sigma\alpha}^{1\perp} \sin(wt) \quad (3.51)$$

$$m_{\Sigma\beta}(t) = M_{\Sigma\beta}^{1\parallel} \cos(wt) + M_{\Sigma\beta}^{1\perp} \sin(wt) \quad (3.52)$$

$$m_{\Sigma 0}(t) = M_{\Sigma 0}^{dc} \quad (3.53)$$

$$m_{\Delta\alpha}(t) = M_{\Delta\alpha}^{1\parallel} \cos(wt) + M_{\Delta\alpha}^{1\perp} \sin(wt) \quad (3.54)$$

$$m_{\Delta\beta}(t) = M_{\Delta\beta}^{1\parallel} \cos(wt) + M_{\Delta\beta}^{1\perp} \sin(wt) \quad (3.55)$$

$$m_{\Delta 0}(t) = M_{\Delta 0}^{dc}. \quad (3.56)$$

The only disturbance terms in the model that require conversion into the DPM are the AC sources, which are assigned fundamental frequency components, as they are assumed to be purely sinusoidal. Note that each harmonic is represented by a set of parallel (cosine) and a perpendicular (sine) component. The uppercase average values, e.g. $I_{\Delta g\beta}^{1\parallel}(t)$ and $M_{\Sigma\beta}^{1\parallel}(t)$ are DC valued in steady-state. Also note that time dependence of the dynamic phasors is not explicitly shown for compact notation, e.g. $M_{\Sigma 0}^{dc}(t)$ and

$M_{\Sigma\beta}^{1\perp}(t)$ are equivalent to $M_{\Sigma 0}^{dc}$ and $M_{\Sigma\beta}^{1\perp}$, respectively.

To obtain the equations for the dynamic phasors, Equations (3.35)-(3.54) are substituted into Equation (3.31), then the corresponding multiplications are performed. After, the equations are separated into those that contain sines and cosines with the same frequency, and the system is solved for each of the dynamic phasors, e.g. $\frac{d}{dt}I_{\Sigma\alpha}^{1\parallel}(t)$ process is extremely tedious, albeit quite straightforward. A detailed tutorial of this process can be found in [70], [73].

The resulting DPM in the $\alpha\beta 0$ -frame representing the structure in Figure 3.5 is presented as:

$$\frac{d}{dt} \begin{bmatrix} \widetilde{\mathbf{X}}_i^* \\ \widetilde{\mathbf{X}}_v^* \end{bmatrix} = \begin{bmatrix} \tilde{A}_{11} & \tilde{A}_{12} \\ \tilde{A}_{21} & 0_{22 \times 22} \end{bmatrix} \begin{bmatrix} \widetilde{\mathbf{X}}_i^* \\ \widetilde{\mathbf{X}}_v^* \end{bmatrix} + \begin{bmatrix} \tilde{N} \\ 0_{22 \times 5} \end{bmatrix} [\widetilde{\mathbf{W}}^*], \quad (3.57)$$

where:

$$\widetilde{\mathbf{X}}_i^* = [I_{\Sigma\alpha}^{1\parallel} \ I_{\Sigma\alpha}^{1\perp} \ I_{\Sigma\alpha}^{2\parallel} \ I_{\Sigma\alpha}^{2\perp} \ I_{\Sigma\beta}^{1\parallel} \ I_{\Sigma\beta}^{1\perp} \ I_{\Sigma\beta}^{2\parallel} \ I_{\Sigma\beta}^{2\perp} \ I_{\Sigma 0}^{dc} \ I_{\Sigma 0}^{3\parallel} \ I_{\Sigma 0}^{3\perp} \ I_{\Delta g\alpha}^{1\parallel} \dots \quad (3.58)$$

$$\dots \ I_{\Delta g\alpha}^{1\perp} \ I_{\Delta g\alpha}^{2\parallel} \ I_{\Delta g\alpha}^{2\perp} \ I_{\Delta g\beta}^{1\parallel} \ I_{\Delta g\beta}^{1\perp} \ I_{\Delta g\beta}^{2\parallel} \ I_{\Delta g\beta}^{2\perp} \ I_{\Delta t\alpha}^{1\parallel} \ I_{\Delta t\alpha}^{1\perp} \ I_{\Delta t\alpha}^{2\parallel} \dots$$

$$\dots \ I_{\Delta t\alpha}^{2\perp} \ I_{\Delta t\beta}^{1\parallel} \ I_{\Delta t\beta}^{1\perp} \ I_{\Delta t\beta}^{2\parallel} \ I_{\Delta t\beta}^{2\perp} \ I_{\Delta t0}^{dc} \ I_{\Delta t0}^{3\parallel} \ I_{\Delta t0}^{3\perp}]$$

$$\widetilde{\mathbf{X}}_v^* = [\Sigma V_{\Sigma\alpha}^{1\parallel} \ \Sigma V_{\Sigma\alpha}^{1\perp} \ \Sigma V_{\Sigma\alpha}^{2\parallel} \ \Sigma V_{\Sigma\alpha}^{2\perp} \ \Sigma V_{\Sigma\beta}^{1\parallel} \ \Sigma V_{\Sigma\beta}^{1\perp} \ \Sigma V_{\Sigma\beta}^{2\parallel} \ \Sigma V_{\Sigma\beta}^{2\perp} \dots \quad (3.59)$$

$$\dots \ \Sigma V_{\Sigma 0}^{dc} \ \Sigma V_{\Sigma 0}^{3\parallel} \ \Sigma V_{\Sigma 0}^{3\perp} \ \Sigma V_{\Delta t\alpha}^{1\parallel} \ \Sigma V_{\Delta t\alpha}^{1\perp} \ \Sigma V_{\Delta t\alpha}^{2\parallel} \ \Sigma V_{\Delta t\alpha}^{2\perp} \dots$$

$$\dots \ \Sigma V_{\Delta t\beta}^{1\parallel} \ \Sigma V_{\Delta t\beta}^{1\perp} \ \Sigma V_{\Delta t\beta}^{2\parallel} \ \Sigma V_{\Delta t\beta}^{2\perp} \ \Sigma V_{\Delta t0}^{dc} \ \Sigma V_{\Delta t0}^{3\parallel} \ \Sigma V_{\Delta t0}^{3\perp}]$$

$$\widetilde{\mathbf{W}}^* = [V_{dc1} \ V_{dc2} \ V_{ac,\alpha}^{1\parallel} \ V_{ac,\alpha}^{1\perp} \ V_{ac,\beta}^{1\parallel} \ V_{ac,\beta}^{1\perp}]. \quad (3.60)$$

The system in Equation (3.57) contains 52 states, shown in Equation (3.58) and Equation (3.59), 6 disturbance terms, shown in Equation (3.60), and 10 modulating

signals, which are embedded in the state matrix. The states and disturbance matrices in Equation (3.57) are given in Appendix C.

3.2.2 DPM Derivation for DC/DC Conversion

The DPM for DC/DC conversion is obtained in the same way the DC/DC three-phase model in Section 3.1.4 is derived, which is by reducing the DC/DC/AC DPM. The rows and columns that represent the AC network, i.e. all the terms related to grid current $I_{\Delta g}$, are removed from Equation (3.57). The resulting DPM is represented as:

$$\frac{d}{dt} \begin{bmatrix} \widetilde{\mathbf{X}}_{ir}^* \\ \widetilde{\mathbf{X}}_{vr}^* \end{bmatrix} = \begin{bmatrix} \tilde{A}_{11r} & \tilde{A}_{12r} \\ \tilde{A}_{21r} & 0_{22 \times 22} \end{bmatrix} \begin{bmatrix} \widetilde{\mathbf{X}}_{ir}^* \\ \widetilde{\mathbf{X}}_{vr}^* \end{bmatrix} + \begin{bmatrix} \tilde{N}_r \\ 0_{22 \times 5} \end{bmatrix} \begin{bmatrix} \widetilde{\mathbf{W}}_r^* \end{bmatrix}, \quad (3.61)$$

where the subscript “ r ” means a reduced version of Equation (3.57), where the three-phase AC grid parameters have been eliminated. In Equation (3.61), matrices \tilde{A}_{12r} and \tilde{N}_r are obtained by removing rows 12th to 19th, matrix \tilde{A}_{21r} by removing columns 12th to 19th, and matrix \tilde{A}_{11r} by removing both columns and rows 12th to 19th, from their respective counterparts in Equation (3.57). The reduced state and input vectors are defined as:

$$\widetilde{\mathbf{X}}_{ir}^* = [\begin{array}{cccccccccccc} I_{\Sigma\alpha}^{1\parallel} & I_{\Sigma\alpha}^{1\perp} & I_{\Sigma\alpha}^{2\parallel} & I_{\Sigma\alpha}^{2\perp} & I_{\Sigma\beta}^{1\parallel} & I_{\Sigma\beta}^{1\perp} & I_{\Sigma\beta}^{2\parallel} & I_{\Sigma\beta}^{2\perp} & I_{\Sigma 0}^{dc} & I_{\Sigma 0}^{3\parallel} & I_{\Sigma 0}^{3\perp} & \dots \\ \dots & I_{\Delta t\alpha}^{1\parallel} & I_{\Delta t\alpha}^{1\perp} & I_{\Delta t\alpha}^{2\parallel} & I_{\Delta t\alpha}^{2\perp} & I_{\Delta t\beta}^{1\parallel} & I_{\Delta t\beta}^{1\perp} & I_{\Delta t\beta}^{2\parallel} & I_{\Delta t\beta}^{2\perp} & I_{\Delta t 0}^{dc} & \dots \\ \dots & I_{\Delta t 0}^{3\parallel} & I_{\Delta t 0}^{3\perp} & \end{array}] \quad (3.62)$$

$$\widetilde{\mathbf{X}}_{vr}^* = [\begin{array}{cccccccccccc} \Sigma V_{\Sigma\alpha}^{1\parallel} & \Sigma V_{\Sigma\alpha}^{1\perp} & \Sigma V_{\Sigma\alpha}^{2\parallel} & \Sigma V_{\Sigma\alpha}^{2\perp} & \Sigma V_{\Sigma\beta}^{1\parallel} & \Sigma V_{\Sigma\beta}^{1\perp} & \Sigma V_{\Sigma\beta}^{2\parallel} & \Sigma V_{\Sigma\beta}^{2\perp} & \dots \\ \dots & \Sigma V_{\Sigma 0}^{dc} & \Sigma V_{\Sigma 0}^{3\parallel} & \Sigma V_{\Sigma 0}^{3\perp} & \Sigma V_{\Delta t\alpha}^{1\parallel} & \Sigma V_{\Delta t\alpha}^{1\perp} & \Sigma V_{\Delta t\alpha}^{2\parallel} & \Sigma V_{\Delta t\alpha}^{2\perp} & \dots \\ \dots & \Sigma V_{\Delta t\beta}^{1\parallel} & \Sigma V_{\Delta t\beta}^{1\perp} & \Sigma V_{\Delta t\beta}^{2\parallel} & \Sigma V_{\Delta t\beta}^{2\perp} & \Sigma V_{\Delta t 0}^{dc} & \Sigma V_{\Delta t 0}^{3\parallel} & \Sigma V_{\Delta t 0}^{3\perp} & \end{array}] \quad (3.63)$$

$$\widetilde{\mathbf{W}}_r^* = [\begin{array}{cc} V_{dc1} & V_{dc2} \end{array}] \quad (3.64)$$

The system in Equation (3.61) contains 44 states, shown in Equation (3.62) and Equation (3.63), 2 disturbance terms, shown in Equation (3.63), and 10 modulating signals, which are embedded in the state matrix. The state and disturbance matrices in Equation (3.61) are given in Appendix D.

3.2.3 DPM Validation

In this section, the validation of the developed DPMs is carried out in the same way as the validation in Section 3.1.5. In this instance, however, the switched model is not used to compare the DPM, having demonstrated that the TAM is an excellent match for the switched model, this validation is performed by comparing the TAM and the DPM.

For this validation, one set of results is shown for each of the four topologies in Figure 3.1. Table 3.3 shows the parameters used in each simulation. The parameters have been chosen to demonstrate the versatility of the DPM when it comes to the number of submodules in the upper and lower arms, as well as the capacitance of each submodule. For all four cases, the capacitances are selected to maintain the energy storage of the

converter at an approximate of $50 \frac{kJ}{MW}$. For the case of DC/DC/AC conversion in both topologies, 1 pu power is being transferred from the first DC port to the second DC port and AC port, split equally. For the DC/DC conversion in both topologies, 1 pu power is being transferred from the first DC port to the second DC port. The disturbance is also presented as a power reduction of power transferred of 50% for the AC and 10% for the second DC port, triggered at $t=2s$.

Figures 3.9 to 3.12 show the results for the four simulation cases, comparing the averaged model with the DPM. Tables 3.4 to 3.7 make a comparison of the most important harmonic components for the state variables in each case. The superscript in the state variable indicates which harmonic component is being compared.

Table 3.3: Simulation parameters for the averaged/DPM simulations

Parameter	MP-DCDCAC	MP-DCDC
P_{rated}	480 MW	480 MW
w	$2\pi 60$ rad/s	$2\pi 60$ rad/s
L_1, L_2, L_t, L_a, L_s	82 mH, 0, 40 mH, 50 mH, 20 mH	80 mH, 80 mH, 0, 50 mH, 0
L_e, L_m	9.8 mH, 28 H	9.8 mH, 28 H
R_1, R_2, R_t, R_a, R_s	2.1 Ω , 0 Ω , 1 Ω , 0.4 Ω , 0.6 Ω	2.1 Ω , 0 Ω , 1 Ω , 0.4 Ω , 0 Ω
R_w	0 Ω	0 Ω
C_u, C_L	10 mF, 12 mF	10 mF, 12 mF
N_u, N_L	200, 180	200, 180
V_{dc1}, V_{dc2}	400 kV, 200 kV	400 kV, 200 kV
$Peak\ L-N\ V_{ac}$	180 kV	N/A
Parameter	BP-DCDCAC	BP-DCDC
P_{rated}	768 MW	384 MW
w	$2\pi 60$ rad/s	$2\pi 60$ rad/s
L_1, L_2, L_t, L_a, L_s	82 mH, 82 mH, 0 mH, 50 mH, 20 mH	80 mH, 80 mH, 0, 50 mH, 0
L_e, L_m	9.8 mH, 28 H	9.8 mH, 28 H
R_1, R_2, R_t, R_a, R_s	2.1 Ω , 2.1 Ω , 0 Ω , 0.4 Ω , 0.6 Ω	2.1 Ω , 2.1 Ω , 0 Ω , 0.4 Ω , 0 Ω
R_w	0.1 Ω	0.1 Ω
C_u, C_L	18 mF, 18 mF	9 mF, 9 mF
N_u, N_L	200, 200	200, 200
V_{dc1}, V_{dc2}	320 kV, 320 kV	160 kV, 160 kV
$Peak\ L-N\ V_{ac}$	180 kV	N/A

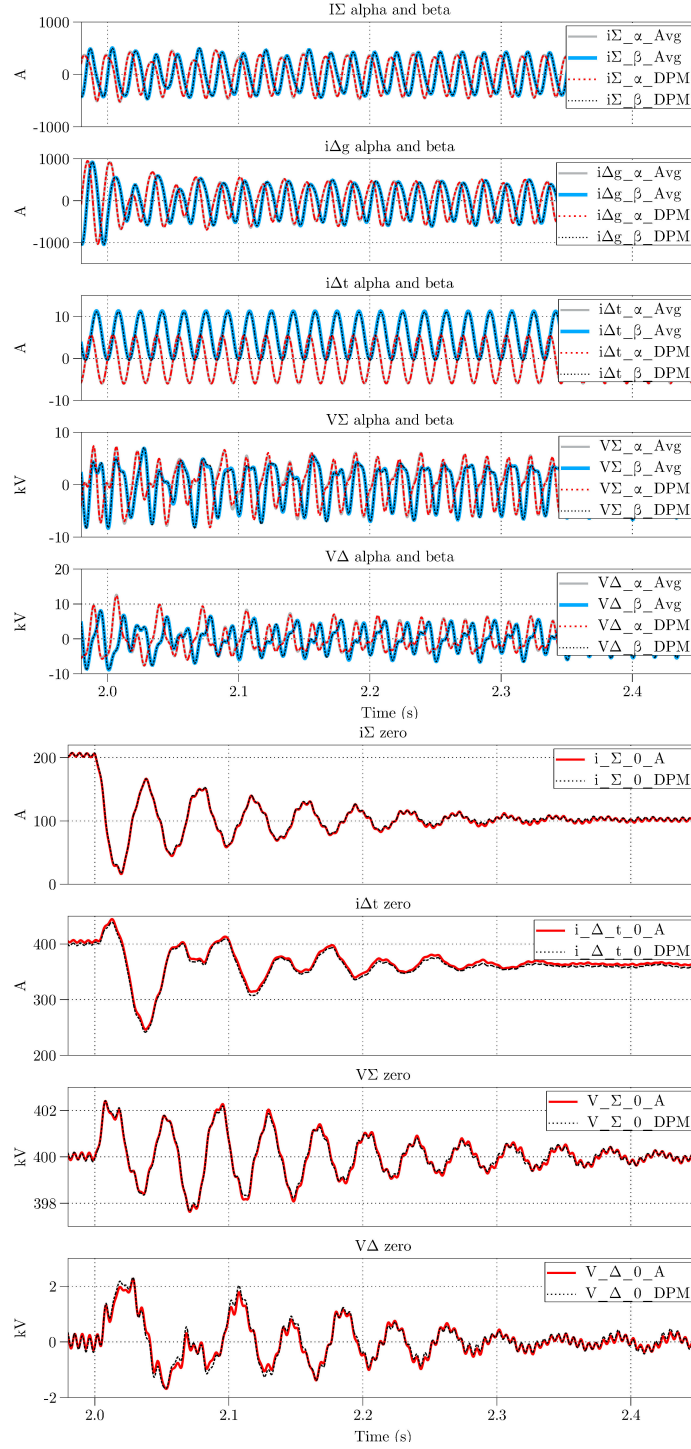


Figure 3.9: MP-DCDCAC; DPM and averaged model simulation results

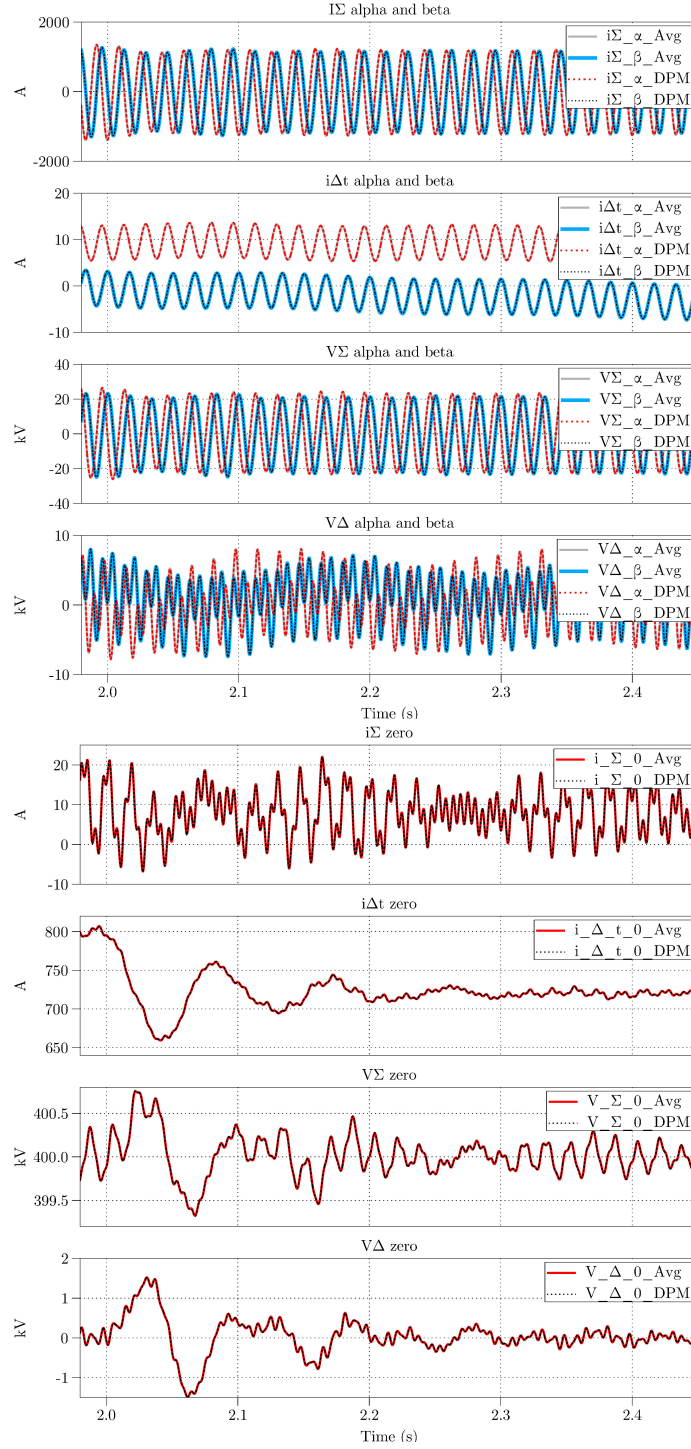


Figure 3.10: MP-DCDC; DPM and averaged model simulation results

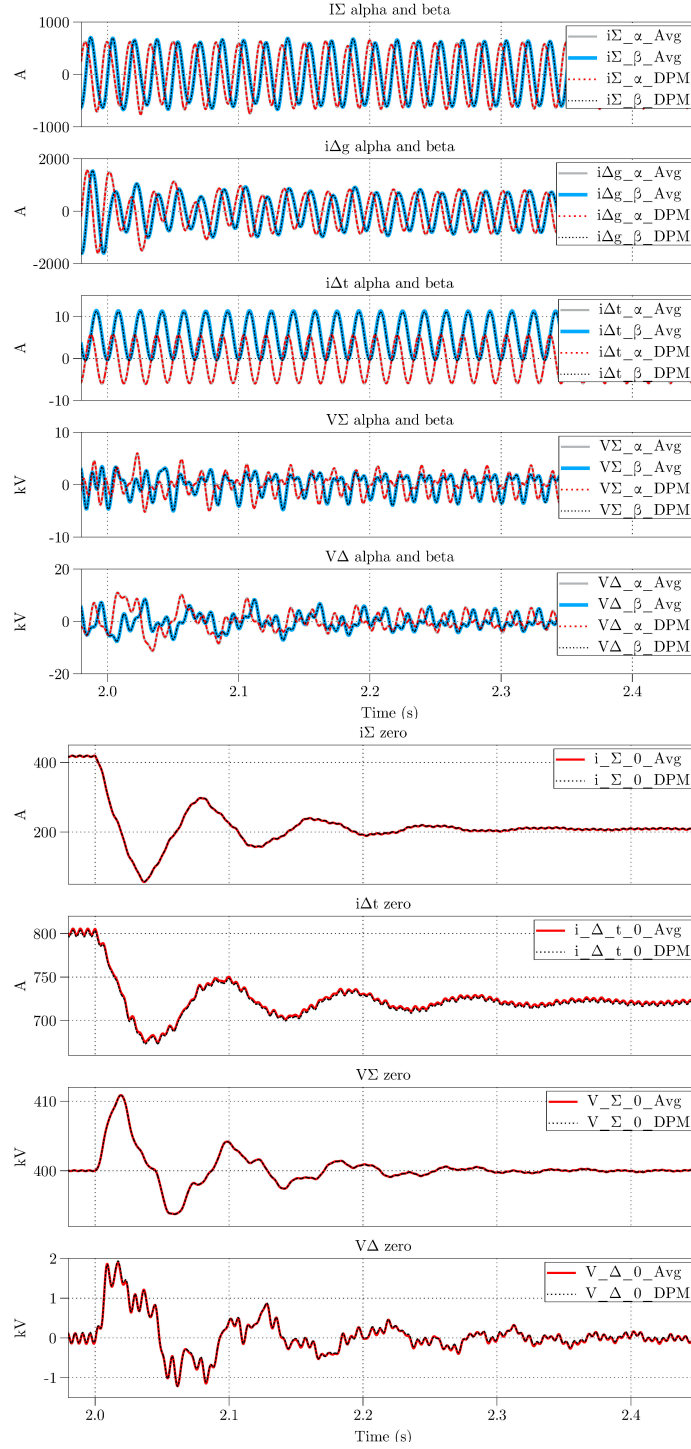


Figure 3.11: BP-DCDCAC; DPM and averaged model simulation results

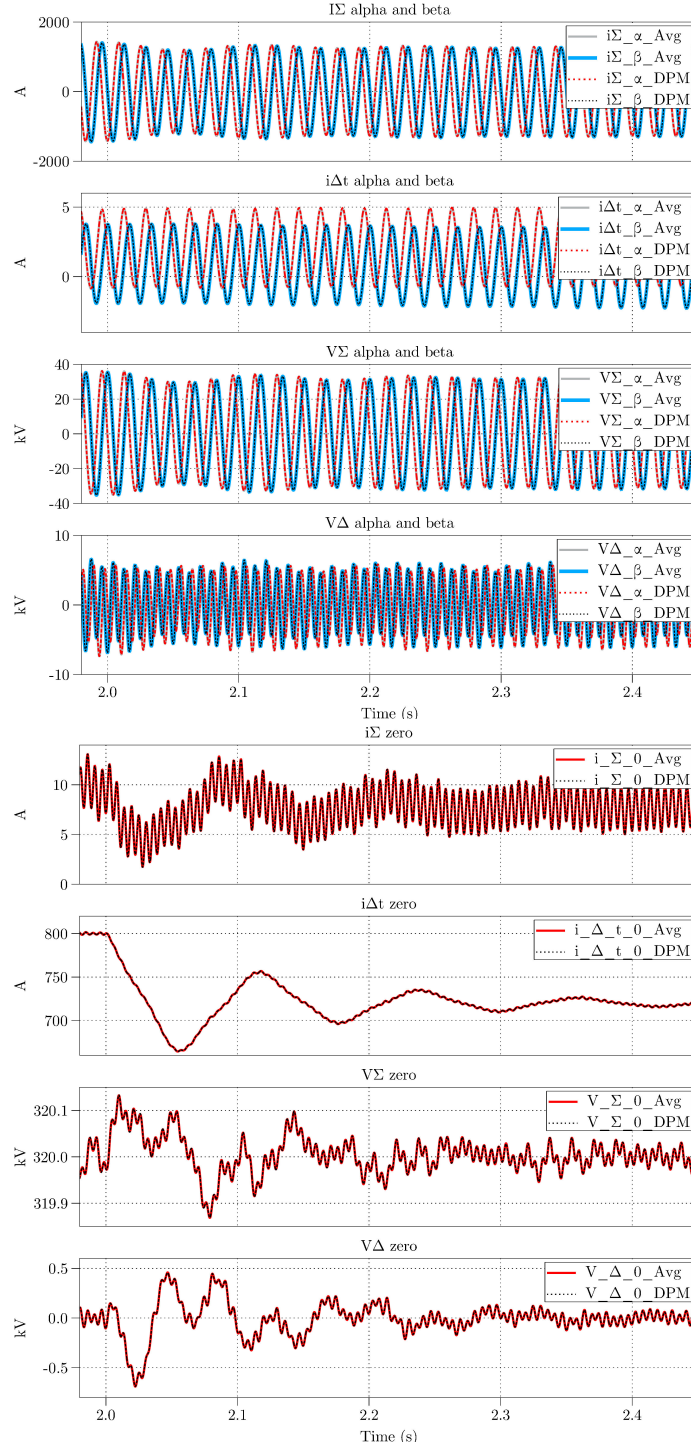


Figure 3.12: BP-DCDC; DPM and averaged model simulation results

Table 3.4: MP-DCDCAC State Variables Steady-State Comparison

State Variable	TAM	DPM	Percent Error
$i_{\Sigma\alpha}^1[A_pk]$	431.434	423.31	1.92%
$i_{\Delta g\alpha}^1[A_pk]$	976.73	983.829	0.72%
$V_{\Sigma\alpha}^1[kV_{pk}]$	5.18522	5.08545	1.96%
$V_{\Sigma\alpha}^2[kV_{pk}]$	3.02994	3.1145	2.72%
$V_{\Delta\alpha}^1[kV_{pk}]$	7.13196	7.28104	2.05%
$V_{\Delta\alpha}^2[kV_{pk}]$	2.48198	2.33423	6.33%
$i_{\Sigma 0}^{dc}[A]$	204.045	205.262	0.59%
$i_{\Delta t\alpha}^{dc}[A]$	403.964	399.974	1.00%
$V_{\Sigma 0}^{dc}[kV]$	399.998	400.002	0.00%

Table 3.5: MP-DCDC State Variables Steady-State Comparison

State Variable	TAM	DPM	Percent Error
$i_{\Sigma\alpha}^1[A_pk]$	1353.38	1353.01	0.03%
$V_{\Sigma\alpha}^1[kV_{pk}]$	25.4928	25.4843	0.03%
$V_{\Sigma\alpha}^2[kV_{pk}]$	1.12191	1.12269	0.07%
$V_{\Delta\alpha}^1[kV_{pk}]$	3.04729	3.04717	0.00%
$V_{\Delta\alpha}^2[kV_{pk}]$	4.65869	4.65561	0.07%
$i_{\Delta t0}^{dc}[A]$	800.296	800.291	0.00%
$V_{\Sigma 0}^{dc}[kV]$	400	400	0.00%

It can be noted that the DC/DC cases have excellent matching between models, and the DC/DC/AC is also very good; however, Appendix E shows the same operating points in which the capacitance is decreased. In the case of the DC/DC/AC conversion, the matching worsens with the decreased capacitance, and hence with increased capacitor

voltage ripple. The same does not occur with the DC/DC conversion cases, which suggests the accuracy of the model is not nearly as sensitive to capacitance selection. A reason for this could be the presence of decoupled harmonics in the AC/DC and DC/DC conversions that cross couple when DC/DC/AC conversion occurs. This suggests that, for an even more precise model for the DC/DC/AC conversion, a more comprehensive spectrum of harmonics has to be selected when developing the DPM beyond the frequencies considered in Equation (3.37) to Equation (3.50).

Table 3.6: BP-DCDCAC State Variables Steady-State Comparison

State Variable	Avg	DPM	Percent Error
$i_{\Sigma\alpha}^1[A_pk]$	663.555	661.217	0.35%
$i_{\Delta g\alpha}^1[A_pk]$	1569.41	1571.61	0.14%
$V_{\Sigma\alpha}^1[kV_{pk}]$	1.96597	1.8981	3.58%
$V_{\Sigma\alpha}^2[kV_{pk}]$	2.74241	2.85204	3.84%
$V_{\Delta\alpha}^1[kV_{pk}]$	5.155	5.18667	0.61%
$V_{\Delta\alpha}^2[kV_{pk}]$	2.2955	2.18447	5.08%
$i_{\Sigma 0}^{dc}[A]$	417.659	418.142	0.12%
$i_{\Delta t\alpha}^{dc}[A]$	801.887	800.001	0.24%
$V_{\Sigma 0}^{dc}[kV]$	400.009	400	0.00%

3.3 Chapter summary

In this chapter, two time-averaged state-space models were developed that can be used to represent the four converter structures in Figure 3.1a - Figure 3.1e. Two of the topologies are for DC/DC/AC conversion and the other two are for DC/DC conversion. The developed TAMs are time-variant and therefore solving for a steady-state operating

Table 3.7: BP-DCDC State Variables Steady-State Comparison

State Variable	Avg	DPM	Percent Error
$i_{\Sigma\alpha}^1[A_pk]$	1430.35	1430.11	0.02%
$V_{\Sigma\alpha}^1[kV_{pk}]$	35.423	35.4162	0.02%
$V_{\Sigma\alpha}^2[kV_{pk}]$	0.879617	0.880158	0.06%
$V_{\Delta\alpha}^1[kV_{pk}]$	1.11742	1.1147	0.24%
$V_{\Delta\alpha}^2[kV_{pk}]$	5.89186	5.88948	0.04%
$i_{\Delta t0}^{dc}[A]$	800.016	800.004	0.00%
$V_{\Sigma 0}^{dc}[kV]$	320	320	0.00%

point other than the trivial case of zero power transfer is not possible; moreover, classical linear state space analysis tools cannot be used given the states are time-varying. To overcome this challenge, two different multi-frequency DPMs in the alpha-beta-zero reference frame are developed from the TAMs that yield time-invariant states (i.e. DC-valued states) at steady state. The stationary reference frame is exploited as it helps decouple harmonic content within the converter.

The TAMs are validated against detailed switched converter models in the software PLECS, with excellent matching shown for all four converter structures, i.e., for both DC/DC/AC and DC/DC conversion. The DPMs are then validated against the TAMs with very good results demonstrated during both steady-state and dynamics. It was observed that the accuracy of the DPMs for DC/DC conversion is, for all practical purposes, insensitive to capacitive energy storage, while, interestingly, the accuracy of the DPMs for DC/DC/AC conversion is a function of converter internal stored energy. Therefore, capacitance selection for the DC/DC/AC models should ensure that a minimum amount of stored energy is maintained, otherwise, excessive capacitor voltage ripple will result, which can deteriorate the model accuracy.

Tables 3.8 and 3.9 provide a summary of the developed TAMs and DPMs, respectively.

Table 3.8: Summary of developed time-averaged models

Converter	State-Space Model	Model Matrices
MP-DCDCAC	Equation (3.31) • Set $L_2 = 0$, $R_2 = 0$	Appendix A
MP-DCDC	Equation (3.34) • Set $L_2 = 0$, $R_2 = 0$	Appendix B
BP-DCDCAC	Equation (3.31) • Set V_{dc1} as the sum of the two DC networks, and V_{dc2} as the second DC network • Set $L_t = 0$, $R_t = 0$	Appendix A
BP-DCDC	Equation (3.34) • Set V_{dc1} as the sum of the two DC networks, and V_{dc2} as the second DC network • Set $L_t = 0$, $R_t = 0$	Appendix B

Table 3.9: Summary of developed DPMs

Converter	State-Space Model	Model Matrices
MP-DCDCAC	Equation (3.57) • Set $L_2 = 0$, $R_2 = 0$	Appendix C
MP-DCDC	Equation (3.61) • Set $L_2 = 0$, $R_2 = 0$	Appendix D
BP-DCDCAC	Equation (3.57) • Set V_{dc1} as the sum of the two DC networks, and V_{dc2} as the second DC network • Set $L_t = 0$, $R_t = 0$	Appendix C
BP-DCDC	Equation (3.61) • Set V_{dc1} as the sum of the two DC networks, and V_{dc2} as the second DC network • Set $L_t = 0$, $R_t = 0$	Appendix D

Chapter 4

DC/DC/AC and DC/DC Converters Case Studies

In this chapter, a systematic solution procedure to obtain the modulating signals for a specified operating point for the two DC/DC/AC and the two DC/DC converters is firstly introduced. By using this algorithm, steady-state waveforms for each of the four converters are shown for different operating points, and an analysis of the converters' operation is given. Studies are carried out to examine the response of the converters to a step-change in one of the parameters.

4.1 DC/DC/AC Conversion

This section covers the systematic solution procedure and the studies carried out that relate to DC/DC/AC conversion.

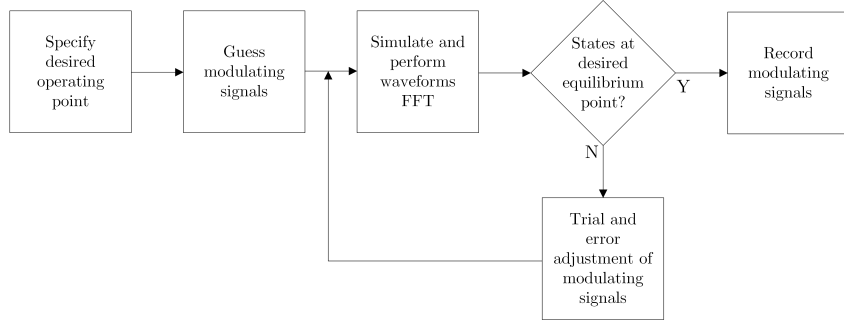


Figure 4.1: Process to obtain modulating signals using TAMs

4.1.1 Challenges in steady-state analysis using TAM

The TAMs developed in section 3.1 provide near perfect matching of the switched model of the generalised converter structure, and are useful for detailed converter dynamics analysis. To obtain the specific steady-state operating points in the converter, however, the TAMs are not directly useful, since their states are time-varying at steady-state and therefore analytically solving for $\frac{dx}{dt} = 0$ is not possible. Solving the TAM system of equations by setting the derivatives of the states to zero would only give the trivial answer of zero power flow between the ports. Moreover, the process of finding modulating signals for the TAMs would look something like the process shown in Figure 4.1, a process that doesn't give accurate results, and is extremely time consuming.

The states of the DPMs, on the other hand, are DC valued at steady-state, and are therefore ideal to use a solver to solve $\frac{dx}{dt} = 0$ for any desired operating point, including solving for the associated equilibria modulating signals.

4.1.2 Steady-State Solution Procedure

The simplest way to operate the converters, as shown in Section 3.1.5 and Section 3.2.3, is open loop modulation where fixed control inputs are used. This necessitates

the open loop modulating signals that yield the desired operating point to be known before running the simulation. To do this, a mathematical software such as Matlab, can be used to find the equilibrium point at which the system meets the specified criteria. This method is successfully applied in [70], [73].

The DPM allows solving for the desired open-loop steady-state control inputs, since the state variables are all constants at steady-state. This means that the system of differential equations that can be used to represent both DC/DC/AC converters, Equation (3.57), can be solved to obtain the control inputs by specifying that the derivatives of the states are zero, which can be represented as:

$$\begin{bmatrix} \tilde{A}_{11} & \tilde{A}_{12} \\ \tilde{A}_{21} & 0_{22 \times 22} \end{bmatrix} \begin{bmatrix} \tilde{\mathbf{X}}_i^* \\ \tilde{\mathbf{X}}_v^* \end{bmatrix} + \begin{bmatrix} \tilde{N} \\ 0_{22 \times 5} \end{bmatrix} [\tilde{\mathbf{W}}^*] = 0. \quad (4.1)$$

To solve a system of nonlinear equations, as the one shown in Equation (4.1), the number of unknown variables has to be equal to the number of equations. The system in Equation (4.1) contains 52 equations and 68 unknown variables (52 states, 6 disturbance terms, and 10 modulating signals), assuming that all converter design parameters have been specified.

The 6 disturbance terms, i.e. the external DC and AC port voltages, are specified by the desired operating point. Since the objective is to have all 10 modulating signals as outputs of the solution procedure, 10 of the other variables need to be specified. The 10 modulating signals, shown in Section 3.2.1 in Equation (3.51) - Equation (3.56), are given here in column vector format:

$$\mathbf{M} = \begin{bmatrix} M_{\Sigma\alpha}^{1||} & M_{\Sigma\alpha}^{1\perp} & M_{\Sigma\beta}^{1||} & M_{\Sigma\beta}^{1\perp} & M_{\Sigma 0}^{dc} & M_{\Delta\alpha}^{1||} & M_{\Delta\alpha}^{1\perp} & M_{\Delta\beta}^{1||} & M_{\Delta\beta}^{1\perp} & M_{\Delta 0}^{dc} \end{bmatrix}^T. \quad (4.2)$$

The solution procedure should yield modulating signals that produce balanced three-phase converter voltages and currents. For this to be accomplished, the eight modulating signals that are either α or β quantities, must satisfy the following constraints:

$$M_{\Sigma\alpha}^{1\parallel} = M_{\Sigma\beta}^{1\perp} \quad (4.3)$$

$$M_{\Delta\alpha}^{1\parallel} = M_{\Delta\beta}^{1\perp} \quad (4.4)$$

$$M_{\Sigma\alpha}^{1\perp} = - M_{\Sigma\beta}^{1\parallel} \quad (4.5)$$

$$M_{\Delta\alpha}^{1\perp} = - M_{\Delta\beta}^{1\parallel}. \quad (4.6)$$

Only one of the four relationships in Equations (4.3) to (4.6) needs to be explicitly specified, and the remaining three relationships will be an outcome of the solution procedure. As an example, both terms in Equation (4.3) can be set as being the same variable in the model. This forces the solver to provide balanced quantities for the other three sets of modulating signals, while simultaneously reducing the number of variables that need to be specified from 10 to 9.

The remaining 9 “free” variables can be specified in whatever way is convenient for the desired converter operation. In this work, for the purpose of DC/DC/AC conversion in both MP and BP structures, the 9 variables are specified as follows:

- $I_{\Sigma\alpha}^{1\perp}$ and $I_{\Sigma\beta}^{1\parallel}$: These two states partially comprise the first harmonic component of the circulating current i_{Σ} , responsible for capacitor charge balancing between arms. The desired operation of the converter includes no reactive power circulation

between the arms to maximise conversion efficiently, and therefore:

$$I_{\Sigma\alpha}^{1\perp} = I_{\Sigma\beta}^{1\parallel} = 0. \quad (4.7)$$

- $I_{\Sigma g\alpha}^{1\parallel}$ and $I_{\Sigma g\beta}^{1\perp}$: These two states are related to the real power flow into the AC port. These are set to achieve a desired P injection into the AC grid, $P_{ac,3\phi}$ as:¹

$$I_{\Sigma g\alpha}^{1\parallel} = I_{\Sigma g\beta}^{1\perp} = \sqrt{2} \frac{P_{ac,3\phi}}{\sqrt{3} \cdot V_{ac,LL,RMS}}. \quad (4.8)$$

- $I_{\Sigma g\alpha}^{1\perp}$ and $I_{\Sigma g\beta}^{1\parallel}$: These two states are related to the reactive power flow into the AC port. These are set to achieve a desired Q injection into the AC grid, $Q_{ac,3\phi}$, as¹:

$$I_{\Sigma g\alpha}^{1\perp} = -I_{\Sigma g\beta}^{1\parallel} = \sqrt{2} \frac{Q_{ac,3\phi}}{\sqrt{3} \cdot V_{ac,LL,RMS}}. \quad (4.9)$$

- $I_{\Delta t0}^{dc}$: Represents one third of the average current that will flow into the d_2 DC port, controlling the desired DC power flow into that port, P_{dc} , according to:

$$I_{\Delta t0}^{dc} = \frac{P_{dc,2}}{3 \cdot V_{dc,2}}. \quad (4.10)$$

- $\Sigma V_{\Sigma 0}^{dc}$ and $\Sigma V_{\Delta 0}^{dc}$: These states are specified to ensure balanced submodule capacitor voltages in the upper and lower arms, according to:

$$\Sigma V_{\Sigma 0}^{dc} = \frac{V_{cap}^{rated}}{2} (N_u + N_L) \quad (4.11)$$

$$\Sigma V_{\Delta 0}^{dc} = \frac{V_{cap}^{rated}}{2} (N_u - N_L). \quad (4.12)$$

¹Voltage $V_{ac,LL,RMS}$ is directly related to the peak AC grid voltage $\alpha\beta$ components contained in the W vector in Equation (4.1).

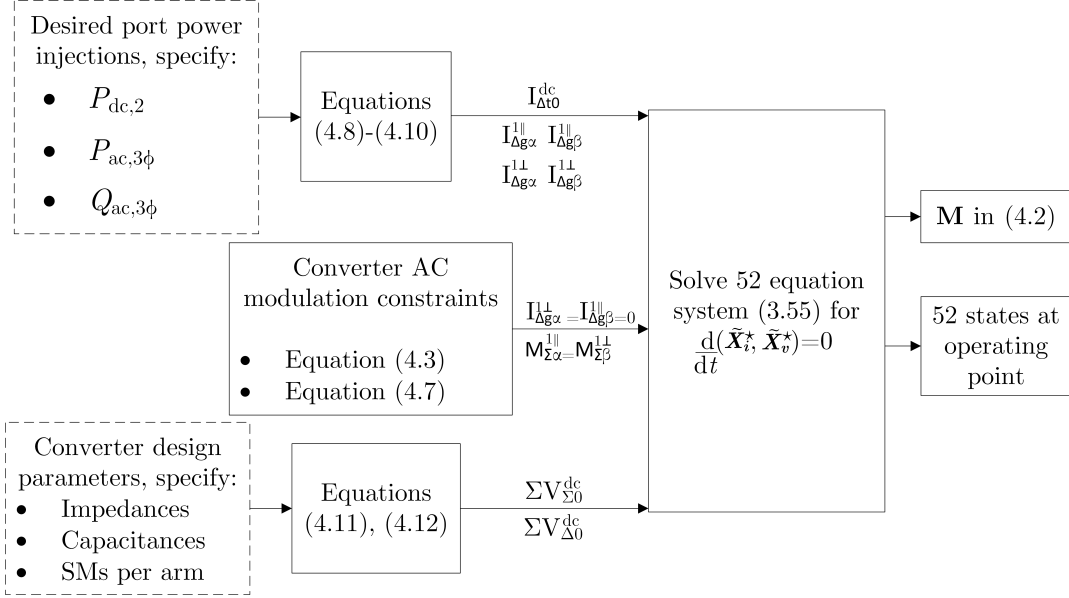


Figure 4.2: Solution procedure visualisation

Figure 4.2 provides a visualisation of the solution procedure. After specifying the nine values as shown, a mathematical solver such as Matlab can be used to solve the values for all the modulating signals that would provide the specified operating point, \mathbf{M} , which can be used to run the simulation of the converter.

Another advantage of the solution procedure is that it also outputs the values for all the other unspecified states at that equilibrium point. Those values can be used to systematically study the converters' steady-state operating point, as will be elaborated below.

4.1.3 MP-DCDCAC Steady-State Analysis

In this section, the solution procedure presented in Section 4.1.2 is used to find the modulating signals required to perform the simulations for six arbitrary steady-state operating points for the MP-DCDCAC converter. Figure 4.3 shows the MP-DCDCAC

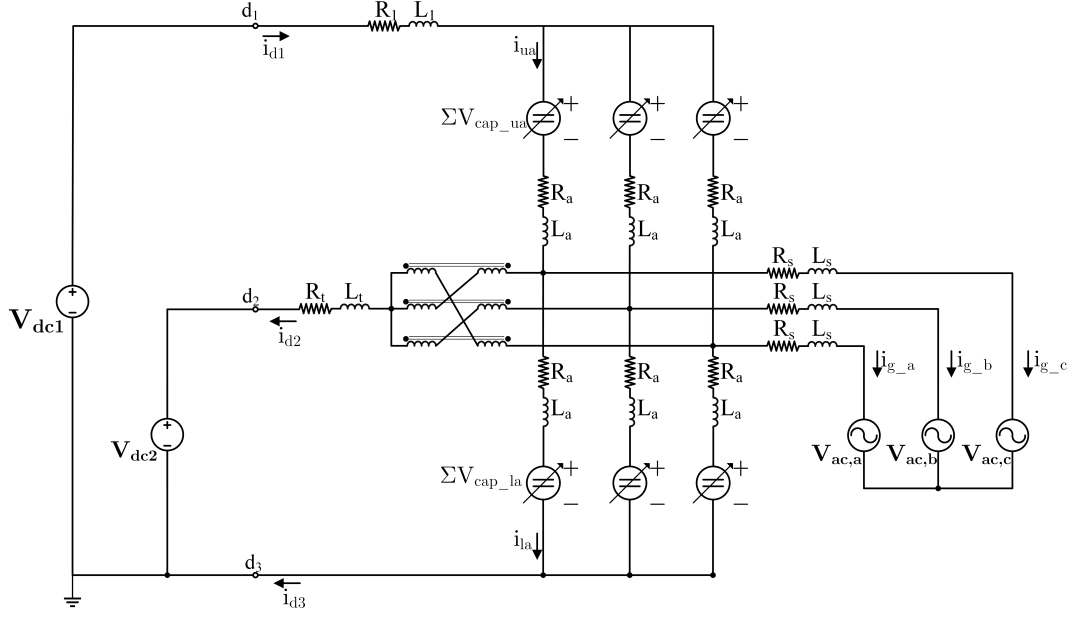


Figure 4.3: MP-DCDCAC converter with current direction convention

converter that is simulated using the DPM, including the conventions for the current directions. The first DC network, connected between ports d_1 and d_3 , will henceforth be named NW_1 ; in the same manner the network connected between ports d_2 and d_3 will be called NW_2 , and the AC network will be called NW_{ac} . The convention for the powers flows to each of the networks, i.e. $P_{dc,1}$, $P_{dc,2}$, and P_{ac} , is that a positive sign means that network is providing power to the converter. Because of these current flows, $P_{dc,1}$ and $P_{dc,2}$ can be defined as:

$$P_{dc,1} = V_{dc,1} \cdot i_{d1}^{dc} \quad (4.13)$$

$$P_{dc,2} = V_{dc,2} \cdot i_{d2}^{dc} \quad (4.14)$$

The MP-DCDCAC is rated for 480 MW, and for all six operating points the NW_1

voltage is set to $V_{dc1} = 400\text{kV}$. The NW_2 voltage, V_{dc1} , is set depending on the ratio G_v , introduced in Section 2.2 in Equation (2.19).

4.1.3.1 400/200kV ($G_v=0.5$) Converter Design

Figures 4.4 to 4.6 show the simulation waveforms for three different port power injections for the MP-DCDCAC at $G_v = 0.5$. The waveforms shown are the upper and lower phase a arm currents, the upper and lower phase a sum of capacitor voltages, the currents entering NW_{ac} , and the three DC port currents. The peak value of the $NW_{ac,L-N}$ voltages are set to 180 kV. Table 4.1 lists the parameters used for these simulations.

Figures 4.4 and 4.5 display simulation results where active power transfer between the external DC and AC systems is performed. Figure 4.4 shows a case where 1 pu power is being transferred from NW_1 to NW_2 and NW_{ac} , being split equally. Figure 4.5 shows a case in which NW_2 receives 1 pu power, while NW_1 and NW_{ac} provide 0.8 and 0.2 pu power, respectively. The DC power transfers are clearly visible through the DC ports currents. In both cases, the AC grid currents are comprised of first and second harmonic currents, being the latter much more noticeable in the second case, as the first harmonic content is much lower.

The first case presents an equal combination of P_Σ and P_Δ converter power transfer mechanisms, as expected from the explanation in Section 2.3, whereas the second case, which is mostly DC/DC conversion, shows P_Σ as the more prominent power transfer mechanism. In both cases, the capacitor voltages are balanced at 400 kV as desired. The third case, Figure 4.6, demonstrates zero power flow between the three networks. There is practically no current flowing through the DC and AC ports; however, a small amount of current is still circulating in the arms, to maintain a balance of the capacitor's voltages. The DC component of the arm capacitor voltages is 400 kV as expected.

Table 4.1: Simulation parameters for MP-DCDCAC using $G_v=0.5$

Parameter	Value
w	$2\pi 60$ rad/s
L_1, L_2, L_t, L_a, L_s	82 mH, 40 mH, 50 mH, 20 mH
L_e, L_m	9.8 mH, 28 H
R_1, R_2, R_t, R_a, R_s	2.1 Ω , 1 Ω , 0.4 Ω , 0.6 Ω
R_w	0.1 Ω
C_u, C_L	10 mF
N_u, N_L	200
Peak L - N V_{ac}	180 kV

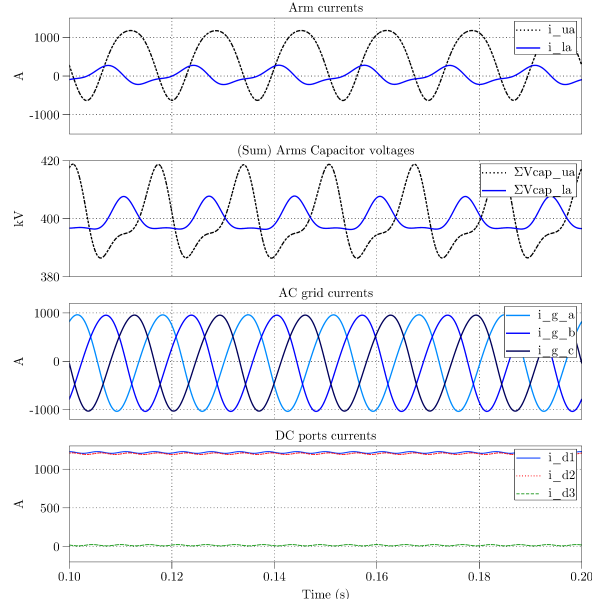


Figure 4.4: Steady-state MP-DCDCAC DPM waveforms for $G_v=0.5$ (400/200 kV); $P_{dc,1}=1$ pu, $P_{dc,2}=-0.5$ pu, $P_{ac}=-0.5$ pu

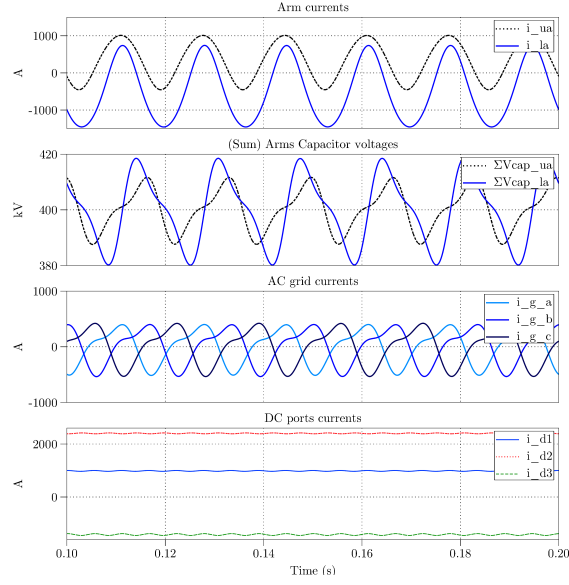


Figure 4.5: Steady-state MP-DCDCAC DPM waveforms for $G_v=0.5$ (400/200 kV); $P_{dc,1}=0.8$ pu, $P_{dc,2}=-1$ pu, $P_{ac}=0.2$ pu

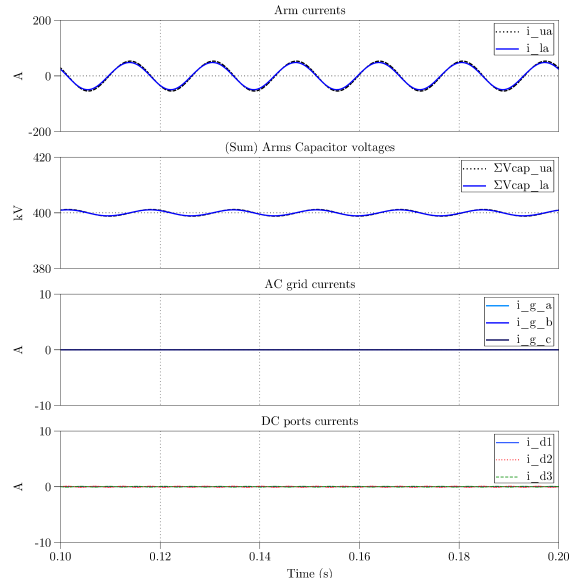


Figure 4.6: Steady-state MP-DCDCAC DPM waveforms for $G_v=0.5$ (400/200 kV); $P_{dc,1}=0$ pu, $P_{dc,2}=0$ pu, $P_{ac}=0$ pu

4.1.3.2 400/320kV ($G_v=0.8$) Converter Design

Figures 4.7 to 4.9 show similar port power injections for the MP-DCDCAC converter as Figures 4.4 to 4.6, but now utilising a DC voltage ratio $G_v=0.8$. These simulations demonstrate the capability of the DPM to utilize a different number of submodules for the upper and lower arms, contrasting to the previous three cases in the previous section, where they were equal. This means that the DC component of ΣV_{cap} at which the capacitor's voltage is balanced will be different for each arm in this section. The converter parameters used in this section are listed in Table 4.2. The number of submodules used in each arm are selected to support the maximum DC+AC voltages each arm will be subjected to, at 2 kV rated voltage for each submodule. This means that the DC component of ΣV_{cap} for the upper and lower arms is set to 160 and 400 kV, respectively, as dictated by Equation (4.11). The peak value of the $NW_{ac,L-N}$ voltages are set to 80 kV, since assuming the use of half-bridge submodules this is the maximum peak that can be synthesised by the arms.

In the case of equal splitting of the power between NW_2 and NW_{ac} , Figure 4.7 shows a common nmode DC component in the arms' currents not present in the 400/200 kV case, given that G_v is no longer 0.5, as expected by the information in Table 2.2, in Section 2.3. It can also be noted that, in this case, there is DC current exiting through the d_3 DC port, given the new voltage balancing requirements for this operation. The grid currents retain the expected first harmonic component behaviour that were present in the $G_v=0.5$ cases, although the second harmonic component is relatively much smaller. Once again, Figure 4.9 demonstrates the ability of the DPM to achieve a zero-power transfer operation, in which a small amount of AC average power is transferred between arms to maintain capacitor voltage balance, and a very small amount of third harmonic current can be seen in the DC ports.

Table 4.2: Simulation parameters for MP-DCDCAC using $G_v=0.8$

Parameter	Value
w	$2\pi 60$ rad/s
L_1, L_2, L_t, L_a, L_s	82 mH, 40 mH, 50 mH, 20 mH
L_e, L_m	9.8 mH, 28 H
R_1, R_2, R_t, R_a, R_s	2.1 Ω , 1 Ω , 0.4 Ω , 0.6 Ω
R_w	0.1 Ω
C_u, C_L	8 mF, 18 mF
N_u, N_L	80, 200
Peak L - N V_{ac}	80 kV

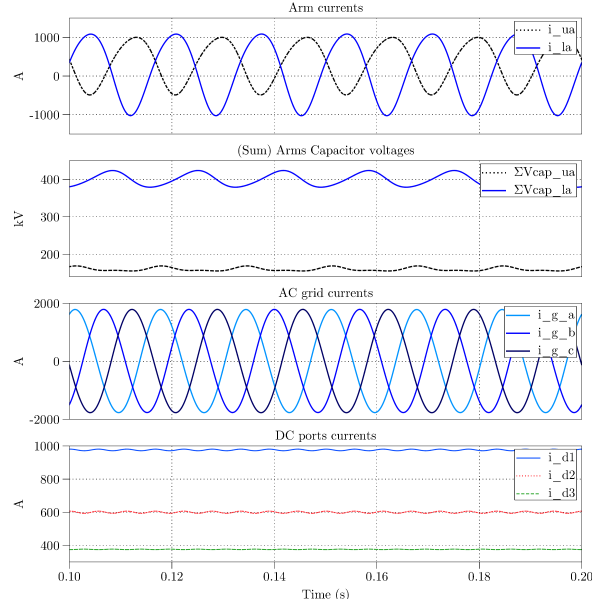


Figure 4.7: Steady-state MP-DCDCAC DPM waveforms for $G_v=0.8$ (400/320 kV); $P_{dc,1}=0.8$ pu, $P_{dc,2}=-0.4$ pu, $P_{ac}=-0.4$ pu

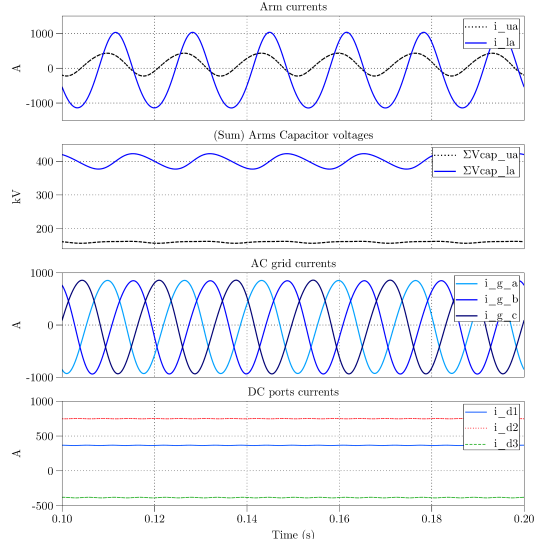


Figure 4.8: Steady-state MP-DCDCAC DPM waveforms for $G_v=0.8$ (400/320 kV); $P_{dc,1}=0.3$ pu, $P_{dc,2}=-0.5$ pu, $P_{ac}=0.2$ pu

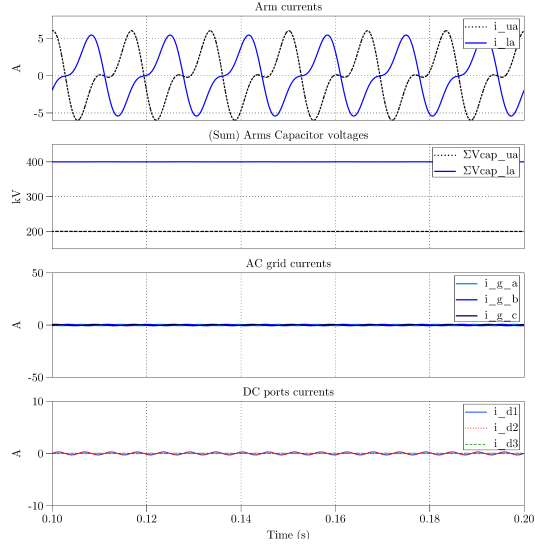


Figure 4.9: Steady-state MP-DCDCAC DPM waveforms for $G_v=0.8$ (400/320 kV); $P_{dc,1}=0$ pu, $P_{dc,2}=0$ pu, $P_{ac}=0$ pu

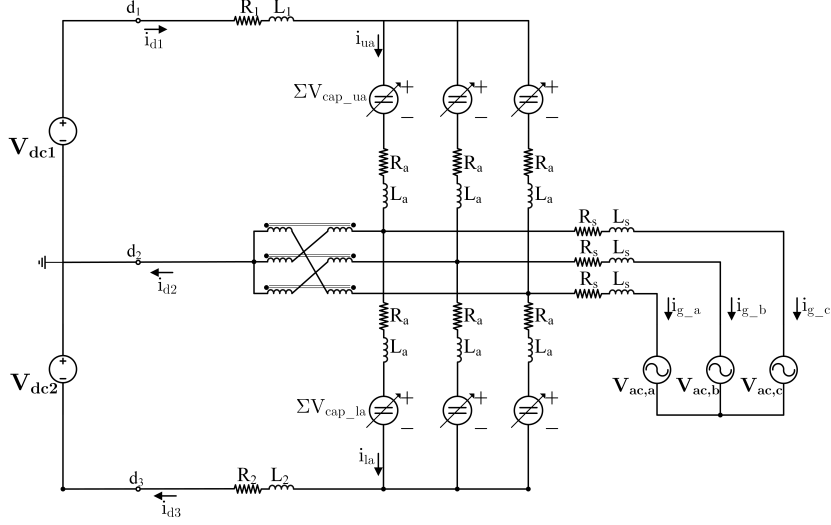


Figure 4.10: BP-DCDCAC converter with current direction convention

4.1.4 BP-DCDCAC Steady-State Analysis

In this section, the solution procedure presented in Section 4.1.2 is used to solve for the modulating signals required to enable open-loop simulations for three different steady-state operating points for the BP-DCDCAC converter. Figure 4.10 shows the BP-DCDCAC converter that is simulated using the DPM, including the conventions for the current directions. This topology is called bipolar because the DC port d_1 is at a positive potential and the DC port d_3 is at a negative potential, whereas in the MP topology d_1 and d_2 were at a positive potential, and d_3 was grounded.

The first DC network, connected between ports d_1 and d_2 , will henceforth be named NW_1 ; in the same manner the network connected between ports d_2 and d_3 will be called NW_2 , and the AC network will be called NW_{ac} . The convention for the powers flows to each of the networks, i.e. $P_{dc,1}$, $P_{dc,2}$, and P_{ac} , is that a positive sign means that network is providing power to the converter.

The BP-DCDCAC is rated for 768 MW, and this converter is ideal for interconnecting

two DC networks that operate at the same voltage level, i.e. bipolar grids. Because of this, for all three operating points, the voltages for NW_1 and NW_2 are set to 320 kV, while the peak value of the $NW_{ac,L-N}$ voltages are set to 320 kV.

It must be noted that a minor difference exists between how one of the specified variables in the solution procedure is set differently for the BP-DCDCAC compared to the MP-DCDCAC. The variable $I_{\Delta t0}^{dc}$ in Figure 4.2 does not represent the same port power transfer mechanism for the BP topology in Figure 4.10 as it did for the MP topology in Figure 4.3. For the latter, it was the average current that was exclusively injected into the second DC network. For the BP topology, $I_{\Delta t0}^{dc}$ represents the average current that flows into the common point between the two DC networks. Therefore, specifying this variable does not directly specify the power flowing in or out of the second DC network.

To address this situation, once again the $\Sigma\Delta$ domain is used to simplify the explanation and analysis of this conversion. Instead of having $P_{dc,1}$ and $P_{dc,2}$ to express the powers in and out of the first and second DC networks, $P_{dc,\Sigma}$ and $P_{dc,\Delta}$ are used to represent the common mode and differential mode of the powers exchanged between the DC networks themselves, respectively. The mapping between these quantities is defined as:

$$\begin{bmatrix} P_{dc,\Sigma} \\ P_{dc,\Delta} \end{bmatrix} = \begin{bmatrix} 1 & 1 \\ 1 & -1 \end{bmatrix} \begin{bmatrix} P_{dc,1} \\ P_{dc,2} \end{bmatrix} \quad (4.15)$$

Given the DC current common to all three converter's legs, i.e. $3 \cdot I_{\Sigma 0}^{dc}$, and assuming both DC networks have the same voltage level, i.e. $V_{dc1} = V_{dc2} = V_{dc}$, $P_{dc,\Sigma}$ and $P_{dc,\Delta}$ can also be defined as:

$$P_{dc,\Sigma} = 2(3 \cdot I_{\Sigma 0}^{dc})V_{dc} \quad (4.16)$$

$$P_{dc,\Delta} = I_{\Delta t 0}^{dc} \cdot V_{dc} \quad (4.17)$$

Since $I_{\Delta t 0}^{dc}$ is proportional to $P_{dc,\Delta}$ and $I_{\Sigma 0}^{dc}$ is proportional to $P_{dc,\Sigma}$, it is now easy to set in the solution procedure $P_{dc,\Delta}$ through $I_{\Delta t 0}^{dc}$, and have $I_{\Sigma 0}^{dc}$ be an outcome that will set $P_{dc,\Sigma}$. The parameters of the converter used for these simulations are shown in Table 4.3.

Table 4.3: Simulation parameters for BP-DCDCAC

Parameter	Value
w	$2\pi 60$ rad/s
L_1, L_2, L_t, L_a, L_s	82 mH, 82 mH, 50 mH, 20 mH
L_e, L_m	9.8 mH, 28 H
R_1, R_2, R_t, R_a, R_s	2.1 Ω , 2.1 Ω , 0.4 Ω , 0.6 Ω , 0.1 Ω
R_w	0.1 Ω
C_u, C_L	10 mF
N_u, N_L	320

4.1.4.1 320/320kV ($G_v=1$) Converter Design

Figures 4.11 to 4.14 show the waveforms for four different port power injections for the BP-DCDCAC. The waveforms shown are the upper and lower phase a arm currents, the upper and lower phase a sum of capacitor voltages, the currents entering NW_{ac} , and the three DC port currents. The last plot also includes the current $3(I_{\Sigma 0}^{dc})$, as it can be of use to understand the powers being transferred between ports for this converter.

Figure 4.11 presents a case in which NW_1 and NW_2 each supply 0.5 pu power (col-

lectively 1 pu) to the NW_{ac} . This case is analogous to a conventional AC/DC converter, and the waveforms are what would be expected of such a conversion. For example, the arms contain large negative sequence second harmonic component that sums to zero at the DC rails. It is interesting to note that, out of all operating points presented in this chapter, this is the only one in which the currents in NW_{ac} do not present a second harmonic component, possibly due to the fact that no DC/DC conversion is occurring.

Figures 4.12 and 4.13 show the simulation waveforms for the operating points in which the power transfers are $P_{dc,1}=0.25$ pu, $P_{dc,2}=-0.5$ pu, $P_{ac}=0.25$ pu and $P_{dc,1}=-0.6$ pu, $P_{dc,2}=0.5$ pu, $P_{ac}=0.1$ pu, respectively. Both present the arms' currents and voltages harmonic spectrum that are expected from both theory and the results of the MP-DCDCAC converter for simultaneous DC/DC/AC conversion. The grid currents are a combination of first and second harmonic, and the converter presents both P_{Σ} and P_{Δ} power transfer mechanisms, the latter being much more noticeable in the case shown in Figure 4.13, as DC/DC conversion is the dominant conversion in this case. It is also interesting noting the inversion of DC currents sign between the two cases, given both DC networks switching their operation, be it providing or receiving power.

Figure 4.14, as with the MP-DCDCAC, demonstrates zero power flow between the three networks. The results are similar to the zero-power flow case of the previous section, noting the small amount of first and second harmonic current in the arms to maintain the capacitor's voltage balance, and the small third harmonic current in all DC port currents. In all cases, the capacitor voltages are balanced at 640 kV, as desired.

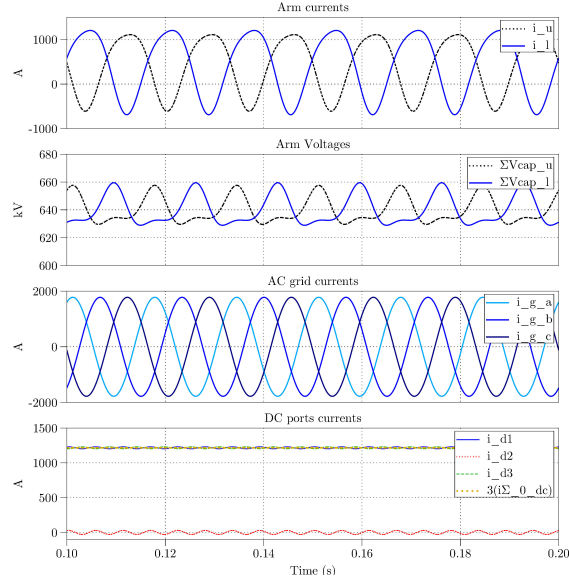


Figure 4.11: Steady-state BP-DCDCAC DPM waveforms; $P_{dc,1}=0.5$ pu, $P_{dc,2}=0.5$ pu, $P_{ac}=-1$ pu

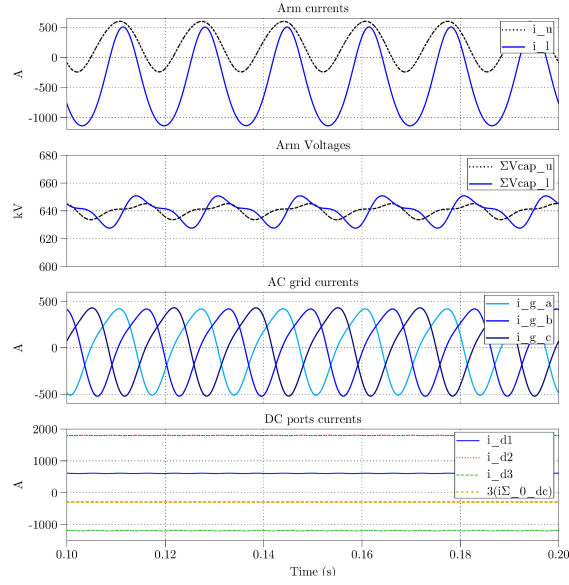


Figure 4.12: Steady-state BP-DCDCAC DPM waveforms; $P_{dc,1}=0.25$ pu, $P_{dc,2}=-0.5$ pu, $P_{ac}=0.25$ pu

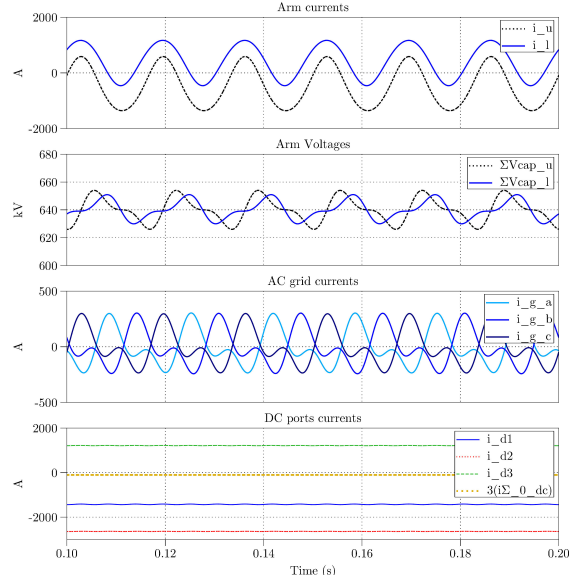


Figure 4.13: Steady-state BP-DCDCAC DPM waveforms; $P_{dc,1}=-0.6$ pu, $P_{dc,2}=0.5$ pu, $P_{ac}=0.1$ pu

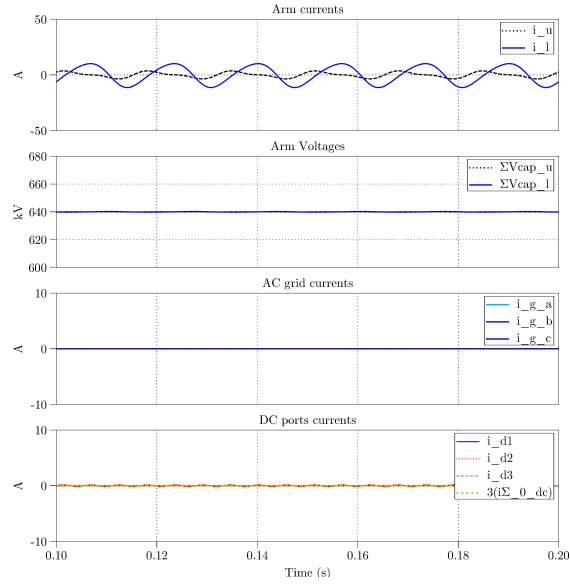


Figure 4.14: Steady-state BP-DCDCAC DPM waveforms; $P_{dc,1}=0$ pu, $P_{dc,2}=0$ pu, $P_{ac}=0$ pu

4.1.5 Varying Parameters Studies

Another useful application for the DPM in Equation (4.1) and solution procedure developed in section Section 4.1.2 is that it can be used to explore the converters' behaviour in response to changing parameters. This can be accomplished by running the solution procedure many times while step-varying one or several of the specified quantities, and collecting the data of interest in each iteration. This section presents a few examples of this use for the MP-DCDCAC converter of section Section 4.1.3, for $G_v=0.5$ and $G_v=0.8$, utilising the parameters of Table 4.1.

Figure 4.15(a) and (b) show how the peak current stress and the percent capacitors voltage peak-to-peak ripple in the upper and lower phase a arms, respectively, change while varying the power flow into NW_2 while having 0.5 pu fixed power flow into NW_{ac} , meaning that power out of NW_1 changes accordingly, for $G_v=0.5$. Figure 4.15(c) and (d) carry out the same analysis but having 1 pu fixed power provided by NW_1 , and varying it from 1 pu into NW_2 , to 1 pu into NW_{ac} , meaning that in all instances $P_{dc,2} + P_{ac}=1$. Figure 4.15(a) and (c) present the peak arms' currents in two ways: (i) only the DC components and (ii) DC plus AC components. The DC only curves are useful to visualise average power transfers. Also, the difference between these two curves is the AC stress. Figure 4.15(a) shows that in both extremes of the graph the arms' peak current stress is caused only by AC components, at -0.5 pu power flow to the NW_2 for the upper arm and 0.5 pu for the lower arm. Figure 4.15(c) demonstrates how the arms are subjected to a different stress pattern than in Figure 4.15(a), given that in this case the upper arm is always processing 1 pu power from NW_1 . The voltage ripple in the arms' capacitors in Figure 4.15(b) and (d) resemble the shape of their respective arms' currents. The converters are usually designed to keep this peak-to-peak ripple below 10%, meaning that the full loading operation of this converter might require the choosing of the capacitors

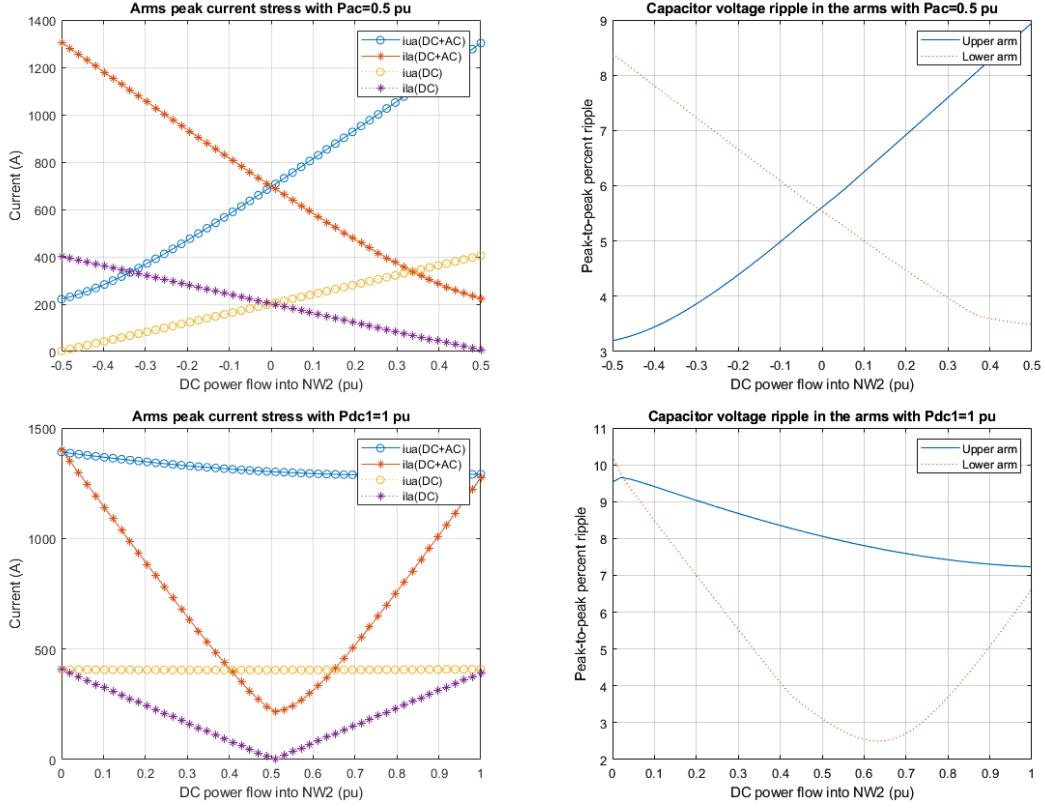


Figure 4.15: Loci of steady-state studies for $G_v=0.5$ for the phase a upper and lower arms: (a) arms' peak current stress with $P_{ac}=0.5$ pu; (b) percent capacitor voltage ripple with $P_{ac}=0.5$; (c) arms' peak current stress with $P_{dc1}=1$ pu; (d) percent capacitor voltage ripple with $P_{dc1}=1$ pu

to be above the $50 \frac{kJ}{MW}$ energy storage selected for these studies.

Figure 4.16 shows the studies presented in Figure 4.15 but with $G_v=0.8$, as discussed in section 4.1.2.2. The patterns of the loci are similar in both sets, as they tell of the behaviour of the converter in those situations. The biggest differences can be found in that the lines for the upper and lower arms no longer intersect in the middle of the graphs for the $P_{ac}=0.5$ cases, and a shift towards the right side of the graph in the $P_{dc1}=1$ pu cases for the quantities representing the lower arm. All four figures demonstrate how

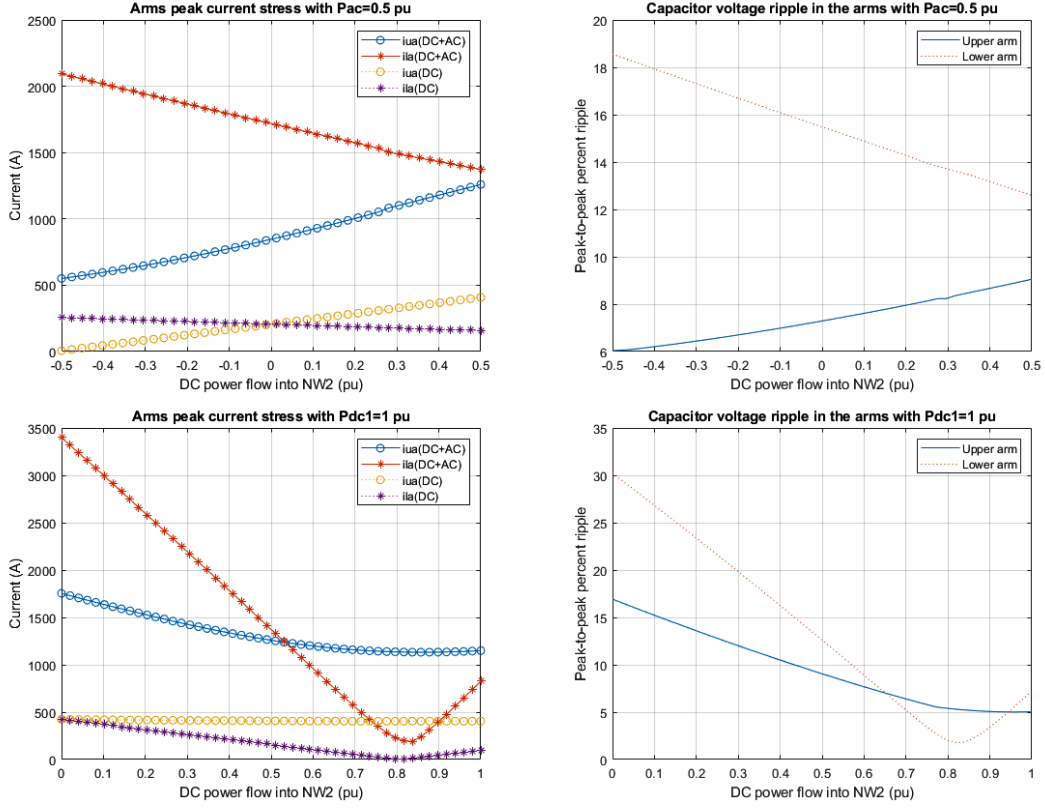


Figure 4.16: Loci of steady-state studies for $G_v=0.8$ for the phase a upper and lower arms: (a) arms' peak current stress with $P_{ac}=0.5$ pu; (b) percent capacitor voltage ripple with $P_{ac}=0.5$; (c) arms' peak current stress with $P_{dc1}=1$ pu; (d) percent capacitor voltage ripple with $P_{dc1}=1$ pu

this converter design is impacted by the limited AC voltage available with half-bridge submodules in this case, since a very high current is required to satisfy the power flows. Figure 4.16(a) shows the stress in the lower arm is very high when the power flows only from NW_2 to NW_{ac} , while a similar thing is shown in Figure 4.16(c) when the power flows from NW_1 to NW_{ac} . Figure 4.16(b) and (d) demonstrate the high peak-to-peak voltage ripple in the arms in the same cases. This information can be used to take decisions during the converter design as to whether prevent these scenarios of high current stress,

or perhaps employ full-bridge submodules in the upper arm.

4.2 DC/DC Conversion

This section covers the solution procedure, steady-state operating point analyses, and varying parameters studies for the DC/DC converters.

4.2.1 Steady-State Solution Procedure

The system of differential equations that can be used to represent both DC/DC converters, originally presented in Section 3.2.2 as Equation (3.61), is represented here as:

$$\begin{bmatrix} \tilde{A}_{11r} & \tilde{A}_{12r} \\ \tilde{A}_{21r} & 0_{22 \times 22} \end{bmatrix} \begin{bmatrix} \widetilde{\mathbf{X}}_{ir}^* \\ \widetilde{\mathbf{X}}_{vr}^* \end{bmatrix} + \begin{bmatrix} \tilde{N}_r \\ 0_{22 \times 5} \end{bmatrix} \begin{bmatrix} \widetilde{\mathbf{W}}_r^* \end{bmatrix} = 0 \quad (4.18)$$

The derivatives of the states are set to zero in Equation (4.18), as this is the objective of the solver to obtain the modulating signals which serve as control inputs for the simulations. The solution procedure for the DC/DC converters is the same as the one presented in section 4.1.2 for the DC/DC/AC converters, the only difference being that the system in Equation (4.18) now contains 44 equations and 56 unknown variables (44 states, 2 disturbance terms, and 10 modulating signals), assuming that all converter design parameters have been specified.

The disturbance terms, i.e. external DC port voltages, are specified by the desired operating point. Once again, the objective is to have all 10 modulating signals as outputs of the solution procedure, which again requires 10 specified terms. The difference in this case is that the four AC grid parameters that were being specified for the DC/DC/AC,

Equations (4.8) and (4.9), can no longer be specified given the lack of an AC port. One way to reduce the number of variables that need to be specified is to use the remaining three relationships presented in section 4.1.2, equations Equations (4.4) to (4.6), since only Equation (4.3) was used in the DC/DC/AC solution procedure, reducing the number of unknowns to 11, only requiring one more to be specified.

To solve this, a constraint in the form of one more differential equation is added to the system in Equation (4.18), given by:

$$(V_{\Sigma 0}^{dc} + V_{\Delta t 0}^{dc})(M_{\Sigma \alpha}^{1\parallel} + M_{\Delta \alpha}^{1\parallel}) - \hat{V}_{\Delta ac} = 0 \quad (4.19)$$

Equation (4.19) provides a constraint in the possible values of $M_{\Sigma \alpha}^{1\parallel}$ and $M_{\Delta \alpha}^{1\parallel}$, by stressing that the parallel component of the upper arm's AC voltage has to be collinear with the reference vector (0°). The rest of the specified values are the same as the ones given in Figure 4.2.

4.2.2 MP-DCDC Steady-State Analysis

In this section, the solution procedure explained in section 4.2.1 is used to find the modulating signals required to perform the simulations for six different steady-state operating points for the MP-DCDC converter. Figure 4.17 shows the MP-DCDC converter that is simulated using the DPM, including the conventions for the current directions. The first DC network, connected between ports d_1 and d_3 , will henceforth be named NW_1 ; in the same manner the network connected between ports d_2 and d_3 will be called NW_2 . Since in these converters only two networks are present, the definition of the operating points only provides the power being supplied by NW_1 , $P_{dc,1}$, and a positive sign means NW_1 is supplying power.

The MP-DCDC is rated for 480 MW, and the voltages for corresponding to the DC

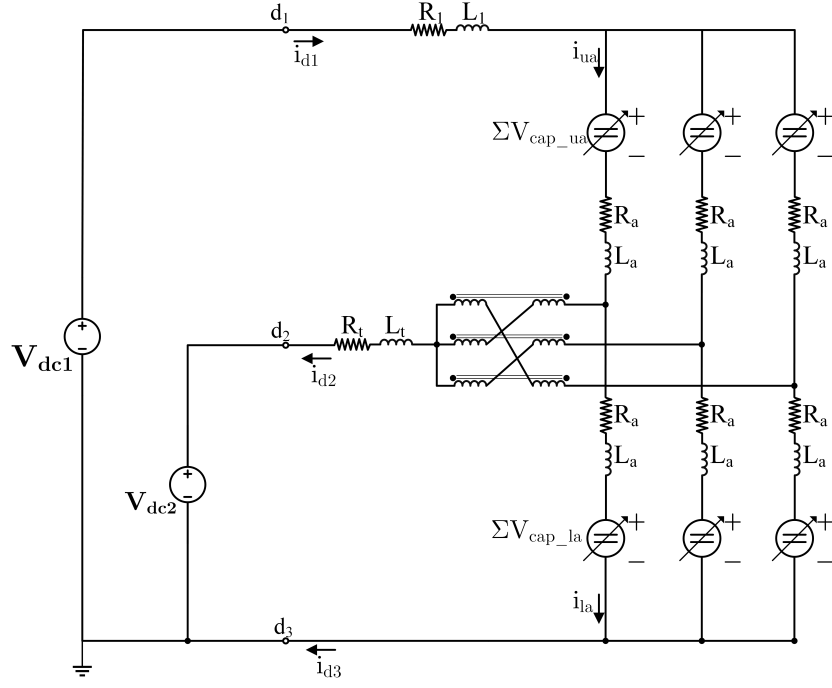


Figure 4.17: MP-DCDC converter with current direction convention

ports NW_1 to NW_2 vary in the different G_v scenarios.

4.2.2.1 500/250kV ($G_v=0.5$) Converter Design

Figures 4.18 to 4.20 show the simulation waveforms for three different port power injections, $P_{dc,1}=1$ pu, $P_{dc,1}=-1$ pu, and $P_{dc,1}=0$ pu, for the MP-DCDC at $G_v=0.5$. The waveforms shown are the upper and lower phase a arm currents, the upper and lower phase a sum of capacitor voltages, and the three DC port currents. Table 4.4 provides the parameters used for these simulations.

Figures 4.18 and 4.19 demonstrate active power transfer between the DC ports, as it can be appreciated by the DC port currents. The common mode arm's current is exclusively AC current, while the differential mode current is exclusively DC, as expected.

Since this is DC/DC conversion under $G_v=0.5$, the DC component of both arms' currents is the same value, around 320 A, but opposite signs for upper and lower arms. Figure 4.20 demonstrates a situation of no power being exchanged between DC ports, and the only visible waveform is a small AC component in the arms' currents to maintain capacitor voltage balance. In all cases, the capacitor voltages are balanced at 500 kV as desired.

Table 4.4: Simulation parameters for MP-DCDC using $G_v=0.5$

Parameter	Value
w	$2\pi 60$ rad/s
L_1, L_2, L_t, L_a, L_s	82 mH, 40 mH, 50 mH, 20 mH
L_e, L_m	9.8 mH, 28 H
R_1, R_2, R_t, R_a, R_s	2.1 Ω , 1 Ω , 0.4 Ω , 0.6 Ω
R_w	0.1 Ω
C_u, C_L	8 mF
N_u, N_L	250

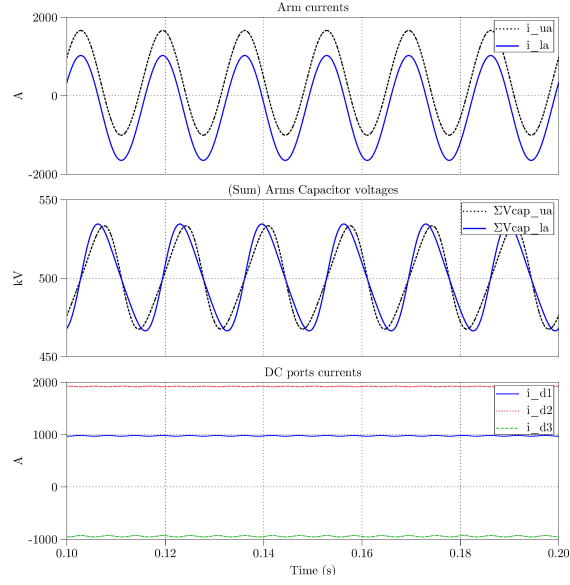


Figure 4.18: Steady-state MP-DCDC DPM waveforms for $G_v=0.5$ (500/250 kV); $P_{dc,1}=1$ pu

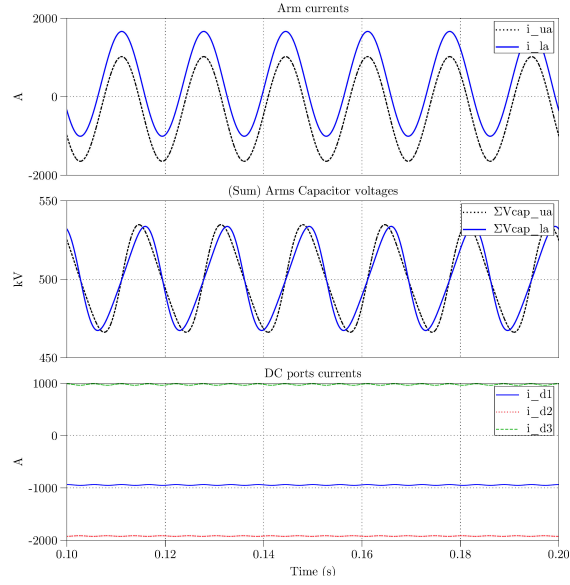


Figure 4.19: Steady-state MP-DCDC DPM waveforms for $G_v=0.5$ (500/250 kV); $P_{dc,1}=-1$ pu

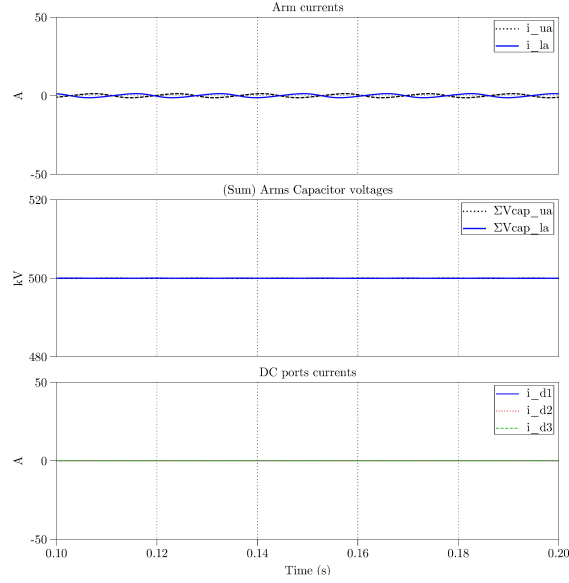


Figure 4.20: Steady-state MP-DCDC DPM waveforms for $G_v=0.5$ (500/250 kV); $P_{dc,1}=0$ pu

4.2.2.2 400/320kV ($G_v=0.8$) Converter Design

Figures 4.21 to 4.23 show the same port power injections for the MP-DCDC converter as Figures 4.18 to 4.20, but now utilising $G_v=0.8$. The waveforms shown are the upper and lower phase a arm currents, the upper and lower phase a sum of capacitor voltages, and the three DC port currents. Table 4.5 provides the parameters used for these simulations.

Figures 4.21 and 4.22 show cases with active power transfer between DC ports. As in the waveforms in the previous section, the arms' currents differential mode current is exclusively DC, however in these cases there is also a DC component in the common mode current. This corresponds with the information in Table 2.2, in Section 2.3, where it was stated that a DC common mode current would exist if $G_v \neq 0.5$. A very small component of third harmonic current is present in the arms' currents and voltages, a

component often neglected in the phasor modelling of DC/DC converters, as its effect is almost negligible. Figure 4.23 demonstrates a situation of no power being exchanged between DC ports, and only AC current in the arms to maintain capacitor voltage balance is noticeable. In contrast to simulations in Section 4.1, the DC port currents show no sign of third harmonic current in the zero-power transfer scenario. In all cases, the capacitor voltages are balanced at 160 and 400 kV for the upper and lower arms, respectively, as desired.

Table 4.5: Simulation parameters for MP-DCDC using $G_v=0.8$

Parameter	Value
w	$2\pi 60$ rad/s
L_1, L_2, L_t, L_a, L_s	82 mH, 40 mH, 50 mH, 20 mH
L_e, L_m	9.8 mH, 28 H
R_1, R_2, R_t, R_a, R_s	2.1 Ω , 1 Ω , 0.4 Ω , 0.6 Ω
R_w	0.1 Ω
C_u, C_L	12 mF, 14 mF
N_u, N_L	80, 200

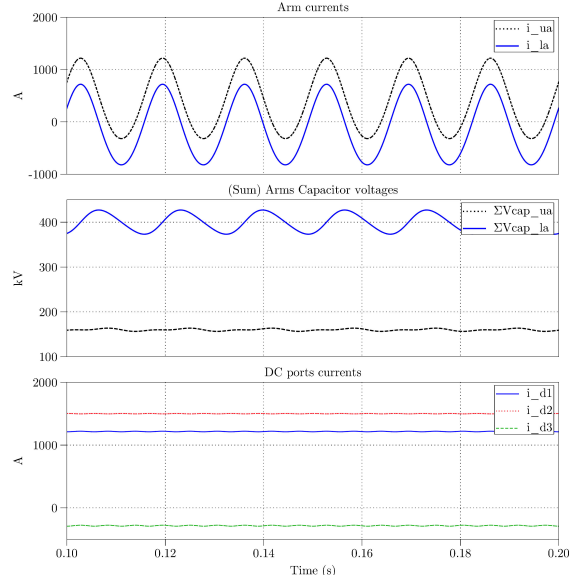


Figure 4.21: Steady-state MP-DCDC DPM waveforms for $G_v=0.8$ (400/320 kV); $P_{dc,1}=1$ pu

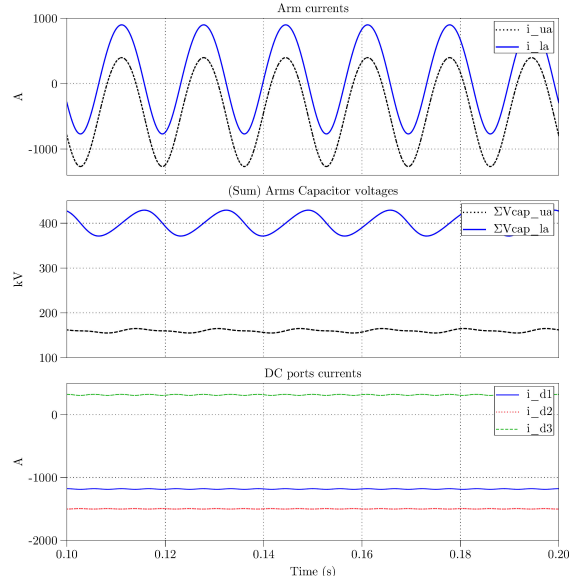


Figure 4.22: Steady-state MP-DCDC DPM waveforms for $G_v=0.8$ (400/320 kV); $P_{dc,1}=-1$ pu

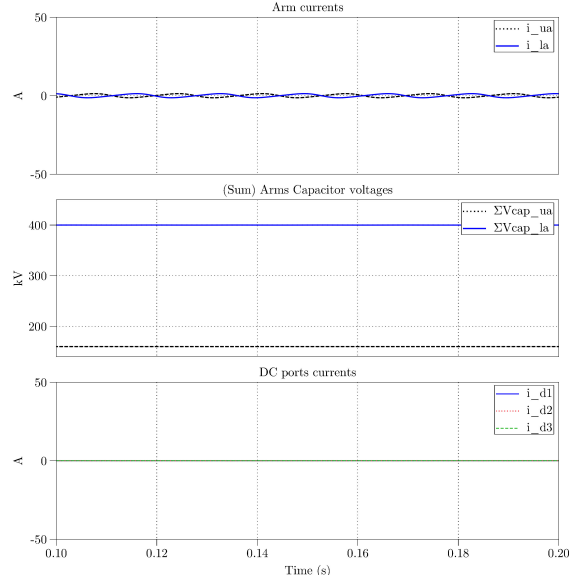


Figure 4.23: Steady-state MP-DCDC DPM waveforms for $G_v=0.8$ (400/320 kV); $P_{dc,1}=0$ pu

4.2.3 BP-DCDC Steady-State Analysis

In this section, the DC/DC solution procedure presented in Section 4.2.1 is used to solve for the modulating signals required to enable open-loop simulations for three different steady-state operating points for the BP-DCDCAC converter. Figure 4.24 shows the BP-DCDC converter that is simulated using the DPM, including the conventions for the current directions. This converter topology can be considered as an inverting topology, contrasting with the more common DC/DC conversion in which the DC networks are linked by non-inverting topologies [19], [33], [34]. The inverting DC-DC topology in Figure 4.3 (without the AC port) is used as the core building block of the multiport DC/DC converter in [9].

The BP-DCDC is rated for 384 MW. For all three operating points the voltages for NW_1 and NW_2 are set to 320 kV, consistent with a bipolar DC grid application.

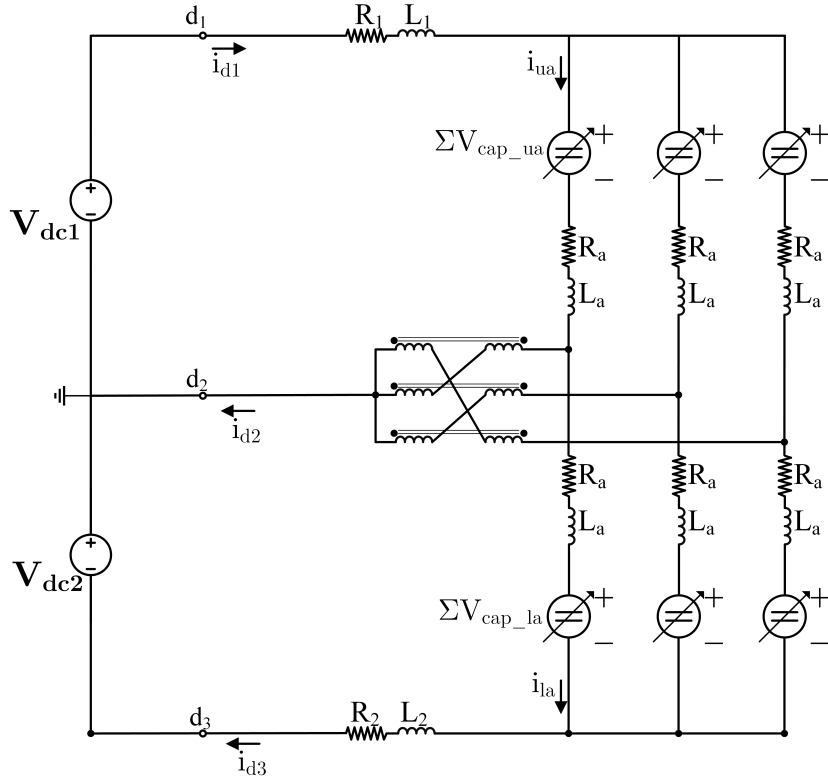


Figure 4.24: BP-DCDC converter with current direction convention

Table 4.6: Simulation parameters for BP-DCDC

Parameter	Value
w	$2\pi 60$ rad/s
L_1, L_2, L_t, L_a, L_s	82 mH, 82 mH, 50 mH, 20 mH
L_e, L_m	9.8 mH, 28 H
R_1, R_2, R_t, R_a, R_s	2.1 Ω , 2.1 Ω , 0.4 Ω , 0.6 Ω , 0.1 Ω
R_w	0.1 Ω
C_u, C_L	8 mF
N_u, N_L	320

The differences between the solution procedure of the MP-DCDCAC and BP-DCDCAC explained in Section 4.1.4 apply here as well. Table 4.6 shows the parameters used in these simulations.

4.2.3.1 320/320kV ($G_v=1$) Converter Design

Figures 4.25 to 4.27 show the same port power injections for the BP-DCDC as the cases for the MP-DCDC. The waveforms shown are the upper and lower phase a arm currents, the upper and lower phase a sum of capacitor voltages, and the three DC port currents. Table 4.6 provides the parameters used for these simulations.

Figures 4.25 and 4.26 show the scenarios where full pu power is being transferred from NW_1 to NW_2 and the reversed operation, respectively. As in the previous cases in this DC/DC conversion section, the waveforms in these two cases are mirrored, demonstrating bidirectional power flow. It's interesting to note that in both cases the term $3(I_{\Sigma 0}^{dc})$ is zero. As mentioned in Section 2.3, DC/DC conversion requires only P_{Δ} as power transfer mechanism, and contrasting to the simulations for the BP-DCDCAC converter, $I_{\Sigma 0}^{dc}$ has no effect in this conversion. This means that P_{Δ} alone, and by extension id_2 , can explain which network is supplying and which one is receiving power.

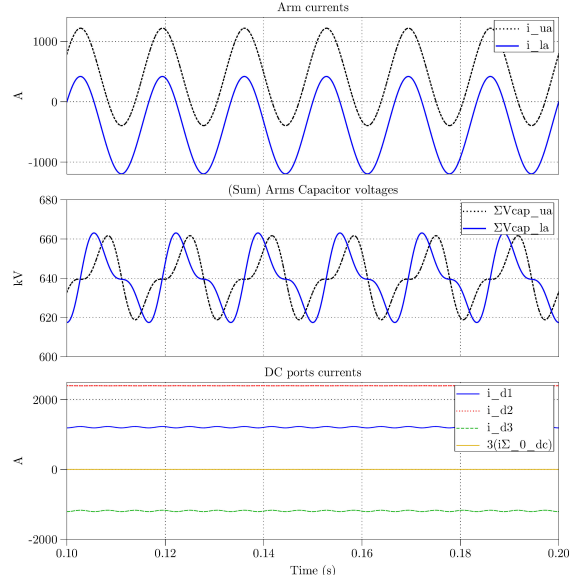


Figure 4.25: Steady-state BP-DCDC DPM waveforms for $G_v=1$ (320/320 kV); $P_{dc,1} = 1$ pu

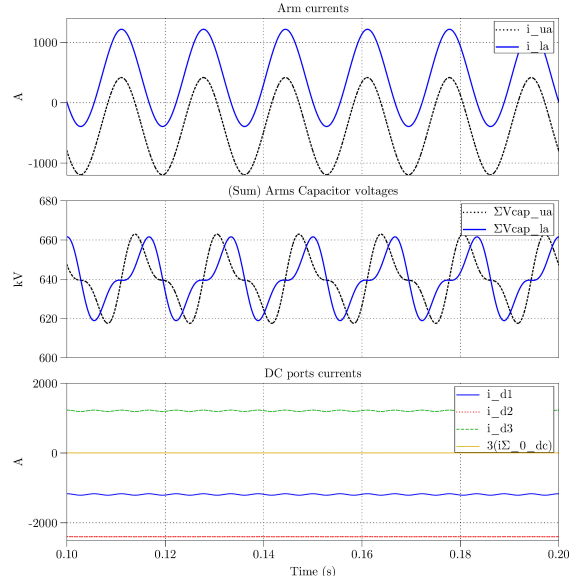


Figure 4.26: Steady-state BP-DCDC DPM waveforms for $G_v=1$ (320/320 kV); $P_{dc,1} = -1$ pu

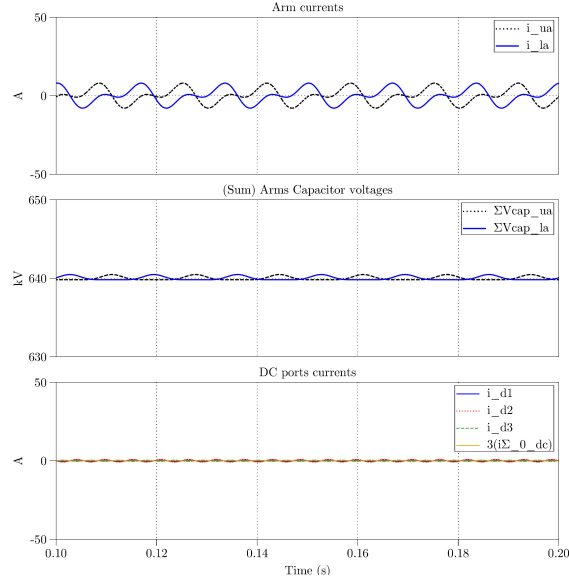


Figure 4.27: Steady-state BP-DCDC DPM waveforms for $G_v=1$ (320/320 kV); $P_{dc,1} = 0$ pu

4.2.4 Varying Parameters Studies

As in Section 4.1.4, the DPM in equation Equation (4.18) and the revised solution procedure is here used to demonstrate the converter's behaviour in response to changing parameters. This section presents a few examples of this use for the MP-DCDC converter of Section 4.2.2, for $G_v=0.5$ and $G_v=0.8$, utilising the parameters of Table 4.4 for the $G_v=0.5$ and Table 4.5 for the $G_v=0.8$ cases.

Figure 4.28 shows the four studies performed in this section, in all of them the power flow is varied from 1 pu power received by NW_1 to 1 pu power received by NW_2 . Figure 4.28(a) and (b) demonstrate how the peak current stress and the percent capacitors voltage peak-to-peak ripple in the upper and lower phase a arms, respectively, change while varying the power flow, at a ratio of $G_v=0.5$. These plots show symmetry about the $P_{dc,1}=0$ operating point, which is expected according to the literature in DC/DC

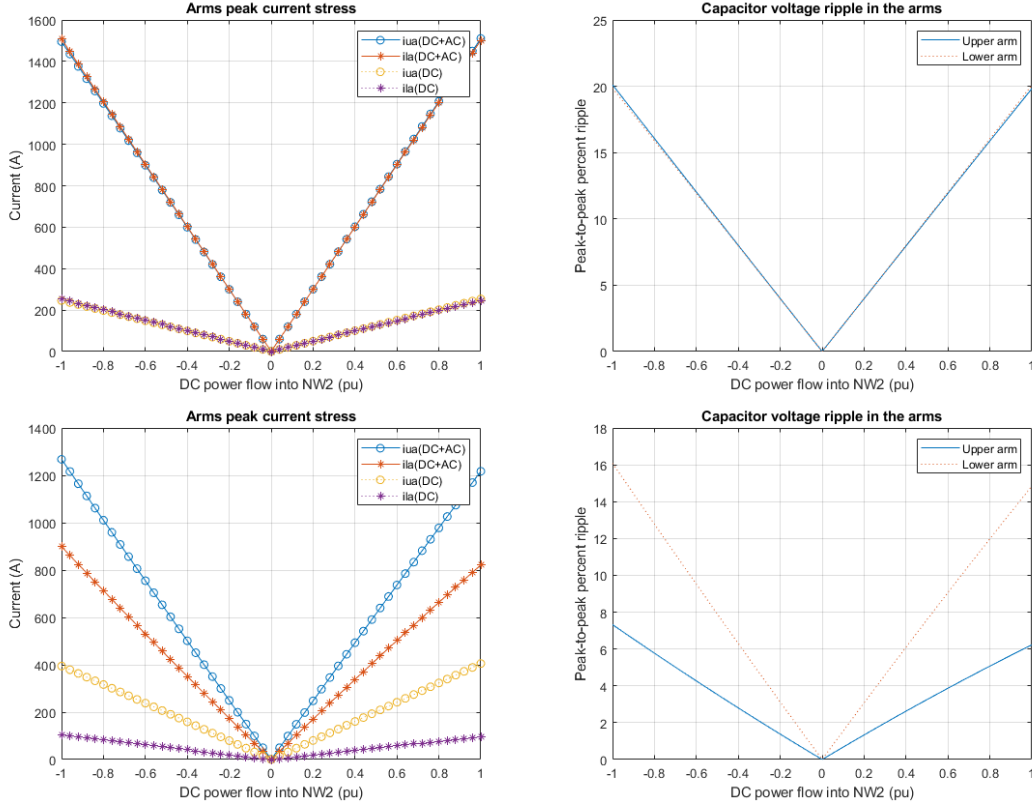


Figure 4.28: Loci of steady-state studies for the phase a upper and lower arms: (a) arms' peak current stress for $G_v=0.5$; (b) percent capacitor voltage ripple for $G_v=0.5$; (c) arms' peak current stress for $G_v=0.8$; (d) percent capacitor voltage ripple for $G_v=0.8$

conversion with this G_v ratio, as presented in [70]. Figure 4.28(c) and (d), meanwhile, show the same parameters but with a ratio of $G_v=0.8$, and, as expected, the upper and lower arms are no longer subjected to the same stresses. These results can be used to properly design a practical converter, i.e., if the currents in the arms exceed the limits of the devices to be used, or if the voltage ripple is to be kept within a certain limit, the proper measures can be taken by analysing the operating ranges to which the converter will be subjected, and designing accordingly.

4.3 Chapter Summary

In this chapter, the derived DPMs for the four topologies of interest in this thesis have been subjected to steady-state and varying parameters studies, for different DC step ratios G_v . For the steady-state studies, different operating points have been simulated for each converter, where the power injections to the external networks have been specified, and waveforms for several steady-state quantities in the converters are examined. For the varying parameters studies, a variable in the operating point is step-varied through a predetermined range with the goal of observing how these changes affect converter performance, i.e. capacitor voltage ripple and current stress in the arms. In all cases, the converters' behaviour validates the theoretical information presented in Chapter 2, including the harmonic components that are required in specific converter's tasks, and the power transfer mechanisms present in DC/DC and DC/DC/AC conversion processes.

The shown studies are only a small sample of all the studies that can be performed using the DPMs, which provide insight into the operation of these novel converters, and demonstrate the versatility of the developed models.

Chapter 5

Conclusion

As DC transmission gathers increasing interest as another viable way for transmission and distribution of power, hybrid AC/DC grids appear to be the power system of the future. The technology to link AC and DC systems, as well as different levels of DC systems, will become ever more crucial as the currently AC dominated transmission and distribution systems require interconnection with HVDC and MVDC systems. MMC converters with the ability to simultaneously perform DC/DC and AC/DC conversions are attractive devices that can help realise future highly meshed hybrid AC/DC grids. This thesis has undertaken the task to develop and validate benchmark models that the research community can utilise to study the emerging classes of DC/DC/AC and DC/DC MMCs.

5.1 Contributions

This thesis provides the following core contributions:

1. An $\alpha\beta 0$ -frame TAM of a generalised MMC structure is derived that includes multiple harmonic components to capture the different power transfer mechanisms involved in AC/DC and DC/DC conversion processes. This unified model is used to represent two different DC/DC/AC MMC topologies; minor modifications are then made to adapt this model to represent two different DC/DC MMC topologies. All four TAMs permit the user to specify all the impedances in the converters structure and at the ports, as well as balanced or unbalanced networks' voltages, and values for arms' number of cells and capacitances, which can be different between the upper and lower arms. This provides a wide range of versatility for converter studies, and improves on the conventional modelling of converters, where upper and lower arms' capacitances and cell numbers are traditionally set to be equal. The derived TAMs show excellent agreement with PLECS switched model simulations.
2. The aforementioned benchmark $\alpha\beta 0$ -frame TAM can be used by researches to study the DC/DC/AC and DC/DC classes of MMCs. This thesis uses the TAM to derive a unified $\alpha\beta 0$ DPM that accounts for DC through third harmonic components, providing a time-invariant (at steady-state) non-linear model that can be used for a wide range of studies not easily performed with the TAM. These models offer the same versatility provided by the TAMs. Similar to the TAM, the unified DPM is then manipulated to create four different models for DC/DC/AC and DC/DC MMCs, which show very good agreement with the derived TAMs. This thesis focuses on using the DPMs for steady-state operating point analyses of the four different MMC topologies. Interestingly, this work reveals the DC/DC/AC DPMs accuracy is somewhat sensitive to the chosen capacitance in the cells, suggesting an even broader spectrum of harmonic content has to be selected for the DPM when a small amount of converter internal energy storage is desired. The DC/DC DPMs did not demonstrate any such sensitivity to internal energy storage.

3. A comprehensive solution procedure is formulated that allows a user to solve for any desired operating point for the DPMs, yielding the full set of open-loop modulating signals and full state solution, while only requiring the user to input basic data such as port power injections and terminal voltages. This is not possible to achieve using only the TAMs. The solution procedure is essential to exploiting the DPMs for study of the converters' steady-state operation in a systematic manner, as demonstrated with various case studies in this work.

5.2 Future Work

This work presents groundwork for more research into DC/DC/AC MMCs to be made. The developed models provide a sound foundation for future work in HVDC, MVDC, and hybrid grids. A few tentative future works include:

1. Experimental validation of the DC/DC/AC and DC/DC DPMs, and investigation into the potential to adapt the solution procedure equations to real-time predictions.
2. Investigate the addition of harmonic components to the modulating signals embedded in the DPMs to study capacitor voltage reduction techniques and suppression of unwanted harmonic currents.
3. Carry out small-signal stability studies and explore the use of conventional linear control design tools such as root locus and bode plots, via linearization of the DPMs.
4. Study the capabilities of the presented models utilising full-bridge submodules.
5. Investigate the use of the DPMs for accelerating simulation of their switched-model counterparts.

References

- [1] M. Barnes, D. V. Hertem, S. P. Teeuwsen, and M. Callavik, “HVDC systems in smart grids”, *Proc. IEEE*, vol. 105, no. 11, pp. 2082–2098, 2017.
- [2] G. Shi, X. Cai, C. Sun, Y. Chang, and R. Yang, “All-DC offshore wind farm with parallel connection: An overview”, *IET Conf. Publ.*, vol. 2016, no. CP696, 2016.
- [3] P. Bresesti, W. L. Kling, R. L. Hendriks, and R. Vailati, “HVDC connection of offshore wind farms to the transmission system”, *IEEE Trans. ENERGY Convers.*, vol. 22, no. 1, pp. 37–43, 2007.
- [4] G. H. Kim, M. H. Kang, J. H. Ahn, S. H. Chae, and E. H. Kim, “Operation of dc series connected offshore wind farm by using tap changing transformer with MMC-HVDC”, *5th Int. Conf. Renew. Energy Gener. Appl. ICREGA 2018*, vol. 2018-Jan, pp. 291–295, 2018.
- [5] J. Zhou and J. Wu, “Overview on VSC-HVDC systems based on PV”, *Proc. - 2018 IEEE Int. Power Electron. Appl. Conf. Expo. PEAC 2018*, pp. 1–4, 2018.
- [6] S. Isik, H. Nath, M. Alharbi, and S. Bhattacharya, “Direct PV integration to MMC based point to point HVDC link”, *Conference Record of the 3rd IEEE International Workshop on Electronic Power Grid*, vol. eGrid 2018, pp. 1–5, 2018.

- [7] N. Kawakami and Y. Iijima, "Overview of battery energy storage systems for stabilization of renewable energy in japan", *2012 Int. Conf. Renew. Energy Res. Appl. ICRERA 2012*, pp. 1–5, 2012.
- [8] H. Singh and S. Vadhera, "Comparative analysis between SMES and BESS in application of VSC-HVDC system", *12th IEEE Int. Conf. Electron. Energy, Environ. Commun. Comput. Control (E3-C3), INDICON 2015*, vol. 105, pp. 1–6, 2016.
- [9] S. H. Kung and G. J. Kish, "Multiport modular multilevel converter for DC systems", *IEEE Trans. Power Deliv.*, vol. 34, no. 1, pp. 73–83, 2019.
- [10] L. Michi, G. Donnini, and C. Giordano, "New HVDC technology in pan-european power system planning", *AEIT HVDC Int. Conf. AEIT HVDC 2019*, pp. 1–6, 2019.
- [11] L. Michi, "An overview of the HVDC transmission system models in planning tools: The italian experience", *2019 AEIT HVDC Int. Conf. AEIT HVDC 2019*, pp. 1–6, 2019.
- [12] P. Kundur, *Power Systems Stability and Control*, 1st. McGraw-Hill, 1994.
- [13] N. Ahmed, "HVDC SuperGrids with modular multilevel converters - the power transmission backbone of the future", *International Multi-Conference on Systems, Signals and Devices, SSD 2012*, pp. 1–7, 2012.
- [14] N. Ahmed, A. Haider, D. V. Hertem, L. Zhang, and H. P. Nee, "Prospects and challenges of future HVDC SuperGrids with modular multilevel converters", *Proceedings of the 2011 14th European Conference on Power Electronics and Applications, EPE 2011*, pp. 1–10, 2011.
- [15] O. E. Oni, I. E. Davidson, and K. N. I. Mbangula, "A review of LCC-HVDC and VSC-HVDC technologies and applications", *EEEIC 2016 - Int. Conf. Environ. Electr. Eng.*, pp. 1–7, 2016.

- [16] A. Lesnicar and R. Marquardt, “An innovative modular multilevel converter topology suitable for a wide power range - power tech conference proceedings, 2003 IEEE bologna”, *2003 IEEE Bol. PowerTech - Conf. Proc.*, vol. 3, pp. 1–6, 2003.
- [17] A. Nami, J. Liang, F. Dijkhuizen, and G. D. Demetriades, “Modular multilevel converters for HVDC applications: Review on converter cells and functionalities”, *IEEE Trans. Power Electron.*, vol. 30, no. 1, pp. 18–36, 2015.
- [18] A. Schön and M. M. Bakran, “Comparison of modular multilevel converter based HV DC-DC-converters”, *2016 18th Eur. Conf. Power Electron. Appl. EPE 2016 ECCE Eur.*, pp. 10–17, 2016.
- [19] G. J. Kish, “On the emerging class of non-isolated modular multilevel DC-DC converters for DC and hybrid AC-DC systems”, *IEEE Trans. Smart Grid*, vol. 10, no. 2, pp. 1762–1771, 2019.
- [20] S. P. Teeuwsen, “Simplified dynamic model of a voltage-sourced converter with modular multilevel converter design”, *2009 IEEE/PES Power Syst. Conf. Expo. PSCE 2009*, pp. 1–6, 2009.
- [21] S. Norrga, L. Ängquist, K. Ilves, L. Harnefors, and H. P. Nee, “Decoupled steady-state model of the modular multilevel converter with half-bridge cells”, *IET Conf. Publ.*, vol. 2012, no. 592 CP, 2012.
- [22] S. Rohner, S. Bernet, M. Hiller, and R. Sommer, “Modulation, losses, and semiconductor requirements of modular multilevel converters”, *IEEE Trans. Ind. Electron.*, vol. 57, no. 8, pp. 2633–2642, 2010.
- [23] M. Hagiwara, R. Maeda, and H. Akagi, “Control and analysis of the modular multilevel cascade converter based on double-star chopper-cells (MMCC-DSCC)”, *IEEE Trans. Power Electron.*, vol. 26, no. 6, pp. 2649–1658, 2011.

- [24] —, “Theoretical analysis and control of the modular multilevel cascade converter based on double-star chopper-cells (MMCC-DSCC)”, *2010 Int. Power Electron. Conf. - ECCE Asia -, IPEC 2010*, vol. 1, pp. 2029–2036, 2010.
- [25] W. Rik, W. A. A. D. Doncker, and D. M. Divan, “A three-phase soft-switched high-power-density dc /dc converter for high-power applications”, *IEEE Trans. Ind. Appl.*, vol. 27, no. 1, 1991.
- [26] M. J. Carrizosa, A. Bennaib, P. Alou, and G. Damm, “DC transformer for DC/DC connection in HVDC network”, *2013 15th Eur. Conf. Power Electron. Appl. EPE 2013*, pp. 1–10, 2013.
- [27] A. Tyagi and K. R. Padiyar, “Dynamic analysis and simulation of a VSC based back-to-back HVDC link”, *Proc. India Int. Conf. Power Electron. IICPE 2006*, no. 2, pp. 232–238, 2006.
- [28] T. Luth, M. M. C. Merlin, T. C. Green, F. Hassan, and C. D. Barker, “High-frequency operation of a DC/AC/DC system for HVDC applications”, *IEEE Trans. Power Electron.*, vol. 29, no. 8, pp. 4107–4115, 2014.
- [29] I. A. Gowaid, G. P. Adam, S. Ahmed, D. Holliday, and B. W. Williams, “Analysis and design of a modular multilevel converter with trapezoidal modulation for medium and high voltage DC-DC transformer”, *IEEE Trans. Power Electron.*, vol. 30, no. 10, pp. 5439–5457, 2015.
- [30] B. Zhao, Q. Song, J. Li, Y. Wang, and W. Liu, “High-frequency-link modulation methodology of dc-dc transformer based on modular multilevel converter for HVDC application: Comprehensive analysis and experimental verification”, *IEEE Trans. Power Electron.*, vol. 32, no. 5, pp. 3413–3424, 2017.

- [31] A. Schön and M. M. Bakran, “A new HVDC-DC converter with inherent fault clearing capability”, *2013 15th Eur. Conf. Power Electron. Appl. EPE 2013*, 2013.
- [32] —, “High power HVDC-DC converters for the interconnection of HVDC lines with different line topologies”, *2014 Int. Power Electron. Conf. IPEC-Hiroshima - ECCE Asia 2014.*, vol. 28, no. 10, pp. 3255–3262, 2014.
- [33] J. A. Ferreira, “The multilevel modular DC converter”, *IEEE Trans. Power Electron.*, vol. 28, no. 10, pp. 4460–4465, 2013.
- [34] S. Norrga, L. Angquist, and A. Antonopoulos, “The polyphase cascaded-cell DC/DC converter”, *2013 IEEE Energy Convers. Congr. Expo. ECCE 2013*, pp. 4082–4088, 2013.
- [35] G. J. Kish and P. W. Lehn, “A modular bidirectional DC power flow controller with fault blocking capability for DC networks”, *2013 IEEE 14th Work. Control Model. Power Electron. COMPEL 2013*, pp. 1–7, 2013.
- [36] M. M. Bakran and A. Schön, *DC to DC converter*, WO 2016/138949 A1, 2016.
- [37] G. J. Kish, M. Ranjram, and P. W. Lehn, “A modular multilevel DC/DC converter with fault blocking capability for HVDC interconnects”, *IEEE Trans. Power Electron.*, vol. 30, no. 1, pp. 148–162, 2015.
- [38] G. K. Papastergiou and G. G. Stamatiou, *AC/DC multicell power converter for dual terminal HVDC connection*, US20140375122A1, 2014.
- [39] S. Cui, J. H. Lee, J. Hu, R. W. D. Doncker, and S. K. Sul, “A modular multilevel converter with a zigzag transformer for bipolar MVDC distribution systems”, *IEEE Trans. Power Electron.*, vol. 34, no. 2, pp. 1038–1043, 2019.

- [40] Y. Li, D. Liu, and G. J. Kish, "Generalized DC-DC-AC MMC structure for MVDC and HVDC applications", *2019 20th Work. Control Model. Power Electron. COM-PEL 2019*, pp. 1–8, 2019.
- [41] M. Rouhani and G. J. Kish, "Multiport DC-DC-AC modular multilevel converters for hybrid AC/DC power systems", *IEEE Trans. Power Deliv.*, vol. 35, no. 1, pp. 408–419, 2019.
- [42] S. H. Kung and G. J. Kish, "A modular multilevel HVDC buck-boost converter derived from its switched-mode counterpart", *IEEE Trans. Power Deliv.*, vol. 33, no. 1, pp. 82–92, 2018.
- [43] H. Alyami and Y. Mohamed, "Review and development of MMC employed in VSC-HVDC systems", *Can. Conf. Electr. Comput. Eng.*, pp. 1–6, 2017.
- [44] H. Y. Kanaan and K. Al-Haddad, "Modeling and simulation of dc-dc power converters in CCM and DCM using the switching functions approach: Application to the buck and cuk converters", *Proc. Int. Conf. Power Electron. Drive Syst.*, vol. 1, pp. 468–473, 2005.
- [45] G. P. Adam, P. Li, I. A. Gowaid, and B. W. Williams, "Generalized switching function model of modular multilevel converter", *Proc. IEEE Int. Conf. Ind. Technol.*, vol. 2015-June, no. June, pp. 2702–2707, 2015.
- [46] H. Saad, K. Jacobs, W. Lin, and D. Jovcic, "Modelling of MMC including half-bridge and full-bridge submodules for EMT study", *19th Power Syst. Comput. Conf. PSCC 2016*, pp. 1–7, 2016.
- [47] I. C. Damian, M. Eremia, and M. Sanduleac, "Fault analysis of a high voltage direct current link using detailed equivalent models for modular multilevel converters", *Proc. 2019 8th Int. Conf. Mod. Power Syst. MPS 2019*, pp. 1–6, 2019.

- [48] U. N. Gnanarathna, A. M. Gole, and R. P. Jayasinghe, “Efficient modeling of modular multilevel HVDC converters (MMC) on electromagnetic transient simulation programs”, *IEEE Trans. Power Deliv.*, vol. 26, no. 1, pp. 316–324, 2011.
- [49] S. Nanou and S. Papathanassiou, “Generic average-value modeling of MMC-HVDC links considering submodule capacitor dynamics”, *2017 52nd Int. Univ. Power Eng. Conf. UPEC 2017*, vol. 2017-Jan, pp. 1–5, 2017.
- [50] S. Isik, M. Alharbi, S. Acharya, and S. Bhattacharya, “Performance comparison of detailed and averaging model of a grid connected 401-level MMC system under system fault conditions”, *Proc. IECON 2018 - 44th Annu. Conf. IEEE Ind. Electron. Soc.*, vol. 1, pp. 3979–3984, 2018.
- [51] J. Xu, A. M. Gole, and C. Zhao, “The use of averaged-value model of modular multilevel converter in DC grid”, *IEEE Trans. Power Deliv.*, vol. 30, no. 2, pp. 519–528, 2015.
- [52] G. J. Kish and P. W. Lehn, “Modeling techniques for dynamic and steady-state analysis of modular multilevel DC/DC converters”, *IEEE Trans. Power Deliv.*, vol. 31, no. 6, pp. 2502–2510, 2016.
- [53] G. J. Kish, C. Holmes, and P. W. Lehn, “Dynamic modeling of modular multilevel DC/DC converters for HVDC systems”, *2014 IEEE 15th Work. Control Model. Power Electron. COMPEL 2014*, pp. 1–7, 2014.
- [54] S. R. Sanders, J. M. Noworolski, X. Z. Liu, and G. C. Verghese, “Generalized averaging method for power conversion circuits”, *IEEE Trans. Power Electron.*, vol. 6, no. 2, pp. 251–259, 1991.

- [55] S. M. Kotian and K. N. Shubhanga, “Dynamic phasor modelling and simulation”, *12th IEEE Int. Conf. Electron. Energy, Environ. Commun. Comput. Control (E3-C3), INDICON 2015*, vol. 4, no. 2, pp. 1–6, 2016.
- [56] M. A. Kulasza, “Generalized dynamic phasor-based simulation for power systems”, PhD thesis, University of Manitoba, 2014.
- [57] J. Rupasinghe, S. Filizadeh, and L. Wang, “A dynamic phasor model of an MMC with extended frequency range for emt simulations”, *IEEE J. Emerg. Sel. Top. Power Electron.*, vol. 7, no. 1, pp. 30–40, 2019.
- [58] X. Lu, W. Lin, J. Wen, W. Yao, T. An, and Y. Li, “Dynamic phasor modelling and operating characteristic analysis of half-bridge MMC”, *2016 IEEE 8th Int. Power Electron. Motion Control Conf. IPEMC-ECCE Asia 2016*, no. Hb Mmc, pp. 2615–2621, 2016.
- [59] D. Jovcic and A. A. Jamshidifar, “MMC converter detailed phasor model including second harmonic”, *IEEE PES Innov. Smart Grid Technol. Conf. Eur.*, vol. 2015-Jan, no. January, pp. 1–5, 2015.
- [60] Ö. C. Sakinci and J. Beerten, “Generalized dynamic phasor modeling of the MMC for small-signal stability analysis”, *IEEE Trans. Power Deliv.*, vol. 34, no. 3, pp. 991–1000, 2019.
- [61] D. Jovcic and A. J. Far, “Phasor model of modular multilevel converter with circulating current suppression control”, *IEEE Trans. Power Deliv.*, vol. 30, no. 4, pp. 1889–1897, 2015.
- [62] A. Antonopoulos, L. Ångquist, and H. P. Nee, “On dynamics and voltage control of the modular multilevel converter”, *2009 13th Eur. Conf. Power Electron. Appl. EPE '09*, pp. 1–10, 2009.

- [63] F. Martinez-Rodrigo, D. Ramirez, A. B. Rey-Boue, S. D. Pablo, and L. C. H.-D. Lucas, “Modular multilevel converters: Control and applications”, *Energies-MDPI*, vol. 10, no. 11, 2017.
- [64] S. Du, A. Dekka, B. Wu, and N. Zargari, *MODULAR MULTILEVEL CONVERTERS Analysis, Control, and Applications*, 1st. Wiley-IEEE Press, 2017.
- [65] M. Saeedifard and R. Iravani, “Dynamic performance of a modular multilevel back-to-back HVDC system”, *IEEE Trans. Power Deliv.*, vol. 25, no. 4, pp. 2903–2912, 2010.
- [66] T. Soong and P. W. Lehn, “Internal power flow of a modular multilevel converter with distributed energy resources”, *IEEE J. Emerg. Sel. Top. Power Electron.*, vol. 2, no. 4, pp. 1127–1138, 2014.
- [67] K. Huang and J. A. Ferreira, “Two operational modes of the modular multilevel DC converter”, *9th Int. Conf. Power Electron. - ECCE Asia Green World with Power Electron. ICPE 2015-ECCE Asia*, pp. 1347–1354, 2015.
- [68] H. Yang, J. Qin, S. Debnath, and M. Saeedifard, “Hasor domain steady-state modeling and design of the DC-DC modular multilevel converter”, *IEEE Trans. Power Deliv.*, vol. 31, no. 5, pp. 2054–2063, 2016.
- [69] S. H. Kung and G. J. Kish, “A unified modular multilevel DC/DC converter structure with flexible AC power transfer controls”, *2017 IEEE 18th Work. Control Model. Power Electron. COMPEL 2017*, pp. 2–7, 2017.
- [70] G. J. Kish, “A new class of modular multilevel DC/DC converters for HVDC systems”, PhD thesis, University of Toronto, 2016.
- [71] E. Clarke, *CIRCUIT ANALYSIS OF A-C POWER SYSTEMS*, 1st. NJ, Hoboken: John Wiley & Sons, 1943.

- [72] R. Arachchige, T. Janesh, and K. Rupasinghe, “A dynamic phasor model of a modular multilevel converter for EMT co-simulation”, PhD thesis, University of Manitoba, 2017.
- [73] M. Ranjram, “A multi-port power flow controller for HVDC networks”, PhD thesis, University of Toronto, 2015.
- [74] M. Rouhani, “Multiport DC-DC-AC modular multilevel converters for hybrid AC/DC power systems”, PhD thesis, University of Alberta, 2019.

Appendix A

DC/DC/AC TAM Matrices

The following matrices are for the DC/DC/AC TAM given by Equation (3.31). To reduce the size of the given sub-matrices, several constants are defined as C_{xxy} , where “xx” describes the type of constant, i.e., “ RL ” for a constant with units of resistance times inductance, and “y” takes values of 1,2,3... depending on how many variables share the same unit type. Since the A sub-matrices are of considerable length column-wise, they are divided in several matrices that are numbered with a superscript with only one digit, counting from left to right. The model in Equation (3.31) is repeated here for reference as:

$$\frac{d}{dt} \begin{bmatrix} \mathbf{X}_i^* \\ \mathbf{X}_v^* \end{bmatrix} = \begin{bmatrix} \dot{A}_{11} & \dot{A}_{12} \\ \dot{A}_{21} & 0_{6 \times 6} \end{bmatrix} \begin{bmatrix} \mathbf{X}_i^* \\ \mathbf{X}_v^* \end{bmatrix} + \begin{bmatrix} \dot{N} \\ 0_{6 \times 5} \end{bmatrix} \begin{bmatrix} \mathbf{W}^* \end{bmatrix}$$

$$\dot{A}_{11} = \begin{bmatrix} -\frac{R_a}{L_a} & 0 & 0 & 0 & 0 & 0 & 0 & 0 \\ 0 & -\frac{R_a}{L_a} & 0 & 0 & 0 & 0 & 0 & 0 \\ 0 & 0 & -\frac{C_{RL1}}{2C_{LL1}} & 0 & 0 & 0 & 0 & \frac{C_{RL}}{4C_{LL1}} \\ 0 & 0 & 0 & -\frac{R_s + R_a C_{PU1}}{L_s + L_a C_{PU1}} & 0 & \frac{2L_a R_w - (2L_e + 3L_m)R_a}{C_{LL2}} & 0 & 0 \\ 0 & 0 & 0 & 0 & -\frac{R_s + R_a C_{PU1}}{L_s + L_a C_{PU1}} & 0 & \frac{2L_a R_w - (2L_e + 3L_m)R_a}{C_{LL2}} & 0 \\ 0 & 0 & 0 & -\frac{L_s R_a - L_a R_s}{C_{LL2}} & 0 & -\frac{L_s R_a + 4L_s R_w + 2L_a R_w}{C_{LL2}} & 0 & 0 \\ 0 & 0 & 0 & 0 & -\frac{L_s R_a - L_a R_s}{C_{LL2}} & 0 & -\frac{L_s R_a + 4L_s R_w + 2L_a R_w}{C_{LL2}} & 0 \\ 0 & 0 & -\frac{C_{RL4}}{C_{LL1}} & 0 & 0 & 0 & 0 & -\frac{C_{RL3}}{2C_{LL1}} \end{bmatrix}$$

$$C_{RL1} = 9L_1 R_2 + 9L_2 R_1 + 3L_1 R_a + 3L_a R_1 + 3L_2 R_a + 3L_a R_2 + 12L_e R_1 + 12L_e R_2 + 18L_t R_1 + 18L_t R_2 + 2L_a R_a + 8L_e R_a + 12L_t R_t$$

$$C_{LL1} = L_a^2 + 9L_1 L_2 + 9L_1 L_t + 9L_2 L_t + 6L_1 L_e + 6L_2 L_e + 6L_a L_t + 4L_a L_e + 3L_1 L_a + 9L_2 L_a$$

$$C_{RL4} = 3(3L_1 R_2 - 3L_2 R_1 - L_a R_1 - L_2 R_a + L_a R_2)$$

$$C_{PU1} = \frac{2L_e + 3L_m}{L_a + 4L_e + 6L_m}$$

$$C_{LL2} = 2L_a L_e + 3L_a L_m + L_a L_s + 4L_e L_s + 6L_m L_s$$

$$C_{RL2} = 9L_1 R_2 - 9L_2 R_1 + 3L_1 R_a - 3L_a R_1 - 3L_2 R_a + 3L_a R_2 - 12L_e R_1 + 12L_e R_2 + 18L_1 R_t - 18L_t R_1 - 18L_2 R_t + 18L_t R_2 + 12L_1 R_w - 12L_2 R_w$$

$$C_{RL3} = 9L_1 R_2 + 9L_2 R_1 + 3L_1 R_a + 3L_a R_1 + 3L_2 R_a + 3L_a R_2 + 18L_1 R_t + 18L_2 R_t + 12L_1 R_w + 12L_2 R_w + 2L_a R_a + 12L_a R_t + 8L_a R_w$$

$$\dot{A}_{12} = [\dot{A}_{12}^1 \quad \dot{A}_{12}^2]$$

$$\dot{A}_{12}^1 = \begin{bmatrix} -\frac{2M_{\Sigma 0} + M_{\Sigma \alpha}}{2L_a} & -\frac{M_{\Sigma \beta}}{2L_a} & -\frac{M_{\Sigma \alpha}}{L_a} \\ -\frac{M_{\Sigma \beta}}{2L_a} & -\frac{2M_{\Sigma 0} + M_{\Sigma \alpha}}{2L_a} & -\frac{M_{\Sigma \beta}}{L_a} \\ \frac{3M_{\Delta \alpha}(L_1 - L_2) - 2M_{\Sigma \alpha} C_L}{2L_a(2L_a + 8L_e)C_{PU2}} & \frac{3M_{\Delta \beta}(L_1 - L_2) - 2M_{\Sigma \beta} C_L}{2L_a(2L_a + 8L_e)C_{PU2}} & \frac{3M_{\Delta 0}(L_1 - L_2) - 2M_{\Sigma 0} C_L}{2L_a(L_a + 4L_e)C_{PU2}} \\ -\frac{(2M_{\Delta 0} + M_{\Delta \alpha})(2L_e + 3L_m)}{C_{LL2}} & \frac{M_{\Delta \beta}(2L_e + 3L_m)}{C_{LL2}} & \frac{2M_{\Delta \alpha}(2L_e + 3L_m)}{C_{LL2}} \\ \frac{M_{\Delta \beta}(2L_e + 3L_m)}{C_{LL2}} & -\frac{(2M_{\Delta 0} + M_{\Delta \alpha})(2L_e + 3L_m)}{C_{LL2}} & -\frac{2M_{\Delta \beta}(2L_e + 3L_m)}{C_{LL2}} \\ -\frac{C_{LL2}}{L_s(2M_{\Delta 0} + M_{\Delta \alpha})} & \frac{C_{LL2}}{M_{\Delta \beta} L_s} & -\frac{C_{LL2}}{2L_s M_{\Delta \alpha}} \\ \frac{C_{LL2}}{M_{\Delta \beta} L_s} & -\frac{C_{LL2}}{L_s(2M_{\Delta 0} + M_{\Delta \alpha})} & \frac{C_{LL2}}{2L_s M_{\Delta \beta}} \\ \frac{3M_{\Sigma \alpha}(L_1 - L_2) - 3L_a M_{\Delta \alpha} \left(\frac{L_1 + L_2}{L_a + 2}\right)}{L_a(2L_a + 8L_e)C_{PU2}} & \frac{3M_{\Sigma \beta}(L_1 - L_2) - 3L_a M_{\Delta \beta} \left(\frac{L_1 + L_2}{L_a + 2}\right)}{L_a(2L_a + 8L_e)C_{PU2}} & \frac{3M_{\Sigma 0}(L_1 - L_2) - 3L_a M_{\Delta 0} \left(\frac{L_1 + L_2}{L_a + 2}\right)}{L_a(2L_a + 8L_e)C_{PU2}} \end{bmatrix}$$

$$C_{PU2} = \left(\frac{3L_1 + 3L_2}{2L_a + 1} \right) \left(\frac{3L_1 + 3L_2 + 12L_t}{2L_a + 8L_e} \right) - \left(\frac{(3L_1 - 3L_2)^2}{4L_a(L_a + 4L_e)} \right)$$

$$C_L = \left(\frac{3L_1 + 3L_2 + 12L_t}{2L_a + 8L_e} + 1 \right) (L_a + 4L_e)$$

$$\begin{aligned}
\hat{A}_{21}^5 &= \begin{bmatrix} \left(\frac{Nu}{4Cu}\right)(M_{\Delta\alpha} + M_{\Sigma\alpha}) + \left(\frac{Nl}{4Cl}\right)(M_{\Delta\alpha} - M_{\Sigma\alpha}) \\ \left(\frac{Nu}{4Cu}\right)(M_{\Delta\beta} + M_{\Sigma\beta}) + \left(\frac{Nl}{4Cl}\right)(M_{\Delta\beta} - M_{\Sigma\beta}) \\ \left(\frac{Nu}{4Cu}\right)(M_{\Delta 0} + M_{\Sigma 0}) + \left(\frac{Nl}{4Cl}\right)(M_{\Delta 0} - M_{\Sigma 0}) \\ \left(\frac{Nu}{4Cu}\right)(M_{\Delta\alpha} + M_{\Sigma\alpha}) - \left(\frac{Nl}{4Cl}\right)(M_{\Delta\alpha} - M_{\Sigma\alpha}) \\ \left(\frac{Nu}{4Cu}\right)(M_{\Delta\beta} + M_{\Sigma\beta}) - \left(\frac{Nl}{4Cl}\right)(M_{\Delta\beta} - M_{\Sigma\beta}) \\ \left(\frac{Nu}{4Cu}\right)(M_{\Delta 0} + M_{\Sigma 0}) - \left(\frac{Nl}{4Cl}\right)(M_{\Delta 0} - M_{\Sigma 0}) \end{bmatrix} \\
\dot{N} &= \begin{bmatrix} 0 & 0 & 0 & 0 & 0 \\ 0 & 0 & 0 & 0 & 0 \\ \frac{3L_2 + L_a + 4L_e + 4L_t}{2C_{LL1}} & \frac{3(L_1 - L_2)}{3L_a(L_a + 4L_e)C_{PU2}} & 0 & 0 & -\frac{3(L_1 - L_2)}{2(L_a + 2L_s)(L_a + 4L_e)C_{PU2}} \\ 0 & 0 & \frac{-1}{L_s + L_a C_{PU1}} & 0 & 0 \\ 0 & 0 & 0 & \frac{-1}{L_s + L_a C_{PU}} & 0 \\ 0 & 0 & \frac{L_a}{C_{LL}} & 0 & 0 \\ 0 & 0 & 0 & \frac{L_a}{C_{LL2}} & 0 \\ \frac{3L_2 + L_a}{C_{LL}} & \frac{-\frac{3(L_1 - L_2)}{L_a + 2}}{(L_a + 4L_e)C_{PU}} & 0 & 0 & \frac{3L_a \left(\frac{L_1 - L_2}{L_a + 2}\right)}{(L_a + 2L_s)(L_a + 4L_e)C_{PU}} \end{bmatrix}
\end{aligned}$$

Appendix B

DC/DC TAM Matrices

The following matrices are for the DC/DC TAM given by Equation (3.34). To reduce the size of the given sub-matrices, several constants are defined as C_{xxy} , where “xx” describes the type of constant, i.e., “ RL ” for a constant with units of resistance times inductance, and “y” takes values of 1,2,3... depending on how many variables share the same unit. Since the A sub-matrices are of considerable length column-wise, they are divided in several matrices that are numbered with a superscript with only one digit, counting from left to right. The model in equation Equation (3.34) is repeated here for reference as:

$$\frac{d}{dt} \begin{bmatrix} \mathbf{X}_{ir}^* \\ \mathbf{X}_v^* \end{bmatrix} = \begin{bmatrix} \dot{A}_{11r} & \dot{A}_{12r} \\ \dot{A}_{21r} & 0_{6 \times 6} \end{bmatrix} \begin{bmatrix} \mathbf{X}_{ir}^* \\ \mathbf{X}_v^* \end{bmatrix} + \begin{bmatrix} \dot{N}_r \\ 0_{6 \times 5} \end{bmatrix} \begin{bmatrix} \mathbf{W}_r^* \end{bmatrix}, \quad (\text{B.1})$$

$$\dot{A}_{11r} = \begin{bmatrix} -\frac{R_a}{L_a} & 0 & 0 & 0 & 0 & 0 \\ 0 & -\frac{R_a}{L_a} & 0 & 0 & 0 & 0 \\ 0 & 0 & -\frac{C_{RL1}}{2C_{LL1}} & 0 & 0 & \frac{C_{RL2}}{4C_{LL1}} \\ 0 & 0 & 0 & \frac{-R_a - 4R_w}{L_a + 4L_e + 6L_m} & 0 & 0 \\ 0 & 0 & 0 & 0 & \frac{-R_a - 4R_w}{L_a + 4L_e + 6L_m} & 0 \\ 0 & 0 & -\frac{C_{RL4}}{C_{LL1}} & 0 & 0 & -\frac{C_{RL3}}{2C_{LL1}} \end{bmatrix}$$

$$C_{RL} = 9L_1R_2 + 9L_2R_1 + 3L_1R_a + 3L_aR_1 + 3L_2R_a + 3L_aR_2 + 12L_eR_1 + 12L_eR_2 + 18L_tR_1 + 18L_tR_2 + 2L_aR_a + 8L_eR_a + 12L_tR_t$$

$$C_{LL1} = L_a^2 + 9L_1L_2 + 9L_1L_t + 9L_2L_t + 6L_1L_e + 6L_2L_e + 6L_aL_t + 4L_aL_e + 3L_1L_a + 9L_2L_a$$

$$C_{RL4} = 3(3L_1R_2 - 3L_2R_1 - L_aR_1 - L_2R_a + L_aR_2)$$

$$C_{RL2} = 9L_1R_2 - 9L_2R_1 + 3L_1R_a - 3L_aR_1 - 3L_2R_a + 3L_aR_2 - 12L_eR_1 + 12L_eR_2 + 18L_tR_1 - 18L_tR_2 + 18L_tR_t + 12L_1R_w - 12L_2R_w$$

$$C_{RL3} = 9L_1R_2 + 9L_2R_1 + 3L_1R_a + 3L_aR_1 + 3L_2R_a + 3L_aR_2 + 18L_tR_t + 18L_2R_t + 12L_1R_w + 12L_2R_w + 2L_aR_a + 12L_aR_t + 8L_aR_w$$

$$\dot{A}_{12r} = [\dot{A}_{12r}^1 \quad \dot{A}_{12r}^2]$$

$$\dot{A}_{12r}^1 = \begin{bmatrix} -\frac{2M_{\Sigma 0} + M_{\Sigma \alpha}}{2L_a} & -\frac{M_{\Sigma \beta}}{2L_a} & -\frac{M_{\Sigma \alpha}}{L_a} \\ -\frac{M_{\Sigma \beta}}{2L_a} & -\frac{2M_{\Sigma 0} + M_{\Sigma \alpha}}{2L_a} & -\frac{M_{\Sigma \beta}}{L_a} \\ \frac{3M_{\Delta \alpha}(L_1 - L_2) - 2M_{\Sigma \alpha}C_L}{2L_a(2L_a + 8L_e)C_{PU2}} & \frac{3M_{\Delta \beta}(L_1 - L_2) - 2M_{\Sigma \beta}C_L}{2L_a(2L_a + 8L_e)C_{PU2}} & \frac{3M_{\Delta 0}(L_1 - L_2) - 2M_{\Sigma 0}C_L}{2L_a(L_a + 4L_e)C_{PU2}} \\ -\frac{L_s(2M_{\Delta 0} + M_{\Delta \alpha})}{C_{LL2}} & \frac{M_{\Delta \beta}L_s}{C_{LL2}} & -\frac{2L_sM_{\Delta \alpha}}{C_{LL2}} \\ \frac{M_{\Delta \beta}L_s}{C_{LL2}} & -\frac{L_s(2M_{\Delta 0} + M_{\Delta \alpha})}{C_{LL2}} & -\frac{2L_sM_{\Delta \beta}}{C_{LL2}} \\ \frac{3M_{\Sigma \alpha}(L_1 - L_2) - 3L_aM_{\Delta \alpha}\left(\frac{L_1 + L_2}{L_a + 2}\right)}{L_a(2L_a + 8L_e)C_{PU2}} & \frac{3M_{\Sigma \beta}(L_1 - L_2) - 3L_aM_{\Delta \beta}\left(\frac{L_1 + L_2}{L_a + 2}\right)}{L_a(2L_a + 8L_e)C_{PU2}} & \frac{3M_{\Sigma 0}(L_1 - L_2) - 3L_aM_{\Delta 0}\left(\frac{L_1 + L_2}{L_a + 2}\right)}{L_a(2L_a + 8L_e)C_{PU2}} \end{bmatrix}$$

$$C_{PU2} = \left(\frac{3L_1 + 3L_2}{2L_a + 1}\right)\left(\frac{3L_1 + 3L_2 + 12L_t}{2L_a + 8L_e}\right) - \left(\frac{(3L_1 - 3L_2)^2}{4L_a(L_a + 4L_e)}\right)$$

$$C_L = \left(\frac{3L_1 + 3L_2 + 12L_t}{2L_a + 8L_e} + 1\right)(L_a + 4L_e)$$

$$\dot{A}_{12r}^2 = \begin{bmatrix} -\frac{2M_{\Delta 0} + M_{\Delta \alpha}}{2L_a} & -\frac{M_{\Delta \beta}}{2L_a} & -\frac{M_{\Delta \alpha}}{L_a} \\ -\frac{M_{\Delta \beta}}{2L_a} & -\frac{2M_{\Delta 0} + M_{\Delta \alpha}}{2L_a} & -\frac{M_{\Delta \beta}}{L_a} \\ \frac{3M_{\Sigma \alpha}(L_1 - L_2) - 2M_{\Delta \alpha}C_L}{2L_a(2L_a + 8L_e)C_{PU2}} & \frac{3M_{\Sigma \beta}(L_1 - L_2) - 2M_{\Delta \beta}C_L}{2L_a(2L_a + 8L_e)C_{PU2}} & \frac{3M_{\Sigma 0}(L_1 - L_2) - 2M_{\Delta 0}C_L}{2L_a(L_a + 4L_e)C_{PU2}} \\ -\frac{L_s(2M_{\Sigma 0} + M_{\Sigma \alpha})}{C_{LL2}} & \frac{M_{\Sigma \beta}L_s}{C_{LL2}} & -\frac{2L_sM_{\Sigma \alpha}}{C_{LL2}} \\ \frac{M_{\Sigma \beta}L_s}{C_{LL2}} & -\frac{L_s(2M_{\Sigma 0} + M_{\Sigma \alpha})}{C_{LL2}} & -\frac{2L_sM_{\Sigma \beta}}{C_{LL2}} \\ \frac{3M_{\Delta \alpha}(L_1 - L_2) - 3L_aM_{\Sigma \alpha}\left(\frac{L_1 + L_2}{L_a + 2}\right)}{L_a(2L_a + 8L_e)C_{PU2}} & \frac{3M_{\Delta \beta}(L_1 - L_2) - 3L_aM_{\Sigma \beta}\left(\frac{L_1 + L_2}{L_a + 2}\right)}{L_a(2L_a + 8L_e)C_{PU2}} & \frac{3M_{\Delta 0}(L_1 - L_2) - 3L_aM_{\Sigma 0}\left(\frac{L_1 + L_2}{L_a + 2}\right)}{L_a(2L_a + 8L_e)C_{PU2}} \end{bmatrix}$$

$$\dot{A}_{21r} = [\dot{A}_{21r}^1 \quad \dot{A}_{21r}^2 \quad \dot{A}_{21r}^3 \quad \dot{A}_{21r}^4]$$

125

Appendix C

DC/DC/AC DPM Matrices

The following matrices are for the DC/DC/AC DPM given by Equation (3.57) . To reduce the size of the given sub-matrices, several constants are defined as C_{xxy} , where “xx” describes the type of constant, i.e., “ RL ” for a constant with units of resistance times inductance, and “y” takes values of 1,2,3... depending on how many variables share the same unit. This model includes second and third harmonic components for the modulating signals, but due to time constraints they were not investigated in the thesis’ body, and are always set to 0 for simulation purposes. The model in equation Equation (3.57) is repeated here for reference as:

$$\frac{d}{dt} \begin{bmatrix} \widetilde{\mathbf{X}}_i^* \\ \widetilde{\mathbf{X}}_v^* \end{bmatrix} = \begin{bmatrix} \tilde{A}_{11} & \tilde{A}_{12} \\ \tilde{A}_{21} & 0_{22 \times 22} \end{bmatrix} \begin{bmatrix} \widetilde{\mathbf{X}}_i^* \\ \widetilde{\mathbf{X}}_v^* \end{bmatrix} + \begin{bmatrix} \tilde{N} \\ 0_{22 \times 5} \end{bmatrix} \begin{bmatrix} \widetilde{\mathbf{W}}^* \end{bmatrix}, \quad (\text{C.1})$$

$$\tilde{A}_{11} = \begin{bmatrix} \tilde{A}_{11}^{11} & \tilde{A}_{11}^{12} & \tilde{A}_{11}^{13} & \tilde{A}_{11}^{14} & \tilde{A}_{11}^{15} & \tilde{A}_{11}^{16} & \tilde{A}_{11}^{17} \\ [0]_{22 \times 8} & \tilde{A}_{11}^{22} & \tilde{A}_{11}^{23} & \tilde{A}_{11}^{24} & \tilde{A}_{11}^{25} & \tilde{A}_{11}^{26} & \tilde{A}_{11}^{27} \end{bmatrix}$$

$$\tilde{A}_{11}^{11} = \begin{bmatrix} -\frac{R_a}{L_a} & -\omega & 0 & 0 & 0 & 0 & 0 & 0 \\ \omega & -\frac{R_a}{L_a} & 0 & 0 & 0 & 0 & 0 & 0 \\ 0 & 0 & -\frac{R_a}{L_a} & -2\omega & 0 & 0 & 0 & 0 \\ 0 & 0 & 2\omega & -\frac{R_a}{L_a} & 0 & 0 & 0 & 0 \\ 0 & 0 & 0 & 0 & -\frac{R_a}{L_a} & -\omega & 0 & 0 \\ 0 & 0 & 0 & 0 & \omega & -\frac{R_a}{L_a} & 0 & 0 \\ 0 & 0 & 0 & 0 & 0 & 0 & -\frac{R_a}{L_a} & -2\omega \\ 0 & 0 & 0 & 0 & 0 & 0 & 2\omega & -\frac{R_a}{L_a} \end{bmatrix}$$

$$\tilde{A}_{11}^{12} = \begin{bmatrix} [0]_{8 \times 3} \\ \frac{C_{RL1}}{2C_{LL1}} & 0 & 0 \\ 0 & -\frac{C_{RL}}{2C_{LL}} & -3\omega \\ 0 & 3\omega & -\frac{C_{RL1}}{2C_{LL}} \end{bmatrix} \quad \tilde{A}_{11}^{22} = \begin{bmatrix} [0]_{16 \times 3} \\ \frac{C_{RL4}}{C_{LL1}} & 0 & 0 \\ 0 & \frac{C_{RL4}}{C_{LL1}} & 0 \\ 0 & 0 & \frac{C_{RL4}}{C_{LL1}} \end{bmatrix}$$

$$C_{RL1} = 9L_1R_2 + 9L_2R_1 + 3L_1R_a + 3L_aR_1 + 3L_2R_a + 3L_aR_2 + 12L_eR_1 + 12L_eR_2 + 18L_tR_1 + 18L_tR_2 + 2L_aR_a + 8L_eR_a + 12L_tR_t$$

$$C_{LL1} = L_a^2 + 9L_1L_2 + 9L_1L_t + 9L_2L_t + 6L_1L_e + 6L_2L_e + 6L_aL_t + 4L_aL_e + 3L_1L_a + 9L_2L_a$$

$$C_{RL4} = 3(3L_1R_2 - 3L_2R_1 + L_1R_a - L_aR_1 - L_2R_a + L_aR_2)$$

$$\tilde{A}_{11}^{13} = \begin{bmatrix} [0]_{11 \times 4} \\ -\frac{R_s + R_a C_{PU1}}{L_s + L_a C_{PU1}} & -\omega & 0 & 0 \\ \omega & -\frac{R_s + R_a C_{PU1}}{L_s + L_a C_{PU1}} & 0 & 0 \\ 0 & 0 & -\frac{R_s + R_a C_{PU1}}{L_s + L_a C_{PU1}} & -2\omega \\ 0 & 0 & 2\omega & -\frac{R_s + R_a C_{PU1}}{L_s + L_a C_{PU1}} \end{bmatrix}$$

$$\tilde{A}_{11}^{23} = \begin{bmatrix} [0]_{4 \times 4} \\ -\frac{L_s R_a - L_a R_s}{C_{LL2}} & 0 & 0 & 0 \\ 0 & -\frac{L_s R_a - L_a R_s}{C_{LL2}} & 0 & 0 \\ 0 & 0 & -\frac{L_s R_a - L_a R_s}{C_{LL2}} & 0 \\ 0 & 0 & 0 & -\frac{L_s R_a - L_a R_s}{C_{LL}} \end{bmatrix}$$

$$[0]_{7 \times 4}$$

$$\begin{aligned}
\tilde{A}_{11}^{14} &= \begin{bmatrix} \frac{R_s + R_a C_{PU1}}{L_s + L_a C_{PU1}} & -\omega & 0 & 0 \\ \omega & -\frac{R_s + R_a C_{PU1}}{L_s + L_a C_{PU1}} & 0 & 0 \\ 0 & 0 & -\frac{R_s + R_a C_{PU1}}{L_s + L_a C_{PU1}} & -2\omega \\ 0 & 0 & 2\omega & -\frac{R_s + R_a C_{PU1}}{L_s + L_a C_{PU1}} \end{bmatrix} \begin{matrix} [0]_{15 \times 4} \\ \\ \\ \end{matrix} \\
\tilde{A}_{11}^{24} &= \begin{bmatrix} -\frac{L_s R_a - L_a R_s}{C_{LL2}} & 0 & 0 & 0 \\ 0 & -\frac{L_s R_a - L_a R_s}{C_{LL2}} & 0 & 0 \\ 0 & 0 & -\frac{L_s R_a - L_a R_s}{C_{LL2}} & 0 \\ 0 & 0 & 0 & -\frac{L_s R_a - L_a R_s}{C_{LL2}} \end{bmatrix} \begin{matrix} [0]_{4 \times 4} \\ \\ \\ \end{matrix} \\
\tilde{A}_{11}^{15} &= \begin{bmatrix} \frac{2L_a R_w - R_a(2L_e + 3L_m)}{C_{LL2}} & 0 & 0 & 0 \\ 0 & \frac{2L_a R_w - R_a(2L_e + 3L_m)}{C_{LL2}} & 0 & 0 \\ 0 & 0 & \frac{2L_a R_w - R_a(2L_e + 3L_m)}{C_{LL2}} & 0 \\ 0 & 0 & 0 & \frac{2L_a R_w - R_a(2L_e + 3L_m)}{C_{LL2}} \end{bmatrix} \begin{matrix} [0]_{3 \times 4} \\ [0]_{11 \times 4} \\ \\ \end{matrix} \\
\tilde{A}_{11}^{25} &= \begin{bmatrix} \frac{L_s R_a + 4L_s R_w + 2L_a R_w}{C_{LL2}} & -\omega & 0 & 0 \\ \omega & -\frac{L_s R_a + 4L_s R_w + 2L_a R_w}{C_{LL2}} & 0 & 0 \\ 0 & 0 & -\frac{L_s R_a + 4L_s R_w + 2L_a R_w}{C_{LL2}} & -2\omega \\ 0 & 0 & 2\omega & -\frac{L_s R_a + 4L_s R_w + 2L_a R_w}{C_{LL2}} \end{bmatrix} \begin{matrix} [0]_{4 \times 4} \\ \\ \\ [0]_{7 \times 4} \end{matrix} \\
C_{PU1} &= \frac{2L_e + 3L_m}{L_a + 4L_e + 6L_m} \\
C_{LL} &= 2L_a L_e + 3L_a L_m + L_a L_s + 4L_e L_s + 6L_m L_s \\
\tilde{A}_{11}^{16} &= \begin{bmatrix} \frac{2L_a R_w - R_a(2L_e + 3L_m)}{C_{LL2}} & 0 & 0 & 0 \\ 0 & \frac{2L_a R_w - R_a(2L_e + 3L_m)}{C_{LL2}} & 0 & 0 \\ 0 & 0 & \frac{2L_a R_w - R_a(2L_e + 3L_m)}{C_{LL2}} & 0 \\ 0 & 0 & 0 & \frac{2L_a R_w - R_a(2L_e + 3L_m)}{C_{LL2}} \end{bmatrix} \begin{matrix} [0]_{15 \times 4} \\ \\ \\ \end{matrix}
\end{aligned}$$

$$\tilde{A}_{11}^{26} = \left[\begin{array}{cccc} & & [0]_{4 \times 4} & \\ -\frac{L_s R_a + 4L_s R_w + 2L_a R_w}{C_{LL2}} & -\omega & 0 & 0 \\ \omega & -\frac{L_s R_a + 4L_s R_w + 2L_a R_w}{C_{LL2}} & 0 & 0 \\ 0 & 0 & -\frac{L_s R_a + 4L_s R_w + 2L_a R_w}{C_{LL2}} & -2\omega \\ 0 & 0 & 2\omega & -\frac{L_s R_a + 4L_s R_w + 2L_a R_w}{C_{LL2}} \end{array} \right]$$

$$\tilde{A}_{11}^{17} = \left[\begin{array}{ccc} [0]_{8 \times 3} & & \\ \frac{C_{RL2}}{4C_{LL1}} & 0 & 0 \\ 0 & \frac{C_{RL2}}{4C_{LL1}} & 0 \\ 0 & 0 & \frac{C_{RL2}}{4C_{LL1}} \end{array} \right] \quad \tilde{A}_{11}^{22} = \left[\begin{array}{ccc} [0]_{16 \times 3} & & \\ -\frac{C_{RL3}}{2C_{LL1}} & 0 & 0 \\ 0 & -\frac{C_{RL3}}{2C_{LL1}} & -3\omega \\ 0 & 3\omega & -\frac{C_{RL3}}{2C_{LL1}} \end{array} \right]$$

$$C_{RL2} = 9L_1 R_2 - 9L_2 R_1 + 3L_1 R_a - 3L_a R_1 - 3L_2 R_a + 3L_a R_2 - 12L_e R_1 + 12L_e R_2 + 18L_1 R_t - 18L_t R_1 - 18L_2 R_t + 18L_t R_2 + 12L_1 R_w - 12L_2 R_w$$

$$C_{RL3} = 9L_1 R_2 + 9L_2 R_1 + 3L_1 R_a + 3L_a R_1 + 3L_2 R_a + 3L_a R_2 + 18L_1 R_t + 18L_2 R_t + 12L_1 R_w + 12L_2 R_w + 2L_a R_a + 12L_a R_t + 8L_a R_w$$

$$\tilde{A}_{12} = \left[\begin{array}{cccccccccccc} \tilde{A}_{12}^{11} & \tilde{A}_{12}^{12} & \tilde{A}_{12}^{13} & \tilde{A}_{12}^{14} & \tilde{A}_{12}^{15} & \tilde{A}_{12}^{16} & \tilde{A}_{12}^{17} & \tilde{A}_{12}^{18} & \tilde{A}_{12}^{19} & \tilde{A}_{12}^{10} \\ \tilde{A}_{12}^{21} & \tilde{A}_{12}^{22} & \tilde{A}_{12}^{23} & \tilde{A}_{12}^{24} & \tilde{A}_{12}^{25} & \tilde{A}_{12}^{26} & \tilde{A}_{12}^{27} & \tilde{A}_{12}^{28} & \tilde{A}_{12}^{29} & \tilde{A}_{12}^{20} \\ \tilde{A}_{12}^{31} & \tilde{A}_{12}^{32} & \tilde{A}_{12}^{33} & \tilde{A}_{12}^{34} & \tilde{A}_{12}^{35} & \tilde{A}_{12}^{36} & \tilde{A}_{12}^{37} & \tilde{A}_{12}^{38} & \tilde{A}_{12}^{39} & \tilde{A}_{12}^{30} \end{array} \right]$$

$$\tilde{A}_{12}^{11} = \left[\begin{array}{cc} -\frac{M_{\Sigma 0}^{dc}}{L_a} - \frac{M_{\Sigma \alpha}^{2\parallel}}{4L_a} & -\frac{M_{\Sigma \alpha}^{2\perp}}{4L_a} \\ -\frac{M_{\Sigma \alpha}^{2\perp}}{4L_a} & -\frac{M_{\Sigma 0}^{dc}}{L_a} + \frac{M_{\Sigma \alpha}^{2\parallel}}{4L_a} \\ -\frac{M_{\Sigma 0}^{3\parallel}}{2L_a} - \frac{M_{\Sigma \alpha}^{1\parallel}}{4L_a} & \frac{M_{\Sigma \alpha}^{1\perp}}{4L_a} - \frac{M_{\Sigma 0}^{3\perp}}{2L_a} \\ -\frac{M_{\Sigma \alpha}^{1\perp}}{4L_a} - \frac{M_{\Sigma 0}^{3\perp}}{2L_a} & \frac{M_{\Sigma 0}^{3\parallel}}{2L_a} - \frac{M_{\Sigma \alpha}^{1\parallel}}{4L_a} \\ \frac{M_{\Sigma \beta}^{2\parallel}}{4L_a} & \frac{M_{\Sigma \beta}^{2\perp}}{4L_a} \\ \frac{M_{\Sigma \beta}^{2\perp}}{4L_a} & -\frac{M_{\Sigma \beta}^{2\parallel}}{4L_a} \\ \frac{M_{\Sigma \beta}^{1\parallel}}{4L_a} & -\frac{M_{\Sigma \beta}^{1\perp}}{4L_a} \\ \frac{M_{\Sigma \beta}^{1\perp}}{4L_a} & \frac{M_{\Sigma \beta}^{1\parallel}}{4L_a} \\ \frac{M_{\Delta \alpha}^{1\parallel}(3(L_1 - L_2))}{8C_{PU}(L_a^2 + 4L_a L_e)} - \frac{M_{\Sigma \alpha}^{1\parallel} C_L}{4C_{PU2}(L_a^2 + 4L_a L_e)} & \frac{M_{\Delta \alpha}^{1\perp}(3(L_1 - L_2))}{8C_{PU}(L_a^2 + 4L_a L_e)} - \frac{M_{\Sigma \alpha}^{1\perp} C_L}{4C_{PU}(L_a^2 + 4L_a L_e)} \\ \frac{M_{\Delta \alpha}^{2\parallel}(3(L_1 - L_2))}{8C_{PU}(L_a^2 + 4L_a L_e)} - \frac{M_{\Sigma \alpha}^{2\parallel} C_L}{4C_{PU}(L_a^2 + 4L_a L_e)} & \frac{M_{\Delta \alpha}^{2\perp} C_L}{8C_{PU2}(L_a^2 + 4L_a L_e)} - \frac{M_{\Delta \alpha}^{2\perp}(3(L_1 - L_2))}{8C_{PU}(L_a^2 + 4L_a L_e)} \\ \frac{M_{\Delta \alpha}^{2\perp}(3(L_1 - L_2))}{8C_{PU}(L_a^2 + 4L_a L_e)} - \frac{M_{\Sigma \alpha}^{2\perp} C_L}{4C_{PU2}(L_a^2 + 4L_a L_e)} & \frac{M_{\Delta \alpha}^{2\parallel} C_L}{8C_{PU2}(L_a^2 + 4L_a L_e)} - \frac{M_{\Sigma \alpha}^{2\parallel} C_L}{4C_{PU}(L_a^2 + 4L_a L_e)} \end{array} \right]$$

$$\begin{aligned}
C_{PU2} &= \left(\frac{3L_1 + 3L_2}{2L_a + 1} \right) \left(\frac{3L_1 + 3L_2 + 12L_t}{2L_a + 8L_e} \right) - \left(\frac{(3L_1 - 3L_2)^2}{4L_a(L_a + 4L_e)} \right) \\
C_L &= \left(\frac{3L_1 + 3L_2 + 12L_t}{2L_a + 8L_e} + 1 \right) (L_a + 4L_e) \\
\tilde{A}_{12}^{12} &= \begin{bmatrix}
-\frac{M_{\Sigma 0}^{3\parallel}}{2L_a} - \frac{M_{\Sigma \alpha}^{1\parallel}}{4L_a} & -\frac{M_{\Sigma \alpha}^{1\perp}}{4L_a} - \frac{M_{\Sigma 0}^{3\perp}}{2L_a} \\
\frac{M_{\Sigma \alpha}^{1\perp}}{4L_a} - \frac{M_{\Sigma 0}^{3\perp}}{2L_a} & \frac{M_{\Sigma 0}^{3\parallel}}{2L_a} - \frac{M_{\Sigma \alpha}^{2\parallel}}{4L_a} \\
-\frac{M_{\Sigma 0}^{dc}}{L_a} & 0 \\
0 & -\frac{M_{\Sigma 0}^{dc}}{L_a} \\
\frac{M_{\Sigma \beta}^{1\parallel}}{4L_a} & \frac{M_{\Sigma \beta}^{1\perp}}{4L_a} \\
-\frac{M_{\Sigma \beta}^{1\perp}}{4L_a} & \frac{M_{\Sigma \beta}^{1\parallel}}{4L_a} \\
0 & 0 \\
0 & 0 \\
\frac{M_{\Delta \alpha}^{2\parallel}(3(L_1 - L_2))}{8C_{PU2}(L_a^2 + 4L_a L_e)} - \frac{M_{\Sigma \alpha}^{2\parallel} C_L}{4C_{PU2}(L_a^2 + 4L_a L_e)} & \frac{M_{\Delta \alpha}^{2\perp}(3(L_1 - L_2))}{8C_{PU2}(L_a^2 + 4L_a L_e)} - \frac{M_{\Sigma \alpha}^{2\perp} C_L}{4C_{PU2}(L_a^2 + 4L_a L_e)} \\
\frac{M_{\Delta \alpha}^{1\parallel}(3(L_1 - L_2))}{8C_{PU2}(L_a^2 + 4L_a L_e)} - \frac{M_{\Sigma \alpha}^{1\parallel} C_L}{4C_{PU2}(L_a^2 + 4L_a L_e)} & \frac{M_{\Delta \alpha}^{1\perp} C_L}{4C_{PU2}(L_a^2 + 4L_a L_e)} - \frac{M_{\Sigma \alpha}^{1\perp}(3(L_1 - L_2))}{8C_{PU2}(L_a^2 + 4L_a L_e)} \\
\frac{M_{\Delta \alpha}^{1\perp}(3(L_1 - L_2))}{8C_{PU2}(L_a^2 + 4L_a L_e)} - \frac{M_{\Sigma \alpha}^{1\perp} C_L}{4C_{PU2}(L_a^2 + 4L_a L_e)} & \frac{M_{\Delta \alpha}^{1\parallel}(3(L_1 - L_2))}{8C_{PU2}(L_a^2 + 4L_a L_e)} - \frac{M_{\Sigma \alpha}^{1\parallel} C_L}{4C_{PU2}(L_a^2 + 4L_a L_e)}
\end{bmatrix}
\end{aligned}$$

$$\begin{aligned}
\tilde{A}_{12}^{13} = & \left[\begin{array}{cc}
\frac{M_{\Sigma\beta}^{2\parallel}}{4L_a} & \frac{M_{\Sigma\beta}^{2\perp}}{4L_a} \\
\frac{M_{\Sigma\beta}^{2\perp}}{4L_a} & -\frac{M_{\Sigma\beta}^{2\parallel}}{4L_a} \\
\frac{M_{\Sigma\beta}^{1\parallel}}{4L_a} & -\frac{M_{\Sigma\beta}^{1\perp}}{4L_a} \\
\frac{M_{\Sigma\beta}^{1\perp}}{4L_a} & \frac{M_{\Sigma\beta}^{1\parallel}}{4L_a} \\
-\frac{M_{\Sigma 0}^{dc}}{L_a} + \frac{M_{\Sigma\alpha}^{2\parallel}}{4L_a} & \frac{M_{\Sigma\alpha}^{2\perp}}{4L_a} \\
\frac{M_{\Sigma\alpha}^{2\perp}}{4L_a} & -\frac{M_{\Sigma 0}^{dc}}{L_a} - \frac{M_{\Sigma\alpha}^{2\parallel}}{4L_a} \\
-\frac{M_{\Sigma 0}^{3\parallel}}{2L_a} + \frac{M_{\Sigma\alpha}^{1\parallel}}{4L_a} & -\frac{M_{\Sigma\alpha}^{1\perp}}{4L_a} - \frac{M_{\Sigma 0}^{3\perp}}{2L_a} \\
\frac{M_{\Sigma\alpha}^{1\perp}}{4L_a} - \frac{M_{\Sigma 0}^{3\perp}}{2L_a} & \frac{M_{\Sigma 0}^{3\parallel}}{2L_a} + \frac{M_{\Sigma\alpha}^{1\parallel}}{4L_a} \\
\frac{M_{\Delta\beta}^{1\parallel}(3(L_1 - L_2))}{8C_{PU2}(L_a^2 + 4L_a L_e)} - \frac{M_{\Sigma\beta}^{1\parallel} C_L}{4C_{PU2}(L_a^2 + 4L_a L_e)} & \frac{M_{\Delta\beta}^{1\perp}(3(L_1 - L_2))}{8C_{PU2}(L_a^2 + 4L_a L_e)} - \frac{M_{\Sigma\beta}^{1\perp} C_L}{4C_{PU2}(L_a^2 + 4L_a L_e)} \\
\frac{M_{\Delta\beta}^{2\parallel}(3(L_1 - L_2))}{8C_{PU2}(L_a^2 + 4L_a L_e)} - \frac{M_{\Sigma\beta}^{2\parallel} C_L}{4C_{PU2}(L_a^2 + 4L_a L_e)} & \frac{M_{\Delta\beta}^{2\perp} C_L}{8C_{PU2}(L_a^2 + 4L_a L_e)} - \frac{M_{\Delta\beta}^{2\perp}(3(L_1 - L_2))}{8C_{PU2}(L_a^2 + 4L_a L_e)} \\
\frac{M_{\Delta\beta}^{2\perp}(3(L_1 - L_2))}{8C_{PU2}(L_a^2 + 4L_a L_e)} - \frac{M_{\Sigma\beta}^{2\perp} C_L}{4C_{PU2}(L_a^2 + 4L_a L_e)} & \frac{M_{\Delta\beta}^{2\parallel}(3(L_1 - L_2))}{8C_{PU2}(L_a^2 + 4L_a L_e)} - \frac{M_{\Sigma\beta}^{2\parallel} C_L}{4C_{PU2}(L_a^2 + 4L_a L_e)}
\end{array} \right] \\
\tilde{A}_{12}^{14} = & \left[\begin{array}{cc}
\frac{M_{\Sigma\beta}^{1\parallel}}{4L_a} & \frac{M_{\Sigma\beta}^{1\perp}}{4L_a} \\
-\frac{M_{\Sigma\beta}^{1\perp}}{4L_a} & \frac{M_{\Sigma\beta}^{1\parallel}}{4L_a} \\
0 & 0 \\
0 & 0 \\
-\frac{M_{\Sigma 0}^{3\parallel}}{2L_a} + \frac{M_{\Sigma\alpha}^{1\parallel}}{4L_a} & \frac{M_{\Sigma\alpha}^{1\perp}}{4L_a} - \frac{M_{\Sigma 0}^{3\perp}}{2L_a} \\
\frac{M_{\Sigma\alpha}^{1\perp}}{4L_a} - \frac{M_{\Sigma 0}^{3\perp}}{2L_a} & \frac{M_{\Sigma 0}^{3\parallel}}{2L_a} + \frac{M_{\Sigma\alpha}^{1\parallel}}{4L_a} \\
-\frac{M_{\Sigma 0}^{dc}}{L_a} & 0 \\
0 & -\frac{M_{\Sigma 0}^{dc}}{L_a} \\
\frac{M_{\Delta\beta}^{2\parallel}(3(L_1 - L_2))}{8C_{PU2}(L_a^2 + 4L_a L_e)} - \frac{M_{\Sigma\beta}^{2\parallel} C_L}{4C_{PU2}(L_a^2 + 4L_a L_e)} & \frac{M_{\Delta\beta}^{2\perp}(3(L_1 - L_2))}{8C_{PU2}(L_a^2 + 4L_a L_e)} - \frac{M_{\Sigma\beta}^{2\perp} C_L}{4C_{PU2}(L_a^2 + 4L_a L_e)} \\
\frac{M_{\Delta\beta}^{1\parallel}(3(L_1 - L_2))}{8C_{PU2}(L_a^2 + 4L_a L_e)} - \frac{M_{\Sigma\beta}^{1\parallel} C_L}{4C_{PU2}(L_a^2 + 4L_a L_e)} & \frac{M_{\Delta\beta}^{1\perp} C_L}{8C_{PU2}(L_a^2 + 4L_a L_e)} - \frac{M_{\Delta\beta}^{1\perp}(3(L_1 - L_2))}{8C_{PU2}(L_a^2 + 4L_a L_e)} \\
\frac{M_{\Delta\beta}^{1\perp}(3(L_1 - L_2))}{8C_{PU2}(L_a^2 + 4L_a L_e)} - \frac{M_{\Sigma\beta}^{1\perp} C_L}{4C_{PU2}(L_a^2 + 4L_a L_e)} & \frac{M_{\Delta\beta}^{1\parallel} C_L}{8C_{PU2}(L_a^2 + 4L_a L_e)} - \frac{M_{\Sigma\beta}^{1\parallel} C_L}{4C_{PU2}(L_a^2 + 4L_a L_e)} \\
\frac{M_{\Delta\beta}^{1\parallel}(3(L_1 - L_2))}{8C_{PU2}(L_a^2 + 4L_a L_e)} - \frac{M_{\Sigma\beta}^{1\parallel} C_L}{4C_{PU2}(L_a^2 + 4L_a L_e)} & \frac{M_{\Delta\beta}^{1\perp} C_L}{8C_{PU2}(L_a^2 + 4L_a L_e)} - \frac{M_{\Sigma\beta}^{1\perp} C_L}{4C_{PU2}(L_a^2 + 4L_a L_e)}
\end{array} \right]
\end{aligned}$$

$$\begin{aligned}
\bar{A}_{12}^{15} = & \left[\begin{array}{ccc}
-\frac{M_{\Sigma\alpha}^{1\parallel}}{L_a} & -\frac{M_{\Sigma\alpha}^{2\parallel}}{2L_a} & -\frac{M_{\Sigma\alpha}^{2\perp}}{2L_a} \\
-\frac{M_{\Sigma\alpha}^{1\perp}}{L_a} & \frac{M_{\Sigma\alpha}^{2\perp}}{2L_a} & -\frac{M_{\Sigma\alpha}^{2\parallel}}{2L_a} \\
-\frac{M_{\Sigma\alpha}^{2\parallel}}{L_a} & -\frac{M_{\Sigma\alpha}^{1\parallel}}{2L_a} & -\frac{M_{\Sigma\alpha}^{1\perp}}{2L_a} \\
-\frac{M_{\Sigma\alpha}^{2\perp}}{L_a} & \frac{M_{\Sigma\alpha}^{1\perp}}{2L_a} & -\frac{M_{\Sigma\alpha}^{1\parallel}}{2L_a} \\
-\frac{M_{\Sigma\beta}^{1\parallel}}{L_a} & -\frac{M_{\Sigma\beta}^{2\parallel}}{2L_a} & -\frac{M_{\Sigma\beta}^{2\perp}}{2L_a} \\
-\frac{M_{\Sigma\beta}^{1\perp}}{L_a} & \frac{M_{\Sigma\beta}^{2\perp}}{2L_a} & -\frac{M_{\Sigma\beta}^{2\parallel}}{2L_a} \\
-\frac{M_{\Sigma\beta}^{2\parallel}}{L_a} & -\frac{M_{\Sigma\beta}^{1\parallel}}{2L_a} & -\frac{M_{\Sigma\beta}^{1\perp}}{2L_a} \\
-\frac{M_{\Sigma\beta}^{2\perp}}{L_a} & \frac{M_{\Sigma\beta}^{1\perp}}{2L_a} & -\frac{M_{\Sigma\beta}^{1\parallel}}{2L_a}
\end{array} \right] \\
& \begin{array}{ccccc}
\frac{3M_{\Delta 0}^{dc}(L_1 - L_2)}{2C_{PU2}(L_a^2 + 4L_a L_e)} & \frac{M_{\Sigma 0}^{dc} C_L}{C_{PU2}(L_a^2 + 4L_a L_e)} & \frac{M_{\Delta 0}^{3\parallel}(3(L_1 - L_2))}{2C_{PU2}(L_a^2 + 4L_a L_e)} - \frac{M_{\Sigma 0}^{3\parallel} C_L}{2C_{PU2}(L_a^2 + 4L_a L_e)} & \frac{M_{\Delta 0}^{3\perp}(3(L_1 - L_2))}{2C_{PU2}(L_a^2 + 4L_a L_e)} & \frac{M_{\Sigma 0}^{3\perp} C_L}{2C_{PU2}(L_a^2 + 4L_a L_e)} \\
\frac{3M_{\Delta 0}^{3\parallel}(L_1 - L_2)}{2C_{PU2}(L_a^2 + 4L_a L_e)} & \frac{M_{\Sigma 0}^{3\parallel} C_L}{C_{PU2}(L_a^2 + 4L_a L_e)} & \frac{M_{\Delta 0}^{dc}(3(L_1 - L_2))}{2C_{PU2}(L_a^2 + 4L_a L_e)} - \frac{M_{\Sigma 0}^{dc} C_L}{C_{PU2}(L_a^2 + 4L_a L_e)} & 0 & 0 \\
\frac{3M_{\Delta 0}^{3\perp}(L_1 - L_2)}{2C_{PU2}(L_a^2 + 4L_a L_e)} & \frac{M_{\Sigma 0}^{3\perp} C_L}{C_{PU2}(L_a^2 + 4L_a L_e)} & 0 & \frac{M_{\Delta 0}^{dc}(3(L_1 - L_2))}{2C_{PU2}(L_a^2 + 4L_a L_e)} & \frac{M_{\Sigma 0}^{dc} C_L}{C_{PU2}(L_a^2 + 4L_a L_e)}
\end{array} \\
\bar{A}_{12}^{16} = & \left[\begin{array}{ccc}
-\frac{M_{\Delta 0}^{dc}}{L_a} - \frac{M_{\Delta\alpha}^{2\parallel}}{4L_a} & & -\frac{M_{\Delta\alpha}^{2\perp}}{4L_a} \\
-\frac{M_{\Delta\alpha}^{2\perp}}{4L_a} & & -\frac{M_{\Delta 0}^{dc}}{L_a} + \frac{M_{\Delta\alpha}^{2\parallel}}{4L_a} \\
-\frac{M_{\Delta 0}^{3\parallel}}{2L_a} - \frac{M_{\Delta\alpha}^{1\parallel}}{4L_a} & & \frac{M_{\Delta\alpha}^{1\perp}}{4L_a} - \frac{M_{\Delta 0}^{3\perp}}{2L_a} \\
-\frac{M_{\Delta\alpha}^{1\perp}}{4L_a} - \frac{M_{\Delta 0}^{3\perp}}{2L_a} & & \frac{M_{\Delta\alpha}^{2\perp}}{4L_a} - \frac{M_{\Delta\beta}^{2\parallel}}{4L_a} \\
\frac{M_{\Delta\beta}^{2\parallel}}{4L_a} & & \frac{M_{\Delta\beta}^{2\perp}}{4L_a} - \frac{M_{\Delta\alpha}^{1\parallel}}{4L_a} \\
\frac{M_{\Delta\beta}^{2\perp}}{4L_a} - \frac{M_{\Delta\alpha}^{1\parallel}}{4L_a} & & \frac{M_{\Delta\beta}^{1\perp}}{4L_a} - \frac{M_{\Delta\alpha}^{1\parallel}}{4L_a} \\
\frac{M_{\Delta\beta}^{1\perp}}{4L_a} - \frac{M_{\Delta\alpha}^{1\parallel}}{4L_a} & & \frac{M_{\Delta\beta}^{1\parallel}}{4L_a} - \frac{M_{\Delta\alpha}^{1\perp}}{4L_a} \\
\frac{M_{\Sigma\alpha}^{1\parallel}(3(L_1 - L_2))}{8C_{PU2}(L_a^2 + 4L_a L_e)} - \frac{M_{\Delta\alpha}^{1\parallel} C_L}{4C_{PU2}(L_a^2 + 4L_a L_e)} & & \frac{M_{\Sigma\alpha}^{1\perp}(3(L_1 - L_2))}{8C_{PU2}(L_a^2 + 4L_a L_e)} - \frac{M_{\Delta\alpha}^{1\perp} C_L}{4C_{PU2}(L_a^2 + 4L_a L_e)} \\
\frac{M_{\Sigma\alpha}^{2\parallel}(3(L_1 - L_2))}{8C_{PU2}(L_a^2 + 4L_a L_e)} - \frac{M_{\Delta\alpha}^{2\parallel} C_L}{4C_{PU2}(L_a^2 + 4L_a L_e)} & & \frac{M_{\Sigma\alpha}^{2\perp}(3(L_1 - L_2))}{8C_{PU2}(L_a^2 + 4L_a L_e)} - \frac{M_{\Delta\alpha}^{2\perp} C_L}{4C_{PU2}(L_a^2 + 4L_a L_e)} \\
\frac{M_{\Sigma\alpha}^{2\perp}(3(L_1 - L_2))}{8C_{PU2}(L_a^2 + 4L_a L_e)} - \frac{M_{\Delta\alpha}^{2\perp} C_L}{4C_{PU2}(L_a^2 + 4L_a L_e)} & & \frac{M_{\Sigma\alpha}^{1\parallel}(3(L_1 - L_2))}{8C_{PU2}(L_a^2 + 4L_a L_e)} - \frac{M_{\Delta\alpha}^{1\parallel} C_L}{4C_{PU2}(L_a^2 + 4L_a L_e)}
\end{array} \right]
\end{aligned}$$

$$\begin{aligned}
\tilde{A}_{12}^{17} = & \left[\begin{array}{cc}
-\frac{M_{\Delta 0}^{3\parallel}}{2L_a} - \frac{M_{\Delta\alpha}^{1\parallel}}{4L_a} & -\frac{M_{\Delta\alpha}^{1\perp}}{4L_a} - \frac{M_{\Delta 0}^{3\perp}}{2L_a} \\
\frac{M_{\Delta\alpha}^{1\perp}}{4L_a} - \frac{M_{\Delta 0}^{3\perp}}{2L_a} & \frac{M_{\Delta 0}^{3\parallel}}{2L_a} - \frac{M_{\Delta\alpha}^{2\parallel}}{4L_a} \\
-\frac{M_{\Delta 0}^{dc}}{L_a} & 0 \\
0 & -\frac{M_{\Delta 0}^{dc}}{L_a} \\
\frac{M_{\Delta\beta}^{1\parallel}}{4L_a} & \frac{M_{\Delta\beta}^{1\perp}}{4L_a} \\
-\frac{M_{\Delta\beta}^{1\perp}}{4L_a} & \frac{M_{\Delta\beta}^{1\parallel}}{4L_a} \\
0 & 0 \\
0 & 0 \\
\frac{M_{\Sigma\alpha}^{2\parallel}(3(L_1 - L_2))}{8C_{PU2}(L_a^2 + 4L_aL_e)} - \frac{M_{\Delta\alpha}^{2\parallel}C_L}{4C_{PU2}(L_a^2 + 4L_aL_e)} & \frac{M_{\Sigma\alpha}^{2\perp}(3(L_1 - L_2))}{8C_{PU2}(L_a^2 + 4L_aL_e)} - \frac{M_{\Delta\alpha}^{2\perp}C_L}{4C_{PU2}(L_a^2 + 4L_aL_e)} \\
\frac{M_{\Sigma\alpha}^{1\parallel}(3(L_1 - L_2))}{8C_{PU2}(L_a^2 + 4L_aL_e)} - \frac{M_{\Delta\alpha}^{1\parallel}C_L}{4C_{PU2}(L_a^2 + 4L_aL_e)} & \frac{M_{\Delta\alpha}^{1\perp}C_L}{4C_{PU2}(L_a^2 + 4L_aL_e)} - \frac{M_{\Sigma\alpha}^{1\perp}(3(L_1 - L_2))}{8C_{PU2}(L_a^2 + 4L_aL_e)} \\
\frac{M_{\Sigma\alpha}^{1\perp}(3(L_1 - L_2))}{8C_{PU2}(L_a^2 + 4L_aL_e)} - \frac{M_{\Delta\alpha}^{1\perp}C_L}{4C_{PU2}(L_a^2 + 4L_aL_e)} & \frac{M_{\Sigma\alpha}^{1\parallel}(3(L_1 - L_2))}{8C_{PU2}(L_a^2 + 4L_aL_e)} - \frac{M_{\Delta\alpha}^{1\parallel}C_L}{4C_{PU2}(L_a^2 + 4L_aL_e)}
\end{array} \right] \\
\tilde{A}_{12}^{18} = & \left[\begin{array}{cc}
\frac{M_{\Delta\beta}^{2\parallel}}{4L_a} & \frac{M_{\Delta\beta}^{2\perp}}{4L_a} \\
\frac{M_{\Delta\beta}^{2\perp}}{4L_a} & -\frac{M_{\Delta\beta}^{2\parallel}}{4L_a} \\
\frac{M_{\Delta\beta}^{1\parallel}}{4L_a} & -\frac{M_{\Delta\beta}^{1\perp}}{4L_a} \\
\frac{M_{\Delta\beta}^{1\perp}}{4L_a} & \frac{M_{\Delta\beta}^{1\parallel}}{4L_a} \\
-\frac{M_{\Delta 0}^{dc}}{L_a} + \frac{M_{\Delta\alpha}^{2\parallel}}{4L_a} & \frac{M_{\Delta\alpha}^{2\perp}}{4L_a} \\
\frac{M_{\Delta\alpha}^{2\perp}}{4L_a} & -\frac{M_{\Delta 0}^{dc}}{L_a} - \frac{M_{\Delta\alpha}^{2\parallel}}{4L_a} \\
-\frac{M_{\Delta 0}^{3\parallel}}{2L_a} + \frac{M_{\Delta\alpha}^{1\parallel}}{4L_a} & -\frac{M_{\Delta\alpha}^{1\perp}}{4L_a} - \frac{M_{\Delta 0}^{3\perp}}{2L_a} \\
\frac{M_{\Delta\alpha}^{1\perp}}{4L_a} - \frac{M_{\Delta 0}^{3\perp}}{2L_a} & \frac{M_{\Delta 0}^{3\parallel}}{2L_a} + \frac{M_{\Delta\alpha}^{1\parallel}}{4L_a} \\
\frac{M_{\Sigma\beta}^{1\parallel}(3(L_1 - L_2))}{8C_{PU2}(L_a^2 + 4L_aL_e)} - \frac{M_{\Delta\beta}^{1\parallel}C_L}{4C_{PU2}(L_a^2 + 4L_aL_e)} & \frac{M_{\Sigma\beta}^{1\perp}(3(L_1 - L_2))}{8C_{PU2}(L_a^2 + 4L_aL_e)} - \frac{M_{\Delta\beta}^{1\perp}C_L}{4C_{PU2}(L_a^2 + 4L_aL_e)} \\
\frac{M_{\Sigma\beta}^{2\parallel}(3(L_1 - L_2))}{8C_{PU2}(L_a^2 + 4L_aL_e)} - \frac{M_{\Delta\beta}^{2\parallel}C_L}{4C_{PU2}(L_a^2 + 4L_aL_e)} & \frac{M_{\Delta\beta}^{2\perp}C_L}{4C_{PU2}(L_a^2 + 4L_aL_e)} - \frac{M_{\Sigma\beta}^{2\perp}(3(L_1 - L_2))}{8C_{PU2}(L_a^2 + 4L_aL_e)} \\
\frac{M_{\Sigma\beta}^{2\perp}(3(L_1 - L_2))}{8C_{PU2}(L_a^2 + 4L_aL_e)} - \frac{M_{\Delta\beta}^{2\perp}C_L}{4C_{PU2}(L_a^2 + 4L_aL_e)} & \frac{M_{\Sigma\beta}^{2\parallel}(3(L_1 - L_2))}{8C_{PU2}(L_a^2 + 4L_aL_e)} - \frac{M_{\Delta\beta}^{2\parallel}C_L}{4C_{PU2}(L_a^2 + 4L_aL_e)} \\
\frac{M_{\Sigma\beta}^{1\perp}(3(L_1 - L_2))}{8C_{PU2}(L_a^2 + 4L_aL_e)} - \frac{M_{\Delta\beta}^{1\perp}C_L}{4C_{PU2}(L_a^2 + 4L_aL_e)} & \frac{M_{\Sigma\beta}^{1\parallel}(3(L_1 - L_2))}{8C_{PU2}(L_a^2 + 4L_aL_e)} - \frac{M_{\Delta\beta}^{1\parallel}C_L}{4C_{PU2}(L_a^2 + 4L_aL_e)}
\end{array} \right]
\end{aligned}$$

$$\tilde{A}_{12}^{19} = \left[\begin{array}{cc} \frac{M_{\Delta\beta}^{1\parallel}}{4L_a} & \frac{M_{\Delta\beta}^{1\perp}}{4L_a} \\ -\frac{M_{\Delta\beta}^{1\perp}}{4L_a} & \frac{M_{\Delta\beta}^{1\parallel}}{4L_a} \\ 0 & 0 \\ 0 & 0 \\ -\frac{M_{\Delta 0}^{3\parallel}}{2L_a} + \frac{M_{\Delta\alpha}^{1\parallel}}{4L_a} & \frac{M_{\Delta\alpha}^{1\perp}}{4L_a} - \frac{M_{\Delta 0}^{3\perp}}{2L_a} \\ -\frac{M_{\Delta\alpha}^{1\perp}}{4L_a} - \frac{M_{\Delta 0}^{3\perp}}{2L_a} & \frac{M_{\Delta 0}^{3\parallel}}{2L_a} + \frac{M_{\Delta\alpha}^{2\parallel}}{4L_a} \\ -\frac{M_{\Delta 0}^{dc}}{L_a} & 0 \\ 0 & -\frac{M_{\Delta 0}^{dc}}{L_a} \\ \frac{M_{\Sigma\beta}^{2\parallel}(3(L_1 - L_2))}{8C_{PU2}(L_a^2 + 4L_a L_e)} - \frac{M_{\Delta\beta}^{2\parallel} C_L}{4C_{PU2}(L_a^2 + 4L_a L_e)} & \frac{M_{\Sigma\beta}^{2\perp}(3(L_1 - L_2))}{8C_{PU2}(L_a^2 + 4L_a L_e)} - \frac{M_{\Delta\beta}^{2\perp} C_L}{4C_{PU}(L_a^2 + 4L_a L_e)} \\ \frac{M_{\Sigma\beta}^{1\parallel}(3(L_1 - L_2))}{8C_{PU2}(L_a^2 + 4L_a L_e)} - \frac{M_{\Delta\beta}^{1\parallel} C_L}{4C_{PU}(L_a^2 + 4L_a L_e)} & \frac{M_{\Sigma\beta}^{1\perp} C_L}{4C_{PU2}(L_a^2 + 4L_a L_e)} - \frac{M_{\Sigma\beta}^{1\perp}(3(L_1 - L_2))}{8C_{PU2}(L_a^2 + 4L_a L_e)} \\ \frac{M_{\Sigma\beta}^{1\perp}(3(L_1 - L_2))}{8C_{PU2}(L_a^2 + 4L_a L_e)} - \frac{M_{\Delta\beta}^{1\perp} C_L}{4C_{PU2}(L_a^2 + 4L_a L_e)} & \frac{M_{\Sigma\beta}^{1\parallel}(3(L_1 - L_2))}{8C_{PU2}(L_a^2 + 4L_a L_e)} - \frac{M_{\Delta\beta}^{1\parallel} C_L}{4C_{PU2}(L_a^2 + 4L_a L_e)} \end{array} \right]$$

$$\tilde{A}_{12}^{110} = \left[\begin{array}{ccc} -\frac{M_{\Delta\alpha}^{1\parallel}}{L_a} & -\frac{M_{\Delta\alpha}^{2\parallel}}{2L_a} & -\frac{M_{\Delta\alpha}^{2\perp}}{2L_a} \\ -\frac{M_{\Delta\alpha}^{1\perp}}{L_a} & \frac{M_{\Delta\alpha}^{2\perp}}{2L_a} & -\frac{M_{\Delta\alpha}^{2\parallel}}{2L_a} \\ -\frac{M_{\Delta\alpha}^{2\parallel}}{L_a} & -\frac{M_{\Delta\alpha}^{1\parallel}}{2L_a} & -\frac{M_{\Delta\alpha}^{1\perp}}{2L_a} \\ -\frac{M_{\Delta\alpha}^{2\perp}}{L_a} & \frac{M_{\Delta\alpha}^{1\perp}}{2L_a} & -\frac{M_{\Delta\alpha}^{1\parallel}}{2L_a} \\ -\frac{M_{\Delta\beta}^{1\parallel}}{L_a} & -\frac{M_{\Delta\beta}^{2\parallel}}{2L_a} & -\frac{M_{\Delta\beta}^{2\perp}}{2L_a} \\ -\frac{M_{\Delta\beta}^{1\perp}}{L_a} & \frac{M_{\Delta\beta}^{2\perp}}{2L_a} & -\frac{M_{\Delta\beta}^{2\parallel}}{2L_a} \\ -\frac{M_{\Delta\beta}^{2\parallel}}{L_a} & -\frac{M_{\Delta\beta}^{1\parallel}}{2L_a} & -\frac{M_{\Delta\beta}^{1\perp}}{2L_a} \\ -\frac{M_{\Delta\beta}^{2\perp}}{L_a} & \frac{M_{\Delta\beta}^{1\perp}}{2L_a} & -\frac{M_{\Delta\beta}^{1\parallel}}{2L_a} \\ \frac{3M_{\Sigma 0}^{dc}(L_1 - L_2)}{2C_{PU2}(L_a^2 + 4L_a L_e)} - \frac{M_{\Delta 0}^{dc} C_L}{C_{PU2}(L_a^2 + 4L_a L_e)} & \frac{M_{\Sigma 0}^{3\parallel}(3(L_1 - L_2))}{2C_{PU}(L_a^2 + 4L_a L_e)} - \frac{M_{\Delta 0}^{3\parallel} C_L}{2C_{PU2}(L_a^2 + 4L_a L_e)} & \frac{M_{\Sigma 0}^{3\perp}(3(L_1 - L_2))}{2C_{PU2}(L_a^2 + 4L_a L_e)} - \frac{M_{\Delta 0}^{3\perp} C_L}{2C_{PU2}(L_a^2 + 4L_a L_e)} \\ \frac{3M_{\Sigma 0}^{3\parallel}(L_1 - L_2)}{2C_{PU2}(L_a^2 + 4L_a L_e)} - \frac{M_{\Delta 0}^{3\parallel} C_L}{C_{PU2}(L_a^2 + 4L_a L_e)} & \frac{M_{\Sigma 0}^{dc}(3(L_1 - L_2))}{2C_{PU2}(L_a^2 + 4L_a L_e)} - \frac{M_{\Delta 0}^{dc} C_L}{C_{PU2}(L_a^2 + 4L_a L_e)} & 0 \\ \frac{3M_{\Sigma 0}^{3\perp}(L_1 - L_2)}{2C_{PU}(L_a^2 + 4L_a L_e)} - \frac{M_{\Delta\beta}^{3\perp} C_L}{C_{PU}(L_a^2 + 4L_a L_e)} & 0 & \frac{M_{\Sigma 0}^{dc}(3(L_1 - L_2))}{2C_{PU}(L_a^2 + 4L_a L_e)} - \frac{M_{\Delta 0}^{dc} C_L}{C_{PU}(L_a^2 + 4L_a L_e)} \end{array} \right]$$

$$\begin{aligned}
\tilde{A}_{12}^{21} = & \left[\begin{array}{c} \frac{M_{\Delta 0}^{dc}(4L_e + 6L_m)}{C_{LL2}} - \frac{M_{\Delta \alpha}^{2\parallel}(2L_e + 3L_m)}{2C_{LL2}} \\ - \frac{M_{\Delta \alpha}^{2\perp}(2L_e + 3L_m)}{2C_{LL2}} \\ \frac{M_{\Delta 0}^{3\parallel}(2L_e + 3L_m)}{C_{LL2}} - \frac{M_{\Delta \alpha}^{1\parallel}(2L_e + 3L_m)}{2C_{LL2}} \\ \frac{M_{\Delta \alpha}^{1\perp}(2L_e + 3L_m)}{2C_{LL2}} - \frac{M_{\Delta 0}^{3\perp}(2L_e + 3L_m)}{C_{LL2}} \\ \frac{M_{\Delta \beta}^{2\parallel}(2L_e + 3L_m)}{2C_{LL2}} \\ \frac{M_{\Delta \beta}^{2\perp}(2L_e + 3L_m)}{2C_{LL2}} \\ \frac{M_{\Delta \beta}^{1\parallel}(2L_e + 3L_m)}{2C_{LL2}} \\ \frac{M_{\Delta \beta}^{1\perp}(2L_e + 3L_m)}{2C_{LL2}} \end{array} \right] \\
\tilde{A}_{12}^{22} = & \left[\begin{array}{c} \frac{M_{\Delta 0}^{3\parallel}(2L_e + 3L_m)}{C_{LL2}} - \frac{M_{\Delta \alpha}^{1\parallel}(2L_e + 3L_m)}{2C_{LL2}} \\ \frac{M_{\Delta \alpha}^{1\perp}(2L_e + 3L_m)}{2C_{LL2}} - \frac{M_{\Delta 0}^{3\perp}(2L_e + 3L_m)}{C_{LL2}} \\ - \frac{M_{\Delta 0}^{dc}(4L_e + 6L_m)}{C_{LL2}} \\ 0 \\ \frac{M_{\Delta \beta}^{1\parallel}(2L_e + 3L_m)}{2C_{LL2}} \\ - \frac{M_{\Delta \beta}^{1\perp}(2L_e + 3L_m)}{2C_{LL2}} \\ 0 \\ 0 \end{array} \right]
\end{aligned}$$

$$\begin{aligned}
\bar{A}_{12}^{23} = & \left[\begin{array}{cc}
\frac{M_{\Delta\beta}^{2\parallel}(2L_e + 3L_m)}{2C_{LL2}} & \frac{M_{\Delta\beta}^{2\perp}(2L_e + 3L_m)}{2C_{LL2}} \\
\frac{M_{\Delta\beta}^{2\perp}(2L_e + 3L_m)}{2C_{LL2}} & -\frac{M_{\Delta\beta}^{2\parallel}(2L_e + 3L_m)}{2C_{LL}} \\
\frac{M_{\Delta\beta}^{1\parallel}(2L_e + 3L_m)}{2C_{LL2}} & -\frac{M_{\Delta\beta}^{1\perp}(2L_e + 3L_m)}{2C_{LL2}} \\
\frac{M_{\Delta\beta}^{1\perp}(2L_e + 3L_m)}{2C_{LL}} & \frac{M_{\Delta\beta}^{1\parallel}(2L_e + 3L_m)}{2C_{LL}} \\
-\frac{M_{\Delta 0}^{dc}(4L_e + 6L_m)}{C_{LL2}} + \frac{M_{\Delta\alpha}^{2\parallel}(2L_e + 3L_m)}{2C_{LL2}} & \frac{M_{\Delta\alpha}^{2\perp}(2L_e + 3L_m)}{2C_{LL2}} \\
\frac{M_{\Delta\alpha}^{2\perp}(2L_e + 3L_m)}{2C_{LL2}} & -\frac{M_{\Delta 0}^{dc}(4L_e + 6L_m)}{C_{LL}} - \frac{M_{\Delta\alpha}^{2\parallel}(2L_e + 3L_m)}{2C_{LL2}} \\
-\frac{M_{\Delta 0}^{3\parallel}(2L_e + 3L_m)}{C_{LL2}} + \frac{M_{\Delta\alpha}^{1\parallel}(2L_e + 3L_m)}{2C_{LL2}} & \frac{M_{\Delta\alpha}^{1\perp}(2L_e + 3L_m)}{2C_{LL}} - \frac{M_{\Delta 0}^{3\perp}(2L_e + 3L_m)}{C_{LL2}} \\
\frac{M_{\Delta\alpha}^{1\perp}(2L_e + 3L_m)}{2C_{LL}} - \frac{M_{\Delta 0}^{3\perp}(2L_e + 3L_m)}{C_{LL}} & \frac{M_{\Delta 0}^{3\parallel}(2L_e + 3L_m)}{C_{LL2}} + \frac{M_{\Delta\alpha}^{1\parallel}(2L_e + 3L_m)}{2C_{LL2}}
\end{array} \right] \\
\bar{A}_{12}^{24} = & \left[\begin{array}{cc}
\frac{M_{\Delta\beta}^{1\parallel}(2L_e + 3L_m)}{2C_{LL2}} & \frac{M_{\Delta\beta}^{1\perp}(2L_e + 3L_m)}{2C_{LL2}} \\
-\frac{M_{\Delta\beta}^{1\perp}(2L_e + 3L_m)}{2C_{LL2}} & \frac{M_{\Delta\beta}^{1\parallel}(2L_e + 3L_m)}{2C_{LL2}} \\
0 & 0 \\
0 & 0 \\
-\frac{M_{\Delta 0}^{3\parallel}(2L_e + 3L_m)}{C_{LL}} + \frac{M_{\Delta\alpha}^{1\parallel}(2L_e + 3L_m)}{2C_{LL2}} & \frac{M_{\Delta\alpha}^{1\perp}(2L_e + 3L_m)}{2C_{LL2}} - \frac{M_{\Delta 0}^{3\perp}(2L_e + 3L_m)}{C_{LL}} \\
\frac{M_{\Delta\alpha}^{1\perp}(2L_e + 3L_m)}{2C_{LL}} - \frac{M_{\Delta 0}^{3\perp}(2L_e + 3L_m)}{C_{LL2}} & \frac{M_{\Delta 0}^{3\parallel}(2L_e + 3L_m)}{C_{LL2}} + \frac{M_{\Delta\alpha}^{1\parallel}(2L_e + 3L_m)}{2C_{LL2}} \\
-\frac{M_{\Delta 0}^{dc}(4L_e + 6L_m)}{C_{LL}} & 0 \\
0 & -\frac{M_{\Delta 0}^{dc}(4L_e + 6L_m)}{C_{LL}}
\end{array} \right]
\end{aligned}$$

$$\begin{aligned}
\tilde{A}_{12}^{25} = & \left[\begin{array}{c} \frac{M_{\Delta\alpha}^{1\parallel}(4L_e + 6L_m)}{C_{LL2}} - \frac{M_{\Delta\alpha}^{2\parallel}(2L_e + 3L_m)}{C_{LL2}} - \frac{M_{\Delta\alpha}^{2\perp}(2L_e + 3L_m)}{C_{LL2}} \\ \frac{M_{\Delta\alpha}^{1\perp}(4L_e + 6L_m)}{C_{LL2}} - \frac{M_{\Delta\alpha}^{2\perp}(2L_e + 3L_m)}{C_{LL2}} - \frac{M_{\Delta\alpha}^{2\parallel}(2L_e + 3L_m)}{C_{LL2}} \\ \frac{M_{\Delta\alpha}^{2\parallel}(4L_e + 6L_m)}{C_{LL2}} - \frac{M_{\Delta\alpha}^{1\parallel}(2L_e + 3L_m)}{C_{LL2}} - \frac{M_{\Delta\alpha}^{1\perp}(2L_e + 3L_m)}{C_{LL2}} \\ \frac{M_{\Delta\alpha}^{2\perp}(4L_e + 6L_m)}{C_{LL2}} - \frac{M_{\Delta\alpha}^{1\perp}(2L_e + 3L_m)}{C_{LL2}} - \frac{M_{\Delta\alpha}^{1\parallel}(2L_e + 3L_m)}{C_{LL2}} \\ \frac{M_{\Delta\beta}^{1\parallel}(4L_e + 6L_m)}{C_{LL2}} - \frac{M_{\Delta\beta}^{2\parallel}(2L_e + 3L_m)}{C_{LL2}} - \frac{M_{\Delta\beta}^{2\perp}(2L_e + 3L_m)}{C_{LL2}} \\ \frac{M_{\Delta\beta}^{1\perp}(4L_e + 6L_m)}{C_{LL2}} - \frac{M_{\Delta\beta}^{2\perp}(2L_e + 3L_m)}{C_{LL2}} - \frac{M_{\Delta\beta}^{2\parallel}(2L_e + 3L_m)}{C_{LL2}} \\ \frac{M_{\Delta\beta}^{2\parallel}(4L_e + 6L_m)}{C_{LL2}} - \frac{M_{\Delta\beta}^{1\parallel}(2L_e + 3L_m)}{C_{LL2}} - \frac{M_{\Delta\beta}^{1\perp}(2L_e + 3L_m)}{C_{LL2}} \\ \frac{M_{\Delta\beta}^{2\perp}(4L_e + 6L_m)}{C_{LL2}} - \frac{M_{\Delta\beta}^{1\perp}(2L_e + 3L_m)}{C_{LL2}} - \frac{M_{\Delta\beta}^{1\parallel}(2L_e + 3L_m)}{C_{LL2}} \end{array} \right] \\
\tilde{A}_{12}^{26} = & \left[\begin{array}{c} \frac{M_{\Sigma 0}^{dc}(4L_e + 6L_m)}{C_{LL2}} - \frac{M_{\Sigma\alpha}^{2\parallel}(2L_e + 3L_m)}{2C_{LL2}} - \frac{M_{\Sigma\alpha}^{2\perp}(2L_e + 3L_m)}{2C_{LL2}} \\ - \frac{M_{\Sigma\alpha}^{2\perp}(2L_e + 3L_m)}{2C_{LL2}} - \frac{M_{\Sigma 0}^{dc}(4L_e + 6L_m)}{C_{LL2}} + \frac{M_{\Sigma\alpha}^{2\parallel}(2L_e + 3L_m)}{2C_{LL2}} \\ \frac{M_{\Sigma 0}^{3\parallel}(2L_e + 3L_m)}{C_{LL2}} - \frac{M_{\Sigma\alpha}^{1\parallel}(2L_e + 3L_m)}{2C_{LL2}} - \frac{M_{\Sigma\alpha}^{1\perp}(2L_e + 3L_m)}{2C_{LL2}} - \frac{M_{\Sigma 0}^{3\perp}(2L_e + 3L_m)}{C_{LL2}} \\ \frac{M_{\Sigma\alpha}^{1\perp}(2L_e + 3L_m)}{2C_{LL2}} - \frac{M_{\Sigma 0}^{3\perp}(2L_e + 3L_m)}{C_{LL2}} - \frac{M_{\Sigma 0}^{3\parallel}(2L_e + 3L_m)}{C_{LL2}} - \frac{M_{\Sigma\alpha}^{1\parallel}(2L_e + 3L_m)}{2C_{LL2}} \\ \frac{M_{\Sigma\beta}^{2\parallel}(2L_e + 3L_m)}{2C_{LL2}} - \frac{M_{\Sigma\beta}^{2\perp}(2L_e + 3L_m)}{2C_{LL2}} \\ \frac{M_{\Sigma\beta}^{2\perp}(2L_e + 3L_m)}{2C_{LL2}} - \frac{M_{\Sigma\beta}^{2\parallel}(2L_e + 3L_m)}{2C_{LL2}} \\ \frac{M_{\Sigma\beta}^{1\parallel}(2L_e + 3L_m)}{2C_{LL2}} - \frac{M_{\Sigma\beta}^{1\perp}(2L_e + 3L_m)}{2C_{LL2}} \\ \frac{M_{\Sigma\beta}^{1\perp}(2L_e + 3L_m)}{2C_{LL2}} - \frac{M_{\Sigma\beta}^{1\parallel}(2L_e + 3L_m)}{2C_{LL2}} \end{array} \right]
\end{aligned}$$

$$\begin{aligned}
\tilde{A}_{12}^{27} = & \left[\begin{array}{cc} -\frac{M_{\Sigma 0}^{3\parallel}(2L_e + 3L_m)}{C_{LL2}} - \frac{M_{\Sigma\alpha}^{1\parallel}(2L_e + 3L_m)}{2C_{LL2}} & -\frac{M_{\Sigma\alpha}^{1\perp}(2L_e + 3L_m)}{2C_{LL2}} - \frac{M_{\Sigma 0}^{3\perp}(2L_e + 3L_m)}{C_{LL2}} \\ \frac{M_{\Sigma\alpha}^{1\perp}(2L_e + 3L_m)}{2C_{LL2}} - \frac{M_{\Sigma 0}^{3\perp}(2L_e + 3L_m)}{C_{LL2}} & \frac{M_{\Sigma 0}^{3\parallel}(2L_e + 3L_m)}{C_{LL2}} - \frac{M_{\Sigma\alpha}^{1\parallel}(2L_e + 3L_m)}{2C_{LL2}} \\ -\frac{M_{\Sigma 0}^{dc}(4L_e + 6L_m)}{C_{LL2}} & 0 \\ 0 & -\frac{M_{\Sigma 0}^{dc}(4L_e + 6L_m)}{C_{LL2}} \\ \frac{M_{\Sigma\beta}^{1\parallel}(2L_e + 3L_m)}{2C_{LL2}} & \frac{M_{\Sigma\beta}^{1\perp}(2L_e + 3L_m)}{2C_{LL2}} \\ -\frac{M_{\Sigma\beta}^{1\perp}(2L_e + 3L_m)}{2C_{LL2}} & \frac{M_{\Sigma\beta}^{1\parallel}(2L_e + 3L_m)}{2C_{LL2}} \\ 0 & 0 \\ 0 & 0 \end{array} \right] \\
\tilde{A}_{12}^{28} = & \left[\begin{array}{cc} \frac{M_{\Sigma\beta}^{2\parallel}(2L_e + 3L_m)}{2C_{LL2}} & \frac{M_{\Sigma\beta}^{2\perp}(2L_e + 3L_m)}{2C_{LL2}} \\ \frac{M_{\Sigma\beta}^{2\perp}(2L_e + 3L_m)}{2C_{LL2}} & -\frac{M_{\Sigma\beta}^{2\parallel}(2L_e + 3L_m)}{2C_{LL2}} \\ \frac{M_{\Sigma\beta}^{1\parallel}(2L_e + 3L_m)}{2C_{LL2}} & -\frac{M_{\Sigma\beta}^{1\perp}(2L_e + 3L_m)}{2C_{LL}} \\ \frac{M_{\Sigma\beta}^{1\perp}(2L_e + 3L_m)}{2C_{LL}} & \frac{M_{\Sigma\beta}^{1\parallel}(2L_e + 3L_m)}{2C_{LL}} \\ -\frac{M_{\Sigma 0}^{dc}(4L_e + 6L_m)}{C_{LL2}} + \frac{M_{\Sigma\alpha}^{2\parallel}(2L_e + 3L_m)}{2C_{LL}} & \frac{M_{\Sigma\alpha}^{2\perp}(2L_e + 3L_m)}{2C_{LL}} \\ \frac{M_{\Sigma\alpha}^{2\perp}(2L_e + 3L_m)}{2C_{LL2}} & -\frac{M_{\Sigma 0}^{dc}(4L_e + 6L_m)}{C_{LL2}} - \frac{M_{\Sigma\alpha}^{2\parallel}(2L_e + 3L_m)}{2C_{LL2}} \\ -\frac{M_{\Sigma 0}^{3\parallel}(2L_e + 3L_m)}{C_{LL}} + \frac{M_{\Sigma\alpha}^{1\parallel}(2L_e + 3L_m)}{2C_{LL2}} & \frac{M_{\Sigma\alpha}^{1\perp}(2L_e + 3L_m)}{2C_{LL}} - \frac{M_{\Sigma 0}^{3\perp}(2L_e + 3L_m)}{C_{LL}} \\ \frac{M_{\Sigma\alpha}^{1\perp}(2L_e + 3L_m)}{2C_{LL2}} - \frac{M_{\Sigma 0}^{3\perp}(2L_e + 3L_m)}{C_{LL}} & \frac{M_{\Sigma 0}^{3\parallel}(2L_e + 3L_m)}{C_{LL2}} + \frac{M_{\Sigma\alpha}^{1\parallel}(2L_e + 3L_m)}{2C_{LL2}} \end{array} \right]
\end{aligned}$$

$$\begin{aligned}
\tilde{A}_{12}^{29} = & \left[\begin{array}{cc} \frac{M_{\Sigma\beta}^{1\parallel}(2L_e + 3L_m)}{2C_{LL2}} & \frac{M_{\Sigma\beta}^{1\perp}(2L_e + 3L_m)}{2C_{LL2}} \\ -\frac{M_{\Sigma\beta}^{1\perp}(2L_e + 3L_m)}{2C_{LL2}} & \frac{M_{\Sigma\beta}^{1\parallel}(2L_e + 3L_m)}{2C_{LL2}} \\ 0 & 0 \\ 0 & 0 \\ -\frac{M_{\Sigma 0}^{3\parallel}(2L_e + 3L_m)}{C_{LL2}} + \frac{M_{\Sigma\alpha}^{1\parallel}(2L_e + 3L_m)}{2C_{LL2}} & \frac{M_{\Sigma\alpha}^{1\perp}(2L_e + 3L_m)}{2C_{LL2}} - \frac{M_{\Sigma 0}^{3\perp}(2L_e + 3L_m)}{C_{LL2}} \\ \frac{M_{\Sigma\alpha}^{1\perp}(2L_e + 3L_m)}{2C_{LL2}} - \frac{M_{\Sigma 0}^{3\perp}(2L_e + 3L_m)}{C_{LL2}} & \frac{M_{\Sigma 0}^{3\parallel}(2L_e + 3L_m)}{C_{LL2}} + \frac{M_{\Sigma\alpha}^{1\parallel}(2L_e + 3L_m)}{2C_{LL2}} \\ -\frac{M_{\Sigma 0}^{dc}(4L_e + 6L_m)}{C_{LL2}} & 0 \\ 0 & -\frac{M_{\Sigma 0}^{dc}(4L_e + 6L_m)}{C_{LL2}} \end{array} \right] \\
\tilde{A}_{12}^{210} = & \left[\begin{array}{ccc} \frac{M_{\Sigma\alpha}^{1\parallel}(4L_e + 6L_m)}{C_{LL2}} & -\frac{M_{\Sigma\alpha}^{2\parallel}(2L_e + 3L_m)}{C_{LL2}} & -\frac{M_{\Sigma\alpha}^{2\perp}(2L_e + 3L_m)}{C_{LL2}} \\ -\frac{M_{\Sigma\alpha}^{1\perp}(4L_e + 6L_m)}{C_{LL2}} & \frac{M_{\Sigma\alpha}^{2\perp}(2L_e + 3L_m)}{C_{LL2}} & -\frac{M_{\Sigma\alpha}^{2\parallel}(2L_e + 3L_m)}{C_{LL2}} \\ \frac{M_{\Sigma\alpha}^{2\parallel}(4L_e + 6L_m)}{C_{LL2}} & -\frac{M_{\Sigma\alpha}^{1\parallel}(2L_e + 3L_m)}{C_{LL2}} & -\frac{M_{\Sigma\alpha}^{1\perp}(2L_e + 3L_m)}{C_{LL}} \\ -\frac{M_{\Sigma\alpha}^{2\perp}(4L_e + 6L_m)}{C_{LL2}} & \frac{M_{\Sigma\alpha}^{1\perp}(2L_e + 3L_m)}{C_{LL2}} & -\frac{M_{\Sigma\alpha}^{1\parallel}(2L_e + 3L_m)}{C_{LL2}} \\ \frac{M_{\Sigma\beta}^{1\parallel}(4L_e + 6L_m)}{C_{LL2}} & -\frac{M_{\Sigma\beta}^{2\parallel}(2L_e + 3L_m)}{C_{LL2}} & -\frac{M_{\Sigma\beta}^{2\perp}(2L_e + 3L_m)}{C_{LL2}} \\ -\frac{M_{\Sigma\beta}^{1\perp}(4L_e + 6L_m)}{C_{LL2}} & \frac{M_{\Sigma\beta}^{2\perp}(2L_e + 3L_m)}{C_{LL2}} & -\frac{M_{\Sigma\beta}^{2\parallel}(2L_e + 3L_m)}{C_{LL2}} \\ \frac{M_{\Sigma\beta}^{2\parallel}(4L_e + 6L_m)}{C_{LL2}} & -\frac{M_{\Sigma\beta}^{1\parallel}(2L_e + 3L_m)}{C_{LL2}} & -\frac{M_{\Sigma\beta}^{1\perp}(2L_e + 3L_m)}{C_{LL}} \\ -\frac{M_{\Sigma\beta}^{2\perp}(4L_e + 6L_m)}{C_{LL2}} & \frac{M_{\Sigma\beta}^{1\perp}(2L_e + 3L_m)}{C_{LL}} & -\frac{M_{\Sigma\beta}^{1\parallel}(2L_e + 3L_m)}{C_{LL}} \end{array} \right]
\end{aligned}$$

$$\begin{aligned}
\bar{A}_{12}^{31} = & \left[\begin{array}{cc}
-\frac{2M_{\Delta 0}^{dc} L_s}{C_{LL}} - \frac{M_{\Delta \alpha}^{2\parallel} L_s}{2C_{LL2}} & -\frac{M_{\Delta \alpha}^{2\perp} L_s}{2C_{LL2}} \\
-\frac{M_{\Delta \alpha}^{2\perp} L_s}{2C_{LL}} & -\frac{2M_{\Delta 0}^{dc} L_s}{C_{LL}} + \frac{M_{\Delta \alpha}^{2\parallel} L_s}{2C_{LL}} \\
-\frac{M_{\Delta 0}^{3\parallel} L_s}{C_{LL2}} - \frac{M_{\Delta \alpha}^{1\parallel} L_s}{2C_{LL2}} & \frac{M_{\Delta \alpha}^{1\perp} L_s}{2C_{LL2}} - \frac{M_{\Delta 0}^{3\perp} L_s}{C_{LL2}} \\
-\frac{M_{\Delta \alpha}^{1\perp} L_s}{2C_{LL}} - \frac{M_{\Delta 0}^{3\perp} L_s}{C_{LL2}} & \frac{M_{\Delta 0}^{3\parallel} L_s}{C_{LL2}} - \frac{M_{\Delta \alpha}^{1\parallel} L_s}{2C_{LL2}} \\
\frac{M_{\Delta \beta}^{2\parallel} L_s}{2C_{LL2}} & \frac{M_{\Delta \beta}^{2\perp} L_s}{2C_{LL2}} \\
\frac{M_{\Delta \beta}^{2\perp} L_s}{2C_{LL}} & -\frac{M_{\Delta \beta}^{2\parallel} L_s}{2C_{LL}} \\
\frac{M_{\Delta \beta}^{1\parallel} L_s}{2C_{LL}} & -\frac{M_{\Delta \beta}^{1\perp} L_s}{2C_{LL}} \\
\frac{M_{\Delta \beta}^{1\perp} L_s}{2C_{LL2}} & \frac{M_{\Delta \beta}^{1\parallel} L_s}{2C_{LL2}} \\
\frac{3M_{\Sigma \alpha}^{1\parallel} (L_1 - L_2)}{4C_{PU2}(L_a^2 + 4L_a L_e)} - \frac{M_{\Delta \alpha}^{1\parallel} (3(L_1 + L_2) + 2L_a)}{4C_{PU2}(L_a^2 + 4L_a L_e)} & \frac{3M_{\Sigma \alpha}^{1\perp} (L_1 - L_2)}{4C_{PU} (L_a^2 + 4L_a L_e)} - \frac{M_{\Delta \alpha}^{1\perp} (3(L_1 + L_2) + 2L_a)}{4C_{PU} (L_a^2 + 4L_a L_e)} \\
\frac{3M_{\Sigma \alpha}^{2\parallel} (L_1 - L_2)}{4C_{PU} (L_a^2 + 4L_a L_e)} - \frac{M_{\Delta \alpha}^{2\parallel} (3(L_1 + L_2) + 2L_a)}{4C_{PU2}(L_a^2 + 4L_a L_e)} & \frac{3M_{\Sigma \alpha}^{2\perp} (L_1 - L_2)}{4C_{PU} (L_a^2 + 4L_a L_e)} - \frac{M_{\Delta \alpha}^{2\perp} (3(L_1 + L_2) + 2L_a)}{4C_{PU2}(L_a^2 + 4L_a L_e)} \\
\frac{3M_{\Sigma \alpha}^{2\perp} (L_1 - L_2)}{4C_{PU} (L_a^2 + 4L_a L_e)} - \frac{M_{\Delta \alpha}^{2\perp} (3(L_1 + L_2) + 2L_a)}{4C_{PU} (L_a^2 + 4L_a L_e)} & \frac{3M_{\Sigma \alpha}^{2\parallel} (L_1 - L_2)}{4C_{PU2}(L_a^2 + 4L_a L_e)} - \frac{M_{\Delta \alpha}^{2\parallel} (3(L_1 + L_2) + 2L_a)}{4C_{PU2}(L_a^2 + 4L_a L_e)}
\end{array} \right] \\
\bar{A}_{12}^{32} = & \left[\begin{array}{cc}
-\frac{M_{\Delta 0}^{3\parallel} L_s}{C_{LL2}} - \frac{M_{\Delta \alpha}^{1\parallel} L_s}{2C_{LL2}} & \frac{M_{\Delta \alpha}^{1\perp} L_s}{2C_{LL2}} - \frac{M_{\Delta 0}^{3\perp} L_s}{C_{LL}} \\
\frac{M_{\Delta \alpha}^{1\perp} L_s}{2C_{LL2}} - \frac{M_{\Delta 0}^{3\perp} L_s}{C_{LL2}} & \frac{M_{\Delta 0}^{3\parallel} L_s}{C_{LL2}} - \frac{M_{\Delta \alpha}^{1\parallel} L_s}{2C_{LL2}} \\
-\frac{2M_{\Delta 0}^{dc} L_s}{C_{LL}} & 0 \\
0 & -\frac{2M_{\Delta 0}^{dc} L_s}{C_{LL2}} \\
\frac{M_{\Delta \beta}^{1\parallel} L_s}{2C_{LL2}} & \frac{M_{\Delta \beta}^{1\perp} L_s}{2C_{LL2}} \\
-\frac{M_{\Delta \beta}^{1\perp} L_s}{2C_{LL2}} & \frac{M_{\Delta \beta}^{1\parallel} L_s}{2C_{LL2}} \\
0 & 0 \\
0 & 0 \\
\frac{3M_{\Sigma \alpha}^{2\parallel} (L_1 - L_2)}{4C_{PU2}(L_a^2 + 4L_a L_e)} - \frac{M_{\Delta \alpha}^{2\parallel} (3(L_1 + L_2) + 2L_a)}{4C_{PU2}(L_a^2 + 4L_a L_e)} & \frac{3M_{\Sigma \alpha}^{2\perp} (L_1 - L_2)}{4C_{PU2}(L_a^2 + 4L_a L_e)} - \frac{M_{\Delta \alpha}^{2\perp} (3(L_1 + L_2) + 2L_a)}{4C_{PU} (L_a^2 + 4L_a L_e)} \\
\frac{3M_{\Sigma \alpha}^{1\parallel} (L_1 - L_2)}{4C_{PU2}(L_a^2 + 4L_a L_e)} - \frac{M_{\Delta \alpha}^{1\parallel} (3(L_1 + L_2) + 2L_a)}{4C_{PU} (L_a^2 + 4L_a L_e)} & \frac{M_{\Delta \alpha}^{1\perp} (3(L_1 + L_2) + 2L_a)}{4C_{PU2}(L_a^2 + 4L_a L_e)} - \frac{3M_{\Sigma \alpha}^{1\perp} (L_1 - L_2)}{4C_{PU2}(L_a^2 + 4L_a L_e)} \\
\frac{3M_{\Sigma \alpha}^{1\perp} (L_1 - L_2)}{4C_{PU} (L_a^2 + 4L_a L_e)} - \frac{M_{\Delta \alpha}^{1\perp} (3(L_1 + L_2) + 2L_a)}{4C_{PU2}(L_a^2 + 4L_a L_e)} & \frac{3M_{\Sigma \alpha}^{2\parallel} (L_1 - L_2)}{4C_{PU2}(L_a^2 + 4L_a L_e)} - \frac{M_{\Delta \alpha}^{2\parallel} (3(L_1 + L_2) + 2L_a)}{4C_{PU2}(L_a^2 + 4L_a L_e)}
\end{array} \right]
\end{aligned}$$

$$\begin{aligned}
\tilde{A}_{12}^{33} = & \left[\begin{array}{c} \frac{M_{\Delta\beta}^{2\parallel} L_s}{2C_{LL2}} \\ \frac{M_{\Delta\beta}^{2\perp} L_s}{2C_{LL2}} \\ \frac{M_{\Delta\beta}^{1\parallel} L_s}{2C_{LL2}} \\ \frac{M_{\Delta\beta}^{1\perp} L_s}{2C_{LL2}} \\ -\frac{2M_{\Delta 0}^{dc} L_s}{C_{LL2}} + \frac{M_{\Delta\alpha}^{2\parallel} L_s}{2C_{LL2}} \\ \frac{M_{\Delta\alpha}^{2\perp} L_s}{2C_{LL2}} \\ -\frac{M_{\Delta 0}^{3\parallel} L_s}{C_{LL2}} + \frac{M_{\Delta\alpha}^{1\parallel} L_s}{2C_{LL2}} \\ \frac{M_{\Delta\alpha}^{1\perp} L_s}{2C_{LL2}} - \frac{M_{\Delta 0}^{3\perp} L_s}{C_{LL}} \\ \frac{3M_{\Sigma\beta}^{1\parallel} (L_1 - L_2)}{4C_{PU2}(L_a^2 + 4L_a L_e)} - \frac{M_{\Delta\beta}^{1\parallel} (3(L_1 + L_2) + 2L_a)}{4C_{PU2}(L_a^2 + 4L_a L_e)} \\ \frac{3M_{\Sigma\beta}^{2\parallel} (L_1 - L_2)}{4C_{PU2}(L_a^2 + 4L_a L_e)} - \frac{M_{\Delta\beta}^{2\parallel} (3(L_1 + L_2) + 2L_a)}{4C_{PU2}(L_a^2 + 4L_a L_e)} \\ \frac{3M_{\Sigma\beta}^{2\perp} (L_1 - L_2)}{4C_{PU2}(L_a^2 + 4L_a L_e)} - \frac{M_{\Delta\beta}^{2\perp} (3(L_1 + L_2) + 2L_a)}{4C_{PU}(L_a^2 + 4L_a L_e)} \end{array} \right] \\
& \left[\begin{array}{c} \frac{M_{\Delta\beta}^{2\perp} L_s}{2C_{LL2}} \\ \frac{M_{\Delta\beta}^{1\parallel} L_s}{2C_{LL2}} \\ \frac{M_{\Delta\beta}^{1\perp} L_s}{2C_{LL2}} \\ 0 \\ 0 \\ -\frac{M_{\Delta 0}^{3\parallel} L_s}{C_{LL2}} + \frac{M_{\Delta\alpha}^{1\parallel} L_s}{2C_{LL2}} \\ -\frac{M_{\Delta\alpha}^{1\perp} L_s}{2C_{LL2}} - \frac{M_{\Delta 0}^{3\perp} L_s}{C_{LL2}} \\ -\frac{2M_{\Delta 0}^{dc} L_s}{C_{LL2}} \\ 0 \\ \frac{3M_{\Sigma\beta}^{2\parallel} (L_1 - L_2)}{4C_{PU2}(L_a^2 + 4L_a L_e)} - \frac{M_{\Delta\beta}^{2\parallel} (3(L_1 + L_2) + 2L_a)}{4C_{PU2}(L_a^2 + 4L_a L_e)} \\ \frac{3M_{\Sigma\beta}^{1\parallel} (L_1 - L_2)}{4C_{PU}(L_a^2 + 4L_a L_e)} - \frac{M_{\Delta\beta}^{1\parallel} (3(L_1 + L_2) + 2L_a)}{4C_{PU2}(L_a^2 + 4L_a L_e)} \\ \frac{3M_{\Sigma\beta}^{1\perp} (L_1 - L_2)}{4C_{PU}(L_a^2 + 4L_a L_e)} - \frac{M_{\Delta\beta}^{1\perp} (3(L_1 + L_2) + 2L_a)}{4C_{PU2}(L_a^2 + 4L_a L_e)} \end{array} \right] \\
\tilde{A}_{12}^{34} = & \left[\begin{array}{c} \frac{M_{\Delta\beta}^{1\parallel} L_s}{2C_{LL2}} \\ -\frac{M_{\Delta\beta}^{1\perp} L_s}{2C_{LL2}} \\ 0 \\ 0 \\ -\frac{M_{\Delta\alpha}^{1\perp} L_s}{2C_{LL2}} - \frac{M_{\Delta 0}^{3\perp} L_s}{C_{LL2}} \\ -\frac{2M_{\Delta 0}^{dc} L_s}{C_{LL2}} \\ 0 \\ \frac{3M_{\Sigma\beta}^{2\parallel} (L_1 - L_2)}{4C_{PU2}(L_a^2 + 4L_a L_e)} - \frac{M_{\Delta\beta}^{2\parallel} (3(L_1 + L_2) + 2L_a)}{4C_{PU2}(L_a^2 + 4L_a L_e)} \\ \frac{3M_{\Sigma\beta}^{1\parallel} (L_1 - L_2)}{4C_{PU}(L_a^2 + 4L_a L_e)} - \frac{M_{\Delta\beta}^{1\parallel} (3(L_1 + L_2) + 2L_a)}{4C_{PU2}(L_a^2 + 4L_a L_e)} \\ \frac{3M_{\Sigma\beta}^{1\perp} (L_1 - L_2)}{4C_{PU}(L_a^2 + 4L_a L_e)} - \frac{M_{\Delta\beta}^{1\perp} (3(L_1 + L_2) + 2L_a)}{4C_{PU2}(L_a^2 + 4L_a L_e)} \end{array} \right] \\
& \left[\begin{array}{c} \frac{M_{\Delta\beta}^{1\perp} L_s}{2C_{LL2}} \\ \frac{M_{\Delta\beta}^{1\parallel} L_s}{2C_{LL2}} \\ \frac{M_{\Delta\beta}^{1\perp} L_s}{2C_{LL2}} \\ 0 \\ 0 \\ \frac{M_{\Delta\alpha}^{1\perp} L_s}{2C_{LL2}} - \frac{M_{\Delta 0}^{3\perp} L_s}{C_{LL2}} \\ \frac{M_{\Delta 0}^{3\parallel} L_s}{C_{LL2}} + \frac{M_{\Delta\alpha}^{1\parallel} L_s}{2C_{LL2}} \\ 0 \\ -\frac{2M_{\Delta 0}^{dc} L_s}{C_{LL2}} \\ \frac{3M_{\Sigma\beta}^{2\perp} (L_1 - L_2)}{4C_{PU2}(L_a^2 + 4L_a L_e)} - \frac{M_{\Delta\beta}^{2\perp} (3(L_1 + L_2) + 2L_a)}{4C_{PU2}(L_a^2 + 4L_a L_e)} \\ \frac{3M_{\Sigma\beta}^{1\parallel} (L_1 - L_2)}{4C_{PU2}(L_a^2 + 4L_a L_e)} - \frac{M_{\Delta\beta}^{1\parallel} (3(L_1 + L_2) + 2L_a)}{4C_{PU2}(L_a^2 + 4L_a L_e)} \\ \frac{3M_{\Sigma\beta}^{1\perp} (L_1 - L_2)}{4C_{PU}(L_a^2 + 4L_a L_e)} - \frac{M_{\Delta\beta}^{1\perp} (3(L_1 + L_2) + 2L_a)}{4C_{PU}(L_a^2 + 4L_a L_e)} \end{array} \right]
\end{aligned}$$

142

$$\begin{aligned}
\tilde{A}_{12}^{37} = & \left[\begin{array}{cc}
-\frac{M_{\Sigma 0}^{3\parallel} L_s}{C_{LL2}} - \frac{M_{\Sigma \alpha}^{1\parallel} L_s}{2C_{LL2}} & -\frac{M_{\Sigma \alpha}^{1\perp} L_s}{2C_{LL2}} - \frac{M_{\Sigma 0}^{3\perp} L_s}{C_{LL2}} \\
\frac{M_{\Sigma \alpha}^{1\perp} L_s}{2C_{LL2}} - \frac{M_{\Sigma 0}^{3\perp} L_s}{C_{LL}} & \frac{M_{\Sigma 0}^{3\parallel} L_s}{C_{LL}} - \frac{M_{\Sigma \alpha}^{1\parallel} L_s}{2C_{LL}} \\
-\frac{2M_{\Sigma 0}^{dc} L_s}{C_{LL2}} & 0 \\
0 & -\frac{2M_{\Sigma 0}^{dc} L_s}{C_{LL2}} \\
\frac{M_{\Sigma \beta}^{1\parallel} L_s}{2C_{LL}} & \frac{M_{\Sigma \beta}^{1\perp} L_s}{2C_{LL}} \\
-\frac{M_{\Sigma \beta}^{1\perp} L_s}{2C_{LL}} & \frac{M_{\Sigma \beta}^{1\parallel} L_s}{2C_{LL2}} \\
0 & 0 \\
0 & 0 \\
\frac{3M_{\Delta \alpha}^{2\parallel} (L_1 - L_2)}{4C_{PU2}(L_a^2 + 4L_a L_e)} - \frac{M_{\Sigma \alpha}^{2\parallel} (3(L_1 + L_2) + 2L_a)}{4C_{PU} (L_a^2 + 4L_a L_e)} & \frac{3M_{\Delta \alpha}^{2\perp} (L_1 - L_2)}{4C_{PU} (L_a^2 + 4L_a L_e)} - \frac{M_{\Sigma \alpha}^{2\perp} (3(L_1 + L_2) + 2L_a)}{4C_{PU2}(L_a^2 + 4L_a L_e)} \\
\frac{3M_{\Delta \alpha}^{1\parallel} (L_1 - L_2)}{4C_{PU2}(L_a^2 + 4L_a L_e)} - \frac{M_{\Sigma \alpha}^{1\parallel} (3(L_1 + L_2) + 2L_a)}{4C_{PU2}(L_a^2 + 4L_a L_e)} & \frac{M_{\Sigma \alpha}^{1\perp} (3(L_1 + L_2) + 2L_a)}{4C_{PU} (L_a^2 + 4L_a L_e)} - \frac{3M_{\Delta \alpha}^{1\perp} (L_1 - L_2)}{4C_{PU2}(L_a^2 + 4L_a L_e)} \\
\frac{3M_{\Delta \alpha}^{1\perp} (L_1 - L_2)}{4C_{PU2}(L_a^2 + 4L_a L_e)} - \frac{M_{\Sigma \alpha}^{1\perp} (3(L_1 + L_2) + 2L_a)}{4C_{PU} (L_a^2 + 4L_a L_e)} & \frac{3M_{\Delta \alpha}^{1\parallel} (L_1 - L_2)}{4C_{PU2}(L_a^2 + 4L_a L_e)} - \frac{M_{\Sigma \alpha}^{1\parallel} (3(L_1 + L_2) + 2L_a)}{4C_{PU} (L_a^2 + 4L_a L_e)}
\end{array} \right] \\
\tilde{A}_{12}^{38} = & \left[\begin{array}{cc}
\frac{M_{\Sigma \beta}^{2\parallel} L_s}{2C_{LL}} & \frac{M_{\Sigma \beta}^{2\perp} L_s}{2C_{LL}} \\
\frac{M_{\Sigma \beta}^{2\perp} L_s}{2C_{LL}} & -\frac{M_{\Sigma \beta}^{2\parallel} L_s}{2C_{LL2}} \\
\frac{M_{\Sigma \beta}^{1\parallel} L_s}{2C_{LL2}} & -\frac{M_{\Sigma \beta}^{1\perp} L_s}{2C_{LL}} \\
\frac{M_{\Sigma \beta}^{1\perp} L_s}{2C_{LL2}} & \frac{M_{\Sigma \beta}^{1\parallel} L_s}{2C_{LL2}} \\
-\frac{2M_{\Sigma 0}^{dc} L_s}{C_{LL2}} + \frac{M_{\Sigma \alpha}^{2\parallel} L_s}{2C_{LL}} & \frac{M_{\Sigma \alpha}^{2\perp} L_s}{2C_{LL2}} \\
\frac{M_{\Sigma \alpha}^{2\perp} L_s}{2C_{LL}} & -\frac{2M_{\Sigma 0}^{dc} L_s}{C_{LL}} - \frac{M_{\Sigma \alpha}^{2\parallel} L_s}{2C_{LL2}} \\
-\frac{M_{\Sigma 0}^{3\parallel} L_s}{C_{LL2}} + \frac{M_{\Sigma \alpha}^{1\parallel} L_s}{2C_{LL2}} & -\frac{M_{\Sigma \alpha}^{1\perp} L_s}{2C_{LL2}} - \frac{M_{\Sigma 0}^{3\perp} L_s}{C_{LL}} \\
\frac{M_{\Sigma \alpha}^{1\perp} L_s}{2C_{LL2}} - \frac{M_{\Sigma 0}^{3\perp} L_s}{C_{LL}} & \frac{M_{\Sigma 0}^{3\parallel} L_s}{C_{LL2}} + \frac{M_{\Sigma \alpha}^{1\parallel} L_s}{2C_{LL2}} \\
\frac{3M_{\Delta \beta}^{1\parallel} (L_1 - L_2)}{4C_{PU} (L_a^2 + 4L_a L_e)} - \frac{M_{\Sigma \beta}^{1\parallel} (3(L_1 + L_2) + 2L_a)}{4C_{PU2}(L_a^2 + 4L_a L_e)} & \frac{3M_{\Delta \beta}^{1\perp} (L_1 - L_2)}{4C_{PU} (L_a^2 + 4L_a L_e)} - \frac{M_{\Sigma \beta}^{1\perp} (3(L_1 + L_2) + 2L_a)}{4C_{PU} (L_a^2 + 4L_a L_e)} \\
\frac{3M_{\Delta \beta}^{2\parallel} (L_1 - L_2)}{4C_{PU2}(L_a^2 + 4L_a L_e)} - \frac{M_{\Sigma \beta}^{2\parallel} (3(L_1 + L_2) + 2L_a)}{4C_{PU} (L_a^2 + 4L_a L_e)} & \frac{M_{\Sigma \beta}^{2\perp} (3(L_1 + L_2) + 2L_a)}{4C_{PU} (L_a^2 + 4L_a L_e)} - \frac{3M_{\Delta \beta}^{2\perp} (L_1 - L_2)}{4C_{PU} (L_a^2 + 4L_a L_e)} \\
\frac{3M_{\Delta \beta}^{2\perp} (L_1 - L_2)}{4C_{PU} (L_a^2 + 4L_a L_e)} - \frac{M_{\Sigma \beta}^{2\perp} (3(L_1 + L_2) + 2L_a)}{4C_{PU2}(L_a^2 + 4L_a L_e)} & \frac{3M_{\Delta \beta}^{2\parallel} (L_1 - L_2)}{4C_{PU} (L_a^2 + 4L_a L_e)} - \frac{M_{\Sigma \beta}^{2\parallel} (3(L_1 + L_2) + 2L_a)}{4C_{PU} (L_a^2 + 4L_a L_e)}
\end{array} \right]
\end{aligned}$$

$$\begin{aligned}
\tilde{A}_{12}^{39} = & \left[\begin{array}{cc} \frac{M_{\Sigma\beta}^{1\parallel} L_s}{2C_{LL2}} & \frac{M_{\Sigma\beta}^{1\perp} L_s}{2C_{LL}} \\ -\frac{M_{\Sigma\beta}^{1\perp} L_s}{2C_{LL}} & \frac{M_{\Sigma\beta}^{1\parallel} L_s}{2C_{LL2}} \\ 0 & 0 \\ 0 & 0 \\ -\frac{M_{\Sigma 0}^{3\parallel} L_s}{C_{LL}} + \frac{M_{\Sigma\alpha}^{1\parallel} L_s}{2C_{LL2}} & \frac{M_{\Sigma\alpha}^{1\perp} L_s}{2C_{LL2}} - \frac{M_{\Sigma 0}^{3\perp} L_s}{C_{LL2}} \\ -\frac{M_{\Sigma\alpha}^{1\perp} L_s}{2C_{LL}} - \frac{M_{\Sigma 0}^{3\perp} L_s}{C_{LL}} & \frac{M_{\Sigma 0}^{3\parallel} L_s}{C_{LL}} + \frac{M_{\Sigma\alpha}^{1\parallel} L_s}{2C_{LL}} \\ -\frac{2M_{\Sigma 0}^{dc} L_s}{C_{LL}} & 0 \\ 0 & -\frac{2M_{\Sigma 0}^{dc} L_s}{C_{LL}} \\ \frac{3M_{\Delta\beta}^{2\parallel} (L_1 - L_2)}{4C_{PU2}(L_a^2 + 4L_a L_e)} - \frac{M_{\Sigma\beta}^{2\parallel} (3(L_1 + L_2) + 2L_a)}{4C_{PU} (L_a^2 + 4L_a L_e)} & \frac{3M_{\Delta\beta}^{2\perp} (L_1 - L_2)}{4C_{PU} (L_a^2 + 4L_a L_e)} - \frac{M_{\Sigma\beta}^{2\perp} (3(L_1 + L_2) + 2L_a)}{4C_{PU2}(L_a^2 + 4L_a L_e)} \\ \frac{3M_{\Delta\beta}^{1\parallel} (L_1 - L_2)}{4C_{PU2}(L_a^2 + 4L_a L_e)} - \frac{M_{\Sigma\beta}^{1\parallel} (3(L_1 + L_2) + 2L_a)}{4C_{PU2}(L_a^2 + 4L_a L_e)} & \frac{M_{\Sigma\beta}^{1\perp} (3(L_1 + L_2) + 2L_a)}{4C_{PU2}(L_a^2 + 4L_a L_e)} - \frac{3M_{\Delta\beta}^{1\perp} (L_1 - L_2)}{4C_{PU2}(L_a^2 + 4L_a L_e)} \\ \frac{3M_{\Delta\beta}^{1\perp} (L_1 - L_2)}{4C_{PU2}(L_a^2 + 4L_a L_e)} - \frac{M_{\Sigma\beta}^{1\perp} (3(L_1 + L_2) + 2L_a)}{4C_{PU} (L_a^2 + 4L_a L_e)} & \frac{3M_{\Delta\beta}^{1\parallel} (L_1 - L_2)}{4C_{PU} (L_a^2 + 4L_a L_e)} - \frac{M_{\Sigma\beta}^{1\parallel} (3(L_1 + L_2) + 2L_a)}{4C_{PU2}(L_a^2 + 4L_a L_e)} \end{array} \right] \\
\tilde{A}_{12}^{310} = & \left[\begin{array}{ccc} \frac{2M_{\Sigma\alpha}^{1\parallel} L_s}{C_{LL2}} & -\frac{M_{\Sigma\alpha}^{2\parallel} L_s}{C_{LL}} & -\frac{M_{\Sigma\alpha}^{2\perp} L_s}{C_{LL}} \\ \frac{2M_{\Sigma\alpha}^{1\perp} L_s}{C_{LL2}} & \frac{M_{\Sigma\alpha}^{2\perp} L_s}{C_{LL}} & -\frac{M_{\Sigma\alpha}^{2\parallel} L_s}{C_{LL}} \\ \frac{2M_{\Sigma\alpha}^{2\parallel} L_s}{C_{LL2}} & -\frac{M_{\Sigma\alpha}^{1\parallel} L_s}{C_{LL}} & -\frac{M_{\Sigma\alpha}^{1\perp} L_s}{C_{LL2}} \\ \frac{2M_{\Sigma\alpha}^{2\perp} L_s}{C_{LL2}} & \frac{M_{\Sigma\alpha}^{1\perp} L_s}{C_{LL}} & -\frac{M_{\Sigma\alpha}^{1\parallel} L_s}{C_{LL2}} \\ \frac{2M_{\Sigma\beta}^{1\parallel} L_s}{C_{LL}} & -\frac{M_{\Sigma\beta}^{2\parallel} L_s}{C_{LL2}} & -\frac{M_{\Sigma\beta}^{2\perp} L_s}{C_{LL2}} \\ \frac{2M_{\Sigma\beta}^{1\perp} L_s}{C_{LL}} & \frac{M_{\Sigma\beta}^{2\perp} L_s}{C_{LL2}} & -\frac{M_{\Sigma\beta}^{2\parallel} L_s}{C_{LL2}} \\ \frac{2M_{\Sigma\beta}^{2\parallel} L_s}{C_{LL}} & -\frac{M_{\Sigma\beta}^{1\parallel} L_s}{C_{LL2}} & -\frac{M_{\Sigma\beta}^{1\perp} L_s}{C_{LL2}} \\ \frac{2M_{\Sigma\beta}^{2\perp} L_s}{C_{LL}} & \frac{M_{\Sigma\beta}^{1\perp} L_s}{C_{LL}} & -\frac{M_{\Sigma\beta}^{1\parallel} L_s}{C_{LL2}} \\ \frac{3M_{\Sigma 0}^{dc} (L_1 - L_2)}{C_{PU2}(L_a^2 + 4L_a L_e)} - \frac{M_{\Sigma 0}^{dc} (3L_1 + 3L_2 + 2L_a)}{C_{PU2}(L_a^2 + 4L_a L_e)} & \frac{3M_{\Sigma 0}^{3\parallel} (L_1 - L_2)}{2C_{PU2}(L_a^2 + 4L_a L_e)} - \frac{M_{\Sigma 0}^{3\parallel} (3L_1 + 3L_2 + 2L_a)}{2C_{PU2}(L_a^2 + 4L_a L_e)} & \frac{3M_{\Sigma 0}^{3\perp} (L_1 - L_2)}{2C_{PU2}(L_a^2 + 4L_a L_e)} - \frac{M_{\Sigma 0}^{3\perp} (3L_1 + 3L_2 + 2L_a)}{2C_{PU2}(L_a^2 + 4L_a L_e)} \\ \frac{3M_{\Sigma 0}^{3\parallel} (L_1 - L_2)}{C_{PU2}(L_a^2 + 4L_a L_e)} - \frac{M_{\Sigma 0}^{3\parallel} (3L_1 + 3L_2 + 2L_a)}{C_{PU} (L_a^2 + 4L_a L_e)} & \frac{3M_{\Sigma 0}^{3\perp} (L_1 - L_2)}{C_{PU} (L_a^2 + 4L_a L_e)} - \frac{M_{\Sigma 0}^{3\perp} (3L_1 + 3L_2 + 2L_a)}{C_{PU2}(L_a^2 + 4L_a L_e)} & 0 \\ \frac{3M_{\Sigma 0}^{3\perp} (L_1 - L_2)}{C_{PU2}(L_a^2 + 4L_a L_e)} - \frac{M_{\Sigma 0}^{3\perp} (3L_1 + 3L_2 + 2L_a)}{C_{PU} (L_a^2 + 4L_a L_e)} & 0 & \frac{3M_{\Sigma 0}^{dc} (L_1 - L_2)}{C_{PU} (L_a^2 + 4L_a L_e)} - \frac{M_{\Sigma 0}^{dc} (3L_1 + 3L_2 + 2L_a)}{C_{PU2}(L_a^2 + 4L_a L_e)} \end{array} \right] \\
\tilde{A}_{21} = & \begin{bmatrix} \tilde{A}_{21}^{11} & \tilde{A}_{21}^{12} & \tilde{A}_{21}^{13} & \tilde{A}_{21}^{14} & \tilde{A}_{21}^{15} & \tilde{A}_{21}^{16} & \tilde{A}_{21}^{17} & \tilde{A}_{21}^{18} & \tilde{A}_{21}^{19} & \tilde{A}_{21}^{110} & \tilde{A}_{21}^{111} & \tilde{A}_{21}^{112} & \tilde{A}_{21}^{113} & \tilde{A}_{21}^{114} \\ \tilde{A}_{21}^{21} & \tilde{A}_{21}^{22} & \tilde{A}_{21}^{23} & \tilde{A}_{21}^{24} & \tilde{A}_{21}^{25} & \tilde{A}_{21}^{26} & \tilde{A}_{21}^{27} & \tilde{A}_{21}^{28} & \tilde{A}_{21}^{29} & \tilde{A}_{21}^{210} & \tilde{A}_{21}^{211} & \tilde{A}_{21}^{212} & \tilde{A}_{21}^{213} & \tilde{A}_{21}^{214} \end{bmatrix}
\end{aligned}$$

145

146

147

148

149

150

151

152

153

154

$$\tilde{N} = \begin{bmatrix} 0 & 0 & 0 & 0 & 0 & 0 \\ 0 & 0 & 0 & 0 & 0 & 0 \\ 0 & 0 & 0 & 0 & 0 & 0 \\ 0 & 0 & 0 & 0 & 0 & 0 \\ 0 & 0 & 0 & 0 & 0 & 0 \\ 0 & 0 & 0 & 0 & 0 & 0 \\ 0 & 0 & 0 & 0 & 0 & 0 \\ 0 & 0 & 0 & 0 & 0 & 0 \\ \frac{3L_2 + L_a + 4L_e + 6L_t}{2C_{LL}} & \frac{3L_1 - 3L_2}{2L_a(L_a + 4L_e)C_{PU2}} & 0 & 0 & 0 & 0 \\ 0 & 0 & 0 & 0 & 0 & 0 \\ 0 & 0 & 0 & 0 & 0 & 0 \\ 0 & 0 & \frac{-1}{L_s + (L_a C_{PU1})} & 0 & 0 & 0 \\ 0 & 0 & 0 & \frac{-1}{L_s + (L_a C_{PU1})} & 0 & 0 \\ 0 & 0 & 0 & 0 & 0 & 0 \\ 0 & 0 & 0 & 0 & 0 & 0 \\ 0 & 0 & 0 & 0 & \frac{-1}{L_s + (L_a C_{PU1})} & 0 \\ 0 & 0 & 0 & 0 & 0 & \frac{-1}{L_s + (L_a C_{PU1})} \\ 0 & 0 & 0 & 0 & 0 & 0 \\ 0 & 0 & \frac{L_a}{C_{LL2}} & 0 & 0 & 0 \\ 0 & 0 & 0 & \frac{L_a}{C_{LL}} & 0 & 0 \\ 0 & 0 & 0 & 0 & 0 & 0 \\ 0 & 0 & 0 & 0 & 0 & 0 \\ 0 & 0 & 0 & 0 & 0 & 0 \\ 0 & 0 & 0 & 0 & \frac{L_a}{C_{LL}} & 0 \\ 0 & 0 & 0 & 0 & 0 & \frac{L_a}{C_{LL2}} \\ 0 & 0 & 0 & 0 & 0 & 0 \\ 0 & 0 & 0 & 0 & 0 & 0 \\ \frac{3L_2 + L_a}{C_{LL}} & \frac{-3L_1 - 3L_2}{L_a + 2} & 0 & 0 & 0 & 0 \\ 0 & 0 & 0 & 0 & 0 & 0 \\ 0 & 0 & 0 & 0 & 0 & 0 \end{bmatrix}$$

Appendix D

DC/DC DPM Matrices

The following matrices are for the DC/DC DPM given by Equation (3.61). To reduce the size of the given sub-matrices, several constants are defined as C_{xxy} , where “xx” describes the type of constant, i.e., “ RL ” for a constant with units of resistance times inductance, and “y” takes values of 1,2,3... depending on how many variables share the same unit. This model includes second and third harmonic components for the modulating signals, but due to time constraints they were not investigated in the thesis’ body, and are always set to 0 for simulation purposes. The model in equation Equation (3.61) is repeated here for reference as:

$$\frac{d}{dt} \begin{bmatrix} \widetilde{\mathbf{X}}_{ir}^* \\ \widetilde{\mathbf{X}}_{vr}^* \end{bmatrix} = \begin{bmatrix} \tilde{A}_{11r} & \tilde{A}_{12r} \\ \tilde{A}_{21r} & 0_{22 \times 22} \end{bmatrix} \begin{bmatrix} \widetilde{\mathbf{X}}_{ir}^* \\ \widetilde{\mathbf{X}}_{vr}^* \end{bmatrix} + \begin{bmatrix} \tilde{N}_r \\ 0_{22 \times 5} \end{bmatrix} \begin{bmatrix} \widetilde{\mathbf{W}}_r^* \end{bmatrix}, \quad (\text{D.1})$$

$$\tilde{A}_{11r} = \begin{bmatrix} \tilde{A}_{11r}^{11} & \tilde{A}_{11r}^{12} & [0]_{11 \times 4} & [0]_{15 \times 4} & \tilde{A}_{11r}^{15} \\ [0]_{22 \times 8} & \tilde{A}_{11r}^{22} & \tilde{A}_{11}^{23} & \tilde{A}_{11r}^{24} & \tilde{A}_{11r}^{25} \end{bmatrix}$$

$$\tilde{A}_{11r}^{11} = \begin{bmatrix} -\frac{R_a}{L_a} & -\omega & 0 & 0 & 0 & 0 & 0 & 0 \\ \omega & -\frac{R_a}{L_a} & 0 & 0 & 0 & 0 & 0 & 0 \\ 0 & 0 & -\frac{R_a}{L_a} & -2\omega & 0 & 0 & 0 & 0 \\ 0 & 0 & 2\omega & -\frac{R_a}{L_a} & 0 & 0 & 0 & 0 \\ 0 & 0 & 0 & 0 & -\frac{R_a}{L_a} & -\omega & 0 & 0 \\ 0 & 0 & 0 & 0 & \omega & -\frac{R_a}{L_a} & 0 & 0 \\ 0 & 0 & 0 & 0 & 0 & 0 & -\frac{R_a}{L_a} & -2\omega \\ 0 & 0 & 0 & 0 & 0 & 0 & 2\omega & -\frac{R_a}{L_a} \end{bmatrix}$$

$$\tilde{A}_{11}^{12} = \begin{bmatrix} \begin{matrix} [0]_{8 \times 3} \\ -\frac{C_{RL}}{2C_{LL1}} & 0 & 0 \end{matrix} \\ 0 & -\frac{C_{RL1}}{2C_{LL1}} & -3\omega \\ 0 & 3\omega & -\frac{C_{RL1}}{2C_{LL1}} \end{bmatrix} \quad \tilde{A}_{11}^{22} = \begin{bmatrix} \begin{matrix} [0]_{8 \times 3} \\ \frac{C_{RL4}}{C_{LL1}} & 0 & 0 \end{matrix} \\ 0 & \frac{C_{RL4}}{C_{LL1}} & 0 \\ 0 & 0 & \frac{C_{RL4}}{C_{LL1}} \end{bmatrix}$$

$$\tilde{A}_{11}^{12} = \begin{bmatrix} \begin{matrix} [0]_{8 \times 3} \\ -\frac{C_{RL}}{2C_{LL1}} & 0 & 0 \end{matrix} \\ 0 & -\frac{C_{RL1}}{2C_{LL1}} & -3\omega \\ 0 & 3\omega & -\frac{C_{RL1}}{2C_{LL1}} \end{bmatrix} \quad \tilde{A}_{11}^{22} = \begin{bmatrix} \begin{matrix} [0]_{8 \times 3} \\ \frac{C_{RL4}}{C_{LL1}} & 0 & 0 \end{matrix} \\ 0 & \frac{C_{RL4}}{C_{LL1}} & 0 \\ 0 & 0 & \frac{C_{RL4}}{C_{LL1}} \end{bmatrix}$$

$$C_{RL1} = 9L_1R_2 + 9L_2R_1 + 3L_1R_a + 3L_aR_1 + 3L_2R_a + 3L_aR_2 + 12L_eR_1 + 12L_eR_2 + 18L_tR_1 + 18L_tR_2 + 2L_aR_a + 8L_eR_a + 12L_tR_t$$

$$C_{LL1} = L_a^2 + 9L_1L_2 + 9L_1L_t + 9L_2L_t + 6L_1L_e + 6L_2L_e + 6L_aL_t + 4L_aL_e + 3L_1L_a + 9L_2L_a$$

$$C_{RL4} = 3(3L_1R_2 - 3L_2R_1 + L_1R_a - L_aR_1 - L_2R_a + L_aR_2)$$

$$\tilde{A}_{11}^{23} = \begin{bmatrix} \begin{matrix} -\frac{R_a - 4R_w}{L_a + 4L_e + 6L_m} & -\omega & 0 & 0 \\ \omega & -\frac{R_a - 4R_w}{L_a + 4L_e + 6L_m} & 0 & 0 \\ 0 & 0 & \frac{-R_a - 4R_w}{L_a + 4L_e + 6L_m} & -2\omega \\ 0 & 0 & 2\omega & \frac{-R_a - 4R_w}{L_a + 4L_e + 6L_m} \end{matrix} \end{bmatrix}$$

[0]_{7x4}

$$\tilde{A}_{11}^{24} = \begin{bmatrix} \frac{-R_a - 4R_w}{L_a + 4L_e + 6L_m} & -\omega & 0 & 0 \\ \omega & \frac{-R_a - 4R_w}{L_a + 4L_e + 6L_m} & 0 & 0 \\ 0 & 0 & \frac{-R_a - 4R_w}{L_a + 4L_e + 6L_m} & -2\omega \\ 0 & 0 & 2\omega & \frac{-R_a - 4R_w}{L_a + 4L_e + 6L_m} \end{bmatrix}$$

[0]_{3x4}

$$\tilde{A}_{11}^{17} = \begin{bmatrix} \frac{C_{RL2}}{4C_{LL1}} & 0 & 0 \\ 0 & \frac{C_{RL2}}{4C_{LL1}} & 0 \\ 0 & 0 & \frac{C_{RL2}}{4C_{LL1}} \end{bmatrix} \quad \tilde{A}_{11}^{22} = \begin{bmatrix} -\frac{C_{RL3}}{2C_{LL1}} & 0 & 0 \\ 0 & -\frac{C_{RL3}}{2C_{LL1}} & -3\omega \\ 0 & 3\omega & -\frac{C_{RL3}}{2C_{LL1}} \end{bmatrix}$$

$$C_{RL2} = 9L_1R_2 - 9L_2R_1 + 3L_1R_a - 3L_2R_1 - 3L_2R_a + 3L_aR_2 - 12L_eR_1 + 12L_eR_2 + 18L_1R_t - 18L_2R_t - 18L_tR_1 - 18L_tR_2 + 12L_1R_w - 12L_2R_w$$

$$C_{RL} = 9L_1R_2 + 9L_2R_1 + 3L_1R_a + 3L_aR_1 + 3L_2R_a + 3L_aR_2 + 18L_1R_t + 18L_2R_t + 12L_1R_w + 12L_2R_w + 2L_aR_a + 12L_aR_t + 8L_aR_w$$

$$\tilde{A}_{12r} = \begin{bmatrix} \tilde{A}_{12r}^{11} & \tilde{A}_{12r}^{12} & \tilde{A}_{12r}^{13} & \tilde{A}_{12r}^{14} & \tilde{A}_{12r}^{15} & \tilde{A}_{12r}^{16} & \tilde{A}_{12r}^{17} & \tilde{A}_{12r}^{18} & \tilde{A}_{12r}^{19} & \tilde{A}_{12r}^{110} \\ \tilde{A}_{12r}^{21} & \tilde{A}_{12r}^{22} & \tilde{A}_{12r}^{23} & \tilde{A}_{12r}^{24} & \tilde{A}_{12r}^{25} & \tilde{A}_{12r}^{26} & \tilde{A}_{12r}^{27} & \tilde{A}_{12r}^{28} & \tilde{A}_{12r}^{29} & \tilde{A}_{12r}^{210} \end{bmatrix}$$

$$\tilde{A}_{12r}^{11} = \begin{bmatrix} -\frac{M_{\Sigma 0}^{dc}}{L_a} - \frac{M_{\Sigma \alpha}^{2\parallel}}{4L_a} & -\frac{M_{\Sigma \alpha}^{2\perp}}{4L_a} \\ -\frac{M_{\Sigma \alpha}^{2\perp}}{4L_a} & -\frac{M_{\Sigma 0}^{dc}}{L_a} + \frac{M_{\Sigma \alpha}^{2\parallel}}{4L_a} \\ \frac{M_{\Sigma 0}^{3\parallel}}{2L_a} - \frac{M_{\Sigma \alpha}^{1\parallel}}{4L_a} & \frac{M_{\Sigma \alpha}^{1\perp}}{4L_a} - \frac{M_{\Sigma 0}^{3\perp}}{2L_a} \\ -\frac{M_{\Sigma \alpha}^{1\perp}}{4L_a} - \frac{M_{\Sigma 0}^{3\perp}}{2L_a} & \frac{M_{\Sigma \beta}^{2\parallel}}{4L_a} \\ \frac{M_{\Sigma \beta}^{2\parallel}}{4L_a} & \frac{M_{\Sigma \beta}^{2\perp}}{4L_a} \\ \frac{M_{\Sigma \beta}^{2\perp}}{4L_a} & -\frac{M_{\Sigma \beta}^{2\parallel}}{4L_a} \\ \frac{M_{\Sigma \beta}^{1\parallel}}{4L_a} & -\frac{M_{\Sigma \beta}^{1\perp}}{4L_a} \\ \frac{M_{\Sigma \beta}^{1\perp}}{4L_a} & \frac{M_{\Sigma \beta}^{1\parallel}}{4L_a} \\ \frac{M_{\Delta \alpha}^{1\parallel}(3(L_1 - L_2))}{8C_{PU2}(L_a^2 + 4L_aL_e)} - \frac{M_{\Sigma \alpha}^{1\parallel}C_L}{4C_{PU2}(L_a^2 + 4L_aL_e)} & \frac{M_{\Delta \alpha}^{1\perp}(3(L_1 - L_2))}{8C_{PU2}(L_a^2 + 4L_aL_e)} - \frac{M_{\Sigma \alpha}^{1\perp}C_L}{4C_{PU2}(L_a^2 + 4L_aL_e)} \\ \frac{M_{\Delta \alpha}^{2\parallel}(3(L_1 - L_2))}{8C_{PU2}(L_a^2 + 4L_aL_e)} - \frac{M_{\Sigma \alpha}^{2\parallel}C_L}{4C_{PU2}(L_a^2 + 4L_aL_e)} & \frac{M_{\Delta \alpha}^{2\perp}(3(L_1 - L_2))}{8C_{PU2}(L_a^2 + 4L_aL_e)} - \frac{M_{\Sigma \alpha}^{2\perp}C_L}{4C_{PU2}(L_a^2 + 4L_aL_e)} \\ \frac{M_{\Delta \alpha}^{2\perp}(3(L_1 - L_2))}{8C_{PU2}(L_a^2 + 4L_aL_e)} - \frac{M_{\Sigma \alpha}^{2\perp}C_L}{4C_{PU2}(L_a^2 + 4L_aL_e)} & \frac{M_{\Delta \alpha}^{2\parallel}(3(L_1 - L_2))}{8C_{PU2}(L_a^2 + 4L_aL_e)} - \frac{M_{\Sigma \alpha}^{2\parallel}C_L}{4C_{PU2}(L_a^2 + 4L_aL_e)} \end{bmatrix}$$

$$C_{PU2} = \left(\frac{3L_1 + 3L_2}{2L_a + 1} \right) \left(\frac{3L_1 + 3L_2 + 12L_t}{2L_a + 8L_e} \right) - \left(\frac{(3L_1 - 3L_2)^2}{4L_a(L_a + 4L_e)} \right)$$

$$C_L = \left(\frac{3L_1 + 3L_2 + 12L_t}{2L_a + 8L_e} + 1 \right) (L_a + 4L_e)$$

$$\tilde{A}_{12r}^{12} = \begin{bmatrix} -\frac{M_{\Sigma 0}^{3\parallel}}{2L_a} - \frac{M_{\Sigma\alpha}^{1\parallel}}{4L_a} & -\frac{M_{\Sigma\alpha}^{1\perp}}{4L_a} - \frac{M_{\Sigma 0}^{3\perp}}{2L_a} & -\frac{M_{\Sigma\alpha}^{1\perp}}{4L_a} - \frac{M_{\Sigma 0}^{3\perp}}{2L_a} & 0 \\ \frac{M_{\Sigma\alpha}^{1\perp}}{4L_a} - \frac{M_{\Sigma 0}^{3\perp}}{2L_a} & \frac{M_{\Sigma 0}^{dc}}{L_a} & 0 & -\frac{M_{\Sigma 0}^{dc}}{L_a} \\ 0 & \frac{M_{\Sigma\beta}^{1\parallel}}{4L_a} & \frac{M_{\Sigma\beta}^{1\perp}}{4L_a} & \frac{M_{\Sigma\beta}^{1\parallel}}{4L_a} \\ \frac{M_{\Sigma\beta}^{1\perp}}{4L_a} & 0 & 0 & 0 \\ \frac{M_{\Delta\alpha}^{2\parallel}(3(L_1 - L_2))}{8C_{PU2}(L_a^2 + 4L_aL_e)} - \frac{M_{\Sigma\alpha}^{2\parallel}C_L}{4C_{PU2}(L_a^2 + 4L_aL_e)} & \frac{M_{\Delta\alpha}^{2\perp}(3(L_1 - L_2))}{8C_{PU2}(L_a^2 + 4L_aL_e)} - \frac{M_{\Sigma\alpha}^{2\perp}C_L}{4C_{PU2}(L_a^2 + 4L_aL_e)} & \frac{M_{\Delta\alpha}^{1\parallel}(3(L_1 - L_2))}{8C_{PU2}(L_a^2 + 4L_aL_e)} - \frac{M_{\Sigma\alpha}^{1\parallel}C_L}{4C_{PU2}(L_a^2 + 4L_aL_e)} & \frac{M_{\Delta\alpha}^{1\perp}(3(L_1 - L_2))}{8C_{PU2}(L_a^2 + 4L_aL_e)} - \frac{M_{\Sigma\alpha}^{1\perp}C_L}{4C_{PU2}(L_a^2 + 4L_aL_e)} \end{bmatrix}$$

$$\bar{A}_{12r}^{13} = \left[\begin{array}{cc} \frac{M_{\Sigma\beta}^{2\parallel}}{4L_a} & \frac{M_{\Sigma\beta}^{2\perp}}{4L_a} \\ \frac{M_{\Sigma\beta}^{2\perp}}{4L_a} & -\frac{M_{\Sigma\beta}^{2\parallel}}{4L_a} \\ \frac{M_{\Sigma\beta}^{1\parallel}}{4L_a} & -\frac{M_{\Sigma\beta}^{1\perp}}{4L_a} \\ \frac{M_{\Sigma\beta}^{1\perp}}{4L_a} & \frac{M_{\Sigma\beta}^{1\parallel}}{4L_a} \\ -\frac{M_{\Sigma 0}^{dc}}{L_a} + \frac{M_{\Sigma\alpha}^{2\parallel}}{4L_a} & \frac{M_{\Sigma\alpha}^{2\perp}}{4L_a} \\ \frac{M_{\Sigma\alpha}^{2\perp}}{4L_a} & -\frac{M_{\Sigma 0}^{dc}}{L_a} - \frac{M_{\Sigma\alpha}^{2\parallel}}{4L_a} \\ -\frac{M_{\Sigma 0}^{3\parallel}}{2L_a} + \frac{M_{\Sigma\alpha}^{1\parallel}}{4L_a} & -\frac{M_{\Sigma\alpha}^{1\perp}}{4L_a} - \frac{M_{\Sigma 0}^{3\perp}}{2L_a} \\ \frac{M_{\Sigma\alpha}^{1\perp}}{4L_a} - \frac{M_{\Sigma 0}^{3\perp}}{2L_a} & \frac{M_{\Sigma 0}^{3\parallel}}{2L_a} + \frac{M_{\Sigma\alpha}^{1\parallel}}{4L_a} \\ \frac{M_{\Delta\beta}^{1\parallel}(3(L_1 - L_2))}{8C_{PU2}(L_a^2 + 4L_aL_e)} - \frac{M_{\Sigma\beta}^{1\parallel}C_L}{4C_{PU2}(L_a^2 + 4L_aL_e)} & \frac{M_{\Delta\beta}^{1\perp}(3(L_1 - L_2))}{8C_{PU2}(L_a^2 + 4L_aL_e)} - \frac{M_{\Sigma\beta}^{1\perp}C_L}{4C_{PU2}(L_a^2 + 4L_aL_e)} \\ \frac{M_{\Delta\beta}^{2\parallel}(3(L_1 - L_2))}{8C_{PU2}(L_a^2 + 4L_aL_e)} - \frac{M_{\Sigma\beta}^{2\parallel}C_L}{4C_{PU2}(L_a^2 + 4L_aL_e)} & \frac{M_{\Sigma\beta}^{2\perp}C_L}{4C_{PU2}(L_a^2 + 4L_aL_e)} - \frac{M_{\Delta\beta}^{2\perp}(3(L_1 - L_2))}{8C_{PU2}(L_a^2 + 4L_aL_e)} \\ \frac{M_{\Delta\beta}^{2\perp}(3(L_1 - L_2))}{8C_{PU2}(L_a^2 + 4L_aL_e)} - \frac{M_{\Sigma\beta}^{2\perp}C_L}{4C_{PU2}(L_a^2 + 4L_aL_e)} & \frac{M_{\Delta\beta}^{2\parallel}(3(L_1 - L_2))}{8C_{PU2}(L_a^2 + 4L_aL_e)} - \frac{M_{\Sigma\beta}^{2\parallel}C_L}{4C_{PU2}(L_a^2 + 4L_aL_e)} \end{array} \right]$$

161

$$\tilde{A}_{12r}^{16} = \left[\begin{array}{cc}
-\frac{M_{\Delta 0}^{dc}}{L_a} - \frac{M_{\Delta \alpha}^{2\parallel}}{4L_a} & -\frac{M_{\Delta \alpha}^{2\perp}}{4L_a} \\
-\frac{M_{\Delta \alpha}^{2\perp}}{4L_a} & -\frac{M_{\Delta 0}^{dc}}{L_a} + \frac{M_{\Delta \alpha}^{2\parallel}}{4L_a} \\
-\frac{M_{\Delta 0}^{3\parallel}}{2L_a} - \frac{M_{\Delta \alpha}^{1\parallel}}{4L_a} & \frac{M_{\Delta \alpha}^{1\perp}}{4L_a} - \frac{M_{\Delta 0}^{3\perp}}{2L_a} \\
-\frac{M_{\Delta \alpha}^{1\perp}}{4L_a} - \frac{M_{\Delta 0}^{3\perp}}{2L_a} & \frac{M_{\Delta 0}^{3\parallel}}{2L_a} - \frac{M_{\Delta \alpha}^{1\parallel}}{4L_a} \\
\frac{M_{\Delta \beta}^{2\parallel}}{4L_a} & \frac{M_{\Delta \beta}^{2\perp}}{4L_a} \\
\frac{M_{\Delta \beta}^{2\perp}}{4L_a} & \frac{M_{\Delta \beta}^{2\parallel}}{4L_a} \\
\frac{M_{\Delta \beta}^{1\parallel}}{4L_a} & \frac{M_{\Delta \beta}^{1\perp}}{4L_a} \\
\frac{M_{\Delta \beta}^{1\perp}}{4L_a} & \frac{M_{\Delta \beta}^{1\parallel}}{4L_a} \\
\frac{M_{\Delta \alpha}^{1\parallel}(3(L_1 - L_2))}{8C_{PU2}(L_a^2 + 4L_a L_e)} - \frac{M_{\Delta \alpha}^{1\parallel} C_L}{4C_{PU2}(L_a^2 + 4L_a L_e)} & \frac{M_{\Delta \alpha}^{1\perp}(3(L_1 - L_2))}{8C_{PU2}(L_a^2 + 4L_a L_e)} - \frac{M_{\Delta \alpha}^{1\perp} C_L}{4C_{PU2}(L_a^2 + 4L_a L_e)} \\
\frac{M_{\Delta \alpha}^{2\parallel}(3(L_1 - L_2))}{8C_{PU2}(L_a^2 + 4L_a L_e)} - \frac{M_{\Delta \alpha}^{2\parallel} C_L}{4C_{PU2}(L_a^2 + 4L_a L_e)} & \frac{M_{\Delta \alpha}^{2\perp}(3(L_1 - L_2))}{8C_{PU2}(L_a^2 + 4L_a L_e)} - \frac{M_{\Delta \alpha}^{2\perp} C_L}{4C_{PU2}(L_a^2 + 4L_a L_e)} \\
\frac{M_{\Delta \alpha}^{2\perp}(3(L_1 - L_2))}{8C_{PU2}(L_a^2 + 4L_a L_e)} - \frac{M_{\Delta \alpha}^{2\perp} C_L}{4C_{PU2}(L_a^2 + 4L_a L_e)} & \frac{M_{\Delta \alpha}^{2\parallel}(3(L_1 - L_2))}{8C_{PU2}(L_a^2 + 4L_a L_e)} - \frac{M_{\Delta \alpha}^{2\parallel} C_L}{4C_{PU2}(L_a^2 + 4L_a L_e)}
\end{array} \right]$$

$$\tilde{A}_{12r}^{17} = \begin{bmatrix} -\frac{M_{\Delta 0}^{3\parallel}}{2L_a} - \frac{M_{\Delta\alpha}^{1\parallel}}{4L_a} & -\frac{M_{\Delta\alpha}^{1\perp}}{4L_a} - \frac{M_{\Delta 0}^{3\perp}}{2L_a} \\ \frac{M_{\Delta\alpha}^{1\perp}}{4L_a} - \frac{M_{\Delta 0}^{3\perp}}{2L_a} & \frac{M_{\Delta 0}^{3\parallel}}{2L_a} - \frac{M_{\Delta\alpha}^{2\parallel}}{4L_a} \\ -\frac{M_{\Delta 0}^{dc}}{L_a} & 0 \\ 0 & -\frac{M_{\Delta 0}^{dc}}{L_a} \\ \frac{M_{\Delta\beta}^{1\parallel}}{4L_a} & \frac{M_{\Delta\beta}^{1\perp}}{4L_a} \\ -\frac{M_{\Delta\beta}^{1\perp}}{4L_a} & \frac{M_{\Delta\beta}^{1\parallel}}{4L_a} \\ 0 & 0 \\ 0 & 0 \\ \frac{M_{\Sigma\alpha}^{2\parallel}(3(L_1 - L_2))}{8C_{PU2}(L_a^2 + 4L_aL_e)} - \frac{M_{\Delta\alpha}^{2\parallel}C_L}{4C_{PU2}(L_a^2 + 4L_aL_e)} & \frac{M_{\Sigma\alpha}^{2\perp}(3(L_1 - L_2))}{8C_{PU2}(L_a^2 + 4L_aL_e)} - \frac{M_{\Delta\alpha}^{2\perp}C_L}{4C_{PU2}(L_a^2 + 4L_aL_e)} \\ \frac{M_{\Sigma\alpha}^{1\parallel}(3(L_1 - L_2))}{8C_{PU2}(L_a^2 + 4L_aL_e)} - \frac{M_{\Delta\alpha}^{1\parallel}C_L}{4C_{PU2}(L_a^2 + 4L_aL_e)} & \frac{M_{\Delta\alpha}^{1\perp}C_L}{4C_{PU2}(L_a^2 + 4L_aL_e)} - \frac{M_{\Sigma\alpha}^{1\perp}(3(L_1 - L_2))}{8C_{PU2}(L_a^2 + 4L_aL_e)} \\ \frac{M_{\Sigma\alpha}^{1\perp}(3(L_1 - L_2))}{8C_{PU2}(L_a^2 + 4L_aL_e)} - \frac{M_{\Delta\alpha}^{1\perp}C_L}{4C_{PU2}(L_a^2 + 4L_aL_e)} & \frac{M_{\Sigma\alpha}^{1\parallel}(3(L_1 - L_2))}{8C_{PU2}(L_a^2 + 4L_aL_e)} - \frac{M_{\Delta\alpha}^{1\parallel}C_L}{4C_{PU2}(L_a^2 + 4L_aL_e)} \end{bmatrix}$$

$$\tilde{A}_{12}^{18} = \left[\begin{array}{cc} \frac{M_{\Delta\beta}^{2\parallel}}{4L_a} & \frac{M_{\Delta\beta}^{2\perp}}{4L_a} \\ \frac{M_{\Delta\beta}^{2\perp}}{4L_a} & -\frac{M_{\Delta\beta}^{2\parallel}}{4L_a} \\ \frac{M_{\Delta\beta}^{1\parallel}}{4L_a} & -\frac{M_{\Delta\beta}^{1\perp}}{4L_a} \\ \frac{M_{\Delta\beta}^{1\perp}}{4L_a} & \frac{M_{\Delta\beta}^{1\parallel}}{4L_a} \\ -\frac{M_{\Delta 0}^{dc}}{L_a} + \frac{M_{\Delta\alpha}^{2\parallel}}{4L_a} & \frac{M_{\Delta\alpha}^{2\perp}}{4L_a} \\ \frac{M_{\Delta\alpha}^{2\perp}}{4L_a} & -\frac{M_{\Delta 0}^{dc}}{L_a} - \frac{M_{\Delta\alpha}^{2\parallel}}{4L_a} \\ -\frac{M_{\Delta 0}^{3\parallel}}{2L_a} + \frac{M_{\Delta\alpha}^{1\parallel}}{4L_a} & -\frac{M_{\Delta\alpha}^{1\perp}}{4L_a} - \frac{M_{\Delta 0}^{3\perp}}{2L_a} \\ \frac{M_{\Delta\alpha}^{1\perp}}{4L_a} - \frac{M_{\Delta 0}^{3\perp}}{2L_a} & \frac{M_{\Delta 0}^{3\parallel}}{2L_a} + \frac{M_{\Delta\alpha}^{1\parallel}}{4L_a} \\ \frac{M_{\Sigma\beta}^{1\parallel}(3(L_1 - L_2))}{8C_{PU}(L_a^2 + 4L_aL_e)} - \frac{M_{\Delta\beta}^{1\parallel}C_L}{4C_{PU}(L_a^2 + 4L_aL_e)} & \frac{M_{\Sigma\beta}^{1\perp}(3(L_1 - L_2))}{8C_{PU}(L_a^2 + 4L_aL_e)} - \frac{M_{\Delta\beta}^{1\perp}C_L}{4C_{PU}(L_a^2 + 4L_aL_e)} \\ \frac{M_{\Sigma\beta}^{2\parallel}(3(L_1 - L_2))}{8C_{PU2}(L_a^2 + 4L_aL_e)} - \frac{M_{\Delta\beta}^{2\parallel}C_L}{4C_{PU}(L_a^2 + 4L_aL_e)} & \frac{M_{\Sigma\beta}^{2\perp}C_L}{4C_{PU2}(L_a^2 + 4L_aL_e)} - \frac{M_{\Sigma\beta}^{2\perp}(3(L_1 - L_2))}{8C_{PU}(L_a^2 + 4L_aL_e)} \\ \frac{M_{\Sigma\beta}^{2\perp}(3(L_1 - L_2))}{8C_{PU}(L_a^2 + 4L_aL_e)} - \frac{M_{\Delta\beta}^{2\perp}C_L}{4C_{PU}(L_a^2 + 4L_aL_e)} & \frac{M_{\Sigma\beta}^{2\parallel}(3(L_1 - L_2))}{8C_{PU}(L_a^2 + 4L_aL_e)} - \frac{M_{\Delta\beta}^{2\parallel}C_L}{4C_{PU}(L_a^2 + 4L_aL_e)} \end{array} \right]$$

$$\begin{aligned}
\tilde{A}_{12r}^{19} = & \left[\begin{array}{c} \frac{M_{\Delta\beta}^{1\parallel}}{4L_a} \\ -\frac{M_{\Delta\beta}^{1\perp}}{4L_a} \\ 0 \\ 0 \\ -\frac{M_{\Delta 0}^{3\parallel}}{2L_a} + \frac{M_{\Delta\alpha}^{1\parallel}}{4L_a} \\ -\frac{M_{\Delta\alpha}^{1\perp}}{4L_a} - \frac{M_{\Delta 0}^{3\perp}}{2L_a} \\ -\frac{M_{\Delta 0}^{dc}}{L_a} \\ 0 \end{array} \right] \left[\begin{array}{c} \frac{M_{\Delta\beta}^{1\perp}}{4L_a} \\ \frac{M_{\Delta\beta}^{1\parallel}}{4L_a} \\ 0 \\ 0 \\ \frac{M_{\Delta\alpha}^{1\perp}}{4L_a} - \frac{M_{\Delta 0}^{3\perp}}{2L_a} \\ \frac{M_{\Delta 0}^{3\parallel}}{2L_a} + \frac{M_{\Delta\alpha}^{2\parallel}}{4L_a} \\ 0 \\ -\frac{M_{\Delta 0}^{dc}}{L_a} \end{array} \right] \\
& \left[\begin{array}{cc} \frac{M_{\Sigma\beta}^{2\parallel}(3(L_1 - L_2))}{8C_{PU2}(L_a^2 + 4L_aL_e)} - \frac{M_{\Delta\beta}^{2\parallel}C_L}{4C_{PU2}(L_a^2 + 4L_aL_e)} & \frac{M_{\Sigma\beta}^{2\perp}(3(L_1 - L_2))}{8C_{PU2}(L_a^2 + 4L_aL_e)} - \frac{M_{\Delta\beta}^{2\perp}C_L}{4C_{PU2}(L_a^2 + 4L_aL_e)} \\ \frac{M_{\Sigma\beta}^{1\parallel}(3(L_1 - L_2))}{8C_{PU2}(L_a^2 + 4L_aL_e)} - \frac{M_{\Delta\beta}^{1\parallel}C_L}{4C_{PU2}(L_a^2 + 4L_aL_e)} & \frac{M_{\Delta\beta}^{1\perp}C_L}{4C_{PU2}(L_a^2 + 4L_aL_e)} - \frac{M_{\Sigma\beta}^{1\perp}(3(L_1 - L_2))}{8C_{PU2}(L_a^2 + 4L_aL_e)} \\ \frac{M_{\Sigma\beta}^{1\perp}(3(L_1 - L_2))}{8C_{PU2}(L_a^2 + 4L_aL_e)} - \frac{M_{\Delta\beta}^{1\perp}C_L}{4C_{PU2}(L_a^2 + 4L_aL_e)} & \frac{M_{\Sigma\beta}^{1\parallel}(3(L_1 - L_2))}{8C_{PU2}(L_a^2 + 4L_aL_e)} - \frac{M_{\Delta\beta}^{1\parallel}C_L}{4C_{PU2}(L_a^2 + 4L_aL_e)} \end{array} \right] \\
\tilde{A}_{12}^{110} = & \left[\begin{array}{ccc} -\frac{M_{\Delta\alpha}^{1\parallel}}{L_a} & -\frac{M_{\Delta\alpha}^{2\parallel}}{2L_a} & -\frac{M_{\Delta\alpha}^{2\perp}}{2L_a} \\ -\frac{M_{\Delta\alpha}^{1\perp}}{L_a} & \frac{M_{\Delta\alpha}^{2\perp}}{2L_a} & -\frac{M_{\Delta\alpha}^{2\parallel}}{2L_a} \\ -\frac{M_{\Delta\alpha}^{2\parallel}}{L_a} & -\frac{M_{\Delta\alpha}^{1\parallel}}{2L_a} & -\frac{M_{\Delta\alpha}^{1\perp}}{2L_a} \\ -\frac{M_{\Delta\alpha}^{2\perp}}{L_a} & \frac{M_{\Delta\alpha}^{1\perp}}{2L_a} & -\frac{M_{\Delta\alpha}^{1\parallel}}{2L_a} \\ -\frac{M_{\Delta\beta}^{1\parallel}}{L_a} & -\frac{M_{\Delta\beta}^{2\parallel}}{2L_a} & -\frac{M_{\Delta\beta}^{2\perp}}{2L_a} \\ -\frac{M_{\Delta\beta}^{1\perp}}{L_a} & \frac{M_{\Delta\beta}^{2\perp}}{2L_a} & -\frac{M_{\Delta\beta}^{2\parallel}}{2L_a} \\ -\frac{M_{\Delta\beta}^{2\parallel}}{L_a} & -\frac{M_{\Delta\beta}^{1\parallel}}{2L_a} & -\frac{M_{\Delta\beta}^{1\perp}}{2L_a} \\ -\frac{M_{\Delta\beta}^{2\perp}}{L_a} & \frac{M_{\Delta\beta}^{1\perp}}{2L_a} & -\frac{M_{\Delta\beta}^{1\parallel}}{2L_a} \end{array} \right] \left[\begin{array}{ccc} \frac{3M_{\Sigma 0}^{dc}(L_1 - L_2)}{2C_{PU2}(L_a^2 + 4L_aL_e)} - \frac{M_{\Delta 0}^{dc}C_L}{C_{PU}(L_a^2 + 4L_aL_e)} & \frac{M_{\Sigma 0}^{3\parallel}(3(L_1 - L_2))}{2C_{PU2}(L_a^2 + 4L_aL_e)} - \frac{M_{\Delta 0}^{3\parallel}C_L}{2C_{PU}(L_a^2 + 4L_aL_e)} & \frac{M_{\Sigma 0}^{3\perp}(3(L_1 - L_2))}{2C_{PU}(L_a^2 + 4L_aL_e)} - \frac{M_{\Delta 0}^{3\perp}C_L}{2C_{PU}(L_a^2 + 4L_aL_e)} \\ \frac{3M_{\Sigma 0}^{3\parallel}(L_1 - L_2)}{2C_{PU}(L_a^2 + 4L_aL_e)} - \frac{M_{\Delta 0}^{3\parallel}C_L}{C_{PU}(L_a^2 + 4L_aL_e)} & \frac{M_{\Sigma 0}^{dc}(3(L_1 - L_2))}{2C_{PU2}(L_a^2 + 4L_aL_e)} - \frac{M_{\Delta 0}^{dc}C_L}{C_{PU2}(L_a^2 + 4L_aL_e)} & 0 \\ \frac{3M_{\Sigma 0}^{3\perp}(L_1 - L_2)}{2C_{PU}(L_a^2 + 4L_aL_e)} - \frac{M_{\Delta 0}^{3\perp}C_L}{C_{PU}(L_a^2 + 4L_aL_e)} & 0 & \frac{M_{\Sigma 0}^{dc}(3(L_1 - L_2))}{2C_{PU2}(L_a^2 + 4L_aL_e)} - \frac{M_{\Delta 0}^{dc}C_L}{C_{PU}(L_a^2 + 4L_aL_e)} \end{array} \right]
\end{aligned}$$

$$\tilde{A}_{12}^{21} = \left[\begin{array}{cc} -\frac{2M_{\Delta 0}^{dc} L_s}{C_{LL}} - \frac{M_{\Delta \alpha}^{2\parallel} L_s}{2C_{LL}} & -\frac{M_{\Delta \alpha}^{2\perp} L_s}{2C_{LL2}} \\ -\frac{M_{\Delta \alpha}^{2\perp} L_s}{2C_{LL}} & -\frac{2M_{\Delta 0}^{dc} L_s}{C_{LL}} + \frac{M_{\Delta \alpha}^{2\parallel} L_s}{2C_{LL2}} \\ -\frac{M_{\Delta 0}^{3\parallel} L_s}{C_{LL}} - \frac{M_{\Delta \alpha}^{1\parallel} L_s}{2C_{LL2}} & \frac{M_{\Delta \alpha}^{1\perp} L_s}{2C_{LL}} - \frac{M_{\Delta 0}^{3\perp} L_s}{C_{LL2}} \\ -\frac{M_{\Delta \alpha}^{1\perp} L_s}{2C_{LL}} - \frac{M_{\Delta 0}^{3\perp} L_s}{C_{LL}} & \frac{M_{\Delta 0}^{3\parallel} L_s}{C_{LL}} - \frac{M_{\Delta \alpha}^{1\parallel} L_s}{2C_{LL}} \\ \frac{M_{\Delta \beta}^{2\parallel} L_s}{2C_{LL}} & \frac{M_{\Delta \beta}^{2\perp} L_s}{2C_{LL2}} \\ \frac{M_{\Delta \beta}^{2\perp} L_s}{2C_{LL}} & \frac{M_{\Delta \beta}^{2\parallel} L_s}{2C_{LL2}} \\ \frac{M_{\Delta \beta}^{1\parallel} L_s}{2C_{LL2}} & \frac{M_{\Delta \beta}^{1\perp} L_s}{2C_{LL2}} \\ \frac{M_{\Delta \beta}^{1\perp} L_s}{2C_{LL2}} & \frac{M_{\Delta \beta}^{1\parallel} L_s}{2C_{LL2}} \\ \frac{3M_{\Sigma \alpha}^{1\parallel} (L_1 - L_2)}{4C_{PU2} (L_a^2 + 4L_a L_e)} - \frac{M_{\Delta \alpha}^{1\parallel} (3(L_1 + L_2) + 2L_a)}{4C_{PU2} (L_a^2 + 4L_a L_e)} & \frac{3M_{\Sigma \alpha}^{1\perp} (L_1 - L_2)}{4C_{PU2} (L_a^2 + 4L_a L_e)} - \frac{M_{\Delta \alpha}^{1\perp} (3(L_1 + L_2) + 2L_a)}{4C_{PU2} (L_a^2 + 4L_a L_e)} \\ \frac{3M_{\Sigma \alpha}^{2\parallel} (L_1 - L_2)}{4C_{PU} (L_a^2 + 4L_a L_e)} - \frac{M_{\Delta \alpha}^{2\parallel} (3(L_1 + L_2) + 2L_a)}{4C_{PU} (L_a^2 + 4L_a L_e)} & \frac{3M_{\Sigma \alpha}^{2\perp} (L_1 - L_2)}{4C_{PU} (L_a^2 + 4L_a L_e)} - \frac{M_{\Delta \alpha}^{2\perp} (3(L_1 + L_2) + 2L_a)}{4C_{PU} (L_a^2 + 4L_a L_e)} \\ \frac{3M_{\Sigma \alpha}^{2\perp} (L_1 - L_2)}{4C_{PU} (L_a^2 + 4L_a L_e)} - \frac{M_{\Delta \alpha}^{2\perp} (3(L_1 + L_2) + 2L_a)}{4C_{PU} (L_a^2 + 4L_a L_e)} & \frac{3M_{\Sigma \alpha}^{2\parallel} (L_1 - L_2)}{4C_{PU} (L_a^2 + 4L_a L_e)} - \frac{M_{\Delta \alpha}^{2\parallel} (3(L_1 + L_2) + 2L_a)}{4C_{PU} (L_a^2 + 4L_a L_e)} \end{array} \right]$$

To maintain the same model nomenclature than in the DC/DC/AC DPM, C_{LL2} remains as it was in the original model, but in this case it is defined as follows and its units are only one “ L ”.

$$C_{LL2} = L_a + 4L_e + 6L_m$$

$$\begin{aligned}
\tilde{A}_{12r}^{22} = & \left[\begin{array}{cc}
-\frac{M_{\Delta 0}^{3\parallel} L_s}{C_{LL}} - \frac{M_{\Delta \alpha}^{1\parallel} L_s}{2C_{LL2}} & -\frac{M_{\Delta \alpha}^{1\perp} L_s}{2C_{LL2}} - \frac{M_{\Delta 0}^{3\perp} L_s}{C_{LL2}} \\
\frac{M_{\Delta 0}^{1\perp} L_s}{2C_{LL}} - \frac{M_{\Delta 0}^{3\perp} L_s}{C_{LL2}} & \frac{M_{\Delta 0}^{3\parallel} L_s}{C_{LL2}} - \frac{M_{\Delta \alpha}^{1\parallel} L_s}{2C_{LL}} \\
-\frac{2M_{\Delta 0}^{dc} L_s}{C_{LL2}} & 0 \\
0 & -\frac{2M_{\Delta 0}^{dc} L_s}{C_{LL}} \\
\frac{M_{\Delta \beta}^{1\parallel} L_s}{2C_{LL2}} & \frac{M_{\Delta \beta}^{1\perp} L_s}{2C_{LL2}} \\
-\frac{M_{\Delta \beta}^{1\perp} L_s}{2C_{LL2}} & \frac{M_{\Delta \beta}^{1\parallel} L_s}{2C_{LL}} \\
0 & 0 \\
0 & 0 \\
\frac{3M_{\Sigma \alpha}^{2\parallel} (L_1 - L_2)}{4C_{PU} (L_a^2 + 4L_a L_e)} - \frac{M_{\Delta \alpha}^{2\parallel} (3(L_1 + L_2) + 2L_a)}{4C_{PU} (L_a^2 + 4L_a L_e)} & \frac{3M_{\Sigma \alpha}^{2\perp} (L_1 - L_2)}{4C_{PU2} (L_a^2 + 4L_a L_e)} - \frac{M_{\Delta \alpha}^{2\perp} (3(L_1 + L_2) + 2L_a)}{4C_{PU} (L_a^2 + 4L_a L_e)} \\
\frac{3M_{\Sigma \alpha}^{1\parallel} (L_1 - L_2)}{4C_{PU2} (L_a^2 + 4L_a L_e)} - \frac{M_{\Delta \alpha}^{1\parallel} (3(L_1 + L_2) + 2L_a)}{4C_{PU2} (L_a^2 + 4L_a L_e)} & \frac{M_{\Delta \alpha}^{1\perp} (3(L_1 + L_2) + 2L_a)}{4C_{PU} (L_a^2 + 4L_a L_e)} - \frac{3M_{\Sigma \alpha}^{1\perp} (L_1 - L_2)}{4C_{PU2} (L_a^2 + 4L_a L_e)} \\
\frac{3M_{\Sigma \alpha}^{1\perp} (L_1 - L_2)}{4C_{PU} (L_a^2 + 4L_a L_e)} - \frac{M_{\Delta \alpha}^{1\perp} (3(L_1 + L_2) + 2L_a)}{4C_{PU} (L_a^2 + 4L_a L_e)} & \frac{3M_{\Sigma \alpha}^{1\parallel} (L_1 - L_2)}{4C_{PU} (L_a^2 + 4L_a L_e)} - \frac{M_{\Delta \alpha}^{1\parallel} (3(L_1 + L_2) + 2L_a)}{4C_{PU2} (L_a^2 + 4L_a L_e)}
\end{array} \right] \\
\tilde{A}_{12}^{23} = & \left[\begin{array}{cc}
\frac{M_{\Delta \beta}^{2\parallel} L_s}{2C_{LL}} & \frac{M_{\Delta \beta}^{2\perp} L_s}{2C_{LL2}} \\
\frac{M_{\Delta \beta}^{2\perp} L_s}{2C_{LL2}} & -\frac{M_{\Delta \beta}^{2\parallel} L_s}{2C_{LL2}} \\
\frac{M_{\Delta \beta}^{1\parallel} L_s}{2C_{LL2}} & -\frac{M_{\Delta \beta}^{1\perp} L_s}{2C_{LL2}} \\
\frac{M_{\Delta \beta}^{1\perp} L_s}{2C_{LL2}} & \frac{M_{\Delta \beta}^{1\parallel} L_s}{2C_{LL2}} \\
-\frac{2M_{\Delta 0}^{dc} L_s}{C_{LL2}} + \frac{M_{\Delta \alpha}^{2\parallel} L_s}{2C_{LL2}} & \frac{M_{\Delta \alpha}^{2\perp} L_s}{2C_{LL2}} \\
\frac{M_{\Delta \alpha}^{2\perp} L_s}{2C_{LL2}} & -\frac{2M_{\Delta 0}^{dc} L_s}{C_{LL2}} - \frac{M_{\Delta \alpha}^{2\parallel} L_s}{2C_{LL2}} \\
-\frac{M_{\Delta 0}^{3\parallel} L_s}{C_{LL2}} + \frac{M_{\Delta \alpha}^{1\parallel} L_s}{2C_{LL2}} & -\frac{M_{\Delta \alpha}^{1\perp} L_s}{2C_{LL2}} - \frac{M_{\Delta 0}^{3\perp} L_s}{C_{LL2}} \\
\frac{M_{\Delta \alpha}^{1\perp} L_s}{2C_{LL2}} - \frac{M_{\Delta 0}^{3\perp} L_s}{C_{LL2}} & \frac{M_{\Delta 0}^{3\parallel} L_s}{C_{LL2}} + \frac{M_{\Delta \alpha}^{1\parallel} L_s}{2C_{LL2}} \\
\frac{3M_{\Sigma \beta}^{1\parallel} (L_1 - L_2)}{4C_{PU2} (L_a^2 + 4L_a L_e)} - \frac{M_{\Delta \beta}^{1\parallel} (3(L_1 + L_2) + 2L_a)}{4C_{PU2} (L_a^2 + 4L_a L_e)} & \frac{3M_{\Sigma \beta}^{1\perp} (L_1 - L_2)}{4C_{PU} (L_a^2 + 4L_a L_e)} - \frac{M_{\Delta \beta}^{1\perp} (3(L_1 + L_2) + 2L_a)}{4C_{PU2} (L_a^2 + 4L_a L_e)} \\
\frac{3M_{\Sigma \beta}^{2\parallel} (L_1 - L_2)}{4C_{PU2} (L_a^2 + 4L_a L_e)} - \frac{M_{\Delta \beta}^{2\parallel} (3(L_1 + L_2) + 2L_a)}{4C_{PU} (L_a^2 + 4L_a L_e)} & \frac{M_{\Delta \beta}^{2\perp} (3(L_1 + L_2) + 2L_a)}{4C_{PU2} (L_a^2 + 4L_a L_e)} - \frac{3M_{\Sigma \beta}^{2\perp} (L_1 - L_2)}{4C_{PU2} (L_a^2 + 4L_a L_e)} \\
\frac{3M_{\Sigma \beta}^{2\perp} (L_1 - L_2)}{4C_{PU2} (L_a^2 + 4L_a L_e)} - \frac{M_{\Delta \beta}^{2\perp} (3(L_1 + L_2) + 2L_a)}{4C_{PU2} (L_a^2 + 4L_a L_e)} & \frac{3M_{\Sigma \beta}^{2\parallel} (L_1 - L_2)}{4C_{PU2} (L_a^2 + 4L_a L_e)} - \frac{M_{\Delta \beta}^{2\parallel} (3(L_1 + L_2) + 2L_a)}{4C_{PU2} (L_a^2 + 4L_a L_e)}
\end{array} \right]
\end{aligned}$$

$$\tilde{A}_{12r}^{24} = \begin{bmatrix} \frac{M_{\Delta\beta}^{1\parallel} L_s}{2C_{LL2}} & \frac{M_{\Delta\beta}^{1\perp} L_s}{2C_{LL2}} \\ -\frac{M_{\Delta\beta}^{1\perp} L_s}{2C_{LL2}} & \frac{M_{\Delta\beta}^{1\parallel} L_s}{2C_{LL2}} \\ 0 & 0 \\ 0 & 0 \\ -\frac{M_{\Delta 0}^{3\parallel} L_s}{C_{LL2}} + \frac{M_{\Delta\alpha}^{1\parallel} L_s}{2C_{LL2}} & \frac{M_{\Delta\alpha}^{1\perp} L_s}{2C_{LL2}} - \frac{M_{\Delta 0}^{3\perp} L_s}{C_{LL2}} \\ -\frac{M_{\Delta\alpha}^{1\perp} L_s}{2C_{LL2}} - \frac{M_{\Delta 0}^{3\perp} L_s}{C_{LL2}} & \frac{M_{\Delta 0}^{3\parallel} L_s}{C_{LL2}} + \frac{M_{\Delta\alpha}^{1\parallel} L_s}{2C_{LL2}} \\ -\frac{2M_{\Delta 0}^{dc} L_s}{C_{LL2}} & 0 \\ 0 & -\frac{2M_{\Delta 0}^{dc} L_s}{C_{LL2}} \\ \frac{3M_{\Sigma\beta}^{2\parallel} (L_1 - L_2)}{4C_{PU2}(L_a^2 + 4L_a L_e)} - \frac{M_{\Delta\beta}^{2\parallel} (3(L_1 + L_2) + 2L_a)}{4C_{PU2}(L_a^2 + 4L_a L_e)} & \frac{3M_{\Sigma\beta}^{2\perp} (L_1 - L_2)}{4C_{PU2}(L_a^2 + 4L_a L_e)} - \frac{M_{\Delta\beta}^{2\perp} (3(L_1 + L_2) + 2L_a)}{4C_{PU}(L_a^2 + 4L_a L_e)} \\ \frac{3M_{\Sigma\beta}^{1\parallel} (L_1 - L_2)}{4C_{PU2}(L_a^2 + 4L_a L_e)} - \frac{M_{\Delta\beta}^{1\parallel} (3(L_1 + L_2) + 2L_a)}{4C_{PU2}(L_a^2 + 4L_a L_e)} & \frac{M_{\Delta\beta}^{1\perp} (3(L_1 + L_2) + 2L_a)}{4C_{PU}(L_a^2 + 4L_a L_e)} - \frac{3M_{\Sigma\beta}^{1\perp} (L_1 - L_2)}{4C_{PU2}(L_a^2 + 4L_a L_e)} \\ \frac{3M_{\Sigma\beta}^{1\perp} (L_1 - L_2)}{4C_{PU2}(L_a^2 + 4L_a L_e)} - \frac{M_{\Delta\beta}^{1\perp} (3(L_1 + L_2) + 2L_a)}{4C_{PU2}(L_a^2 + 4L_a L_e)} & \frac{3M_{\Sigma\beta}^{1\parallel} (L_1 - L_2)}{4C_{PU2}(L_a^2 + 4L_a L_e)} - \frac{M_{\Delta\beta}^{1\parallel} (3(L_1 + L_2) + 2L_a)}{4C_{PU2}(L_a^2 + 4L_a L_e)} \end{bmatrix}$$

$$\tilde{A}_{12r}^{25} = \begin{bmatrix} -\frac{2M_{\Delta\alpha}^{1\parallel} L_s}{C_{LL2}} & -\frac{M_{\Delta\alpha}^{2\parallel} L_s}{C_{LL2}} & -\frac{M_{\Delta\alpha}^{2\perp} L_s}{C_{LL2}} \\ -\frac{2M_{\Delta\alpha}^{1\perp} L_s}{C_{LL2}} & \frac{M_{\Delta\alpha}^{2\perp} L_s}{C_{LL2}} & \frac{M_{\Delta\alpha}^{1\parallel} L_s}{C_{LL2}} \\ -\frac{2M_{\Delta\alpha}^{2\parallel} L_s}{C_{LL2}} & -\frac{M_{\Delta\alpha}^{1\perp} L_s}{C_{LL2}} & -\frac{M_{\Delta\alpha}^{1\parallel} L_s}{C_{LL2}} \\ -\frac{2M_{\Delta\alpha}^{2\perp} L_s}{C_{LL2}} & \frac{M_{\Delta\beta}^{2\parallel} L_s}{C_{LL2}} & \frac{M_{\Delta\beta}^{2\perp} L_s}{C_{LL2}} \\ -\frac{2M_{\Delta\beta}^{1\parallel} L_s}{C_{LL2}} & -\frac{M_{\Delta\beta}^{1\perp} L_s}{C_{LL2}} & -\frac{M_{\Delta\beta}^{1\parallel} L_s}{C_{LL2}} \\ -\frac{2M_{\Delta\beta}^{1\perp} L_s}{C_{LL2}} & \frac{M_{\Delta\beta}^{2\parallel} L_s}{C_{LL2}} & \frac{M_{\Delta\beta}^{2\perp} L_s}{C_{LL2}} \\ -\frac{2M_{\Delta\beta}^{2\parallel} L_s}{C_{LL2}} & -\frac{M_{\Delta\beta}^{1\perp} L_s}{C_{LL2}} & -\frac{M_{\Delta\beta}^{1\parallel} L_s}{C_{LL2}} \\ -\frac{2M_{\Delta\beta}^{2\perp} L_s}{C_{LL2}} & \frac{M_{\Delta\beta}^{1\parallel} L_s}{C_{LL2}} & \frac{M_{\Delta\beta}^{1\perp} L_s}{C_{LL2}} \\ \frac{3M_{\Sigma 0}^{dc} (L_1 - L_2)}{C_{PU2}(L_a^2 + 4L_a L_e)} - \frac{M_{\Delta 0}^{dc} (3L_1 + 3L_2 + 2L_a)}{C_{PU2}(L_a^2 + 4L_a L_e)} & \frac{3M_{\Sigma 0}^{3\parallel} (L_1 - L_2)}{2C_{PU2}(L_a^2 + 4L_a L_e)} - \frac{M_{\Delta 0}^{3\parallel} (3L_1 + 3L_2 + 2L_a)}{2C_{PU2}(L_a^2 + 4L_a L_e)} & \frac{3M_{\Sigma 0}^{3\perp} (L_1 - L_2)}{2C_{PU2}(L_a^2 + 4L_a L_e)} - \frac{M_{\Delta 0}^{3\perp} (3L_1 + 3L_2 + 2L_a)}{2C_{PU2}(L_a^2 + 4L_a L_e)} \\ \frac{3M_{\Sigma 0}^{3\parallel} (L_1 - L_2)}{C_{PU2}(L_a^2 + 4L_a L_e)} - \frac{M_{\Delta 0}^{3\parallel} (3L_1 + 3L_2 + 2L_a)}{C_{PU2}(L_a^2 + 4L_a L_e)} & \frac{3M_{\Sigma 0}^{dc} (L_1 - L_2)}{C_{PU2}(L_a^2 + 4L_a L_e)} - \frac{M_{\Delta 0}^{dc} (3L_1 + 3L_2 + 2L_a)}{C_{PU2}(L_a^2 + 4L_a L_e)} & 0 \\ \frac{3M_{\Sigma 0}^{3\perp} (L_1 - L_2)}{C_{PU2}(L_a^2 + 4L_a L_e)} - \frac{M_{\Delta 0}^{3\perp} (3L_1 + 3L_2 + 2L_a)}{C_{PU2}(L_a^2 + 4L_a L_e)} & 0 & \frac{3M_{\Sigma 0}^{dc} (L_1 - L_2)}{C_{PU2}(L_a^2 + 4L_a L_e)} - \frac{M_{\Delta 0}^{dc} (3L_1 + 3L_2 + 2L_a)}{C_{PU2}(L_a^2 + 4L_a L_e)} \end{bmatrix}$$

$$\begin{aligned}
\tilde{A}_{12r}^{26} = & \left[\begin{array}{c} -\frac{2M_{\Sigma 0}^{dc} L_s}{C_{LL2}} - \frac{M_{\Sigma \alpha}^{2\parallel} L_s}{2C_{LL2}} \\ -\frac{M_{\Sigma \alpha}^{2\perp} L_s}{2C_{LL2}} \\ -\frac{M_{\Sigma 0}^{3\parallel} L_s}{C_{LL2}} - \frac{M_{\Sigma \alpha}^{1\parallel} L_s}{2C_{LL2}} \\ -\frac{M_{\Sigma \alpha}^{1\perp} L_s}{2C_{LL2}} - \frac{M_{\Sigma 0}^{3\perp} L_s}{C_{LL2}} \\ \frac{M_{\Sigma \beta}^{2\parallel} L_s}{2C_{LL2}} \\ \frac{M_{\Sigma \beta}^{2\perp} L_s}{2C_{LL2}} \\ \frac{M_{\Sigma \beta}^{1\parallel} L_s}{2C_{LL2}} \\ \frac{M_{\Sigma \beta}^{1\perp} L_s}{2C_{LL2}} \\ \frac{3M_{\Delta \alpha}^{1\parallel} (L_1 - L_2)}{4C_{PU2} (L_a^2 + 4L_a L_e)} - \frac{M_{\Sigma \alpha}^{1\parallel} (3(L_1 + L_2) + 2L_a)}{4C_{PU2} (L_a^2 + 4L_a L_e)} \\ \frac{3M_{\Delta \alpha}^{2\parallel} (L_1 - L_2)}{4C_{PU2} (L_a^2 + 4L_a L_e)} - \frac{M_{\Sigma \alpha}^{2\parallel} (3(L_1 + L_2) + 2L_a)}{4C_{PU} (L_a^2 + 4L_a L_e)} \\ \frac{3M_{\Delta \alpha}^{2\perp} (L_1 - L_2)}{4C_{PU2} (L_a^2 + 4L_a L_e)} - \frac{M_{\Sigma \alpha}^{2\perp} (3(L_1 + L_2) + 2L_a)}{4C_{PU2} (L_a^2 + 4L_a L_e)} \end{array} \right] \\
& \left[\begin{array}{c} -\frac{M_{\Sigma \alpha}^{2\perp} L_s}{2C_{LL2}} - \frac{M_{\Sigma \alpha}^{2\parallel} L_s}{2C_{LL2}} \\ -\frac{M_{\Sigma 0}^{3\parallel} L_s}{C_{LL2}} - \frac{M_{\Sigma \alpha}^{1\parallel} L_s}{2C_{LL2}} \\ -\frac{2M_{\Sigma 0}^{dc} L_s}{C_{LL2}} \\ 0 \\ \frac{M_{\Sigma \beta}^{1\parallel} L_s}{2C_{LL}} \\ -\frac{M_{\Sigma \beta}^{1\perp} L_s}{2C_{LL2}} \\ 0 \\ 0 \\ \frac{3M_{\Delta \alpha}^{2\parallel} (L_1 - L_2)}{4C_{PU2} (L_a^2 + 4L_a L_e)} - \frac{M_{\Sigma \alpha}^{2\parallel} (3(L_1 + L_2) + 2L_a)}{4C_{PU2} (L_a^2 + 4L_a L_e)} \\ \frac{3M_{\Delta \alpha}^{1\parallel} (L_1 - L_2)}{4C_{PU} (L_a^2 + 4L_a L_e)} - \frac{M_{\Sigma \alpha}^{1\parallel} (3(L_1 + L_2) + 2L_a)}{4C_{PU2} (L_a^2 + 4L_a L_e)} \\ \frac{3M_{\Delta \alpha}^{1\perp} (L_1 - L_2)}{4C_{PU} (L_a^2 + 4L_a L_e)} - \frac{M_{\Sigma \alpha}^{1\perp} (3(L_1 + L_2) + 2L_a)}{4C_{PU} (L_a^2 + 4L_a L_e)} \end{array} \right] \\
\tilde{A}_{12r}^{27} = & \left[\begin{array}{c} -\frac{M_{\Sigma 0}^{3\parallel} L_s}{C_{LL}} - \frac{M_{\Sigma \alpha}^{1\parallel} L_s}{2C_{LL2}} \\ \frac{M_{\Sigma \alpha}^{1\perp} L_s}{2C_{LL}} - \frac{M_{\Sigma 0}^{3\perp} L_s}{C_{LL2}} \\ -\frac{2M_{\Sigma 0}^{dc} L_s}{C_{LL2}} \\ 0 \\ \frac{M_{\Sigma \beta}^{1\parallel} L_s}{2C_{LL}} \\ -\frac{M_{\Sigma \beta}^{1\perp} L_s}{2C_{LL2}} \\ 0 \\ 0 \\ \frac{3M_{\Delta \alpha}^{2\parallel} (L_1 - L_2)}{4C_{PU2} (L_a^2 + 4L_a L_e)} - \frac{M_{\Sigma \alpha}^{2\parallel} (3(L_1 + L_2) + 2L_a)}{4C_{PU2} (L_a^2 + 4L_a L_e)} \\ \frac{3M_{\Delta \alpha}^{1\parallel} (L_1 - L_2)}{4C_{PU} (L_a^2 + 4L_a L_e)} - \frac{M_{\Sigma \alpha}^{1\parallel} (3(L_1 + L_2) + 2L_a)}{4C_{PU2} (L_a^2 + 4L_a L_e)} \\ \frac{3M_{\Delta \alpha}^{1\perp} (L_1 - L_2)}{4C_{PU} (L_a^2 + 4L_a L_e)} - \frac{M_{\Sigma \alpha}^{1\perp} (3(L_1 + L_2) + 2L_a)}{4C_{PU} (L_a^2 + 4L_a L_e)} \end{array} \right] \\
& \left[\begin{array}{c} -\frac{M_{\Sigma \alpha}^{1\perp} L_s}{2C_{LL2}} - \frac{M_{\Sigma 0}^{3\perp} L_s}{C_{LL2}} \\ \frac{M_{\Sigma 0}^{3\parallel} L_s}{C_{LL2}} - \frac{M_{\Sigma \alpha}^{1\parallel} L_s}{2C_{LL2}} \\ 0 \\ -\frac{2M_{\Sigma 0}^{dc} L_s}{C_{LL2}} \\ \frac{M_{\Sigma \beta}^{1\perp} L_s}{2C_{LL2}} \\ \frac{M_{\Sigma \beta}^{1\parallel} L_s}{2C_{LL2}} \\ 0 \\ 0 \\ \frac{3M_{\Delta \alpha}^{2\perp} (L_1 - L_2)}{4C_{PU2} (L_a^2 + 4L_a L_e)} - \frac{M_{\Sigma \alpha}^{2\perp} (3(L_1 + L_2) + 2L_a)}{4C_{PU2} (L_a^2 + 4L_a L_e)} \\ \frac{M_{\Sigma \alpha}^{1\perp} (3(L_1 + L_2) + 2L_a)}{4C_{PU} (L_a^2 + 4L_a L_e)} - \frac{3M_{\Delta \alpha}^{1\perp} (L_1 - L_2)}{4C_{PU} (L_a^2 + 4L_a L_e)} \\ \frac{3M_{\Delta \alpha}^{1\parallel} (L_1 - L_2)}{4C_{PU} (L_a^2 + 4L_a L_e)} - \frac{M_{\Sigma \alpha}^{1\parallel} (3(L_1 + L_2) + 2L_a)}{4C_{PU2} (L_a^2 + 4L_a L_e)} \end{array} \right]
\end{aligned}$$

$$\begin{aligned}
\tilde{A}_{12r}^{28} = & \left[\begin{array}{c} \frac{M_{\Sigma\beta}^{2\parallel} L_s}{2C_{LL}} \\ \frac{M_{\Sigma\beta}^{2\perp} L_s}{2C_{LL}} \\ \frac{M_{\Sigma\beta}^{1\parallel} L_s}{2C_{LL2}} \\ \frac{M_{\Sigma\beta}^{1\perp} L_s}{2C_{LL2}} \\ -\frac{2M_{\Sigma0}^{dc} L_s}{C_{LL}} + \frac{M_{\Sigma\alpha}^{2\parallel} L_s}{2C_{LL2}} \\ \frac{M_{\Sigma\alpha}^{2\perp} L_s}{2C_{LL}} \\ -\frac{M_{\Sigma0}^{3\parallel} L_s}{C_{LL}} + \frac{M_{\Sigma\alpha}^{1\parallel} L_s}{2C_{LL2}} \\ \frac{M_{\Sigma\alpha}^{1\perp} L_s}{2C_{LL}} - \frac{M_{\Sigma0}^{3\perp} L_s}{C_{LL}} \\ \frac{3M_{\Delta\beta}^{1\parallel} (L_1 - L_2)}{4C_{PU2}(L_a^2 + 4L_a L_e)} - \frac{M_{\Sigma\beta}^{1\parallel} (3(L_1 + L_2) + 2L_a)}{4C_{PU2}(L_a^2 + 4L_a L_e)} \\ \frac{3M_{\Delta\beta}^{2\parallel} (L_1 - L_2)}{4C_{PU2}(L_a^2 + 4L_a L_e)} - \frac{M_{\Sigma\beta}^{2\parallel} (3(L_1 + L_2) + 2L_a)}{4C_{PU}(L_a^2 + 4L_a L_e)} \\ \frac{3M_{\Delta\beta}^{2\perp} (L_1 - L_2)}{4C_{PU2}(L_a^2 + 4L_a L_e)} - \frac{M_{\Sigma\beta}^{2\perp} (3(L_1 + L_2) + 2L_a)}{4C_{PU}(L_a^2 + 4L_a L_e)} \\ \frac{3M_{\Delta\beta}^{1\perp} (L_1 - L_2)}{4C_{PU}(L_a^2 + 4L_a L_e)} - \frac{M_{\Sigma\beta}^{1\perp} (3(L_1 + L_2) + 2L_a)}{4C_{PU}(L_a^2 + 4L_a L_e)} \end{array} \right] \\
& \left[\begin{array}{c} \frac{M_{\Sigma\beta}^{2\perp} L_s}{2C_{LL}} \\ \frac{M_{\Sigma\beta}^{1\parallel} L_s}{2C_{LL2}} \\ \frac{M_{\Sigma\beta}^{1\perp} L_s}{2C_{LL2}} \\ 0 \\ 0 \\ -\frac{M_{\Sigma0}^{3\parallel} L_s}{C_{LL}} + \frac{M_{\Sigma\alpha}^{1\parallel} L_s}{2C_{LL2}} \\ -\frac{M_{\Sigma\alpha}^{1\perp} L_s}{2C_{LL2}} - \frac{M_{\Sigma0}^{3\perp} L_s}{C_{LL}} \\ -\frac{2M_{\Sigma0}^{dc} L_s}{C_{LL}} \\ 0 \\ \frac{3M_{\Delta\beta}^{2\parallel} (L_1 - L_2)}{4C_{PU}(L_a^2 + 4L_a L_e)} - \frac{M_{\Sigma\beta}^{2\parallel} (3(L_1 + L_2) + 2L_a)}{4C_{PU2}(L_a^2 + 4L_a L_e)} \\ \frac{3M_{\Delta\beta}^{1\parallel} (L_1 - L_2)}{4C_{PU2}(L_a^2 + 4L_a L_e)} - \frac{M_{\Sigma\beta}^{1\parallel} (3(L_1 + L_2) + 2L_a)}{4C_{PU2}(L_a^2 + 4L_a L_e)} \\ \frac{3M_{\Delta\beta}^{2\perp} (L_1 - L_2)}{4C_{PU2}(L_a^2 + 4L_a L_e)} - \frac{M_{\Sigma\beta}^{2\perp} (3(L_1 + L_2) + 2L_a)}{4C_{PU}(L_a^2 + 4L_a L_e)} \\ \frac{3M_{\Delta\beta}^{1\perp} (L_1 - L_2)}{4C_{PU}(L_a^2 + 4L_a L_e)} - \frac{M_{\Sigma\beta}^{1\perp} (3(L_1 + L_2) + 2L_a)}{4C_{PU2}(L_a^2 + 4L_a L_e)} \end{array} \right] \\
\tilde{A}_{12r}^{29} = & \left[\begin{array}{c} \frac{M_{\Sigma\beta}^{1\parallel} L_s}{2C_{LL2}} \\ \frac{M_{\Sigma\beta}^{1\perp} L_s}{2C_{LL}} \\ 0 \\ 0 \\ -\frac{M_{\Sigma0}^{3\parallel} L_s}{C_{LL}} + \frac{M_{\Sigma\alpha}^{1\parallel} L_s}{2C_{LL2}} \\ -\frac{M_{\Sigma\alpha}^{1\perp} L_s}{2C_{LL2}} - \frac{M_{\Sigma0}^{3\perp} L_s}{C_{LL}} \\ -\frac{2M_{\Sigma0}^{dc} L_s}{C_{LL}} \\ 0 \\ \frac{3M_{\Delta\beta}^{2\parallel} (L_1 - L_2)}{4C_{PU2}(L_a^2 + 4L_a L_e)} - \frac{M_{\Sigma\beta}^{2\parallel} (3(L_1 + L_2) + 2L_a)}{4C_{PU2}(L_a^2 + 4L_a L_e)} \\ \frac{3M_{\Delta\beta}^{1\parallel} (L_1 - L_2)}{4C_{PU2}(L_a^2 + 4L_a L_e)} - \frac{M_{\Sigma\beta}^{1\parallel} (3(L_1 + L_2) + 2L_a)}{4C_{PU2}(L_a^2 + 4L_a L_e)} \\ \frac{3M_{\Delta\beta}^{2\perp} (L_1 - L_2)}{4C_{PU2}(L_a^2 + 4L_a L_e)} - \frac{M_{\Sigma\beta}^{2\perp} (3(L_1 + L_2) + 2L_a)}{4C_{PU}(L_a^2 + 4L_a L_e)} \\ \frac{3M_{\Delta\beta}^{1\perp} (L_1 - L_2)}{4C_{PU}(L_a^2 + 4L_a L_e)} - \frac{M_{\Sigma\beta}^{1\perp} (3(L_1 + L_2) + 2L_a)}{4C_{PU2}(L_a^2 + 4L_a L_e)} \end{array} \right] \\
& \left[\begin{array}{c} \frac{M_{\Sigma\beta}^{1\perp} L_s}{2C_{LL2}} \\ \frac{M_{\Sigma\beta}^{1\parallel} L_s}{2C_{LL}} \\ 0 \\ 0 \\ \frac{M_{\Sigma\alpha}^{1\perp} L_s}{2C_{LL2}} - \frac{M_{\Sigma0}^{3\perp} L_s}{C_{LL}} \\ \frac{M_{\Sigma0}^{3\parallel} L_s}{C_{LL2}} + \frac{M_{\Sigma\alpha}^{1\parallel} L_s}{2C_{LL}} \\ 0 \\ -\frac{2M_{\Sigma0}^{dc} L_s}{C_{LL}} \\ \frac{3M_{\Delta\beta}^{2\perp} (L_1 - L_2)}{4C_{PU2}(L_a^2 + 4L_a L_e)} - \frac{M_{\Sigma\beta}^{2\perp} (3(L_1 + L_2) + 2L_a)}{4C_{PU2}(L_a^2 + 4L_a L_e)} \\ \frac{3M_{\Delta\beta}^{1\perp} (L_1 - L_2)}{4C_{PU2}(L_a^2 + 4L_a L_e)} - \frac{M_{\Sigma\beta}^{1\perp} (3(L_1 + L_2) + 2L_a)}{4C_{PU2}(L_a^2 + 4L_a L_e)} \\ \frac{3M_{\Delta\beta}^{2\parallel} (L_1 - L_2)}{4C_{PU}(L_a^2 + 4L_a L_e)} - \frac{M_{\Sigma\beta}^{2\parallel} (3(L_1 + L_2) + 2L_a)}{4C_{PU}(L_a^2 + 4L_a L_e)} \\ \frac{3M_{\Delta\beta}^{1\parallel} (L_1 - L_2)}{4C_{PU2}(L_a^2 + 4L_a L_e)} - \frac{M_{\Sigma\beta}^{1\parallel} (3(L_1 + L_2) + 2L_a)}{4C_{PU2}(L_a^2 + 4L_a L_e)} \end{array} \right]
\end{aligned}$$

171

172

173

174

175

176

177

$$\tilde{A}_{22r} =$$

Appendix E

Accuracy of DC/DC/AC DPM

The accuracy of the developed DC/DC/AC DPMs in Chapter 3 was found to be susceptible to the amount of internal energy storage in the converter, i.e., it is influenced by the capacitance selection. The lower the capacitance selected, the worse the accuracy became. Here are presented the results of the validation simulations in Section 3.2.3, using the parameters in Table 3.3, but reducing the capacitance in the arms from $50 \frac{kJ}{MW}$ to $30 \frac{kJ}{MW}$. These results show how the DC/DC/AC converter models are sensitive to internal energy storage, while the DC/DC converter models are not.

Table E.1: MP-DCDCAC State Variables Steady-State Comparison Using $30 \frac{kJ}{MW}$

State Variable	TAM	DPM	Percent Error
$i_{\Sigma\alpha}^1[A_pk]$	445.747	412.093	8.17%
$i_{\Delta g\alpha}^1[A_pk]$	970.983	992.357	2.15%
$V_{\Sigma\alpha}^1[kV_{pk}]$	9.1587	8.18674	11.87%
$V_{\Sigma\alpha}^2[kV_{pk}]$	5.87866	6.74617	12.86%
$V_{\Delta\alpha}^1[kV_{pk}]$	12.2899	12.7744	3.79%
$V_{\Delta\alpha}^2[kV_{pk}]$	4.64023	3.75481	23.58%
$i_{\Sigma 0}^{dc}[A]$	201.436	205.38	1.92%
$i_{\Delta t\alpha}^{dc}[A]$	418.186	400	4.55%
$V_{\Sigma 0}^{dc}[kV]$	400.013	400	0.00%

Table E.2: MP-DCDC State Variables Steady-State Comparison Using $30 \frac{kJ}{MW}$

State Variable	TAM	DPM	Percent Error
$i_{\Sigma\alpha}^1[A_pk]$	1610.07	1610.22	0.01%
$V_{\Sigma\alpha}^1[kV_{pk}]$	39.6904	39.694	0.01%
$V_{\Sigma\alpha}^2[kV_{pk}]$	1.73437	1.73496	0.03%
$V_{\Delta\alpha}^1[kV_{pk}]$	5.66615	5.66808	0.03%
$V_{\Delta\alpha}^2[kV_{pk}]$	5.74896	5.74865	0.01%
$i_{\Delta t\alpha}^{dc}[A]$	799.989	700.981	0.00%
$V_{\Sigma 0}^{dc}[kV]$	399.99	399.999	0.00%

Table E.3: BP-DCDCAC State Variables Steady-State Comparison Using $30 \frac{kJ}{MW}$

State Variable	Avg	DPM	Percent Error
$i_{\Sigma\alpha}^1[A]$	660.18	652.9	1.12%
$i_{\Delta g\alpha}^1[A]$	1773.44	1780.03	0.37%
$V_{\Sigma\alpha}^1[kV]$	3.19855	3.00139	6.57%
$V_{\Sigma\alpha}^2[kV]$	5.60515	5.91054	5.17%
$V_{\Delta\alpha}^1[kV]$	10.2753	10.3741	0.95%
$V_{\Delta\alpha}^2[kV]$	3.92826	3.61007	8.81%
$i_{\Sigma 0}^{dc}[A]$	469.463	471.003	0.33%
$i_{\Delta t\alpha}^{dc}[A]$	805.826	800.022	0.73%
$V_{\Sigma 0}^{dc}[kV]$	400.27	400	0.07%

Table E.4: BP-DCDC State Variables Steady-State Comparison Using $30 \frac{kJ}{MW}$

State Variable	Avg	DPM	Percent Error
$i_{\Sigma\alpha}^1[A]$	1288.6	1287.68	0.07%
$V_{\Sigma\alpha}^1[kV]$	55.3164	55.2419	0.13%
$V_{\Sigma\alpha}^2[kV]$	1.44153	1.43979	0.12%
$V_{\Delta\alpha}^1[kV]$	1.72325	1.67467	2.90%
$V_{\Delta\alpha}^2[kV]$	10.7167	10.736	0.18%
$i_{\Delta t\alpha}^{dc}[A]$	799.894	799.958	0.01%
$V_{\Sigma 0}^{dc}[kV]$	319.995	319.997	0.00%

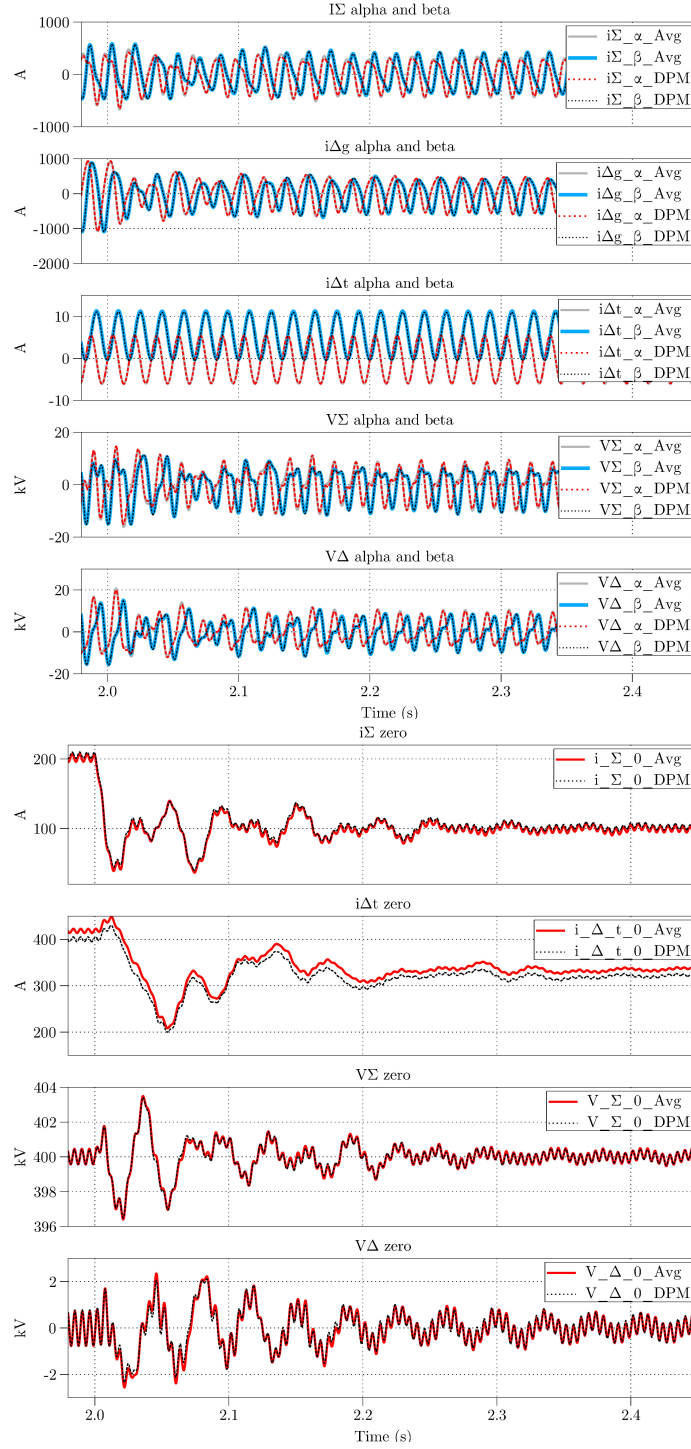


Figure E.1: MP-DCDCAC; DPM and averaged model simulation results using $30 \frac{kJ}{MW}$

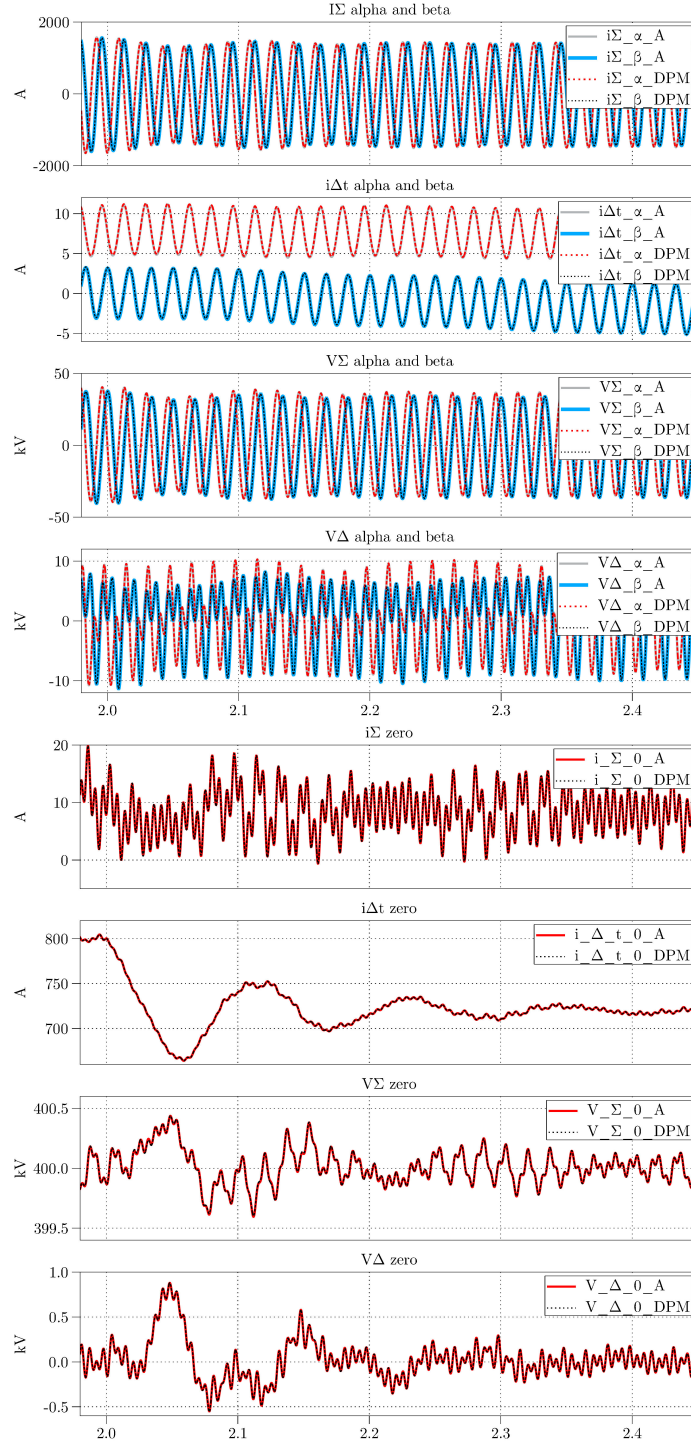


Figure E.2: MP-DCDC; DPM and averaged model simulation results using $30 \frac{kJ}{MW}$

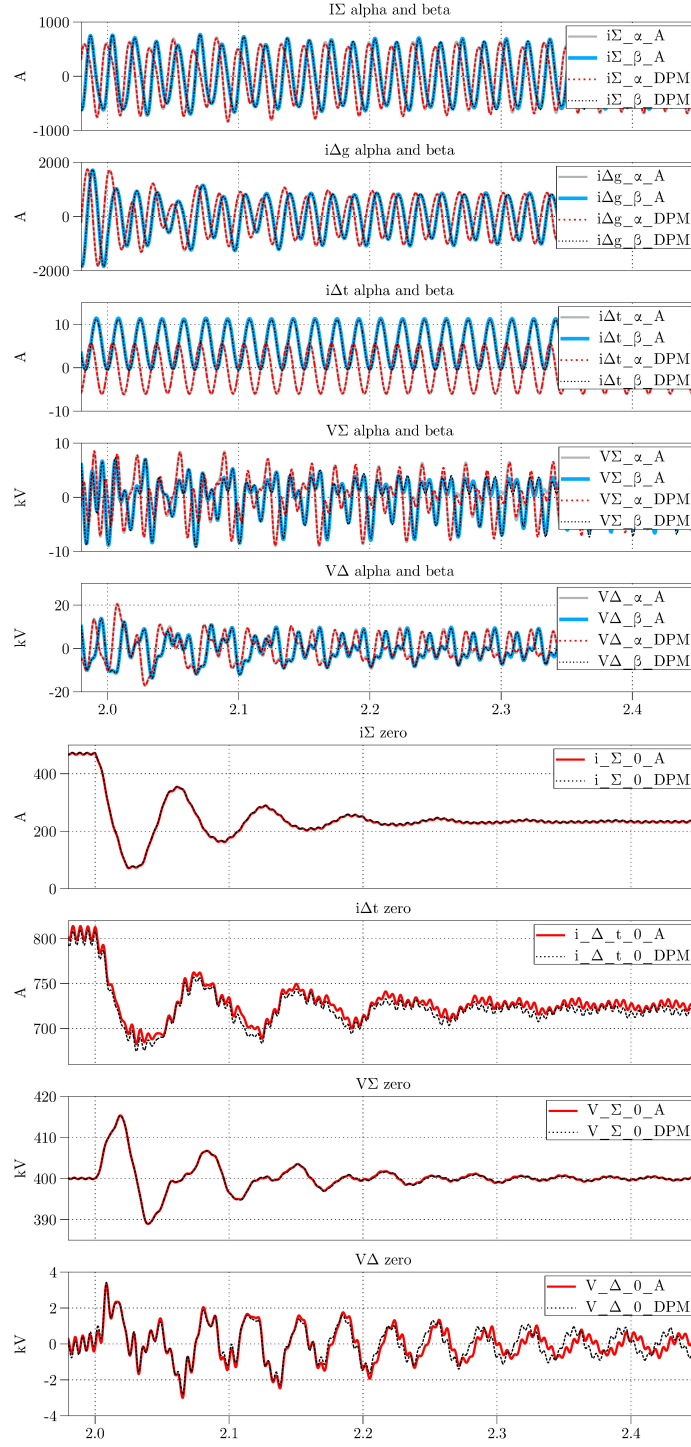


Figure E.3: BP-DCDCAC; DPM and averaged model simulation results using $30 \frac{kJ}{MW}$

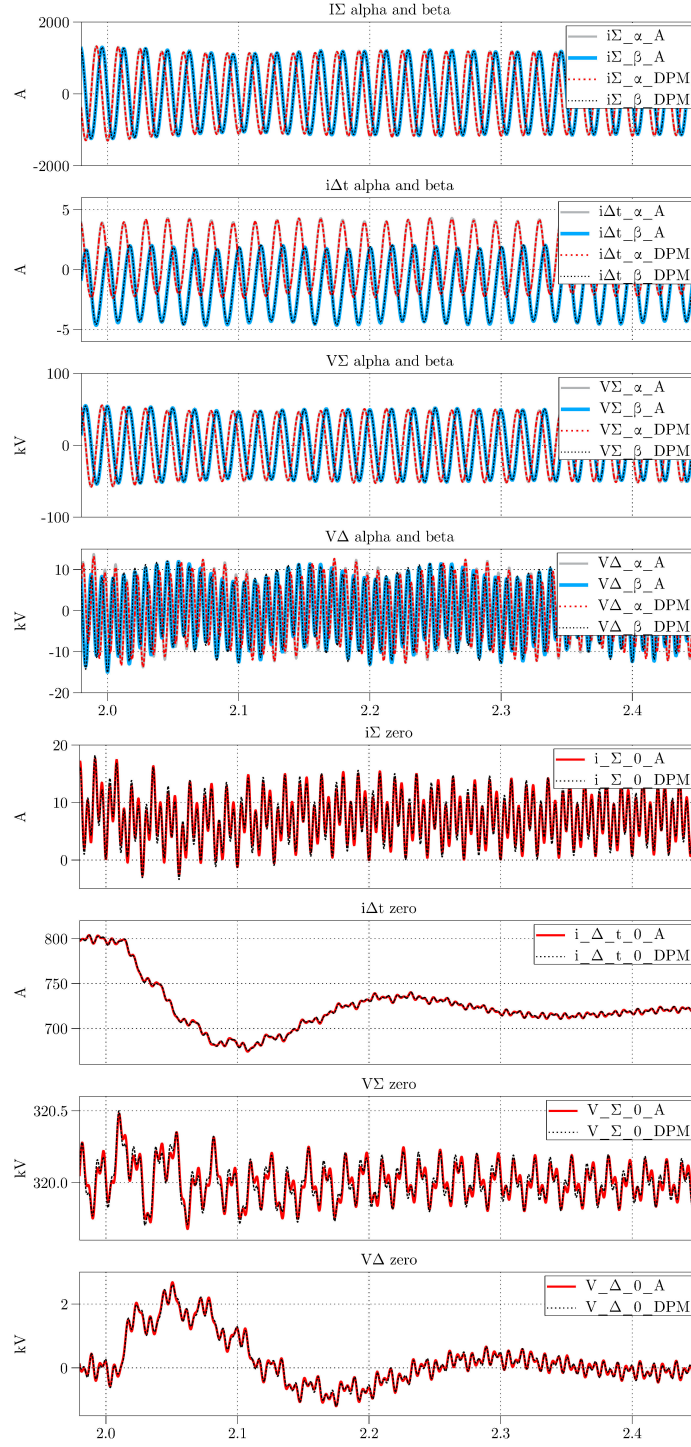


Figure E.4: BP-DCDC; DPM and averaged model simulation results using $30 \frac{kJ}{MW}$